



HAL
open science

IGF1 Receptor Inhibition Amplifies the Effects of Cancer Drugs by Autophagy and Immune-Dependent Mechanisms

Ailing Tian

► **To cite this version:**

Ailing Tian. IGF1 Receptor Inhibition Amplifies the Effects of Cancer Drugs by Autophagy and Immune-Dependent Mechanisms. *Cancer*. Université Paris-Saclay, 2022. English. NNT : 2022UP-ASL040 . tel-03703551

HAL Id: tel-03703551

<https://theses.hal.science/tel-03703551>

Submitted on 24 Jun 2022

HAL is a multi-disciplinary open access archive for the deposit and dissemination of scientific research documents, whether they are published or not. The documents may come from teaching and research institutions in France or abroad, or from public or private research centers.

L'archive ouverte pluridisciplinaire **HAL**, est destinée au dépôt et à la diffusion de documents scientifiques de niveau recherche, publiés ou non, émanant des établissements d'enseignement et de recherche français ou étrangers, des laboratoires publics ou privés.

IGF1 receptor inhibition amplifies the effects of cancer drugs by autophagy and immune-dependent mechanisms

L'inhibition du récepteur IGF1 amplifie les effets des médicaments anticancéreux par l'autophagie et les mécanismes immuno-dépendants

Thèse de doctorat de l'université Paris-Saclay

École doctorale n°582 : Cancérologie : Biologie – Médecine – Santé (CBMS)

Spécialité de doctorat : aspects moléculaires et cellulaires de la biologie

Graduate School : Sciences de la vie et santé. Référent : Faculté de Médecine

Thèse préparée dans l'unité de recherche **Metabolomics and Cell Biology Platforms**
(Gustave Roussy, Université Paris-Saclay)
sous la direction de **Guido KROEMER**, PU-PH

Thèse soutenue à Paris-Saclay, le 14 juin 2022, par

Ailing TIAN

Composition du Jury

Filippo ROSSELLI

DR, Institut Gustave Roussy, Villejuif

Président

Nicolas DUPONT

MCU, Université Paris Cité, Paris

Rapporteur & Examineur

Didac CARMONA-GUTIERREZ

PR associé, University of Graz, Graz

Rapporteur & Examineur

Véronique BAUD

DR, Université Paris Cité, Paris

Examinatrice

Laurie MENGER

CRCN, Institut Gustave Roussy,
Villejuif

Examinatrice

Guido KROEMER

PU-PH, Université Paris- Saclay

Directeur de thèse

CONTENTS

ABSTRACT	1
CONTENTS	3
INTRODUCTION	5
1 Picropodophyllin.....	5
2 Insulin-like growth factor 1 receptor.....	6
2.1 Structure.....	6
2.2 Function.....	7
2.3 IGF-1R signaling pathway.....	8
2.4 IGF-1R expression in tumor cells	8
2.5 IGF-1R and oncogenes.....	9
2.6 IGF-1R inhibitor in cancer therapy.....	9
3 Autophagy.....	12
3.1 The process of autophagy.....	14
3.2 Autophagy-related signaling pathways.....	15
3.2.1 mTOR signaling pathway.....	15
3.2.2 RAS signaling pathway.....	16
3.2.3 MAPK signaling pathway.....	16
3.2.4 FoxO signaling pathway.....	17
3.2.5 p53 signaling pathway.....	17
3.3 Measurement of autophagy.....	17
3.4 Autophagy and tumorigenesis.....	19
3.5 Autophagy and tumor therapy.....	20
4 Immunogenic cell death.....	21
4.1 ICD-related molecules.....	22
4.1.1 ATP.....	22
4.1.2 Calreticulin.....	23
4.1.3 HMGB1.....	24
4.1.4 IFN I.....	25
4.1.5 HSP.....	26
4.2 ICD inducers.....	26

4.2.1 Chemotherapy drugs.....	30
4.2.1.1 Anthracyclines.....	30
4.2.1.2 Cyclophosphamide.....	31
4.2.1.3 Bortezomib.....	31
4.2.1.4 Platinum-based chemotherapy drugs.....	31
4.2.1.5 Natural medicinal chemicals.....	32
4.2.2 Radiotherapy.....	33
4.2.3 Photodynamic therapy.....	34
4.2.4 Oncolytic virus therapy.....	34
4.2.5 Novel ICD inducers.....	35
AIMS OF THE THESIS.....	38
RESULTS.....	40
DISCUSSION.....	41
ACKNOWLEDGEMENT.....	45
REFERENCES.....	47
ANNEX 1: SCIENTIFIC PUBLICATIONS.....	70
ANNEX 2: PAPERS NOT INCLUDED IN THIS THESIS.....	72

INTRODUCTION

1 Picropodophyllin

Picropodophyllin (also known as picropodophyllotoxin (PPP)), is a cyclolignan alkaloid (**Figure 1**) found in the mayapple plant family (*Podophyllum peltatum*), and a small-molecule inhibitor of the insulin-like growth factor 1 receptor (IGF1R) with potential antineoplastic activity. IGF1R is a receptor tyrosine kinase overexpressed in a variety of human cancers and plays a critical role in the growth and survival of many types of cancer cells. PPP specifically inhibits the activity and downregulates the cellular expression of IGF1R without interfering with the activities of other growth factor receptors, such as receptors for insulin, epidermal growth factor (EGFR), platelet-derived growth factor (PDGFR), fibroblast growth factor (FGFR) and mast/stem cell growth factor (KIT). This agent shows potent activity in the suppression of tumor cell proliferation and the induction of tumor cell apoptosis (Linder et al., 2007; Stromberg et al., 2006).

PPP is currently being tested as an orally administrated single-agent treatment in an open-label combined Phase I/II clinical study in advanced cancer patients with solid tumors which progress despite several lines of treatment. In addition, it effectively inhibits rhabdomyosarcoma tumor proliferation and metastasis *in vitro* and in an animal model (Ekman et al., 2011).

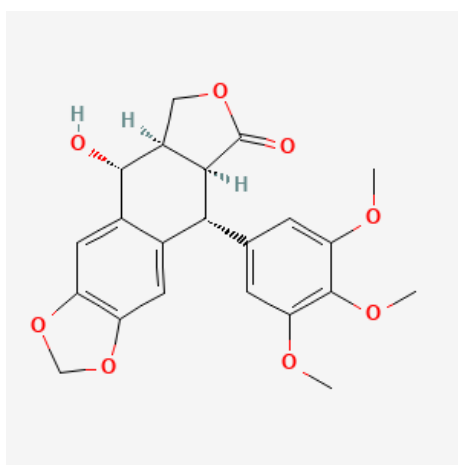


Figure 1. Picropodophyllin chemical structure depiction. (C₂₂H₂₂O₈ - PubChem)

2 Insulin-like growth factor 1 receptor

The insulin-like growth factor 1 receptor (IGF-1R) is a protein found on the surface of human cells. It is a transmembrane receptor that is activated by a hormone called insulin-like growth factor 1 (IGF-1) and by a related hormone called IGF-2. It belongs to the large class of tyrosine kinase receptors. This receptor mediates the effects of IGF-1, which is a polypeptide protein hormone similar in molecular structure to insulin. IGF-1 plays an important role during fetal development and adolescent growth, and continues to have anabolic effects in adults – meaning that it can induce hypertrophy of skeletal muscle and other target tissues. Mice lacking the IGF-1 receptor die late in development, and show a dramatic reduction in body mass, underlining the strong growth-promoting effects of this receptor (Garcia-Mato et al., 2021).

In the insulin-like growth factor (IGF) family system, the IGF-1R is the most important member. It plays a role in up-regulating expression or increasing kinase activity in a variety of neoplasms mediating tumor development and infiltration (Gable et al., 2006). IGF-1R is also related to infestation with pathogenic factors such as *Echinococcus multilocularis*, nematodes (Hemer et al., 2014), and schistosomiasis (You et al., 2010). These properties make IGF-1R an attractive potential target for antitumor and antiparasitic therapy.

2.1 Structure

Human IGF-1R is a transmembrane tetrameric glycoprotein containing 2674 amino acids, whose gene is located at 15q25-26, synthesized in the ribosome, and its precursor is a single-chain polypeptide. The extracellular alpha subunit and the 626 amino acid transmembrane beta subunit constitute a glycoprotein. The α and β subunits form an $\alpha\beta$ half-receptor through a disulfide bond, which together with another $\alpha\beta$ half-receptor, also connected through a disulfide bond, constitutes a complete and mature $\alpha_2\beta_2$ receptor (**Figure 2**).

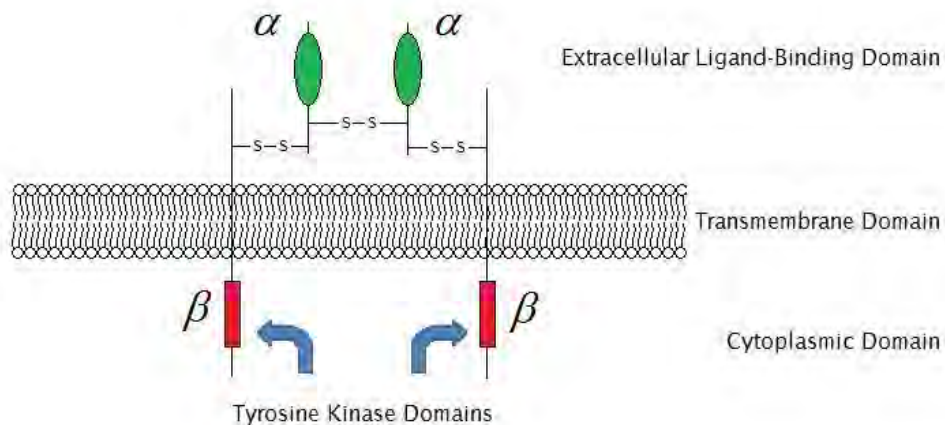


Figure 2. Schematic diagram of the IGF-1R structure. (Wikipedia)

2.2 Function

IGF-1R contains three partial functional domains: the extracellular domain, the transmembrane domain and the tyrosine protein kinase domain (cytoplasmic domain). In most species, including humans and mice, IGF-1R consists, as mentioned, of 2 α subunits and 2 β subunits (Adams et al., 2000). The α subunit of IGF-1R is an extracellular part of the receptor that constitutes the binding region for the ligands IGF-1 and IGF-2, and determines the specificity of ligand binding. The β subunit is a transmembrane structure, located in the intracellular part that is responsible for signal transduction into the cell after receptor activation. It contains the catalytic subunit of tyrosine (Tyr) kinase, which can cross-catalyze the phosphorylation site on the corresponding β subunit for phosphorylation. Different regions of the β subunit can mediate distinct biological activities of IGF-1R, among which the ATP-binding site at K1003 and the tyrosine kinase active regions Y1131, Y1135 and Y1136 are particularly important for the corresponding biological effects of IGF-1R. Mutation of these sites can render IGF-1R unfunctional (Navarro and Baserga, 2001). The binding of ligands to the receptor induces an allosteric interaction between the α and β subunits of the molecule, which activates its tyrosine kinase activity and leads to the self-phosphorylation of multiple tyrosines in the intracellular region. Activation of IGF-1R can activate insulin receptor substrate (IRS)-1, IRS-2, PI3-kinase (PI3-K) and other substrates, and the activation of these substrates

initiates different cell signal transduction pathways, which respectively mediate the biological function of ligands (Yu and Rohan, 2000).

2.3 IGF-1R signaling pathway

When the ligand binds to and activates the receptor, a series of biological effects are triggered. Upon ligand binding to the α subunit of IGF-1R, the β subunit undergoes autophosphorylation, activating the phosphatidylinositol-3-kinase (PI3K)/serine-threonine protein kinase (Akt) pathway and the mitogen-activated protein kinase (MAPK) pathway. On the one hand, the PI3K/Akt pathway promotes the anchorage-independent growth (AIG) of tumor cells, which indicates the metastasis of malignant tumors; on the other hand, the MAPK pathway transmits signals to the nucleus, which is a target involved in cell proliferation. Genes are activated one after another for transcription and expression, which ultimately promotes cell proliferation, infiltration, and metastasis. IGF-1R can also directly bind to phosphatidyl-3,4,5-triphosphate after autophosphorylation of the (PIP3) kinase P85 subunit (Navarro and Baserga, 2001). In addition, in some cells, cell proliferation and apoptosis are also related to the phosphorylation of signal transducer and activator of transcription (STAT) activator caused by IGF-1R. IGF-1R signal transduction can also change cell adhesion and cause malignant growth of cells (Hartog et al., 2007). Therefore, IGF-1R is considered to be an effective target for the treatment of tumors.

2.4 IGF-1R expression in tumor cells

IGF-1R is not only related to normal cell proliferation, apoptosis, body growth and development, but also plays a key role in the formation and maintenance of the malignant phenotype of cells. Occurrence, development, invasion and metastasis are closely related. The proliferation of cells is proportional to the number of IGF-1R molecules on the cell membrane; decreased expression levels or loss of IGF-1R can lead to massive apoptosis of tumor cells; on the contrary, an increase in the expression of IGF-1R can inhibit cell apoptosis. Expression of IGF-1R has been detected in a variety of tumors. Waksanski et al. (Waksanski et al., 2001) showed that compared with normal tissues, the expression of IGF-1 and its receptors in endometrial cancer was significantly increased, and they also found that estrogen can promote the expression of IGF-1R in endometrial

cancer Ishikawas cells. Steller et al. detected the expression of IGF-1R in cervical cancer cell lines. 12 kinds of small cell lung cancer (SCLC), 14 kinds of non-small cell lung cancer (NSCLC) and 2 kinds of breast cancer cell lines were found to express IGF-1R. Tai et al. (Tai et al., 2003) reported that the IGF-1R enzyme participates in actin's entry into the intercellular junction through the signaling pathway of phosphatidylinositol 3-kinase (PI3K) to α -actinin, and promotes the spread of cancer cells, thereby affecting the growth of tumors. Activated and highly expressed IGF-1R can protect cells from apoptotic responses induced by various factors. The results of Nakamura et al. (Nakamura et al., 2004) confirmed that the expression of IGF-1R on the cell membrane can be used to predict the high risk of tumor recurrence in primary tumors, especially in the presence of liver metastases.

2.5 IGF-1R and oncogenes

IGF-1R plays a potential mitogenic and anti-apoptotic role in cell transformation and tumor growth. IGF-1R can regulate cell proliferation by acting on oncogenes and tumor suppressor genes, and then lead to tumor formation and growth. The post-IGF-1R signaling pathway and the expression of Ras, cMYC, FOS and other oncogenes have multiple junctions, which can promote each other and lead to tumorigenesis. p53 and others play a carcinogenic role by increasing the activity of the IGF-1R gene, and IGF-1R can prevent tumor cell apoptosis by downregulating the expression of Fas. Girnita et al. (Girnita et al., 2003) found that the p53 gene indirectly down-regulates the expression of IGF-1R through the mouse gene protein-2 (Mdm2), inhibits tumor cell growth and induces tumor cell apoptosis. Larsson et al. (Larsson et al., 2005) also pointed out that the dysregulation of the p53/Mdm2/IGF-1R pathway is beneficial to the growth of cancer cells, and blocking the expression of p53/Mdm2 can inhibit the signal transduction of IGF-1R.

2.6 IGF-1R inhibitor in cancer therapy

At present, IGF-1R inhibitors are mainly divided into the following types: benzimidazopyridine compounds, pyrrolopyrimidine compounds, pyrazolopyrimidine compounds, pyrrole-5-carbaldehyde compounds, imidazopyrazine compounds, natural sources of small molecule kinase inhibitors and diarylurea compounds.

The benzimidazole pyridine inhibitors BMS-536924 and BMS-554417 developed by Bristol-Myers-Squibb Company are among the compounds with better biological activity, and the current data show that they are still in the preclinical research stage. Wittman et al. (Wittman et al., 2005; Wittman et al., 2007) found that BMS-536924 can effectively inhibit the proliferation of prostate cancer, breast cancer, and lung cancer tumor cells *in vitro* and in clinical trials, and there is sufficient evidence to prove that IGF-1R signal transduction is involved in the above-mentioned proliferation process. Haluska et al. (Haluska et al., 2006) studied the anticancer activity of BMS-554417 *in vitro* and *in vivo*, and found that it can reduce the phosphorylation activity of Akt to block the PI3K/Akt pathway, and ultimately inhibit the activity of IGF-1R and insulin receptor IR. It has been shown to inhibit tumor proliferation *in vitro* and *in vivo*, and it can reduce the volume of xenografted tumor cells.

The pyrrolopyrimidine compounds NVP-AEW541 and NVP-ADW742 developed by Novartis are still in the stage of preclinical research. Mitsiades et al. (Mitsiades et al., 2004) conducted a pathobiological study on the anti-IGF-1R biological activity of NVP-ADW742, and found that NVP-ADW742 had a very good inhibitory effect on various tumor cells, especially against multiple bone marrow cancer cells with conventional therapy (IC₅₀ is 0.1-0.5 μmol/L). The study also found that the PI3K/Akt pathway is an important pathway for NVP-ADW742 to exert its efficacy. Warshamana-Greene et al. (Warshamana-Greene et al., 2005) discovered that the combination of NVP-ADW742 with etoposide and carboplatin can also enhance its sensitivity to small cell lung cancer. Scotland et al. (Scotland et al., 2005) showed that NVP-AEW541 could block MAPK, PI3K/Akt2 pathways and completely inhibit the biological activity of IGF-1R and downstream transduction signals. García-Echeverría et al. (Garcia-Echeverria et al., 2004) found through *in vivo* experiments that NVP-AEW541 can inhibit the signal transduction of IGF-1R in tumor xenografts, and at the same time reduce the growth of IGF-1R-driven fibrosarcoma (IC₅₀ of 0.086 μmol/L), The IC₅₀ of the inhibitory ability to insulin receptor was 2.3 μM, and it had good selectivity.

Abbott has synthesized and studied a series of pyrazolopyrimidine IGF-1R inhibitors. These compounds can inhibit the autophosphorylation of IGF-1R and show moderate drug properties towards IGF-1R. At the same time, these inhibitors have been tested *in vivo*.

The activity was shown to be at least 3 times stronger than the IR inhibitory effect (Mulvihill et al., 2007).

Merck synthesized and studied pyrrole-5-formaldehyde IGF-1R inhibitors (Bell et al., 2005), which are ATP-competitive inhibitors. Studies have found that a reversible covalent complex is formed between a part of the aldehyde groups and lysine residues to mediate and inhibit the signal transduction of IGF-1R (Mulvihill et al., 2008).

Ji et al. (Ji et al., 2007) and Mulvihill et al. (Mulvihill et al., 2009) of OSI Pharmaceuticals synthesized imidazolipizide compounds and studied their IGF-1R inhibitory activity. Among them, PQIP, AQIP and OSI-906 had better activity and effect on inhibiting IGF-1R. Studies have found that these compounds have stronger affinity for IGF-1R than pyrrolopyrimidines, and have stronger molecular solubility. PQIP inhibits the downstream signal transduction and biological activity of IGF-1R by blocking the Akt pathway. At the same time, the activity of other protein kinases is also very low, and it is currently in the late stage of preclinical research. AQIP also prevents cell proliferation and proliferation by blocking the Akt pathway, and then induces cell apoptosis. It not only has high selectivity for IGF-1R, but also its metabolites are very stable (Mulvihill et al., 2009). At the same time, OSI Pharmaceuticals discovered the compound OSI-906 (a novel small-molecule IGF-1R inhibitor) through mixed basic structural design and empirical discovery on the basis of the lead compound. OSI-906 effectively and selectively inhibits IGF-1R autophosphorylation by blocking MAPK and PI3K/Akt2 pathways. Mulvihill et al. (Mulvihill et al., 2009) found that OSI-906 had a very significant anti-tumor effect when taken orally once a day. Currently, OSI-906 is used in clinical phase III trials in locally advanced or metastatic adrenal cortical carcinoma, and in combination with paclitaxel in clinical phase I/II trials in recurrent epithelial ovarian cancer. At the same time, *in vivo* experiments found that OSI-906 could well inhibit the proliferation and spread of tumor cells.

Insmed reports that inM-18 (NDGA), a small molecule kinase inhibitor, is the first small molecule IGF-1R inhibitor to enter clinical phase I studies. It is a polyphenol substance extracted from the creosote bush *Larrea divaricata*, acting as a dual inhibitor of IGF-1R and HER2 receptors, and has been shown to have strong inhibitory effects on prostate cancer, pancreatic cancer, breast cancer and lung cancer (Mulvihill et al., 2009). NDGA

has entered a clinical phase II study (Hartog et al., 2007). Youngen et al. (Youngren et al., 2005) found that picropodophyllin (PPP) inhibited the IGF-1R transduction pathway by blocking the PI3K/Akt pathway, thus inhibiting the growth of tumor cells. The study also found that PPP had no inhibitory effect on IR, so it could avoid the occurrence of diabetes. Lu et al. (Lu et al., 2013) found that PPP is a specific IGF-1R tyrosine kinase inhibitor, which can effectively block the IGF-1R-mediated intracellular signal transduction pathway, thereby inhibiting the growth of tumor cells and promoting apoptosis, but not affecting the growth of normal cells (Youngren et al., 2005). PPP, developed by Biovitrum, is currently in preclinical studies.

Gable et al. (Gable et al., 2006) first discovered diaryl urea compound PQ401 in 2006, which structurally belongs to the group of urea small molecule compounds. *In vivo* experiments confirmed that PQ401 inhibited the growth of mammary adenocarcinoma cells by blocking IGF-1R signaling pathway. *In vitro*, PQ401 was used on human breast cancer MCF-7 cells (with an IC₅₀ between 10 mmol/L to 12 mmol/L, depending on the cell line).

3 Autophagy

Autophagy is a lysosome-dependent catabolic process in cells to meet the metabolic cellular needs and to allow for the renewal of organelles. This process usually relieves cellular damage and nutritional stress. In addition to the physiological role of autophagy in normal cells, autophagy also plays an important role in cancer and other pathological processes. In recent years, people have gradually realized that autophagy plays a complex role in the occurrence and development of cancer. On the one hand, autophagy plays a protective role by removing aged proteins and potentially harmful organelles. On the other hand, autophagy alleviates cell survival, which is harnessed by malignant cells, thus promoting the growth and proliferation of tumors (Dunlop and Tee, 2014). However, the complex role of inducing or inhibiting autophagy in cancer therapy depends on the type of cancer and its microenvironment.

Since its discovery, autophagy has been regarded as a cytoprotective mechanism capable of maintaining cellular homeostasis, facilitating cell survival, and playing a role in the self-digestion of proteins and organelles and the degradation of pathogens under conditions

of cellular nutrient deficiency (Glick et al., 2010). Studies have shown that dysregulation of autophagy is closely related to a variety of diseases including cancer, cardiovascular diseases and autoimmune diseases (Lavandero et al., 2015; White, 2015; Yang et al., 2015b). Autophagy can be divided into macroautophagy, microautophagy, and chaperone-mediated autophagy, depending on the content of the package and the mode of transport (**Figure 3**). The process of macroautophagy involves two stages, one is to encapsulate the cytoplasmic components to be degraded into double-membrane vesicles called autophagosomes, and the other is to transport them into lysosomes. Autophagosomes then fuse with lysosomes, thereby releasing the components to be degraded for lysosome degradation (Glick et al., 2010). Microautophagy is the phagocytosis and degradation of cytoplasmic components by lysosomes directly through the invagination of the lysosomal wall (Li et al., 2012). Chaperone-mediated autophagy is different from the former two in that it is selective (the former two are not selective), and the components to be degraded are degraded directly through the lysosomal wall through chaperone proteins (Bejarano and Cuervo, 2010).

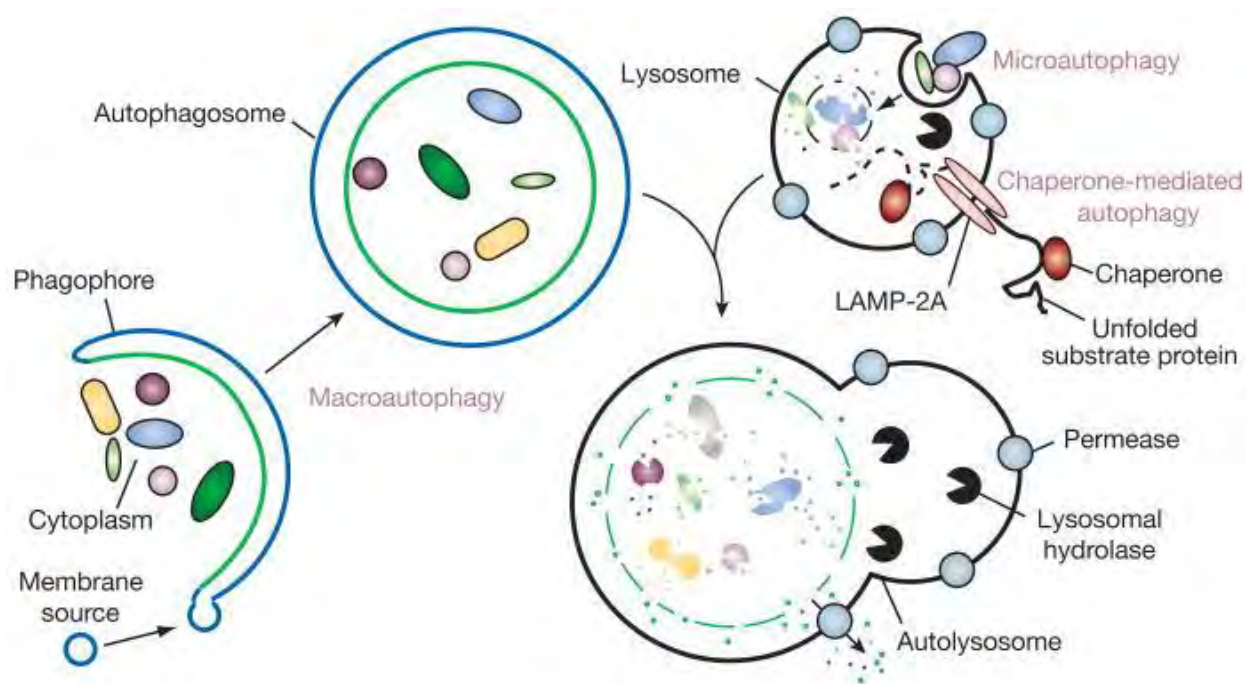


Figure 3. Different types of autophagy. (Mizushima et al., 2008) Microautophagy refers to the sequestration of cytosolic components directly by lysosomes through invaginations in their limiting membrane. The function of this process in higher eukaryotes is not known,

whereas microautophagy-like processes in fungi are involved in selective organelle degradation. In the case of macroautophagy, the cargoes are sequestered within a unique double-membrane cytosolic vesicle, an autophagosome. Sequestration can be either nonspecific, involving the engulfment of bulk cytoplasm, or selective, targeting specific cargoes such as organelles or invasive microbes. The autophagosome is formed by expansion of the phagophore, but the origin of the membrane is unknown. Fusion of the autophagosome with an endosome (not shown) or a lysosome provides hydrolases. Lysis of the autophagosome inner membrane and breakdown of the contents occurs in the autolysosome, and the resulting macromolecules are released back into the cytosol through membrane permeases. CMA involves direct translocation of unfolded substrate proteins across the lysosome membrane through the action of a cytosolic and lysosomal chaperone hsc70, and the integral membrane receptor LAMP-2A (lysosome-associated membrane protein type 2A).

3.1 The process of autophagy

Macroautophagy (hereafter referred to as autophagy) can be mediated by many factors. Nutrient deficiency is a recognized autophagy-inducing factor: cells under nutrient-deficient conditions can use the important proteins and amino acids provided by autophagy to survive (Onodera and Ohsumi, 2005). Hypoxia, infection and DNA damage are also thought to be activators of autophagy, however, whether these factors promote cell survival or induce cell death is controversial (Zhang et al., 2008).

Autophagy is regulated by proteins encoded by more than 30 autophagy-related genes (ATGs) (Feng et al., 2014). The autophagic process includes the formation of autophagosomes, the transport of autophagy substrates to lysosomes, and the degradation of lysosomes in three parts (Kuma and Mizushima, 2010), which are subdivided into initiation of autophagy, vesicle nucleation, vesicle extension, vesicle retraction, autophagosome-lysosome fusion and envelope degradation. The formation of the autophagosome membrane is the first step of autophagy, and the proteins and lipids that form the autophagosome membrane are continuously recruited under the action of the Beclin1-PI3K III complex (He and Levine, 2010), so Beclin1, an ATG member, is one of the key players in autophagy initiation. The resulting small membranous structures,

called pre-autophagosomes, are formed by a specialized region of the endoplasmic reticulum (Nascimbeni et al., 2017), and the Golgi apparatus, mitochondria and other cellular structures may also contribute to the formation of pre-autophagosomes (Bernard and Klionsky, 2013). Recent studies have shown that an elongating synaptotagmin also acts as a regulator of pre-autophagosome formation (Nascimbeni et al., 2017). After the formation of the pre-autophagosome, with the participation of ubiquitin-activating enzyme E1, ubiquitin-conjugating enzyme E2 and ubiquitin-ligase E3 analogs, the bilayer membrane of the pre-autophagosome begins to stretch, and finally encapsulates damaged proteins and organelles, forming autophagosomes (Otomo et al., 2013).

The exact mechanism of autophagosome formation in mammalian cells is unclear, but the LC3 protein family has been shown to play an important role in the formation of autophagosomes. When autophagy is induced, microtubule-associated protein light chain 3 (LC3B) is cleaved to form LC3B-I, which is then further processed to form LC3B-II (Glick et al., 2010). LC3B-II localizes to the inner and outer parts of the autophagosome membrane and is involved in the final membrane fusion step and localization of the autophagosome (Hansen and Johansen, 2011). Once formed, autophagosomes are transferred to, and fused with, lysosomes; autophagosomes can form anywhere in the cytoplasm, however, lysosomes are almost exclusively found in the perinuclear region. The movement of autophagosomes along microtubule trajectories in the cytoskeleton to lysosomes in the perinuclear region is controlled by a variety of proteins including RAB GTPases, membrane fusion proteins (SNAREs) and coat proteins (COPs) (Cardoso et al., 2009; Kimura et al., 2008; Molino et al., 2017; Nakamura and Yoshimori, 2017). Among them, RAB7 is involved in the whole process of autophagosome maturation, tracking and fusion (Guerra and Bucci, 2016). Finally, autophagosomes fuse with lysosomes and release the cellular components to be degraded into lysosomes for degradation.

3.2 Autophagy-related signaling pathways

3.2.1 Mammalian target of rapamycin (mTOR) signaling pathway

Among the various pathways regulating autophagy, the mTOR signaling pathway is crucial. Research has identified an important role for this pathway in regulating cell growth, protein synthesis, metabolism and cell death. mTOR is a kind of serine/threonine kinase

with a molecular weight of 300,000 that is mechanistically located downstream of the phosphoinositide 3-kinase/ protein kinase B (PI3K/Akt) pathway, which significantly regulates cell proliferation. It can bind to a variety of different proteins and form two different mTORs complexes: mTOR1 and mTOR2 (Yang et al., 2015a). When nutrients and growth factors are abundant, mTOR1 is activated and phosphorylates key autophagy-related proteins, resulting in the inhibition of autophagy. On the contrary, when mTOR1 is inhibited, which occurs upon deficiency of energy, amino acids and/or other nutrients, autophagy is induced. The role of mTOR2 in autophagy is unclear (Lu et al., 2015). mTOR1 is regulated by AMP-activated protein kinase (AMPK), and stimulation of AMPK by reducing cellular ATP levels or cellular stress leads to the inhibition of mTOR1. mTOR1 inhibition can prevent the site-specific inhibitory phosphorylation of unc-51-like autophagy-activating kinase 1 (ULK1), which then can freely interact with AMPK, resulting in the phosphorylation of ULK1 at the activation site and leading to autophagy induction. The fact that AMPK regulates both mTOR1 and ULK1 shows the key role of AMPK in autophagy initiation (Sridharan et al., 2011).

3.2.2 Rat sarcoma (RAS) signaling pathway

The RAS protein family consists of guanosine triphosphatase enzymes involved in the control of cell growth and survival. RAS signaling regulates autophagy through two major cellular pathways. Activation of RAS leads to increased stimulation of the PI3K/Akt pathway and upregulation of mTOR1, leading to inhibition of autophagy (Schmukler et al., 2014). Conversely, RAS activation can also be increased by reducing the mitogen-activated protein kinase/extracellular signal-regulated kinases (MAPK/ERK) pathway. It has been demonstrated that HT-29 colon cancer cells induce autophagy when the MAPK/ERK signaling pathway is stimulated (Ogier-Denis et al., 2000).

3.2.3 MAPK signaling pathway

MAPK is a family of serine-threonine kinases that are involved in the regulation of broad cellular responses to growth factor receptor signaling (Lim et al., 2019). Activation of stress-activated protein kinase signaling by MAPK results in the activation of key transcription factors, which in turn regulate the expression of anti-apoptotic genes such as

B-cell lymphoma-2 (Bcl-2). Studies have shown that the binding of Bcl-2 to Beclin-1 can lead to the inhibition of autophagy (Chiang et al., 2018).

3.2.4 FoxO signaling pathway

The FoxO family is a relatively well conserved group of transcription factors. The human FoxO family includes FoxO1 (FKHR), FoxO2 (FoxO6), FoxO3 (FKHRL1) and FoxO4 (AFX). When cells are under stress and starvation conditions, these transcription factors promote autophagy to alleviate this unfavorable condition. Studies have shown (van der Vos et al., 2012) that FoxO3 can enhance the activity of glutamine synthase, and glutamine synthase can inhibit the localization of mTORC1 on lysosomes, so FoxOs may inhibit the mTOR signaling pathway, thereby inducing autophagy. In addition to inducing autophagy, FoxOs also interacts with other related autophagy pathways, thereby regulating the occurrence of autophagy (Webb and Brunet, 2014).

3.2.5 p53 signaling pathway

The p53 gene is a common mutation site in human tumors, and the protein it encodes has four major functional regions: 1. N-terminal transcriptional activation region, which can bind to p53 negative regulators; 2. Central DNA core region; 3. tetramerization domain; 4. C-terminal non-specific DNA binding region (Dai and Gu, 2010). p53 has a dual regulatory effect on autophagy. Under normal circumstances, the level of p53 is regulated by the Beclin1 target sites USP10 and USP13 to deubiquitinate, thereby activating or inhibiting autophagy. Studies have shown (Liu et al., 2011) that the activities of USP10, USP13, Beclin1 and Vps34 are closely related to the expression of p53, and down-regulating its activity can inhibit the expression of p53. When cells are under metabolic stress conditions, p53 can phosphorylate AMPK (Thr127), which in turn inhibits mTOR activity, thereby activating autophagy.

3.3 Measurement of autophagy

The detection and quantitative analysis of autophagy in eukaryotic cells plays an important role in studying the effect of autophagy on eukaryotic growth and development and the relationship between autophagy and disease. At present, there are three main methods for the measurement of autophagosomes: electron microscopy, Western blotting and LC3

immunofluorescence microscopy. Autophagosomes are ultrastructurally defined as double-membrane structures that contain undigested cytoplasm or small organelles (e.g., mitochondria, part of the endoplasmic reticulum) and are not fused to lysosomes. Using electron microscopy to observe the structure of autophagosomes can qualitatively or quantitatively measure the volume of autophagosomes from early to late stages (Yla-Anttila et al., 2009). Autophagy is a dynamic process, and the measurement of the number of autophagosomes can only describe a certain static moment in the process of autophagy, but cannot reflect its overall dynamic activity. Based on this defect, the concept of autophagic flux was introduced to describe autophagic activity, which refers to the entire process of substrates being packaged by autophagosomes and transported to lysosomes for degradation and reuse. The changes in concentration of microtubule-associated protein 1 light chain 3 (LC3) under different conditions are described. In the process of autophagy, LC3 first excises the C-terminal amino acid and converts it into LC3-I scattered in the cytoplasm. LC3-I then combines with phosphatidyl ethanolamine (PE) to form LC3-II that exists stably on the inner and outer membranes of autophagy. LC3-II thus plays an important regulatory role in the entire process of autophagy (Nakatogawa et al., 2009). LC3 is the homolog of the yeast Atg8 gene in mammalian cells, which is located on the surface of pre-autophagic vacuoles and autophagic vacuoles. During the formation of mammalian autophagic vacuoles, LC3 is coordinated by Atg3, Atg5, Atg7, Atg10, Atg12. The composition of ubiquitin-like proteins plays an important role in the processing and modification process, and its expression and the degree of conversion of LC3-I to LC3-II have become important markers of autophagy levels (Wild et al., 2014). Therefore, green fluorescent protein-LC3 (GFP-LC3) can be used as a specific marker for the detection of autophagosomes in cells. However, the increased level of LC3 in cells may be caused by the increase of autophagy activity, or it may be caused by the blocking of autophagosome in the later degradation process. It cannot accurately reflect the autophagic activity of cells. In experiments, it is thus usually necessary to measure the difference in LC3 content between basal autophagy and autophagy-blocked conditions to accurately reflect the dynamic activity of autophagy. The widely used autophagy inhibitors are Chloroquine, Bafilomycin A1 or lysosomal proteases, etc., which lead to the accumulation of autophagosomes by blocking the fusion of autophagosomes and

lysosomes (Kimmelman, 2011). Using western blotting and immunofluorescence microscopy to detect the content of LC3 at the basal level of target cells and normal cells can reflect the autophagy activity of cells, and the measurement of autophagy in the induced state can reflect the autophagy potential of cells. In recent years, in addition to LC3, p62 protein detection has also been used in the evaluation of autophagy levels. p62/SQSTM1 is a multifunctional protein that participates in various signaling pathways (including apoptosis and autophagy), and it contains a domain that binds to LC3 protein. If autophagy is inhibited, SQSTM1 levels rise. The level of p62/SQSTM1 is inversely correlated with the basal autophagy level, and the activity of autophagy can be reflected by continuous measurement of p62 using cellular immunohistochemistry, staining, western blotting and GFP labeling methods (Pircs et al., 2012).

3.4 Autophagy and tumorigenesis

Studies have shown that autophagy plays a "double-edged sword" role in the occurrence and development of tumors, that is, autophagy can both inhibit early tumorigenesis and promote tumor development, and its function depends on the genetic background, developmental stage, and cancer type (Dikic and Elazar, 2018). As a "quality controller" of normal cells, autophagy can limit abnormal mutations caused by metabolic stress damage and genomic instability, thereby inhibiting carcinogenesis. Studies by Liang XH et al. found that the loss of function of ATG proteins, such as Beclin-1, is associated with increased tumor risk (Liang et al., 1999; Qu et al., 2003); studies by Takamura A et al. found that inhibition of ATG protein expression in a mouse model can cause the formation of multiple benign liver tumors (Takamura et al., 2011). However, once the primary tumor has formed, the role of autophagy in tumor cells changes. A growing number of studies have shown that autophagy can be used by tumor cells to adapt to various stressors such as hypoxia or nutrient deprivation, providing support for the metabolism necessary for tumor survival and rapid proliferation, and promoting the growth of most advanced tumors (Guo et al., 2013; Kenific and Debnath, 2015). Studies have also found that autophagy levels in various types of advanced tumors such as pancreatic cancer or activated Ras tumors are significantly higher than the basal autophagy activity in normal tissues (Guo et al., 2011; Yang et al., 2011), thereby helping tumor cells to adapt to treatment-induced stress. This causes such tumors to become resistant to treatment, which is also one of

the main clinical challenges of current tumor treatment. In addition, Vera-Ramirez L et al. found that autophagy is closely related to the survival of dormant cancer cells and the recurrence of metastatic tumors (Vera-Ramirez et al., 2018). Autophagy plays multiple roles in tumor initiation, growth and maintenance.

3.5 Autophagy and tumor therapy

In recent years, more and more studies have shown that autophagy is induced by a variety of tumor treatment methods, including chemotherapy, radiotherapy, and targeted therapy (Chiu et al., 2016; Choi et al., 2012; Michaud et al., 2011; Parodi et al., 2015; Qin et al., 2016; Rosenfeldt et al., 2013). Autophagy stimulated by tumor therapy has a context-dependent effect on tumor cells as it can induce cytotoxicity and cytoprotection. On the one hand, autophagy activation can sensitize tumor cells to chemotherapy and radiotherapy: autophagy induced by chemotherapy in dying tumor cells can facilitate the recruitment of immune effector cells into the tumor through the active release of ATP (Michaud et al., 2011), thereby triggering a tumor-specific immune response to induce tumor cell death. Another study suggested that the inhibition of mTORC1 by calorie restriction, an effective autophagy inducer, also enhances tumor immune surveillance, but this effect was only seen in tumors with high autophagy activity (Pietrocola et al., 2016). Chiu HW et al. found that the autophagy inducer YCW1 could induce ER stress to increase autophagy and enhance the radiosensitivity of breast cancer cells (Chiu et al., 2016), suggesting that radiotherapy-induced autophagy may also have cytotoxic effects. On the other hand, most studies have shown that autophagy promotes chemoresistance. In order to relieve chemotherapy-induced stress, tumor cells can activate autophagy to resist stress and produce cytoprotective effects, resulting in chemoresistance (Choi et al., 2012; Qin et al., 2016). Choi J et al. found that autophagy can promote the resistance to 5-FU treatment in colon cancer (Choi et al., 2012), and autophagy also plays a role in promoting the resistance of ovarian cancer during cisplatin treatment (Qin et al., 2016). In recent years, more and more studies have found that autophagy also plays an important role in promoting the resistance of many targeted therapy drugs. The occurrence of resistance to gefitinib/erlotinib in human lung cancer cells (Han et al., 2011; Jiang et al., 2018), the emergence of imatinib resistance during leukemia treatment (Shingu et al., 2009), the use of temozolomide in the treatment of astrocytoma (Goncalves et al., 2019) and trastuzumab

in the treatment of breast cancer (Cufi et al., 2013) and other processes, have been linked to autophagy playing a role in promoting drug resistance. A study also found that the autophagy inhibitor CQ not only enhanced the anti-tumor effect of radiotherapy in glioblastoma (Huang et al., 2017), but also enhanced the radiosensitivity of bladder cancer cell lines (Wang et al., 2018a), suggesting that radiotherapy induces autophagy in tumor cells.

4 Immunogenic cell death

Over the past decade, scientists have studied the main mechanisms of immunogenic cell death (ICD), a specific mode of cell death that develops in response to antigenic stimulation of dead cells, to achieve a therapeutic effect similar to the injection of an "anti-tumor vaccine". The main mechanism of ICD is that certain characteristic protein molecules on the surface of apoptotic cells can be up-regulated after tumor cells undergo apoptosis stimulated by chemotherapy drugs, which induce dendritic cells to mature and activate tumor-specific T lymphocyte toxicity to kill tumor cells (Galluzzi et al., 2018). It is now well established that radiation therapy, hyperthermia, and certain chemotherapeutic agents induce tumor cell death by means of ICD (Zhou et al., 2019). ICD can induce dead tumor cells to release damage-associated molecular patterns (DAMPs), leading to the activation of tumor-specific immune responses, thereby activating anti-tumor immunity or directly killing tumor cells, exerting long-term efficacy of anti-cancer drugs (Zitvogel et al., 2011). DAMPs of tumor cells include the exposure of calreticulin (CALR) on the surface of pre-apoptotic cells, the secretion of adenosine triphosphate (ATP), and the release of high mobility group box protein B1 (HMGB1) (Colangelo et al., 2016; Martins et al., 2014; Yamazaki et al., 2014). Among them, CALR exposure will release a series of molecular signals, which can not only promote the phagocytosis of tumor cells by dendritic cells, but also induce tumor antigen presentation and tumor-specific T lymphocyte toxicity (Chao et al., 2010). In addition, autophagy of tumor cells needs to be achieved by releasing ATP, to achieve the purpose of aggregation, degradation and destruction of organelles (Michaud et al., 2014). HMGB1 is a non-histone chromatin-binding protein. It has been reported in the literature that its binding to related receptors expressed on dendritic cells is crucial for activating dendritic cells and promoting antigen presentation by dendritic cells

to T cells (Apetoh et al., 2007) (**Figure 4**). Therefore, these features can accurately predict whether chemotherapeutic drugs have the effect of inducing ICD in tumor cells, which provides an important basis for clinical judgment of ICD inducers. The treatment modalities also provide a new way for the clinical treatment of cancer.

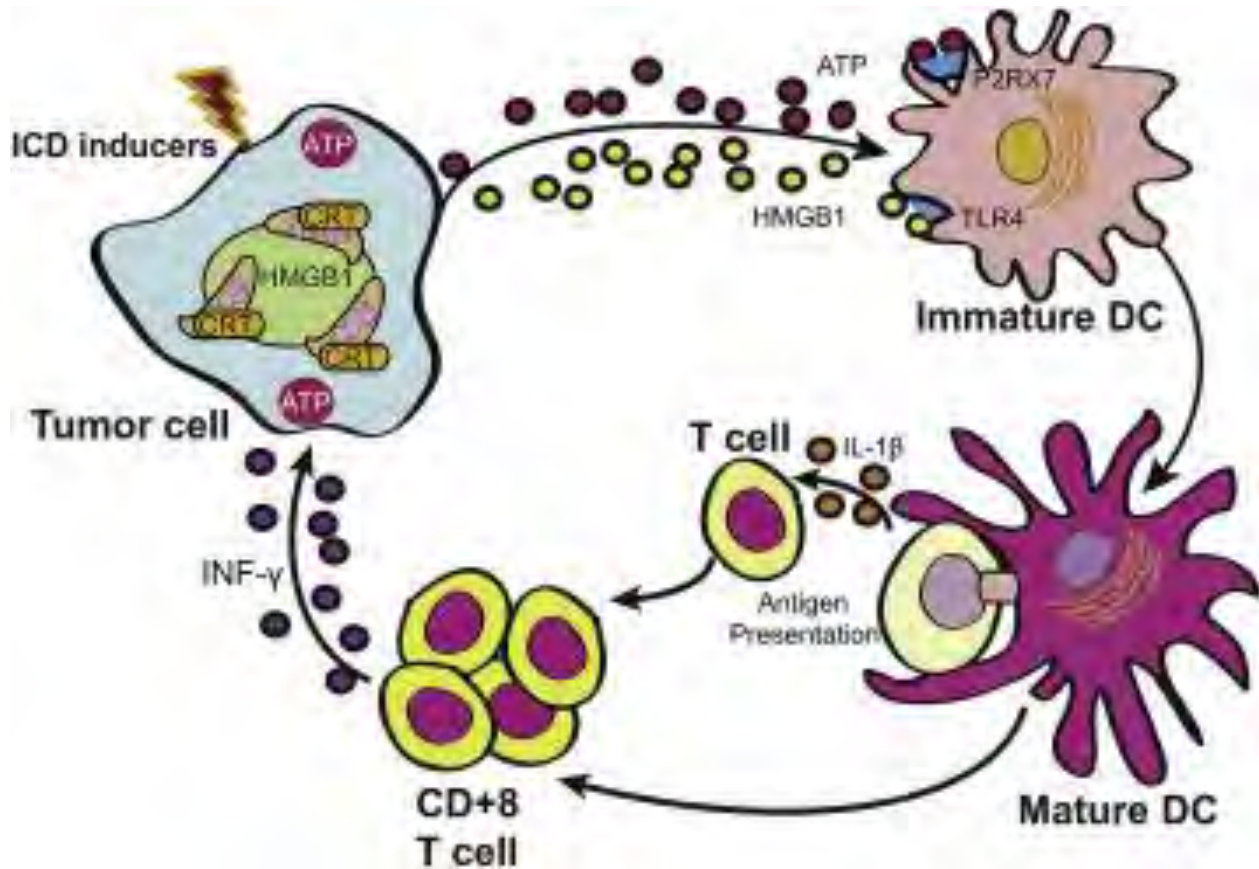


Figure 4. Molecular mechanisms of immunogenic cell death (ICD) in anticancer chemotherapy. (Wang et al., 2018b) ICD inducers stimulate tumor cells to undergo apoptosis; apoptotic cells present certain danger-associated molecular patterns (DAMPs), including exposure of calreticulin (CALR), secretion of adenosine triphosphate (ATP), and release of high mobility group box 1 (HMGB1). These DAMPs lead to the recruitment of dendritic cells (DCs) to the tumor bed, where they engulf tumor cells. Mature DCs then present antigens to tumor-specific cytotoxic T lymphocytes (CTLs), eventually leading to killing of the tumor cells by CTLs.

4.1 ICD-related molecules

4.1.1 ATP

ATP is a direct energy source for cells, but during the ICD process, dying tumor cells release ATP, where it acts as an endogenous danger signal. Several studies have shown that autophagy is essential to the release of high levels of ATP from cells undergoing ICD, but the exact molecular mechanism by which autophagy promotes ATP secretion has not been clarified (Gebremeskel and Johnston, 2015). The release of ATP involves a series of processes such as activation of autophagy, apoptosis, and lysosomal exocytosis before cell death (Martins et al., 2014). Extracellular ATP released by tumor cells acts as a "find me" signal with dual roles of recruiting and activating APCs and inflammasome pathways. The ATP released to the outside of the cell binds to P2X7 and P2Y2 purinergic receptors on APCs (especially dendritic cells, DCs), stimulating their phenotypic maturation and mediating strong chemotaxis (Serrano-Del Valle et al., 2020). Extracellular ATP also activates the caspase-1-dependent NLRP3 complex inflammasome, triggering the secretion of interleukin-1 β (IL-1 β) (Serrano-Del Valle et al., 2020). The generated IL-1 β can prompt $\gamma\delta$ T cells to produce IL-17, which acts on cytotoxic T lymphocytes (CTLs), thereby producing an IFN γ -mediated anti-tumor immune response (Ma et al., 2011). In addition, extracellular ATP also stimulates DCs and macrophages to release pro-inflammatory cytokines, such as tumor necrosis factor- α (TNF- α), IL-1 β and IL-18, to produce tumor-killing activities (Lin et al., 2017).

4.1.2 Calreticulin

CALR is a highly conserved multifunctional calcium-binding protein located within the endoplasmic reticulum (ER), whose main functions are protein chaperones and maintenance of Ca²⁺ homeostasis. CALR is exposed before apoptotic execution on the cell membrane surface, that is, during the process of ICD, CALR translocates from the ER lumen to the cell membrane surface. CALR exposure is one of the key factors for ICD to drive anti-cancer immunity (Gebremeskel and Johnston, 2015; Tanaka et al., 2016). As a powerful "eat me" signal, CALR exposed on the cell membrane surface (ecto-CALR) can enhance the immunogenic recognition and phagocytosis of dead cancer cells by APCs (Sethuraman et al., 2020). Endoplasmic reticulum (ER)-stress is necessary to induce the translocation of ICD-related CALR to the cell membrane surface (Gebremeskel and Johnston, 2015), but the molecular mechanism involves protein kinase R-like ER kinase (PERK)-mediated ER-stress that can phosphorylate eukaryotic translation initiation factor

2 α (eIF2 α) (Wang et al., 2018c), leading to subsequent signaling events, including caspase-8-dependent proteolysis of the ER protein BAP31, activation of the pro-apoptotic protein BAX, transport of CALR from the ER to the Golgi apparatus, and exocytosis of CALR-containing vesicles, ultimately leading to SNARE-mediated relocalization of CALR on the cell surface (Panaretakis et al., 2009; Wang et al., 2018c). CALR forms a stable complex with disulfide isomerase (ERp57) and co-translocates to the cell membrane. Loss of ERp57 can lead to the loss of surface CALR and reduce the phagocytosis of macrophages (Liu et al., 2019). ecto-CALR can bind to multiple receptors on APCs, including CD91, thrombospondin, complement component 1, q subcomponent (C1q) receptors and glycan-binding lectin (Montico et al., 2018), among which ecto-CALR is mainly recognized, phagocytosed and bound by CD91-expressing cells, which can trigger a series of immune events to promote the recruitment of antigen-presenting cells (such as DCs), antigen presentation, and pro-inflammatory cytokines (such as TNF- α and IL-6) release and type 17 helper T cells (Th17) activation (Pawaria and Binder, 2011). Ecto-CALR can induce a series of immune responses, its effects are antagonized or inhibited by small interfering RNA (siRNA)-mediated down-regulation of PERK, which inhibits the phosphorylation of eIF2 α and ER stress, and thereby blocks anthracycline-induced CALR exposure. In addition, the antiphagocytic CD47 as a "don't eat me signal" also antagonizes the effect of ecto-CALR. When there is a high level of CALR on the surface of tumor cells, the expression of CD47 will also increase accordingly. Therefore, blocking or antagonizing CD47 while increasing the plasma membrane exposure of CALR is a strategy to induce ICD, thereby enhancing antitumor therapy.

4.1.3 HMGB1

HMGB1 is a highly conserved and widely distributed nuclear protein in mammalian cells, which plays roles in gene transcription regulation, nucleosome stabilization, and DNA repair. In addition, HMGB1 plays a role as an extracellular signaling molecule in the process of inflammatory cell differentiation, migration and tumor metastasis (Fachri et al., 2021); HMGB1 also promotes DCs maturation, migration, TAA presentation to T cells and production of pro-inflammatory cytokines (Ruan et al., 2020). HMGB1 secreted by tumor cells in the late stage of death binds to a variety of PRRs, including Toll-like receptor 4 (TLR4) and the receptor of advanced glycation end product (RAGE), thereby activating

the receptor of advanced glycation end product (RAGE) in DCs. Mitogen-activated protein kinase (MAPK, p38 and ERK1/2) and nuclear factor kappa B (NF- κ B) (Ruan et al., 2020), promote immune cells to release cytokines such as IL-6 and IL-10, which are then involved in an inflammatory response. HMGB1 can activate the major response genes of myeloid differentiation (MyD88)-dependent signal transduction pathway, inhibit the phagosome-lysosome fusion, thereby promoting the processing and presentation of tumor antigens (Garg et al., 2015; Yamazaki et al., 2014). HMGB1 can also inhibit the activity of immunosuppressive Treg cells (Garg et al., 2015). Studies have shown that in chronic HBV infection, HMGB1 can induce autophagy in peripheral Treg cells through the RAGE-ERK and mTOR pathways (Cheng et al., 2017). HMGB1 was significantly up-regulated in the tumor microenvironment (TME) and positively correlated with patient survival. Tumor cells lacking HMGB1 exhibited impaired ability to induce ICD and antitumor immune responses (Ashrafizadeh et al., 2020).

4.1.4 IFN I

As a group of broad-spectrum antiviral cytokines, IFN I have antiviral infection and immune regulation effects. IFN I is a key family of cytokines that activate effector T lymphocytes and NK cells in the initiation phase of the immune response, can affect the progress of innate and adaptive immune responses, and are essential for microbial defense responses (Ivashkiv and Donlin, 2014; Minute et al., 2020; Serrano-Del Valle et al., 2020). IFN I can induce tumor cell apoptosis and anti-angiogenesis through signal transduction after binding with type I interferon receptor (IFNAR), and can also directly affect the cells of the immune system (Schirmmayer et al., 2019). IFN I directly inhibit the proliferation of tumor and virus-infected cells, and increase the expression of MHC-I class, thereby enhancing antigen recognition, and can also affect the differentiation, maturation and migration of DCs (Hervas-Stubbs et al., 2011). Activation of IFN I responses in tumor cells has become one of the hallmarks of ICD, and the production of IFN I triggers autocrine and paracrine circuits in tumor cells by binding to IFN α and IFN β receptors on tumor cells, resulting in cxc-chemokine ligand 10 (CXCL10) release, play an immunostimulatory effect (Galluzzi et al., 2017; Sistigu et al., 2014). The release of IFN I involves a variety of mechanisms. During chemotherapy, tumor cells will respond to endogenous IFN I due to the release of RNA during cell death (De Beck et al., 2018). DNA-damaging agents also

induce IFN I production in the cytoplasm through dsDNA (De Beck et al., 2018). Yang et al (Yang et al., 2020) found that the sequential combination of IFN β and cisplatin could induce the phosphorylation of eIF2 α more effectively than single treatment, and participate in ER stress, which is crucial for CALR translocation; secondly, upregulation of interferon regulatory factor 1 (IRF1) contributes to the phosphorylation of eIF2 α by IFN β and IFN β -cisplatin. In addition, radiation-induced IFN I enhanced the cross-presentation of DCs (Sato et al., 2020).

4.1.5 HSP

As heat stress proteins, the main function of the heat-shock protein (HSP) family is to assist in protein folding. HSP70 and HSP90 have functions such as stimulating tumor antigen uptake and DCs maturation. High expression of HSP is an important signal for tumor cells to develop ICD. CTLs can recognize HSP-antigen peptides during virus infection and tumor formation. HSP70 and HSP90 can bind to antigenic peptides and undergo receptor-mediated HSP endocytosis. These peptides are shuttled into the antigen-processing pathway of APCs and expressed on class I molecules (Hickman-Miller and Hildebrand, 2004). HSP70 and HSP90 carry tumor antigen peptides and are exposed to the cell surface in the early stage of ICD, and are passively released into the tumor microenvironment in the late stage, and mediate the interaction between cancer cells and immune cells by binding TLRs on DCs and NKG2A on NK cells (Montico et al., 2018). The presentation of HSP-antigen peptides to CTLs can lead to the activation of CTLs, and the presentation to NK cells leads to the loss of inhibitory effect, and the activation of both CTLs and NK cells plays a key tumor-killing role (Hickman-Miller and Hildebrand, 2004).

4.2 ICD inducers

At present, ICD inducers are divided into type I ICD inducers and type II ICD inducers. The type I ICD inducers and type II ICD inducers that have been reported in clinical and preclinical studies are shown in **Table 1**. Type I ICD inducers induce non-ER-targeted apoptosis in tumor cells, causing mild ER stress and release of ICD-related immunogenic molecules; type II ICD inducers selectively target the ER, via ROS-dependent ER stress release danger and apoptosis signals (Rufo et al., 2017). Most clinical antineoplastic drugs, such as anthracyclines, oxaliplatin, bortezomib, cyclophosphamide, and radiation therapy,

belong to type I ICD inducers. Hypericin photodynamic therapy, oncolytic virus therapy, etc. belong to type II ICD inducers. Type I and type II ICD inducers act at different stages of apoptosis, respectively. In the early stage of apoptosis, compared with type I ICD inducers, type II ICD inducers can induce a more severe ER stress response and high levels of ROS, and release more DAMPs, which contribute to the anti-tumor immune response (Pol et al., 2015). However, this long-term persistent response promotes an autoregulatory inflammatory cycle as well as tumor stroma degradation, leading to tumor cell metastasis (Radogna and Diederich, 2018).

Table 1. Inducers of type I and type II Immunogenic cell death and their mechanisms.

ICD inducers		DAMPs	Target of inducing cell death	Mechanism	Reference
Type I ICD inducers	Mitoxantrone and Anthracyclines	ecto-CALR, ERp57, ATP, HSP70, HMGB1	Nucleus (DNA or DNA replication-associated proteins)	<ul style="list-style-type: none"> • Inserts into DNA and inhibits DNA topoisomerase II, exerts cell growth inhibition and cytotoxicity; • Apoptotic cells release ATP as a “find me” signal that recruits monocytes and macrophages to the site of apoptosis; • ATP released by dying tumor cells stimulates the purinergic receptor P2X7 on DCs, causing intracellular K⁺ efflux and activation of the NALP3-ASC inflammasome, driving caspase-1-mediated maturation of pro-IL-1β and secretion of IL-1β; • Anthracycline-induced IL-17 production in $\gamma\delta$T lymphocytes ($\gamma\delta$T17 cells). 	(Elliott et al., 2009; Fucikova et al., 2011; Ghiringhelli et al., 2009; Obeid et al., 2007; Radogna and Diederich, 2018; Tewey et al., 1984)
	Oxaliplatin	ecto-CALR, ERp57, ATP, HSP70, HMGB1	Nucleus (DNA or DNA replication-associated proteins)	<ul style="list-style-type: none"> • Interaction with DNA to form DNA adducts, DNA adducts inhibit transcription and inhibit mismatch repair mechanisms; • Induces DC maturation. 	(Raymond et al., 1998)
	Cyclophosphamide	ecto-CALR, HMGB1	Nucleus (DNA)	<ul style="list-style-type: none"> • Stimulates increased expression of chemokines and their ligands; • Stimulates immune cells to produce cytokines and promotes the conversion of Th2 to Th1. 	(Schiavoni et al., 2011)
	Shikonin	ecto-CALR, HSP70, ectoGRP78	Cytoplasm (tumor-specific pyruvate kinase M2 protein, 20S subunit of the proteasome)	<ul style="list-style-type: none"> • Promotes the phenotypic and functional maturation of DCs, thereby stimulating T cells; • Promotes the differentiation of T cells into Th17 cells; • Restores NK cell cytotoxicity; • Improves CTL activity; • Downregulation of NF-κB signaling reduces tumor-promoting cytokine production. 	(Chen et al., 2012; Chen et al., 2011; Lu et al., 2011)
	7A7 (EGFR-specific antibody)	ecto-CALR, ERp57, HSP70, HSP90	Cell surface (EGFR)	<ul style="list-style-type: none"> • Inhibits tumor cell growth and induces its G0/G1 phase synchronization; • Induces tumor cell apoptosis at high concentrations; • Causes phenotypic maturation of DCs; • Increased tumor infiltration by CD4⁺ T cells, CD8⁺ T cells and DCs. 	(Garrido et al., 2007; Garrido et al., 2011)
	Bortezomib	HSP90	Cytoplasmic (26S proteasome or endoplasmic reticulum-related degradation mechanisms, cancer suppressor 2A)	<ul style="list-style-type: none"> • Generates NK cells and CD8⁺ T cells to inhibit tumor growth; • Promotes antigen cross-presentation between tumor cells and DCs, and tumor antigen-loaded DCs induce IFNγ production in T cells. 	(Chang et al., 2012; Davies et al., 2007; Spisek et al., 2007; Tseng et al., 2012)

	Cardiac glycosides	ecto-CALR, ATP, HMGB1	Cell surface (Na ⁺ , K ⁺ -ATPase)	<ul style="list-style-type: none"> Involved in the SRC kinase-EGFR-MAPK pathway, resulting in tumor cell growth arrest; Inhibits DNA topoisomerase and glycolysis, and promotes apoptosis; ICD can only be triggered in the body when used in combination with other chemotherapy drugs such as mitomycin C or cisplatin. 	(Menger et al., 2012; Prassas and Diamandis, 2008)
	Ultraviolet radiation (UVC)	ecto-CALR, ERp57, ATP, HSP70, HMGB1	Nucleus (DNA or DNA replication-associated proteins)	<ul style="list-style-type: none"> CD8⁺ T cell and NK cell-mediated tumor growth inhibition; UVC-treated tumor cells stimulate DC phagocytosis and maturation, and stimulate IFNγ-producing CD8⁺ T cells; DC antigen processing and proinflammatory cytokine production stimulated by UVC-treated tumor cells. 	(Brusa et al., 2009; Dudek et al., 2013)
	Radiation therapy	ecto-CALR, ERp57, ATP, HSP70, HMGB1	Nucleus (DNA or DNA replication-associated proteins)	<ul style="list-style-type: none"> Induce DNA damage and induce tumor cell apoptosis; DAMPs release, stimulate DCs, and local high-dose radiotherapy increases the number of tumor-infiltrating DCs; Radiation therapy induces ICD, activates DCs, increases infiltration of CD4⁺ and CD8⁺ T cells in tumors, and inhibits Treg. 	(Huang et al., 2007; Selzer and Hebar, 2012)
	High Hydrostatic Pressure (HHP)	ecto-CALR, ATP, HMGB1, HSP70, HSP90	Cellular protein	<ul style="list-style-type: none"> Stimulates DC phagocytosis; Expresses high levels of costimulatory molecules that stimulate the production of large numbers of tumor-specific T lymphocytes. 	(Fucikova et al., 2014)
Type I ICD inducers	Hypericin Photodynamic Therapy (Hyp-PDT)	ecto-CALR, ATP, ectoHSP70, HSP70, HSP90	Endoplasmic reticulum	<ul style="list-style-type: none"> Hypericin is mainly localized to the endoplasmic reticulum, and after irradiation causes Phox-ER stress and activation of different UPR signaling pathways, ultimately leading to Bax/BAK-based mitochondrial apoptosis; Inhibition of pro-tumor cytokine signaling NF-κB activation; Inhibition of tumor cell-derived tumor-promoting cytokines such as TNF, IL-6 and GM-CSF; Inhibit secretion of cancer-derived MMP9 that promotes tumor metastasis. 	(Buytaert et al., 2006; Du et al., 2007; Garg et al., 2012a, b; Garg et al., 2010)
	Coxsackie virus B3	ecto-CALR, ATP, HMGB1	Endoplasmic reticulum	<ul style="list-style-type: none"> Induces ER stress; Increases the number of blood vessels in the tumor; Increases the number of CD8⁺ T lymphocytes. 	(Liu et al., 2012; Miyamoto et al., 2012)
	Pt ^{II} N-heterocyclic carbene complex	ecto-CALR, ATP, HMGB1	Endoplasmic reticulum	<ul style="list-style-type: none"> Induction of ER stress response through PERK activation. 	(Sukkurwala et al., 2014)

4.2.1 Chemotherapy drugs

4.2.1.1 Anthracyclines

Anthracyclines including anthracenediones (mitoxantrone, etc.) and anthrapyrazoles (doxorubicin, epirubicin, daunorubicin, etc.) have been used in the treatment of pediatric sarcoma, leukemia, and the like. Anthracyclines mainly exert cytotoxic effects by intercalating DNA double-stranded bases and inhibiting DNA topoisomerase II. In 2005, doxorubicin was reported as the first inducer of ICD (Casares et al., 2005). Doxorubicin-induced cell death exhibiting characteristics of ICD, such as the release of DAMPs, including pre-apoptotic CALR translocation, ATP secretion in the early stage of apoptosis, HSP70 release in the middle and late stages of apoptosis, and HMGB1 release in the late stage of apoptosis.

Anthracycline-induced ER stress responses are dependent on CALR translocation (Garg et al., 2012a; Panaretakis et al., 2009) and ATP release (Martins et al., 2009). ATP released by dying tumor cells binds to the purinoceptor P2X7 on DCs, causing intracellular K⁺ efflux and inflammasome NALP3 activation, driving caspase1-mediated IL-1 secretion. Anthracycline-treated tumor cells produce type I IFN through autocrine and paracrine pathways, inducing cell death (Michaud et al., 2011). Furthermore, anthracyclines induce the accumulation of IL-17-producing $\gamma\delta$ T cells at the tumor site, prior to the accumulation of cytotoxic T cells at the tumor site (Ma et al., 2011).

Studies have shown that doxorubicin-liposome-microvesicle complexes can enhance doxorubicin-induced ICD. This complex induces increased tumor cell apoptosis, increased CALR exposure and DAMPs release, while further promoting DC maturation (Huang et al., 2018). In addition, studies have shown that the combination of doxorubicin and DC vaccine can enhance the anti-tumor immune response. Mice treated with DC vaccine and doxorubicin had increased numbers of CD8⁺ T lymphocytes in metastases, increased serum IFN γ levels, and inhibited tumor metastatic growth (Kawano et al., 2016).

Anthracyclines are a class of effective ICD inducers, but their clinical application is limited due to their large side effects. Therefore, it is currently necessary to find a therapeutic scheme that can induce ICD and has few side effects.

4.2.1.2 Cyclophosphamide

Cyclophosphamide is one of the most widely used alkylating agents for the treatment of hematological and solid malignancies. Cyclophosphamide possesses significant immunomodulatory activities, most notably its ability to inhibit Treg, thereby eliminating immunosuppression in the tumor microenvironment (Ahlmann and Hempel, 2016). Cyclophosphamide can also induce features that exhibit ICD, including changes in cell surface markers and release of soluble DAMPs (Pol et al., 2015), leading to activation of tumor-specific immune responses.

4.2.1.3 Bortezomib

The proteasome inhibitor bortezomib was approved by the FDA in 2003 and is recommended as a first-line treatment for patients with multiple myeloma. Co-incubation of bortezomib-treated tumor cells with DCs results in antigen-loaded DCs that can induce T cells to produce IFN γ , but addition of HSP90 inhibitors to bortezomib-treated tumor cells reduces the number of IFN γ -producing T cells (Nawrocki et al., 2005). However, the mechanism of action of Bortezomib as an inducer of ICD remains to be further studied.

4.2.1.4 Platinum-based chemotherapy drugs

Platinum-based chemotherapy drugs are crucial in the clinical treatment of tumors. Oxaliplatin directly induces ICD in tumor cells, whereas cisplatin requires an additional inducer to activate its immunogenicity (Martins et al., 2011). Both platinum drugs trigger CALR translocation and release of HSP70, ATP, and HMGB1, but oxaliplatin is an established ICD-inducing drug. Oxaliplatin prevents DNA synthesis by targeting nuclear DNA, inhibits transcription, and inhibits mismatch repair mechanisms (Tesniere et al., 2010). *In vitro* studies showed that co-incubation of DCs with oxaliplatin resulted in increased expression of programmed death receptor ligand 1 (PD-L1) in DC cells, thereby inhibiting T cell proliferation (Tel et al., 2012). This phenomenon suggests that combining oxaliplatin with an anti-PD-L1 antibody for cancer therapy can initiate an effective anti-tumor immune response.

In recent years, other platinum (Pt)-based compounds have also been found to have the characteristics of ICD inducers. PtII N-heterocyclic carbene complexes display the

characteristics of type II ICD inducers, namely, induction of oxidative stress, CALR exposure, and HMGB1 as well as ATP release. Identified as the first small molecule immuno-chemotherapeutic agent, Pt-NHC is another unique cyclic metal complex that selectively localizes to the ER and induces ER stress responses via PERK (Wong et al., 2015). Recently, it was found that a new platinum-based compound R, R-1, 2-cyclohexanediamine pyrophosphate platinum (II) (PT-112) can induce ICD. Clinical studies have shown that PT-112 and PD-L1 immune checkpoint inhibitors have synergy (Kepp and Kroemer, 2020). Immunogenic or immunostimulatory Pt candidates offer potential for the development of platinum-based combination immunochemotherapy agents.

4.2.1.5 Natural medicinal chemicals

Cardiac glycosides (CG) belong to a large family of naturally derived compounds with diverse structures but a common core structure. CG is a type I ICD inducer with a primary target at the alpha subunit of the Na^+/K^+ -ATPase (Diederich et al., 2017). There is a correlation between overexpression of specific α subunits and tumor cell reactivity (Lefranc et al., 2008). CG inhibits Na^+/K^+ -ATPase, increases intracellular Na^+ and Ca^{2+} levels, while depleting intracellular K^+ . High intracellular Na^+ levels block the antiporter activity of $\text{Na}^+/\text{Ca}^{2+}$ exchanger, which is beneficial for the accumulation of Ca^{2+} in the ER and mitochondria. This results in a mild ER or mitochondrial stress response that affects tumor cell proliferation and activity. There is evidence that CG is involved in the SRC kinase-EGFR-MAPK pathway (accompanied by mitochondrial ROS production), resulting in tumor cell growth arrest (Diederich et al., 2017). In addition, the inhibition of DNA topoisomerase activity and the glycolytic pathway by CG also demonstrated the pro-apoptotic effect of CG (Prassas and Diamandis, 2008).

Shikonin is a naphthoquinone compound isolated from the traditional Chinese medicine Shikon, which is an inhibitor of proteasome activity. Shikonin inhibits the 20S subunit of the proteasome, leading to accumulation of polyubiquitinated proteins, and shikonin-treated tumor cells trigger ICD through induced mitochondrial stress, which induces the release of HSP70, HSP90, and HMGB1. Shikonin-treated tumor cell lysates promote DC differentiation and maturation (Chen et al., 2012). Shikonin-treated tumor cells can

promote the differentiation of T cells to Th17 cells, which is very important for ICD-related anti-tumor immunity; in addition, shikonin restores the killing effect of natural killer cells, and studies have shown increased cytotoxic T lymphocyte (CTL) activity in mouse splenocytes immunized with DCs loaded with shikonin-treated tumor cells (Long et al., 2012).

Wogonin is a flavonoid found in *Scutellaria baicalensis*. Wogonin has been shown to induce ICD by triggering the ER stress response, resulting in the exposure of PERK/AKT-dependent CALR and annexin A1 to the cell membrane (Yang et al., 2012). Wogonin produces a potent antitumor immune effect by inducing the release of HMGB1 and ATP, which subsequently activates DCs and induces the release of pro-inflammatory cytokines (Yang et al., 2012).

4.2.2 Radiotherapy

In clinical applications, radiotherapy has been found to induce DNA damage and tumor cell apoptosis as well as in situ ICD in tumor cells and to stimulate T cell-mediated antitumor effects. Radiation therapy selectively kills tumor cells within the irradiated range. There is growing evidence that radiation therapy can use the host's immune system to attack tumor cells in non-irradiated sites. This immune-driven effect not only helps to eliminate tumors at the local irradiation site of the disease, but also eliminates distant metastatic tumor cells, a phenomenon known as abscopal effects. Radiotherapy triggers ICD, which leads to the translocation of CALR to the cell surface and the release of DAMPs such as HMGB1 and ATP, and induces T cells to produce IFN γ *in vitro* and *in vivo*, promoting the antitumor effect of CD8⁺ T cells (Adkins et al., 2014).

Clinically, radiotherapy induces ICD in tumor cells in a dose-dependent manner, usually 2–20 Gy can effectively induce ICD (Golden et al., 2014). Local radiotherapy combined with immune checkpoint inhibitors, such as anti-cytotoxic T lymphocyte antigen 4 (CTLA4) or anti-PD-1, can take advantage of the pro-immunogenic effects of radiotherapy. In addition, radiotherapy combined with some chemotherapeutic drugs can also effectively induce ICD, but the chemotherapeutic drugs may counteract the immunogenicity of radiotherapy, so the specific role of these drugs in radiotherapy needs to be further evaluated.

4.2.3 Photodynamic therapy

Photodynamic therapy (PDT) is a minimally invasive treatment method (van Straten et al., 2017) that can induce type II ICD immune responses. PDT is a selective uptake of photosensitizers by tumor tissues and activated by light of a specific wavelength, resulting in an oxidative stress response, resulting in the destruction of tumor cells located at the site of the photosensitizer action (Garg and Agostinis, 2014). At present, the most intensively studied photosensitizer in this field that can induce ICD is hypericin, an anthraquinone derivative that can target the ER and induce ER stress and activation of the UPR signaling pathway upon irradiation, ultimately leading to cell death (Buytaert et al., 2006). Hypericin-mediated photodynamic therapy (Hyp-PDT) can also inhibit tumor NF- κ B activity. At a certain dose, Hyp-PDT can down-regulate tumor cell-derived tumor-promoting cytokines; in addition, Hyp-PDT can also inhibit the secretion of matrix metalloproteinase 9 (MMP-9), thereby inhibiting tumor metastasis (Du et al., 2007). Currently known photosensitizers that induce ICD include hypericin, 5-alanine (Ji et al., 2015), rose bengal acetate (Panzarini et al., 2014), sugar-binding chloride (Tanaka et al., 2016), phthalocyanines (Liu and Li, 2020), etc. It is being continuously developed and researched.

4.2.4 Oncolytic virus therapy

Viruses can induce and block a variety of cell death pathways. Envelope viruses require membrane proteins and lipids to produce progeny viruses. Thus, the virus induces ER stress and UPR. Oncolytic viruses (OVs) induce cell death similar to chemotherapy-induced ICD. OVs generate pro-inflammatory responses by generating pathogen-associated molecular patterns (PAMPs) and releasing tumor-associated antigens (TAAs), thus serving as an *in situ* tumor vaccine. Cell death induced by multiple OVs exhibited typical features of ICD, including increased surface expression of CALR and elevated levels of extracellular ATP and HMGB1.

Talimogene laherparepvec (T-VEC) is a type 1 herpes simplex virus that expresses the granulocyte-macrophage colony-stimulating factor (GM-CSF) and is currently approved for the treatment of melanoma in the United States and Europe. Studies have shown that after *in vitro* infection with T-VEC, melanoma cells release increased HMGB1, increased

ATP, and increased surface expression of CALR. It was also found that the sensitivity of melanoma cells to T-VEC was negatively correlated with STING expression. Studies have shown that oncolytic HSV-1 can regress tumors with low STING expression. Therefore, T-VEC has the potential to mediate antitumor responses by expressing STING in STING-deficient tumors (Bommareddy et al., 2019).

In addition, coxsackievirus B3 (Liu et al., 2012; Miyamoto et al., 2012) and vaccinia virus (Heinrich et al., 2017) can induce ICD. Coxsackievirus B3 is an RNA virus that replicates in the cytoplasm of host cells, disrupting homeostasis, leading to cell death and accumulation of large amounts of unfolded or misfolded viral envelope proteins in the ER, inducing ER stress. After infection with coxsackievirus B3, non-small cell lung cancer (NSCLC) cells have increased CALR translocation and increased ATP and HMGB1. Coxsackievirus B3 can also enhance the immunogenicity of the tumor microenvironment by increasing the number of intratumoral blood vessels and the number of CD8⁺ T cells, DC, granulocytes, and NK cells accumulate, and the infiltration of inflammatory immune cells increases at the tumor site, contributing to tumor regression (Liu et al., 2012; Miyamoto et al., 2012).

OVs are novel immunotherapies that replicate within solid tumors and interfere with the immune system. OVs replicate preferentially in tumor cells and can be genetically modified to inactivate interfering viral proteins and cause ER stress or activate ROS signaling to induce ICD (van Vloten et al., 2018).

4.2.5 Novel ICD inducers

In recent years, studies have found some new means to combine with ICD inducers to elicit broad antitumor responses, and novel ICD inducers are shown in **Table 2**.

Non-thermal plasmas (NTP) have the potential to induce ICD, and studies have shown that NTP-treated CT26 colorectal cancer cells have increased surface expression of major histocompatibility complex I (MHC I) and CALR. NTP-induced cellular production of ROS and nitric oxide can rapidly alter the cellular oxidative state and induce ER stress. As a unique ROS and nitric oxide delivery system, NTP can successfully induce tumor cell ICD and is a potential cancer adjuvant therapy. The specific mechanism of NTP-induced ICD

needs to be further studied, and the treatment regimen should be further optimized. In addition, immunotherapy is a breakthrough in cancer treatment today, and NTP may be combined with chemotherapy or even therapeutic cancer vaccines (Lin et al., 2018). Nanoparticle-encapsulated doxorubicin and photosensitizer chlorin e6 can effectively stimulate DC recruitment and help DCs better expose and spread TAAs (Ni et al., 2020). Combining chemotherapy, PDT and immunotherapy provides new ideas for cancer treatment.

Retinoic acid inducible gene I (RIG-I) helicase induces an antiviral response program by producing IFN, and its activated tumor cells release high levels of HMGB1, and in addition, its signaling in tumor cells can lead to mitochondrial oxidative stress (Dewell et al., 2014).

Many novel therapies also promote anti-tumor immune responses by inducing tumor cells to undergo ICD. Studies have shown that oncolytic peptides such as LTX-315 and RT53 can induce ICD in tumor cells and release many DAMPs, which are similar to tumor in situ vaccines and promote tumor regression and T cell infiltration in tumor sites (Pasquereau-Kotula et al., 2018; Zhou et al., 2016). Compared with traditional radiotherapy, nano-pulse stimulation (NPS) is an effective non-thermal physical therapy, which uses ultra-short electrical pulses to stimulate tumor cells and inhibit tumor growth. Its mechanism of action is to induce the activation of caspase3/7 in tumor cells, resulting in an increased release of DAMPs, including CALR, ATP and HMGB1 (Nuccitelli et al., 2017). Hybrid protein oxygen nanocarrier therapy is an oxygen self-contained photodynamic therapy that co-targets delivery of photosensitizer and oxygen to tumor cells, induces tumor cell ICD, and releases DAMPs. In a metastatic breast cancer model, hybrid protein oxygen nanocarrier therapy induces antitumor immunity, destroys primary tumors and effectively suppresses distant tumors and lung metastases (Chen et al., 2018). Other physical therapies, such as near-infrared photoimmunotherapy, have also shown potential to induce ICD (Gao et al., 2019).

Table 2. Novel inducers of tumor immunogenic cell death and their mechanisms.

ICD inducers	DAMPs	Mechanism	Reference
RIG-I helicases	ecto-CALR, ERp57, ATP, HSP70, HMGB1	<ul style="list-style-type: none"> • Expression of pro-inflammatory type I interferon; • Upregulation of MHC-I molecules and CD95; • CALR translocates to the cell surface; • Release of HMGB1 and HSP70; • Promotes DC maturation; • Promote efficient phagocytosis of apoptotic tumor cells by CD8a⁺ DC. 	(Duewell et al., 2014)
Oncolytic peptides RT53 and LTX-315	ecto-CALR, ATP, HMGB1	<ul style="list-style-type: none"> • Caspase- and eIF2α-dependent pathways trigger CALR exposure; • ATP and HMGB1 release; • Increased T cell infiltration. 	(Pasquereau-Kotula et al., 2018; Zhou et al., 2016)
Nanopulse stimulation	ecto-CALR, ATP, HMGB1	<ul style="list-style-type: none"> • Stimulates the activation of caspase3/7; • Activation of immune response. 	(Nuccitelli et al., 2017)
Oncolytic virus	ecto-CALR, ATP, HMGB1	<ul style="list-style-type: none"> • Increases the number of HER-2-specific CD8⁺ TILs that secrete IFNγ; • Increased intratumoral infiltration of tumor antigen-specific CD8⁺ T cells. 	(Gujar et al., 2018; Lee and Gujar, 2018)
Hybrid protein oxygen nanocarriers	ecto-CALR, ATP, HMGB1	<ul style="list-style-type: none"> • Promotes the maturation of DCs; • Activation of T lymphocytes, NK cells and TDLNs. 	(Chen et al., 2018)
Near-infrared photoimmunotherapy	ecto-CALR, ATP, HMGB1, HSP70, HSP90	<ul style="list-style-type: none"> • Promotes the maturation of DCs; • Activation of host anti-tumor immune responses. 	(Ogawa et al., 2017)

AIM OF THE THESIS

The development of tumors can be seen as the result of the inability of the human immune system to clear malignant cells. Numerous factors are involved in the process of tumor immune escape, which mainly include tumor-associated antigen loss, insufficient immunogenicity, and an immunosuppressive microenvironmental state caused by insufficient nutrients and specific metabolite accumulation (Chang et al., 2015; Wellenstein and de Visser, 2018). Similarly, the ability of tumor cells to widely adapt to different adverse environments is mainly attributed to the adaptation of the tumor cell metabolism, which is also the main reason for tumor proliferation and metastasis (Vander Heiden and DeBerardinis, 2017). Therefore, both metabolic factors and lack of tumor immune surveillance have been identified as factors driving tumorigenesis and the development of the malignant disease (Pavlova and Thompson, 2016; Vander Heiden and DeBerardinis, 2017). In epidemiological investigations and clinical trials, with the in-depth study of the mechanism of systemic nutritional status affecting immune response, the theory of "immunonutrition" has been developed (O'Sullivan et al., 2019). However, beyond vitamin deficiencies, the detailed molecular mechanisms of systemic macromolecular and small molecule nutrients in immune cell function remain thus far unexplored.

A calorie-restricted diet has favorable anti-inflammatory effects and can improve immune cell function (Buck et al., 2017). Calorie restriction mimetics (CRMs) are a class of drugs or foods that mimic the effects of calorie restriction and are expected to improve health status and even prolong life (Andrejeva and Rathmell, 2017). Studies have shown that starvation and various potential CRMs can increase the expression of insulin-like growth factor-binding protein 1 (IGFBP1) and thereby reduce the level of IGF1 in the blood, ultimately causing changes in the systemic metabolic profile (Prieto et al., 2017); CRMs can reduce the proportion of regulatory T cells (Treg) in cancer nests to improve the efficacy of chemotherapy (Prieto et al., 2017).

CRMs provoke the deacetylation of cellular proteins coupled to an increase in autophagic flux in the absence of toxicity. Pharmacological autophagy enhancement constitutes a preclinically validated strategy for preventing or treating most major age-associated

diseases. Based on these considerations, we engaged in the search for new autophagy inducers acting as additional CRMs by performing a high-content/high-throughput screen on 65 000 distinct compounds on a robotized fluorescence microscopy.

RESULTS

Identification of picropodophyllin as an autophagy inducer

Pharmacological autophagy enhancement constitutes a preclinically validated strategy for preventing or treating most major age-associated diseases. Driven by this consideration, we performed a high-content/high-throughput screen on 65 000 distinct compounds on a robotized fluorescence microscopy platform to identify novel autophagy inducers. Here, we report the discovery of picropodophyllin (PPP) as a potent inducer of autophagic flux that acts on-target.

IGF1 receptor inhibition amplifies the effects of cancer drugs by autophagy and immune-dependent mechanisms

We characterize PPP as an inhibitor of the tyrosine kinase activity of the insulin-like growth factor-1 receptor (IGF1R). Thus, PPP lost its autophagy-stimulatory activity in cells engineered to lack IGF1R or to express a constitutively active AKT serine/threonine kinase 1 (AKT1) mutant. When administered to cancer-bearing mice, PPP improved the therapeutic efficacy of chemoimmunotherapy with a combination of immunogenic cytotoxicants and programmed cell death 1 (PDCD1, better known as PD-1) blockade. These PPP effects were lost when tumors were rendered PPP-insensitive or autophagy-incompetent. In combination with chemotherapy, PPP enhanced the infiltration of tumors by cytotoxic T lymphocytes, while reducing regulatory T cells. In human triple-negative breast cancer patients, the activating phosphorylation of IGF1R correlated with inhibited autophagy, an unfavorable local immune profile, and poor prognosis.

Altogether, these results (displayed as the published article that follows) suggest that IGF1R may constitute a novel and druggable therapeutic target for the treatment of cancer in conjunction with chemoimmunotherapies.

IGF1 receptor inhibition amplifies the effects of cancer drugs by autophagy and immune-dependent mechanisms

Qi Wu,^{1,2,3} Ai-Ling Tian,^{2,3,4} Bei Li,⁵ Marion Leduc,^{2,3} Sabrina Forveille,^{2,3} Peter Hamley,⁶ Warren Galloway,⁶ Wei Xie,^{2,3} Peng Liu,^{2,3} Liwei Zhao,^{2,3} Shuai Zhang,^{2,3,4} Pan Hui,^{2,3,4} Frank Madeo,^{7,8,9} Yi Tu,¹ Oliver Kepp ,^{2,3} Guido Kroemer^{2,3,10,11,12}

To cite: Wu Q, Tian A-L, Li B, *et al.* IGF1 receptor inhibition amplifies the effects of cancer drugs by autophagy and immune-dependent mechanisms. *Journal for ImmunoTherapy of Cancer* 2021;**9**:e002722. doi:10.1136/jitc-2021-002722

► Additional online supplemental material is published online only. To view, please visit the journal online (<http://dx.doi.org/10.1136/jitc-2021-002722>).

QW, A-LT and BL are joint first authors.

Accepted 04 May 2021



© Author(s) (or their employer(s)) 2021. Re-use permitted under CC BY-NC. No commercial re-use. See rights and permissions. Published by BMJ.

For numbered affiliations see end of article.

Correspondence to
Dr Oliver Kepp;
captain.olsen@gmail.com

Professor Yi Tu;
ty701105@163.com

Prof Guido Kroemer;
kroemer@orange.fr

ABSTRACT

Background Pharmacological autophagy enhancement constitutes a preclinically validated strategy for preventing or treating most major age-associated diseases. Driven by this consideration, we performed a high-content/high-throughput screen on 65 000 distinct compounds on a robotized fluorescence microscopy platform to identify novel autophagy inducers.

Results Here, we report the discovery of picropodophyllin (PPP) as a potent inducer of autophagic flux that acts on-target, as an inhibitor of the tyrosine kinase activity of the insulin-like growth factor-1 receptor (IGF1R). Thus, PPP lost its autophagy-stimulatory activity in cells engineered to lack IGF1R or to express a constitutively active AKT serine/threonine kinase 1 (AKT1) mutant. When administered to cancer-bearing mice, PPP improved the therapeutic efficacy of chemoimmunotherapy with a combination of immunogenic cytotoxicants and programmed cell death 1 (PDCD1, better known as PD-1) blockade. These PPP effects were lost when tumors were rendered PPP-insensitive or autophagy-incompetent. In combination with chemotherapy, PPP enhanced the infiltration of tumors by cytotoxic T lymphocytes, while reducing regulatory T cells. In human triple-negative breast cancer patients, the activating phosphorylation of IGF1R correlated with inhibited autophagy, an unfavorable local immune profile, and poor prognosis.

Conclusion Altogether, these results suggest that IGF1R may constitute a novel and druggable therapeutic target for the treatment of cancer in conjunction with chemoimmunotherapies.

INTRODUCTION

Macroautophagy (which we refer to as ‘autophagy’) is a complex intracellular phenomenon in which portions of the cytoplasm including entire organelles are engulfed in autophagosomes that subsequently fuse with lysosomes for the digestion of the luminal cargo. Genetic or acquired defects in this process are linked to a broad spectrum of human diseases ranging from neoplastic to cardiometabolic diseases, inflammatory syndromes and degenerative processes

affecting virtually every organ system and cell type.¹ At the physiological level, autophagy is part of a general stress response that facilitates cellular and organismal adaptation to changing external conditions.² Genetic or pharmacological stimulation of autophagy can extend the healthspan and lifespan of model organisms, thus postponing the stigmata of disease and frailty.^{3–4} For this reason, there is an ever-increasing interest in identifying pharmacological autophagy enhancers.^{5,6}

In the context of cancer, autophagy plays an ambiguous role.^{7,8} On one hand, autophagy is required for maintaining cellular homeostasis and genomic stability,⁹ as well as for facilitating anticancer immunosurveillance,⁵ meaning that the inhibition of autophagy spurs carcinogenesis^{10,11} and disabled autophagy actually constitutes a poor prognostic marker in some cancers.¹² On the other hand, autophagy enhances the fitness of cancer cells and allows them to avoid cell death induction in response to cytotoxicants or targeted therapies.¹³ Thus, the effects of autophagy modulation on tumor progression are highly context dependent. For example, in pancreatic cancer, the induction of autophagy has been suggested as a therapeutic strategy, depending on the genetic makeup of the cancer cells and immune factors.^{14–16} Notwithstanding the ambiguous role of autophagy in carcinogenesis, attempts have been launched to stimulate autophagy for enhancing the therapeutic activity of immunogenic chemotherapies (for instance with anthracyclines and oxaliplatin (OXA)) and immunotherapies.^{5,17–19} In this context, it appears that autophagy has two major effects. First, it can enhance the lysosomal secretion of adenosine triphosphate (ATP) from dying cancer cells, thus enhancing the extracellular

ATP-mediated recruitment of dendritic cell precursors into the tumor.^{5 20} Second, autophagy can contribute to the maintenance of specific T lymphocyte stem cell properties.¹⁸

Driven by the aforementioned considerations, we set out to identify novel autophagy inducers. Here, we report the identification of picropodophyllin (PPP), a cycloignan alkaloid derived from the mayapple plant, as a potent inducer of autophagy that acts through the inhibition of insulin-like growth factor-1 receptor (IGF1R). When administered to tumor-bearing mice, PPP enhanced the efficacy of immunogenic chemotherapy combined with immunotherapy and these effects relied on the induction of autophagy in malignant cells.

MATERIAL AND METHODS

Cell culture and chemicals

Culture media and supplements for cell culture were obtained from Life Technologies (Carlsbad, California, USA) and plastic materials came from Greiner BioOne (Kremsmünster, Austria) and Corning (Corning, New York, USA). Rat adrenal gland PC12 cells stably expressing doxycycline-inducible Q74-GFP were cultured in Roswell Park Memorial Institute (RPMI)-1640 containing 5% fetal bovine serum (FBS) and 10% horse serum.²¹ Human neuroglioma H4 cells, human osteosarcoma U2OS cells, MCA205 murine fibrosarcoma and all the other cells were maintained in Dulbecco's modified Eagle's medium, supplemented with 10% (v/v) FBS, 10 U/mL penicillin sodium and 10 µg/mL streptomycin sulfate at 37°C in a humidified atmosphere with 5% CO₂. Transcription factor EB (TFEB)-deficient (TFEB^{-/-}), transcription factor 3 (TFE3)-deficient (TFE3^{-/-}), TFEB and TFE3-double deficient (TFE DKO), autophagy related 5 (ATG5)-deficient (ATG5^{-/-}), and eukaryotic translation initiation factor 2 alpha kinase 3 (EIF2AK3, better known as PERK)-deficient (PERK^{-/-}) U2OS-green fluorescent protein (GFP)-microtubule associated protein 1 light chain 3 beta (MAP1LC3B, better known as LC3) cell lines and TFEB and TFE3-double deficient (TFE DKO) in H4-GFP-LC3 cells were generated by means of the CRISPR/Cas-mediated genome editing, as per manufacturer's recommendations.¹⁷ U2OS cells stably expressing RFP-LC3 bearing a mutant non-phosphorylation of eukaryotic initiation factor 2α (EIF2A) (eIF2α^{S51A}) were constructed using the CRISPR-Cas9 technology as previously detailed.²² In addition, U2OS cells stably expressing GFP-TFEB were generated by our group in the past.^{17 23} MCA205 cells stably expressing shRNAs interfering with the expression of TFE3/TFEB or ATG5, and overexpressing CD39 and a mutant phosphorylation AKT^{T308D/S473D} were also constructed as the manufacturer.^{5 17 24}

The polyphenol library and PPP were purchased from TargetMol (Boston, MA, USA); Torin1 (TOR), bafilomycin A1, mitoxantrone (MTX) and OXA were obtained from Sigma-Aldrich (St. Louis, MI, USA). Recombinant IGF₁ were obtained from PROSPECBIO (CYT-216,

Rehovot, Israel). Linsitinib (HY-10191) were obtained from MedChemExpress (Shanghai, China).

High-content microscopy

Human osteosarcoma U2OS and neuroglioma H4 cells stably expressing GFP-LC3, GFP-TFEB, GFP-AKT, GFP-AKT R25C, RFP-GFP-LC3-tandem or RFP-GFP-p62-tandem reporter and rat adrenal gland PC12 cells stably expressing doxycycline-inducible Q74-GFP were seeded in 384-well black imaging plates at a density of 2000 cells per well and allowed to adapt for overnight. Cells were treated with the indicated agents, then fixed with 3.7% paraformaldehyde (PFA, w/v in PBS) (F8775, Sigma-Aldrich) at 4°C overnight and stained with 1 µg/mL Hoechst 33342 in PBS. Subsequently, the fixative was exchanged to PBS and the plates were analyzed by automated microscopy. Image acquisition was performed using an ImageXpress Micro XL automated microscope (Molecular Devices, Sunnyvale, California, USA) equipped with a 20 X PlanApo objective (Nikon, Tokyo, Japan), followed by automated image processing with the custom module editor within the MetaXpress software (Molecular Devices). At least four view fields were acquired per well, and experiments involved at least triplicate assessment. Cellular regions of interest, cytoplasm and nucleus, were defined and segmented by using the MetaXpress software (Molecular Devices). After exclusion of cellular debris and dead cells from the dataset, parameters of interest were normalized, statistically evaluated, and graphically depicted with R software. Using R, images were extracted and pixel intensities scaled to be visible (in the same extent for all images of a given experiment). Cell viability was assessed as described before.²⁵

Immunofluorescence

Human osteosarcoma U2OS cells were treated for 6 hour to detect TFE3, then were fixed with 3.7% PFA at 4°C overnight. For staining, fixed cells were permeabilized with 0.1% Triton X100 on ice, and blocked with 5% bovine serum albumin (BSA, w/v in PBS) for 1 hour. Next, cells were incubated with antibodies specific to TFE3 (#ab93808, 1:400, Abcam) at 4°C overnight. After washing with PBS twice, the cells were incubated with AlexaFluor conjugates (Thermo Fisher Scientific) against the primary antibody for 2 hour at ambient temperature. Then cells were washed and imaged by automated fluorescence microscopy as described above. The nuclear intensity of TFE3 was measured and normalized to Ctrl.

Immunohistochemistry

A total of 49 formalin-fixed paraffin-embedded; tissue samples of triple-negative breast cancer were obtained from Renmin Hospital of Wuhan University, People's Republic of China (online supplemental table S1). Patients did not receive financial compensation. Patients with at least 5-year follow-up were included in this retrospective study. All methods were performed in accordance with the relevant guidelines and local regulations.

Immunohistochemical staining was performed by an automatic staining machine (Leica Bond3) or manually processed. Sections were dehydrated and antigenic epitopes were retrieved using a 10 mM citrate buffer and microwaving for 10 min. Specimen were then incubated with for LC3B (#3868, 1:2000, Cell Signaling Technology), phospho-IGF1R (#orb503127, 1:100, Biorbyt, UK), CD163 (#93498, 1:500, Cell Signaling Technology), Foxp3 (#98377, 1:100, Cell Signaling Technology), CD8 (#70306, 1:200, Cell Signaling Technology). Primary antibody staining was detected by peroxidase-conjugated IgG (1:500 diluted P0448, Dako, Glostrup, Denmark). Positive cells were counted on nine randomly chosen tumor areas at 200 magnifications in a double blinded fashion. Quantitative analysis was performed using ImageJ software as described.²⁶ The receiver operating characteristic analysis was used to determine the optimal cut-off values of all proteins expression levels for survival rate.

Immunoblotting

Tissues (~30 mg) were dissociated in Precellys lysing tubes (#CK28_2 mL, Bertin Technologies SAS, France) containing 1 mL of radio immunoprecipitation assay buffer (RIPA) lysis buffer (#89901, Invitrogen, Carlsbad, California, USA) by using the Precellys 24 homogenizer (Bertin Technologies SAS) at 6500 rpm for 5 min, followed by spinning at 14000 g for 15 min to collect the supernatant that contains soluble proteins. For cells, the protein extracts were dissolved in RIPA buffer and obtained by ultrasonication for 3×10 s and centrifuging at 12000 g for 15 min to collect the supernatant that contains soluble proteins. Protein concentration was measured by means of by the BCA Assay (Bio-Rad, Hercules, California, USA). The protein solution was mixed with 4X loading buffer (# NP0008, Invitrogen), and denatured at 100°C for 15 min before subjected to western blotting. The total protein (~30 µg) were resolved on 4%–12% NuPAGE Bis-Tris protein gels (#NP0322, Thermo Fisher Scientific) and electrotransferred to 0.2 µm polyvinylidene fluoride membranes (#1620177, Bio-Rad). The membranes were blocked with 0.05% Tween 20 (#P9416, Sigma Aldrich) v:v in Tris-buffered saline (TBS) (TBST) (#ET220, Euro-medex) supplemented with 5% non-fat powdered milk (w:v in TBS), followed by an overnight incubation at 4°C with primary antibodies specific for LC3B (#2775, 1:1000, Cell Signaling Technology), HA (#ROAHAHA, 1:1000, Sigma-Aldrich), phospho-P70 (Thr389) (#9234, 1:1000, Cell Signaling Technology), P70 (#9202, 1:1000, Cell Signaling Technology), phospho-IGF1R (Tyr1135/1136) (#3024, 1:1000, Cell Signaling Technology), IGF1R (#9750, 1:1000, Cell Signaling Technology), pTFEB (Ser211) (#37681, 1:1000, Cell Signaling Technology), TFEB (#4240, 1:1000, Cell Signaling Technology), TFE3 (#ab93808, 1:1000, Abcam), phospho-AKT (Ser473) (#4060, Cell Signaling Technology), AKT (#4691, Cell Signaling Technology), phospho-mechanistic target of rapamycin (mTOR) (Ser2448) (#2971, Cell Signaling Technology), mTOR (#2983, Cell Signaling Technology),

H3 (#9715, 1:1000, Cell Signaling Technology). Membranes were washed three times for 10 min with TBST before incubation with HRP-conjugated goat-anti-rabbit secondary antibody (CliniScience) for 2 hours at room temperature. Then the membranes were washed again and subjected to chemiluminescence detection with the Amersham ECL Prime detection reagent kit (GE Healthcare, Piscataway, New Jersey, USA) on an ImageQuant LAS 4000 software-assisted imager. The membranes were stripped and reprobated for loading control with anti-actin (# ab 20727, 1:10000, Abcam), anit-glyceraldehyde-3-phosphate dehydrogenase (GAPDH)-specific antibody (#2118, 1:5000, Cell Signaling Technology) or anti-vinculin antibody (#13901, 1:1000, Cell Signaling Technology). Quantification was performed by densitometry using the Image J software.

Plasmid transfection

Cells were seeded, let adhere for 24 hours, and following transfected with the CRISPR-Cas9 plasmid U6gRNA-Cas9-2A-RFP targeting IGF1R (50-ATGATGCGATT CTCGACG-30) or a plasmid coding for AKT carrying the T308D/S473D mutation (#14751, Addgene, Watertown, Massachusetts, USA), according to the manufacturer's advice.

Nuclear extraction experiment

U2OS-GFP-LC3 cells were collected and processed with the Nuclear Extraction Kit (#ab113474, Abcam) following the manufacturer's methods. The GAPDH antibody (#2118, 1:1000, Cell Signaling Technology) was used as cytoplasmic control, and H3 (#9715, 1:1000, Cell Signaling Technology) was selected as nuclear loading and quality control.

Detection of protein deacetylation

U2OS-GFP-LC3 stable expressing cells (~2000 cells/well) were seeded in 384-well microplates overnight. After experimental treatments, cells were fixed with 3.7% PFA containing 1 µg/mL Hoechst 33342 overnight at 4°C. Thereafter, cells were incubated with an antibody specific for acetyl-alpha-tubulin (#5335, 1:500, Cell Signaling Technology) in 5% bovine serum albumin (BSA, w/v in PBS) for 1 hour to block non-specific binding sites and acetylated tubulins, followed by overnight incubation at 4°C with specific antibody to detect acetylated proteins at lysines (#623402, 1:400, BioLegend, San Diego, California, USA). After washing three times with PBS, cells were incubated in AlexaFluor-568 conjugates (Life Technologies) against the primary antibody for 2 hours at room temperature. Fluorescent images were acquired and analyzed as described before.

ATP release assays

Intracellular ATP levels were detected by quinacrine staining (Calbiochem), subsequently the images of quinacrine were observed by means of high-content microscopy and the cytoplasmic intensity of quinacrine was quantitated as described above. Extracellular ATP levels

were measured by the ENLITEN ATP Assay System Bioluminescence Detection Kit (Promega, Madison, Michigan, USA; #FF2000) following the manufacturer's instructions. Luminescence was measured by means of a Paradigm I3 multimode plate reader (Molecular Devices).

Animal model

The animal experiments were approved by the Gustave Roussy ethics committee with the project number: 24771–2020032413235413, and all procedures were performed under the governmental and institutional guidelines and regulations. All mice were maintained in a temperature-controlled and pathogen-free environment with 12 hours light/dark cycles, with food and water ad libitum.

For tumor growth experiments, 7 week-old female wild-type C57BL/6 mice or athymic female nude mice (nu/nu) were obtained from Envigo, France (Envigo, Huntingdon, UK). AT3 wild-type, TC1 wild-type, MCA205 wild-type (WT), overexpressing a CD39 transgene (CD39⁺) or a constitutive active variant of AKT T308D/S473D (4×10^5), MCA205 with ATG5 knockout (WT, 6×10^5) cells were subcutaneously injected into C57BL/6 hosts. When tumors became palpable, mice were treated with 20 mg/kg PPP dissolved in corn oil (Sigma-Aldrich), 25 mg/kg linsitinib (dissolved in 5% DMSO, 10% PEG300, 5% Tween 80, 80% PBS) or an equivalent volume of vehicle alone or in combination with 10 mg/kg (OXA, Sigma-Aldrich) or 200 µg anti-PD-1 antibody (Clone 29 F.1A12, BioXcell, West Lebanon, New Hampshire, USA), by intraperitoneal (i.p.) injection. On the following days, mice well-being and tumor growth were monitored and documented. Animals were sacrificed when tumor size reached endpoint or signs of obvious discomfort were observed following the EU Directive 63/2010 and our Ethical Committee advice.

Ex vivo–phenotyping of the tumor immune infiltrate

Tumors were harvested, weighed and transferred on ice into gentleMACS C tubes (Miltenyi Biotec, Bergisch Gladbach, Germany) containing 1 mL of RPMI medium. Tumors were dissociated first mechanically with scissors, then enzymatically using the mouse tumor dissociation kit (Miltenyi Biotec) and a GentleMACS Octo Dissociator according to the manufacturer's instructions. The dissociated bulk tumor cell suspension was resuspended in RPMI1640, sequentially passed through 70 µm MACS Smart-Strainer (Miltenyi Biotec) and washed twice with PBS. Finally, bulk tumor cells were homogenized in PBS at a concentration corresponding to 250 mg of the initial tumor weight per mL. Prior to staining of tumor-infiltrating lymphocytes (TILs) for flow cytometry analysis, samples (~50 mg) were incubated with LIVE/DEAD Fixable Yellow Dead Cell dye (Thermo Fisher Scientific) to discriminate viable cells from damaged cells. Fc receptors were blocked with anti-mouse CD16/CD32 (clone 2.4G2, Mouse BD Fc Block, BD Pharmingen) before staining with fluorescent-labeled antibodies targeting T-cell

surface markers. Surface staining of murine immune cell populations infiltrating the tumor was performed with the following fluorochrome-conjugated antibodies: anti-CD45-AF700, anti-CD3-BV421, anti-CD8-PE, anti-CD4-Percp.Cy5.5, anti-CD25-PE/Cy7, and anti-PD-1-APC/Cy7 (BioLegend). Then, cells were fixed and permeabilized in eBioscience Foxp3/Transcription Factor Staining Buffer (Thermo Fisher Scientific) and stained for intracellular Foxp3. Finally, stained samples were run through a BD LSR II flow cytometer. Data were acquired using BD FACSDiva software (BD Biosciences) and analyzed using FlowJo software (TreeStar). Absolute counts of leukocytes and tumor cells were normalized considering the following parameters: weight of the harvested tumor and total volume of the dissociated tumor cell suspension (cell concentration typically set to 250 mg/mL in PBS), proportion of the whole cell suspension and proportion of the cell suspension used for cytometry.

Statistical analysis

Unless otherwise mentioned, data are reported as means±SD of triplicate determinations and experiments were repeated at least three yielding similar results. Statistical significance was assessed by Student's t-test. TumGrowth and GraphPad were used to analyze in vivo data arising from murine models.²⁷ The Kaplan-Meier method was used to calculate patient survival and the log-rank test was used to assess the heterogeneity for each prognostic factor. Univariate Cox proportional hazard regressions were used to obtain HRs and their respective 95% CIs to show the strength of the estimated relative risks. Pearson's correlation was used to evaluate the correlation. P values of 0.05 or less were considered to denote significance (*p<0.05; **p<0.01; ***p<0.001; ns, not significant).

RESULTS

Identification of PPP as a potent inducer of autophagic flux

Human osteosarcoma U2OS cells, which are often used as biosensor cell lines,²⁸ were stably transduced with a GFP-LC3 fusion protein and subjected to rounds of selection (to ensure homogeneous GFP-LC3 expression in most cells) and quality control (to ensure adequate formation of GFP-LC3 puncta in response to autophagy induction by the positive control torin1). In a robotized high-content/high throughput screening platform,²⁸ such cells were exposed to ~65 000 compounds (all tested at 10 µM) to identify agents that induce GFP-LC3 puncta at least as efficiently as the positive control (the MTOR inhibitor torin1 used at 300 nM) without cell loss (figure 1A,B). About 200 compounds fulfilled this criterion. We chose to follow-up (PPP, also known as AXL1717) for two reasons. First, in a validation experiment re-evaluating the top 400 compounds from the primary screen, in another smaller screen focusing on a library of polyphenols involving ~1000 compounds and in further low throughput experiments PPP was found

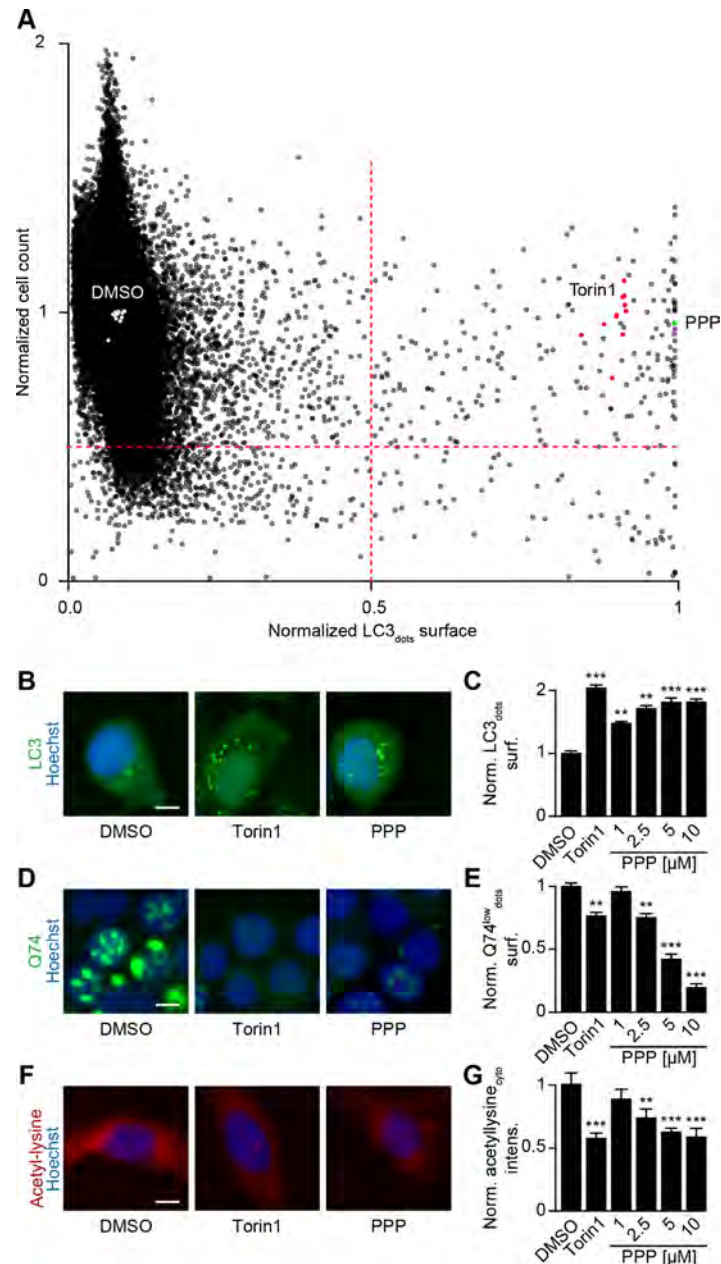


Figure 1 Identification of picropodophyllin (PPP) as autophagy inducer. (A) Human osteosarcoma U2OS stably expressing GFP-LC3 cells and were treated with a chemical library of 65 000 diverse compounds (10 μM) for 6 hours. Torin 1 at 300 nM was used as positive control for autophagy induction. The number of GFP-LC3 positive puncta was measured as a proxy for autophagy and the number of cells that confer a regular nuclear phenotype was assessed as an indicator for viability. We selected the agents that dramatically increase the expression of GFP-LC3 and whose viability is >0.5 times of its expression in control group, are potential autophagy activators. Data were normalized to controls, depicted as means of each campaign. (B, C) U2OS cells stably expressing GFP-LC3 were treated with PPP (1, 2.5, 5, 10 μM) and torin1 (300 nm) was used as control. the surface of GFP-LC3 positive puncta was measured as a proxy for autophagy (C) and representative images are depicted in B. scale bar equals 10 μm. (D, E) Rat adrenal gland PC12 cells expressing an inducible variant of Q74-GFP were treated with doxycycline (1 μg/mL) for 8 hours for the induction of Q74 expression. Then the medium was changed and PPP was added at 1, 2.5, 5 and 10 μM. Torin1 (300 nm) was used as positive control. data is depicted as barchart in E and representative images are shown in D. Scale bar equals 10 μm. (F, G) U2OS cells were treated with PPP and the positive control torin1 (300 nm) for 6 hours, followed by the incubation with specific antibodies to block acetylated tubulin. Thereafter, immunofluorescence was conducted with antibodies against acetylated lysine residues and appropriate AlexaFluor-conjugated secondary antibodies. representative images of acetylation are shown in F, and acetylation intensity in the cytoplasm was measured in G. Scale bar equals 10 μm. Data are means±SD of three replicates (**p<0.01, ***p<0.001 vs DMSO/Ctr, Student's t-test).

to induce autophagic flux in cells expressing distinct flux biosensors, namely a RFP-GFP-LC3 (online supplemental figure S1A), a Q74-GFP construct (online supplemental figure S1B), a RFP-ATG4-GFP-LC3ΔG (online supplemental figure S2A,B), mCherry-GFP-p62 (online supplemental figure S2C,D) and HA-tagged p62 (online supplemental figure S2E-G), confirming that PPP indeed induces autophagic flux. Second, PPP has been described as an inhibitor of IGF1R^{29,30} with potent antitumor effects in preclinical models^{31–33} and acceptable toxicity in clinical phase I and II trials.³⁴

Further experiments confirmed that PPP induced GFP-LC3 puncta (figure 1B,C) and reduced the abundance of the autophagic substrate Q74-GFP (figure 1D,E) in a dose-dependent fashion. In addition, PPP reduced cytoplasmic protein acetylation, as determined by quantitative immunofluorescence staining (figure 1F,G). These effects were detectable at PPP concentrations of 2.5 to 10 μM, which did not affect cellular viability (online supplemental figure S2H). Of note, induction of GFP-LC3 puncta or LC3-II by PPP was lost in *ATG5*^{-/-} U2OS cells (figure 2A–C), was accompanied by the translocation of TFEB and TFE3 into nuclei (figure 2D–H, (online supplemental figure S3A,B), was partially reduced in *TFEB*^{-/-} or *TFE3*^{-/-} cells, and strongly inhibited in *TFEB*^{-/-} *TFE3*^{-/-} double-knockout cells (figure 2I–Q, (online supplemental figure S3C–E). Hence, PPP stimulates autophagic flux through a canonical, ATG5 and TFEB/TFE3-dependent pathway.

PPP induces autophagy through IGF1R inhibition

PPP is known to block the tyrosine kinase activity of IGF1R.^{29,30} Accordingly, PPP-induced GFP-LC3 puncta were not prevented by addition of IGF₁ (figure 3A,B), the agonist ligand of IGF1R. PPP efficiently blocked IGF1-induced IGF1R autophosphorylation, the activating phosphorylation of protein kinase B (best known as AKT), the phosphorylation of MTOR, and the activity of MTOR complex 1 (MTORC1), evaluated by assessing the phosphorylation of the MTORC1 substrates p70^{S6K} and TFEB (figure 3C). Knock-out of IGF1R rendered U2OS cells resistant to the autophagy-inducing effects of PPP (figure 3D–F, online supplemental figure S3F). Conversely, transgenic expression of a constitutively active AKT mutant (T308D/S473D)³⁵ abolished the proautophagic activity of PPP (figure 3G–I, online supplemental figure S4A,B). IGF1 stimulated the membrane translocation of a GFP-AKT fusion protein (but not that of a GFP-AKT^{R25C} mutant that fails to translocate to phosphatidyl inositol-rich membranes),³⁶ and this effect was blocked by PPP (figure 3J,K). Of note, on i.p. injection into mice, PPP inhibited phosphorylation of IGF1, AKT and mTOR, P70^{S6K} and enhanced the abundance of LC3-II in the liver and in the heart (online supplemental figure S5A–K). LC3-II was also enhanced in the brain (online supplemental figure S5L,M). Altogether, these results indicate that PPP induces autophagy through the inhibition of IGF1R and its downstream signals AKT and MTORC1.

IGF1R activation as a negative prognostic factor in breast cancer

A paucity in LC3B puncta, reflecting disabled autophagy in malignant cells, is associated with dismal prognosis of breast cancer, as well as an unfavorable ratio of tumor infiltrating CD8⁺ cytotoxic T lymphocytes (CTLs) over FOXP3⁺ regulatory T cells (Tregs) or CD163⁺ tumor-associated macrophages (TAMs).^{12,37} In a series of 49 stage negative breast cancer patients treated by surgical resection (online supplemental table S1), the activating phosphorylation of IGF1R detectable by immunohistochemistry correlated negatively with the density of LC3 puncta and CD8⁺ CTLs but positively with FOXP3⁺ Tregs and CD163⁺ TAMs (figure 4A–E). Phosphorylation of IGF1R above the median level was associated with poor overall survival compared with low IGF1R phosphorylation (figure 4F). The risk stratification of breast cancer patients could be further improved by including the characteristics of the immune infiltrate. Thus, patients with phospho-IGF1R^{high} CD8^{low}, phospho-IGF1R^{high} FOXP3^{high} and phospho-IGF1R^{high} CD163^{high} breast cancer exhibited the worst overall survival (figure 4G–I). Altogether, these results indicate that activation of IGF1R signaling might affect autophagy as well as breast cancer immunosurveillance in a clinically relevant fashion. We, therefore, decided to evaluate the effects of IGF1 inhibitors on cancer immunosurveillance.

Immune response-amplifying effects of IGF1R inhibition

Autophagy induction can increase the immunogenicity of anthracycline or OXA-induced cell death by favoring the release of ATP.^{5,38} Accordingly, addition of PPP to U2OS cells enhanced the release of ATP from cells, causing a diminution of ATP-sensitive quinacrine fluorescence (figure 5A,B) and an increase in ATP concentrations in culture media in response to low-dose MTX. PPP similarly stimulated the release of ATP in response to low-dose OXA (online supplemental figure S6A,B). The low-dose chemotherapy-induced ATP release was inhibited by knockout of ATG5, knockout of eIF2α kinase 3 EIF2AK3 (best known as PERK, which is required for autophagy induction by MTX),²² the S51A knockin mutation in eIF2α that renders it unphosphorylatable (and blocks autophagy induction),^{22,39} as well as the expression of a constitutively active AKT mutant, AKT^{T308D/S473D} (figure 5C–F).

Considering the fact that PPP induced autophagy in mouse cancer cell lines (online supplemental figure S6C,D), we evaluated the capacity of PPP to improve the efficacy of chemioimmunotherapy against cutaneous MCA205 fibrosarcomas that were orthotopically implanted in histocompatible C57BL/6 mice. PPP alone did not reduce tumor growth. PPP failed to improve the efficacy of immunotherapy with PD-1 blockade, but improved that of chemotherapy with OXA. Moreover, the triple combination of OXA, PD-1 blockade and PPP was more efficient than

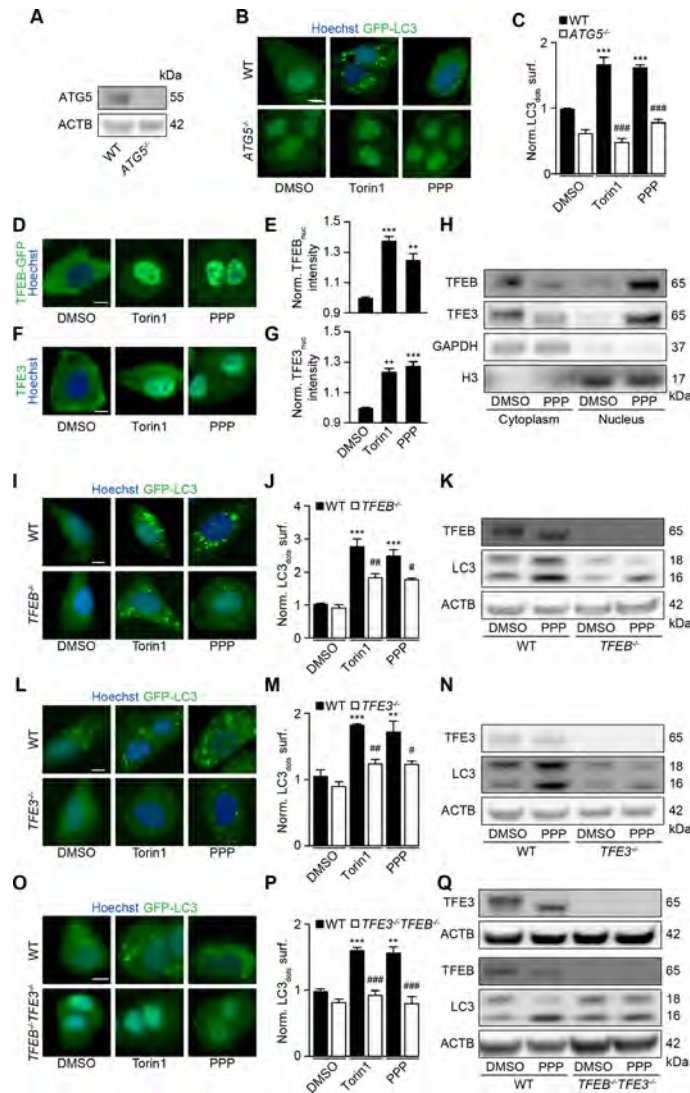


Figure 2 TFEB and TFE3 mediate PPP-induced autophagy. (A–C) U2OS-GFP-LC3 wild-type (WT) or ATG5 knockout cells were treated with PPP (10 μ M) or torin1 (300 nM) for 6 hours. Then the cells were fixed and GFP-LC3 dots were quantified. Scale bar equals 10 μ m. Data are means \pm SD of four replicates *** p <0.001 vs untreated control; ### P <0.001 vs WT; Tukey’s multiple comparisons test). (D, E) U2OS cells stably expressing GFP-TFEB fusion protein were treated with PPP (10 μ M) for 16 hours and torin1 was used as positive control. nuclear GFP intensities were measured (E) and representative images are shown in D. Scale bar equals 10 μ m. Data are means \pm SD of three replicates (** p <0.01, *** p <0.001 vs DMSO/Ctr, Student’s t-test). (F, G) U2OS cells were treated with PPP (10 μ M) for 16 hours and torin1 was used as positive control and then endogenous TFE3 translocation was assessed by immunostaining (F) and TFE3 nuclear intensities are depicted (G). Scale bar equals 10 μ m. Data are means \pm SD of three replicates (** p <0.01, *** p <0.001 vs DMSO/Ctr, Student’s t-test). (H) U2OS cells were treated with PPP (10 μ M) for 16 hours or were left untreated. Cytoplasmic and nuclear fractions were separated and assessed for nuclear translocation of TFEB and TFE3 by SDS-PAGE. band intensities of TFEB, TFE3, GAPDH and H3 were assessed and their ratio (TFEB or TFE3/GAPDH, and TFEB or TFE3/H3) was calculated (online supplemental figure S3). (I–Q) U2OS-GFP-LC3 cells WT or single as well as double knockout for TFEB and TFE3 were treated with PPP (10 μ M) or torin1 for 16 H. LC3 II expression and TFEB/TFE3 deficiency by knockout were checked by SDS-PAGE and parallel immunoblot (K, N, Q). Band intensities of LC3-II and β -actin (ACTB) were assessed, and their ratio (LC3-II/actin) was calculated (online supplemental figure S3). representative images are shown in (I, L, O), and GFP-LC3 dots were quantified as indicator of autophagy (J, M, P). Scale bar equals 10 μ m. Data are means \pm SD of four replicates (*** p <0.001 vs untreated control; # P <0.05, ## P <0.01, ### P <0.001 vs WT; Tukey’s multiple comparisons test). PPP, picropodophyllin SDS-PAGE, sodium dodecyl sulfate polyacrylamide gel electrophoresis.

chemoimmunotherapy with OXA and PD-1 blockade alone (figure 5H–I, online supplemental figure S7A). These effects depend on the immune system because no therapeutic efficacy could be measured in athymic nu/nu mice (that lack mature T lymphocytes) (figure 5J, online supplemental figure S7B).

Immunocompetent mice that had been cured from MCA205 fibrosarcoma by the triple combination (OXA, PD-1 blockade and PPP) were resistant against rechallenge with MCA205 cells but readily developed antigenically unrelated TC1 lung cancer, meaning that they developed immune memory (figure 5K,L).

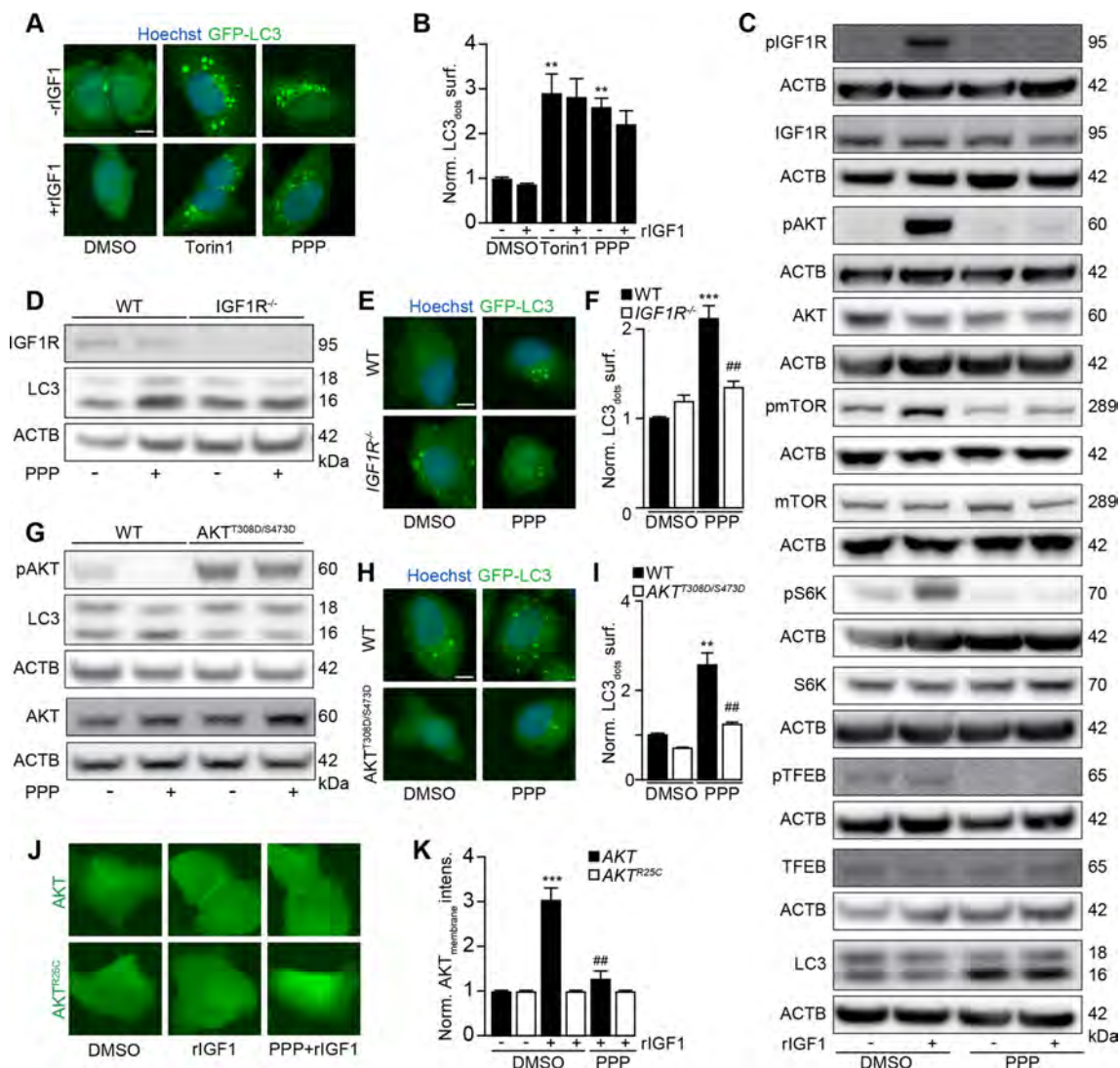


Figure 3 PPP induces autophagy via IGF1R/AKT signaling. (A, B) U2OS-GFP-LC3 cells were incubated in the absence of FBS overnight and were further treated with PPP (10 μ M) or torin1 (300 nm) in the presence or absence of IGF1 (10 nm) for 6 hours. After fixation, GFP-LC3 dots were quantified in B. Scale bar equals 10 μ m. Data are means \pm SD of three replicates (** P <0.01, vs DMSO/Ctr, Student's t-test). (C) Immunoblot exploration of the IGF1R signal pathway. After U2OS cells were incubated in the absence of FBS overnight, then the cells were treated with PPP (10 μ M) together with or without IGF1 (10 nm) for 6 hours. Proteins were separated by SDS-PAGE and parallel immunoblots of pIGF1R (Tyr1135/1136), IGF1R, pAkt (Ser473), Akt, pmTOR (Ser2448), mTOR, pp70 (THR389), p70, pTFEB (Ser211), TFEB, LC3-II and were performed in parallel instances and β -actin (ACTB) was used as loading control (C). (D, E) U2OS wild-type (WT) or IGF1R knockout cells were treated with PPP (10 μ M) for 6 H. SDS-PAGE and immunoblots of IGF1R, LC3 and ACTB were performed (D), band intensities of LC3-II and ACTB were assessed, and their ratio (LC3-II/ACTB) was calculated (online supplemental figure S4). In parallel U2OS-GFP-LC3 WT or IGF1R knockout cells were treated with PPP (10 μ M) for 6 hours then the cells were fixed and GFP-LC3 dots were quantified by microscopy (F). Representative images are shown in E and scale bar equals 10 μ m. Data are means \pm SD of three replicates (** P <0.001 vs untreated control; ## P <0.01 vs WT; Tukey's multiple comparisons test). (G–I) U2OS cells were transfected with constitutive active AKT^{T308D/S473D} and were treated with PPP (10 μ M) for 6 hours. SDS-PAGE and immunoblots of pAKT, AKT, LC3 and ACTB were performed (G), band intensities of LC3-II and ACTB were assessed, and their ratio (LC3-II/ACTB) was calculated (online supplemental figure S4). In parallel U2OS-GFP-LC3 WT or AKT^{T308D/S473D}-expressing cells were treated with PPP (10 μ M) for 6 H then the cells were fixed and GFP-LC3 dots were quantified by microscopy (I). Representative images are shown in H and scale bar equals 10 μ m. Data are means \pm SD of three replicates (** P <0.01 vs untreated control; ## P <0.01 vs WT; Tukey's multiple comparisons test). (J–K) U2OS cells stably expressing GFP-AKT or GFP-AKT^{R25C} were incubated in absence of FBS overnight, then the cells were treated with IGF1 (10 nm) or PPP (10 μ M) combined with IGF1 (10 nm). After 5 min, the membrane translocation of GFP-AKT was detected by microscopy (J) and the membrane intensity of AKT was measured (K). Scale bar equals 10 μ m. Data are means \pm SD of three replicates (** P <0.001 vs DMSO/Ctr, Student's t-test). IGF1, FBS, fetal bovine serum; IGF1, insulin-like growth factor-1; PPP, picropodophyllin; SDS_PAGE, sodium dodecyl sulfate polyacrylamide gel electrophoresis.

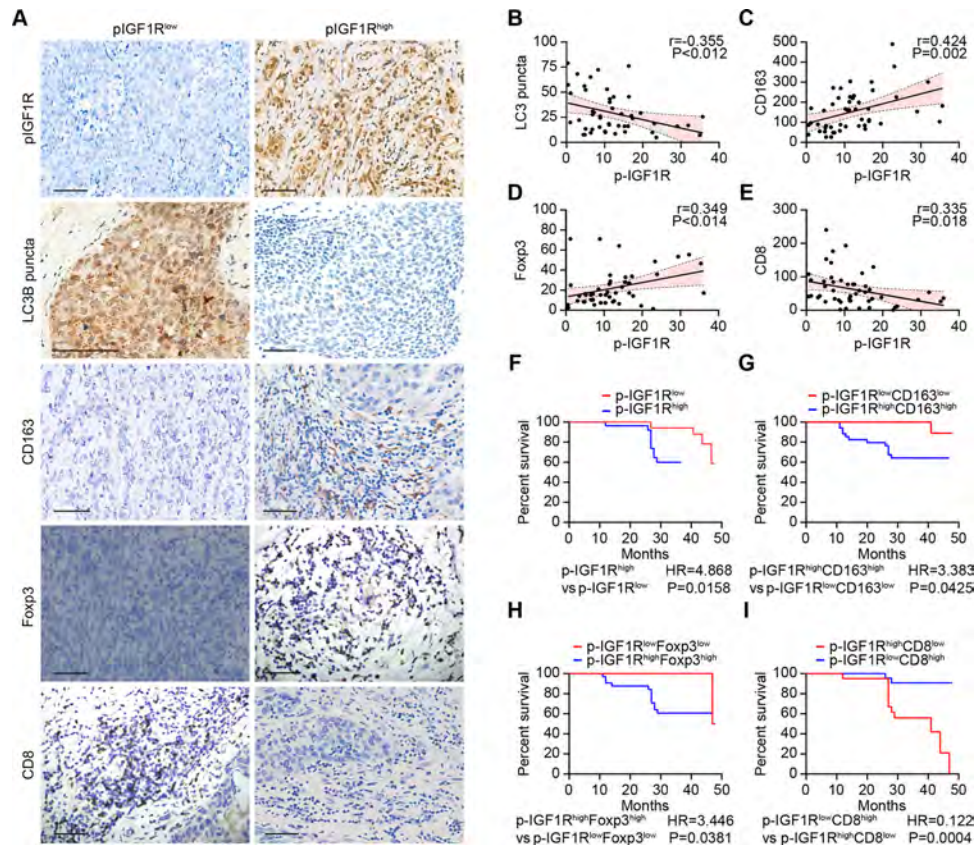


Figure 4 IGF1R signaling correlates with immunosuppressive markers and decreased survival in breast cancer. (A–I) The expression of CD163, FOXP3 and CD8 as well as the phosphorylation of IGF1R and the dot formation of LC3 were quantified in paraffin-embedded biopsies obtained from 49 triple-negative breast cancer patients by ImageJ after staining with specific antibodies. Representative images of phosphorylated-IGF1R, dotted LC3B, and CD163, FOXP3 and CD8 expression are shown in A. The scale bar indicates 100 μ m. Correlation analyses (determined by the Spearman method) of the analyzed parameters for each patient are depicted in B–E. (F–I) Kaplan-Meier survival analysis of patients with biomarker-positive and biomarker-negative immunohistochemistry staining. IGF1R, insulin-like growth factor-1 receptor.

Inhibition of PPP-induced autophagy by AKT^{T308D/S473D} or knockout of *Atg5*, as well as the expression of the ecto-ATPase CD39 abolished the anticancer effects of PPP (figure 5M–O, online supplemental figure S7C–E), supporting the involvement of autophagy-dependent ATP release in PPP effects. PPP did not affect the MCA205 tumor immune infiltrate on its own, but did reduce PD-1 induction by OXA on CD8⁺ T cells (figure 5P–R). Moreover, the combination of PP OXA depleted Tregs from the tumor environment (online supplemental figure 5S) and improved the CD8/Treg ratio (figure 5T).

These immune response-associated effects of IGF1R inhibition were also observed for TC1 non-small cell lung cancer, in which PPP similarly improved the effects of OXA or those of an OXA+ anti-PD-1 combination (figure 6A–C, online supplemental figure S7F). Of note, survival of mice with TC1 cancers was similarly extended by PPP +OXA and PPP +OXA+anti-PD-1 (online supplemental figure S7F). Mice that had been ridden from their TC1 tumors became resistant against rechallenge with the same tumor but not MCA205 fibrosarcomas (figure 6D,E). In mice-bearing AT3 breast cancers, PPP also improve the effects of

OXA +PD-1 blockade (online supplemental figure S6E–G, S7G). Moreover, PPP could be replaced by another IGF1R antagonist, linsitinib, to ameliorate the outcome of chemotherapy with OXA or a combined OXA +anti-PD-1 regimen (figure 6F–H, online supplemental figure S7H). The triple combination (OXA +anti-PD-1+linsitinib) induced several complete remissions as well as immune memory against the tumors that had been eliminated (figure 6I,J). These results underscore the capacity of IGF1R antagonist to enhance the efficacy of chemoimmunotherapy in preclinical models.

DISCUSSION

Together with the insulin receptor, IGF1R is one of the most important trophic receptor tyrosine kinases, stimulating the uptake of nutrients into cells as well as a variety of anabolic reactions.⁴⁰ Inhibition of IGF1R itself or that of the signal transduction cascade acting downstream of IGF1R (the PI3K/AKT/MTOR pathway) potently stimulates autophagy as well as other stress-adaptive mechanisms.^{41–43} Indeed, a vast literature suggests that chronic inhibition of this pathway by caloric restriction,

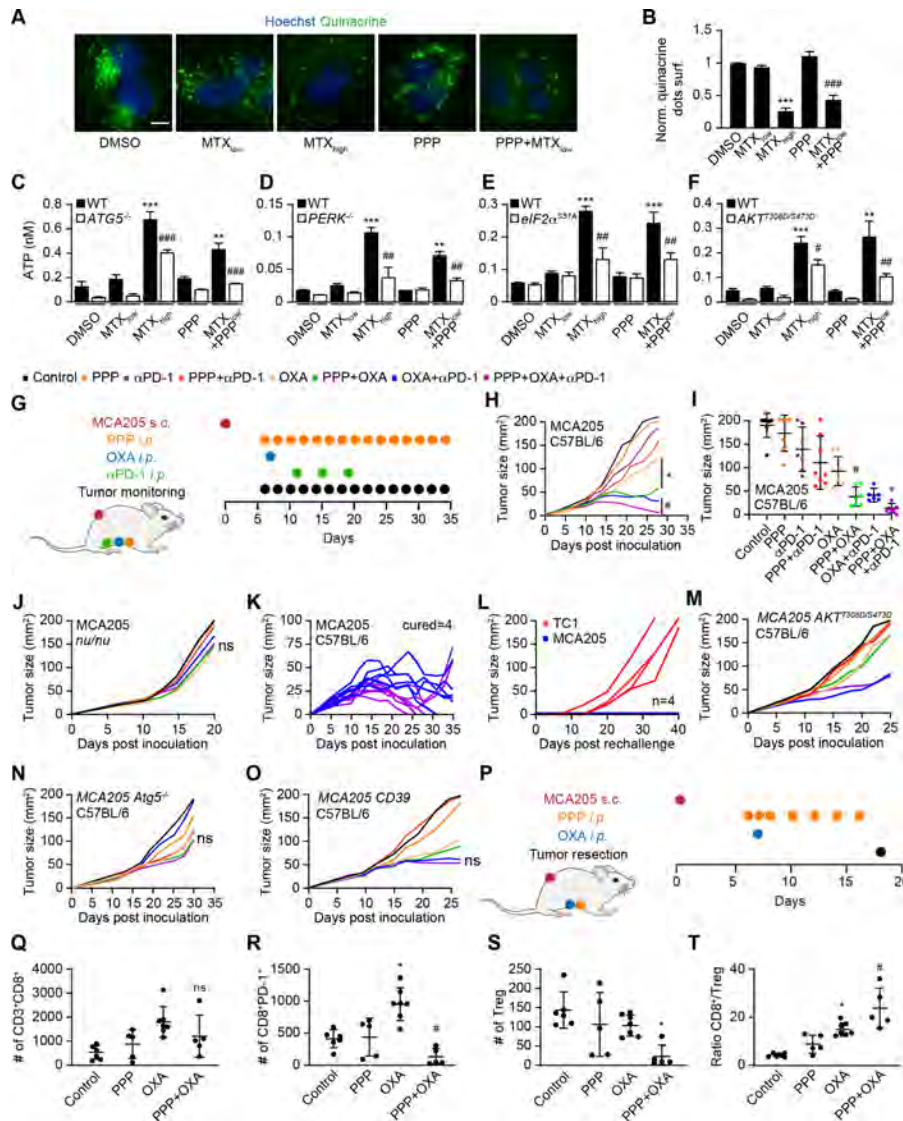


Figure 5 PPP improves autophagy-dependent anticancer chemotherapy in a T lymphocyte-dependent manner. (A, B) Human osteosarcoma cells were treated with PPP (10 μ M) in the presence of a low dose of the ICD inducers mitoxantrone (MTX, 1 μ M) for 6 hours. High-dose MTX (5 μ M) was used as positive controls. Quinacrine staining was used to monitor intracellular ATP content. Representative images are shown in A and quinacrine dots were quantified in B. Scale bar equals 10 μ m. Data are means \pm SD of three replicates (** p <0.001 vs untreated control; ### p <0.001 vs PPP; Tukey's multiple comparisons test). (C–F) Human neuroglioma H4 cells wild-type or Atg5 knockout, human osteosarcoma U2OS wild type, PERK knockout or PEIF2 α S51A knockin cells, murine fibrosarcoma MCA205 wild-type or AKT^{T308D/S473D} knockin cells were treated with PPP (10 μ M) alone or in combination with low doses of the ICD inducers MTX (1 μ M) for 6 H as described above. High-dose MTX (5 μ M) was used as positive controls. The extracellular ATP levels were measured in C–F. Data are means \pm SD of three replicates (** P <0.01, *** P <0.001 vs untreated control; # P <0.05, ## P <0.01, ### P <0.001 vs WT; Tukey's multiple comparisons test). (G–O) In vivo treatment of implanted murine MCA205 fibrosarcoma with oxaliplatin (OXA), anti-PD-1 antibody and PPP, alone or in combination (schematic view in G). (H, I) Growth kinetic of murine fibrosarcoma MCA205 cells evolving in immunocompetent C57BL/6 mice or athymic nu/nu mice (J) or MCA205 fibrosarcoma expressing constitutive active AKT^{T308D/S473D} (M), Atg5 deficient MCA205 ATG5^{-/-} (N) or MCA205 expressing the ectoATPase CD39 (O) evolving in immunocompetent C57BL/6 mice were treated as indicated in (G). When tumors became palpable, mice received systemic intraperitoneal (i.p.) injections of ppp alone or together with OXA or PD-1 blocker. Data are depicted as growth curves (mean \pm SD) (H, L–O) and tumor size distributions at day 24 (I). Individual tumor growth curves of mice treated with OXA and PPP, combined or not with PD-1 blockade are shown (K). The generation of immunological memory was assessed in cured animals by rechallenge with MCA205 and TC-1. Individual tumor growth curves are depicted (L). Data were analyzed with TumGrowth. $n \geq 6$ for mice in each group. (* P < 0.05 or ns, not statistically significant vs OXA; # P <0.05 or ns, not statistically significant vs OXA+PD-1 blockade, Student's t-test, survival plots in online supplemental figure S7). (P) Schematic overview of the treatment of implanted murine MCA205 fibrosarcoma with OXA and PPP, alone or in combination. (P–T) Cytofluorometric analysis of tumor-infiltrating lymphocytes (TIL): CD3⁺CD8⁺ cytotoxic T lymphocytes (Q), CD8⁺PD-1⁺ T lymphocytes (R), CD4⁺FOXP3⁺CD25⁺ regulatory T cells (Treg) (S), and the ratio of CD3⁺CD8⁺ T cells over Treg (T). Data are means \pm SD ($n \geq 5$) (* p <0.05 or ns, not statistically significant vs control; # P <0.05 or ns, not statistically significant vs OXA, Student's t-test). PPP, picropodophyllin.

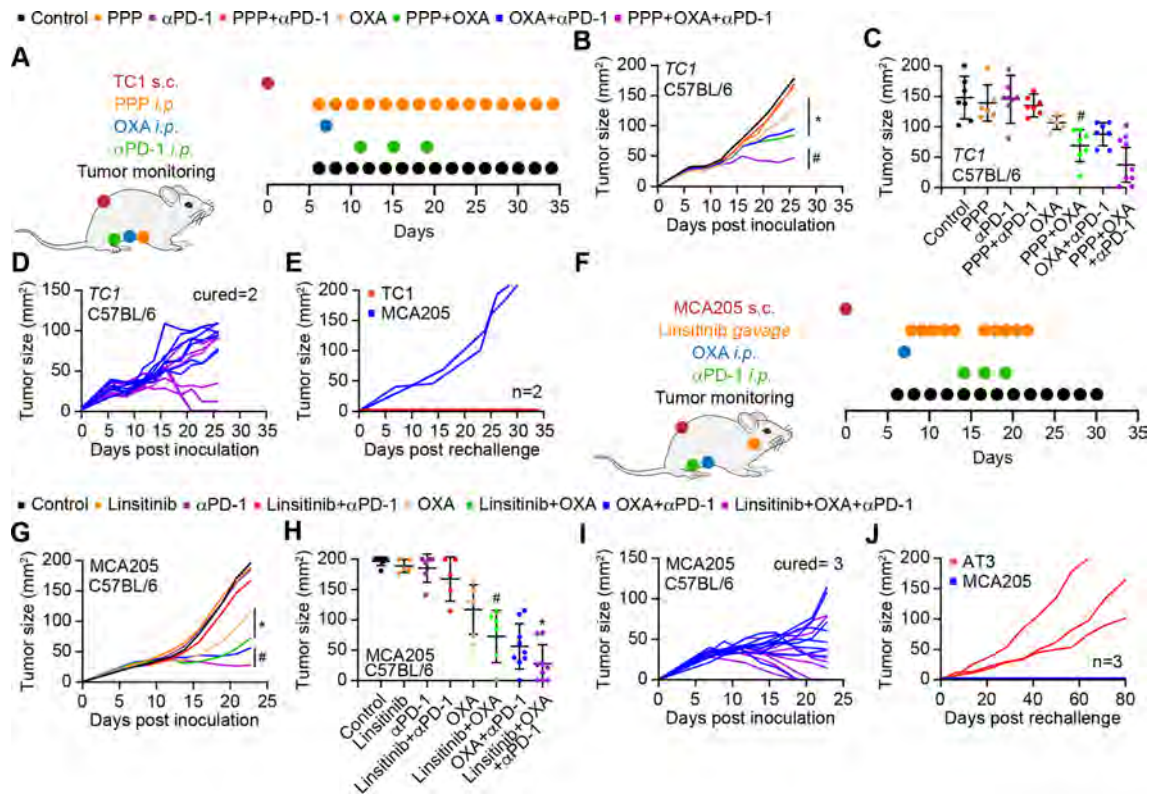


Figure 6 IGF1R inhibition improves the anticancer efficacy of immunotherapy. (A) Schematic overview of the in vivo treatment of murine lung cancer Tc1 cells with oxaliplatin (OXA), anti-PD-1 antibody and PPP, alone or in combination. (B–E) Growth kinetic of Tc1 cells evolving in immunocompetent C57BL/6 mice, treated as indicated in (A). When tumors became palpable, mice received systemic intraperitoneal injection of PPP alone or together with OXA or PD-1 blocker. Data are depicted as (B) growth curves (mean±SD); (C) tumor size distributions at day 24; (D) individual tumor growth curves of mice treated with OXA and PPP, combined or not with PD-1 blockade. The generation of immunological memory was assessed in cured animals by rechallenge with MCA205 and Tc1. Individual tumor growth curves are depicted (E). Data were analyzed with TumGrowth. $n \geq 6$ for mice in each group. (* $P < 0.05$ or ns, not statistically significant vs OXA; # $P < 0.05$ or ns, not statistically significant vs OXA+PD-1 blocker, Student's t-test, survival plots in online supplemental figure S7). (F) Schematic overview of the in vivo treatment of murine fibrosarcoma MCA205 cells with OXA, anti-PD-1 antibody and the selective IGF1R inhibitor linsitinib (Lins), alone or in combination. IGF1R, insulin-like growth factor-1 receptor; PPP, picropodophyllin.

pharmacological inhibitors or loss-of-function mutations has the capacity to extend the healthspan and lifespan in model organisms^{3,44–46} and perhaps in humans as well.⁴⁷

Here, we identified a pharmacological IGF1R inhibitor, PPP, as a potent inducer of autophagic flux that acts on-target, as suggested by several observations. First, PPP inhibited all elements of the signaling cascading, hence reducing the activating phosphorylation of IGF1R, AKT and the MTOR substrate S6K, both in vitro, in cultured human cell lines and in vivo, in the liver and heart from mice, commensurate with the induction of autophagy. Second, PPP lost its capacity to induce autophagy after knockout of IGF1R, which obliges the cells to rewire their metabolism to support by other trophic receptors.^{48,49} Third, most convincingly, artificial activation of the inhibited cascade by expressing a transgene-encoded constitutively active AKT mutant, abolished autophagy induction by PPP. These results unequivocally demonstrate that PPP is activating autophagy through a specific mode of action, without major off-target effects. Of note, as for other autophagy inducers,^{22,50–52} this pathway involved the obligatory phosphorylation of eIF2 α as part of the

integrated stress response. Thus, cells bearing a non-phosphorylatable eIF2 α mutant or lacking the eIF2 α kinase EIF2AK3/PERK were unable to activate the autophagic pathway in response to PPP.

Stimulation of autophagy by fasting or by the administration of CRMs enhances the efficacy of immunogenic chemotherapies (for instance with anthracyclines and OXA) as well as combination regimens of chemotherapies with immune checkpoint inhibitors targeting PD-1.^{5,19,53,54} Accordingly, we found that PPP enhanced the efficacy of anticancer chemotherapies with MTX and OXA, alone or in combination with PD-1 blocking antibodies. PPP on its own had little or no tumor growth inhibitory effects against MCA205 fibrosarcomas, TC1 non-small cell lung cancers and AT3 triple-negative breast cancer. The anticancer effects of PPP were only detectable in combination with chemoimmunotherapy and were lost in tumors that lacked essential genes/proteins involved in the autophagic process (due to knockout of ATG5 or knock-in mutation of eIF2 α) or were rendered

resistant to PPP (by transfection with constitutively active AKT). Moreover, these anticancer effects were accompanied by an increased infiltration of tumors by CTLs together with improvement in the local CTL/Treg ratio, and were lost in immunodeficient mice lacking mature T lymphocytes. Of note, it appears that the autophagy-dependent increase in extracellular ATP from tumor cells³⁸ plays a rate-limiting role in the therapeutic efficacy of PPP, which indeed was lost when cancer cells were genetically manipulated to express the ATP-degrading enzyme CD39 on their surface. Importantly, in one tumor model (TC1), PPP improved the outcome of OXA-based chemotherapy, and this effect was not further improved by PD-1 blockade. This might prove therapeutically relevant in situations where anti-PD-1 cannot be administered.

PPP could be replaced by another IGF1R inhibitor, linsitinib, which has undergone evaluation in clinical trials.^{55–57} Linsitinib increased the efficacy of immunochemotherapy in mice, suggesting that this type of clinical grade IGF1R inhibitor should be evaluated in patients for similar combination effects. Indeed, linsitinib has been administered to patients with cancer either alone^{55–57} or in combination with other anticancer agents thought to mediate direct effects on cancer cells such as the MTORC1 inhibitor everolimus,⁵⁸ the EGFR inhibitor erlotinib⁵⁹ or the chemotherapeutics paclitaxel⁶⁰ and irinotecan,⁶¹ with variable results. However, linsitinib has not been investigated for its potential immune effects and has not been combined with any kind of immunotherapy including PD-1 blockade.

At the clinical level, we observed that the activating phosphorylation of IGF1R detectable by immunohistochemistry correlated with a reduction of LC3B-positive puncta in triple-negative breast cancer patients. This IGF1R phosphorylation also correlated with poor local immunosurveillance as indicated by scarce infiltration by CD8⁺ CTLs but high abundance of FOXP3⁺ regulatory T cells and immunosuppressive CD163⁺ macrophages infiltrating the tumors, as well as dismal prognosis. These results confirm the negative effects of IGF1R signaling on immunosurveillance and disease control in breast cancer patients. A recent report on patients with colorectal cancer treated with chemotherapy together with EGFR or VEGF inhibitor revealed that overactivation of the IGF1R also constitutes a poor prognostic factor, particularly in patients bearing RAS wild-type tumors.⁶² These findings echo prior observations that high expression of IGF1R (though without proof of its activation) is a poor prognostic biomarker in gastric⁶³ and breast cancer.¹

In conclusion, excessive antiautophagic signaling via IGF1R has a major negative effect on anticancer immunosurveillance, thus reducing patient prognosis. However, IGF1R and its downstream signals are amenable to pharmacological inhibition and subsequent improvement of cancer control by the immune

system. These considerations should be incorporated into the future design of clinical trials in which inhibition of the IGF1R/PI3K/AKT/MTOR pathway will be combined with adequate immunostimulation with ICD inducers and/or immune checkpoint inhibitors.

Author affiliations

- ¹Department of Breast and Thyroid Surgery, Renmin Hospital of Wuhan University, Wuhan, Hubei, China
- ²Centre de Recherche des Cordeliers, Equipe labellisée par la Ligue contre le cancer, Université de Paris, Sorbonne Université, Inserm U1138, Institut Universitaire de France, Paris, France
- ³Metabolomics and Cell Biology Platforms, Gustave Roussy Cancer Center, Université Paris Saclay, Villejuif, France
- ⁴Faculty of Medicine, Université Paris Saclay, Kremlin Bicêtre, France
- ⁵Department of Pathology, Renmin Hospital of Wuhan University, Wuhan, Hubei, China
- ⁶Samsara Therapeutics Ltd, Oxford, UK
- ⁷Institute of Molecular Biosciences, NAWI Graz, University of Graz, Graz, Austria
- ⁸BioTechMed-Graz, Graz, Austria
- ⁹Field of Excellence BioHealth, University of Graz, Graz, Austria
- ¹⁰Suzhou Institute for Systems Medicine, Chinese Academy of Medical Sciences, Suzhou, Jiangsu, China
- ¹¹Pôle de Biologie, Hôpital Européen Georges Pompidou, AP-HP, Paris, France
- ¹²Karolinska Institutet, Department of Women's and Children's Health, Karolinska University Hospital, Stockholm, Sweden

Acknowledgements We are grateful to the support of the Gustave Roussy, Université Paris-Saclay, Plateforme Imagerie et Cytométrie (PFIC), UMS AMMICA INSERM US23-CNRS 3655.

Contributors QW, A-LT and BL performed most of the experiments; QW, A-LT and WX performed in vivo experiments, ML, SF, PH and WG conceived and performed the large chemical drug screen, FM, YT, OK and GK conceived the study; PL, LZ, SZ and HP designed (parts of) the study; OK and GK wrote the paper.

Funding QW, A-LT, WX and HP were supported by the Chinese scholarship council. OK receives funding by the Île de France DIM ELICIT initiative. This work was partially supported by a Natural Science Foundation of Hubei grant (Grant No: 2020CFA026) to YT. GK is supported by the Ligue contre le Cancer (équipe labellisée); Agence National de la Recherche (ANR)—Projets blancs; AMMICA US23/CNRS UMS3655; Association pour la recherche sur le cancer (ARC); Association 'Ruban Rose'; Cancéropôle Ile-de-France; Fondation pour la Recherche Médicale (FRM); a donation by Elior; Equipex Onco-Pheno-Screen; European Joint Programme on Rare Diseases (EJPRD); Gustave Roussy Odyssey, the European Union Horizon 2020 Projects Oncobiome and Crimson; Fondation Carrefour; High-end Foreign Expert Program in China (GDW20171100085), Institut National du Cancer (INCa); Inserm (HTE); Institut Universitaire de France; LabEx Immuno-Oncology (ANR-18-IDEX-0001); the RHU Torino Lumière; Seerave Foundation; SIRIC Stratified Oncology Cell DNA Repair and Tumor Immune Elimination (SOCRATE); and SIRIC Cancer Research and Personalized Medicine (CARPEM). This study contributes to the IdEx Université de Paris ANR-18-IDEX-0001. FM is grateful to the Austrian Science Fund FWF (SFB LIPOTOX F3007 and F3012, W1226, P29203, P29262, P27893, P31727) and the Austrian Federal Ministry of Education, Science and Research as well as the University of Graz for grants 'Unkonventionelle Forschung-InterFast and Fast4Health' as well as 'flysleep' (BMWFW-80.109/0001-WF/V/3b/2015). We acknowledge the support of the field of excellence BioHealth, of NAWI Graz and the BioTechMed-Graz flagship project "EPIAge".

Competing interests PH and WG are full-time employees of Samsara Therapeutics. GK, FM and OK are cofounders of Samsara Therapeutics.

Patient consent for publication Not required.

Ethics approval All patients included in the study wrote the informed consent, approved by the Institutional Ethics Committee of the Renmin Hospital of Wuhan University (approval no. 2018K-C09). Animal experiments were conducted in compliance with the European Union (EU) Directive 63/2010 and protocols 2019_030_20590 and were approved by the Ethical Committee of the Gustave Roussy Campus Cancer (CEEA IRCIV/IGR no. 26, registered at the French Ministry of Research).

Provenance and peer review Not commissioned; externally peer reviewed.

Data availability statement Data are available on reasonable request. All data relevant to the study are included in the article or uploaded as online supplemental information. All data supporting the findings of this study are available within the article and its online supplemental information files and from the corresponding author on reasonable request.

Supplemental material This content has been supplied by the author(s). It has not been vetted by BMJ Publishing Group Limited (BMJ) and may not have been peer-reviewed. Any opinions or recommendations discussed are solely those of the author(s) and are not endorsed by BMJ. BMJ disclaims all liability and responsibility arising from any reliance placed on the content. Where the content includes any translated material, BMJ does not warrant the accuracy and reliability of the translations (including but not limited to local regulations, clinical guidelines, terminology, drug names and drug dosages), and is not responsible for any error and/or omissions arising from translation and adaptation or otherwise.

Open access This is an open access article distributed in accordance with the Creative Commons Attribution Non Commercial (CC BY-NC 4.0) license, which permits others to distribute, remix, adapt, build upon this work non-commercially, and license their derivative works on different terms, provided the original work is properly cited, appropriate credit is given, any changes made indicated, and the use is non-commercial. See <http://creativecommons.org/licenses/by-nc/4.0/>.

ORCID iD

Oliver Kepp <http://orcid.org/0000-0002-6081-9558>

REFERENCES

- de Groot S, Charehbili A, van Laarhoven HWM, *et al.* Insulin-like growth factor 1 receptor expression and IGF1R 3129G>T polymorphism are associated with response to neoadjuvant chemotherapy in breast cancer patients: results from the NEOZOTAC trial (BOOG 2010-01). *Breast Cancer Res* 2016;18:3.
- Ho CJ, Samarasekera G, Rothe K, *et al.* Puncta intended: connecting the dots between autophagy and cell stress networks. *Autophagy* 2021;17:1–6.
- Hansen M, Rubinsztein DC, Walker DW. Autophagy as a promoter of longevity: insights from model organisms. *Nat Rev Mol Cell Biol* 2018;19:579–93.
- López-Otín C, Kroemer G. Hallmarks of health. *Cell* 2021;184:33–63.
- Pietrocola F, Pol J, Vacchelli E, *et al.* Caloric restriction mimetics enhance anticancer immunosurveillance. *Cancer Cell* 2016;30:147–60.
- Rubinsztein DC, Codogno P, Levine B. Autophagy modulation as a potential therapeutic target for diverse diseases. *Nat Rev Drug Discov* 2012;11:709–30.
- Galluzzi L, Pietrocola F, Bravo-San Pedro JM, *et al.* Autophagy in malignant transformation and cancer progression. *Embo J* 2015;34:856–80.
- Santana-Codina N, Mancias JD, Kimmelman AC. The role of autophagy in cancer. *Annu Rev Cancer Biol* 2017;1:19–39.
- Hewitt G, Korolchuk VI. Repair, reuse, recycle: the expanding role of autophagy in genome maintenance. *Trends Cell Biol* 2017;27:340–51.
- Cassidy LD, Young ARJ, Young CNJ, *et al.* Temporal inhibition of autophagy reveals segmental reversal of ageing with increased cancer risk. *Nat Commun* 2020;11:307.
- Wang Y, Xiong H, Liu D, *et al.* Autophagy inhibition specifically promotes epithelial-mesenchymal transition and invasion in Ras-mutated cancer cells. *Autophagy* 2019;15:886–99.
- Ladoire S, Penault-Llorca F, Senovilla L, *et al.* Combined evaluation of LC3B puncta and HMGB1 expression predicts residual risk of relapse after adjuvant chemotherapy in breast cancer. *Autophagy* 2015;11:1878–90. doi:10.1080/15548627.2015.1082022
- Amaravadi R, Kimmelman AC, White E. Recent insights into the function of autophagy in cancer. *Genes Dev* 2016;30:1913–30.
- Rosenfeldt MT, O'Prey J, Morton JP, *et al.* P53 status determines the role of autophagy in pancreatic tumour development. *Nature* 2013;504:296–300.
- Karasic TB, O'Hara MH, Loaiza-Bonilla A, *et al.* Effect of gemcitabine and nab-paclitaxel with or without hydroxychloroquine on patients with advanced pancreatic cancer: a phase 2 randomized clinical trial. *JAMA Oncol* 2019;5:993–8.
- Yamamoto K, Venida A, Yano J, *et al.* Autophagy promotes immune evasion of pancreatic cancer by degrading MHC-I. *Nature* 2020;581:100–5.
- Chen G, Xie W, Nah J, *et al.* 3,4-Dimethoxychalcone induces autophagy through activation of the transcription factors TFE3 and TFE8. *EMBO Mol Med* 2019;11:e10469.
- Vodnala SK, Eil R, Kishton RJ, *et al.* T cell stemness and dysfunction in tumors are triggered by a common mechanism. *Science* 2019;363. doi:10.1126/science.aau0135. [Epub ahead of print: 29 Mar 2019].
- Lévesque S, Le Naour J, Pietrocola F, *et al.* A synergistic triad of chemotherapy, immune checkpoint inhibitors, and caloric restriction mimetics eradicates tumors in mice. *Oncoimmunology* 2019;8:e1657375.
- Ma Y, Adjemian S, Mattarollo SR, *et al.* Anticancer chemotherapy-induced intratumoral recruitment and differentiation of antigen-presenting cells. *Immunity* 2013;38:729–41.
- Wang Y, Xie W, Humeau J, *et al.* Autophagy induction by thiostrepton improves the efficacy of immunogenic chemotherapy. *J Immunother Cancer* 2020;8.
- Humeau J, Leduc M, Cerrato G, *et al.* Phosphorylation of eukaryotic initiation factor-2 α (eIF2 α) in autophagy. *Cell Death Dis* 2020;11:433.
- Bezu L, Sauvat A, Humeau J, *et al.* eIF2 α phosphorylation is pathognomonic for immunogenic cell death. *Cell Death Differ* 2018;25:1375–93.
- Pietrocola F, Castoldi F, Markaki M, *et al.* Aspirin recapitulates features of caloric restriction. *Cell Rep* 2018;22:2395–407.
- Sauvat A, Wang Y, Segura F, *et al.* Quantification of cellular viability by automated microscopy and flow cytometry. *Oncotarget* 2015;6:9467–75.
- Varghese F, Bukhari AB, Malhotra R, *et al.* Ihc Profiler: an open source plugin for the quantitative evaluation and automated scoring of immunohistochemistry images of human tissue samples. *PLoS One* 2014;9:e96801.
- Enot DP, Vacchelli E, Jacquilot N, *et al.* TumGrowth: an open-access web tool for the statistical analysis of tumor growth curves. *Oncoimmunology* 2018;7:e1462431.
- Kepp O, Chen G, Carmona-Gutierrez D, *et al.* A discovery platform for the identification of caloric restriction mimetics with broad health-improving effects. *Autophagy* 2020;16:188–9.
- Girnita A, Girnita L, del Prete F, *et al.* Cyclolignans as inhibitors of the insulin-like growth factor-1 receptor and malignant cell growth. *Cancer Res* 2004;64:236–42.
- Vasilcanu D, Girnita A, Girnita L, *et al.* The cyclolignan ppp induces activation loop-specific inhibition of tyrosine phosphorylation of the insulin-like growth factor-1 receptor. link to the phosphatidylinositol-3 kinase/Akt apoptotic pathway. *Oncogene* 2004;23:7854–62.
- Girnita A, All-Ericsson C, Economou MA, *et al.* The insulin-like growth factor-I receptor inhibitor picropodophyllin causes tumor regression and attenuates mechanisms involved in invasion of uveal melanoma cells. *Clin Cancer Res* 2006;12:1383–91.
- Wu X, Sooman L, Wickström M, *et al.* Alternative cytotoxic effects of the postulated IGF-IR inhibitor picropodophyllin in vitro. *Mol Cancer Ther* 2013;12:1526–36.
- Tarnowski M, Tkacz M, Zgutka K, *et al.* Picropodophyllin (ppp) is a potent rhabdomyosarcoma growth inhibitor both in vitro and in vivo. *BMC Cancer* 2017;17:532.
- Bergqvist M, Holgersson G, Bondarenko I, *et al.* Phase II randomized study of the IGF-1R pathway modulator AXL1717 compared to docetaxel in patients with previously treated, locally advanced or metastatic non-small cell lung cancer. *Acta Oncol* 2017;56:441–7.
- Berndt N, Yang H, Trinczek B, *et al.* The Akt activation inhibitor TCN-P inhibits Akt phosphorylation by binding to the pH domain of Akt and blocking its recruitment to the plasma membrane. *Cell Death Differ* 2010;17:1795–804.
- Balla T, Várnai P. Visualizing cellular phosphoinositide pools with GFP-fused protein-modules. *Sci STKE* 2002;2002:pl3.
- Ladoire S, Enot D, Senovilla L, *et al.* The presence of LC3B puncta and HMGB1 expression in malignant cells correlate with the immune infiltrate in breast cancer. *Autophagy* 2016;12:864–75.
- Michaud M, Martins I, Sukkurwala AQ, *et al.* Autophagy-Dependent anticancer immune responses induced by chemotherapeutic agents in mice. *Science* 2011;334:1573–7.
- Shen S, Niso-Santano M, Adjemian S, *et al.* Cytoplasmic STAT3 represses autophagy by inhibiting PKR activity. *Mol Cell* 2012;48:667–80.
- Thompson CB, Bielska AA. Growth factors stimulate anabolic metabolism by directing nutrient uptake. *J Biol Chem* 2019;294:17883–8.
- Gu Y, Wang C, Cohen A. Effect of IGF-1 on the balance between autophagy of dysfunctional mitochondria and apoptosis. *FEBS Lett* 2004;577:357–60.

- 42 Troncoso R, Vicencio JM, Parra V, *et al.* Energy-preserving effects of IGF-1 antagonize starvation-induced cardiac autophagy. *Cardiovasc Res* 2012;93:320–9.
- 43 Galluzzi L, Pietrocola F, Levine B, *et al.* Metabolic control of autophagy. *Cell* 2014;159:1263–76.
- 44 Fontana L, Partridge L, Longo VD. Extending healthy life span—from yeast to humans. *Science* 2010;328:321–6.
- 45 López-Otin C, Galluzzi L, Freije JMP, *et al.* Metabolic control of longevity. *Cell* 2016;166:802–21.
- 46 Leidal AM, Levine B, Debnath J. Autophagy and the cell biology of age-related disease. *Nat Cell Biol* 2018;20:1338–48.
- 47 Vitale G, Pellegrino G, Vollery M, *et al.* Role of IGF-1 system in the modulation of longevity: controversies and new insights from a centenarians' perspective. *Front Endocrinol* 2019;10:27.
- 48 Lee C, Raffaghello L, Longo VD. Starvation, detoxification, and multidrug resistance in cancer therapy. *Drug Resist Updat* 2012;15:114–22.
- 49 Emdal KB, Pedersen A-K, Bekker-Jensen DB, *et al.* Integrated proximal proteomics reveals Irs2 as a determinant of cell survival in ALK-driven neuroblastoma. *Sci Signal* 2018;11. doi:10.1126/scisignal.aap9752. [Epub ahead of print: 20 Nov 2018].
- 50 Tallóczy Z, Jiang W, Virgin HW, *et al.* Regulation of starvation- and virus-induced autophagy by the eIF2alpha kinase signaling pathway. *Proc Natl Acad Sci U S A* 2002;99:190–5.
- 51 Kroemer G, Mariño G, Levine B. Autophagy and the integrated stress response. *Mol Cell* 2010;40:280–93.
- 52 Wengrod JC, Gardner LB. Cellular adaptation to nutrient deprivation: crosstalk between the mTORC1 and eIF2 α signaling pathways and implications for autophagy. *Cell Cycle* 2015;14:2571–7.
- 53 Wu Q, Tian A-L, Durand S, *et al.* Isobacachalcone induces autophagy and improves the outcome of immunogenic chemotherapy. *Cell Death Dis* 2020;11:1015.
- 54 Castoldi F, Humeau J, Martins I, *et al.* Autophagy-Mediated metabolic effects of aspirin. *Cell Death Discov* 2020;6:129.
- 55 Jones RL, Kim ES, Nava-Parada P, *et al.* Phase I study of intermittent oral dosing of the insulin-like growth factor-1 and insulin receptors inhibitor OSI-906 in patients with advanced solid tumors. *Clin Cancer Res* 2015;21:693–700.
- 56 Fassnacht M, Berruti A, Baudin E, *et al.* Linsitinib (OSI-906) versus placebo for patients with locally advanced or metastatic adrenocortical carcinoma: a double-blind, randomised, phase 3 study. *Lancet Oncol* 2015;16:426–35.
- 57 von Mehren M, George S, Heinrich MC, *et al.* Linsitinib (OSI-906) for the treatment of adult and pediatric wild-type gastrointestinal stromal tumors, a sarc phase II study. *Clin Cancer Res* 2020;26:1837–45.
- 58 Bendell JC, Jones SF, Hart L, *et al.* A phase Ib study of linsitinib (OSI-906), a dual inhibitor of IGF-1R and IR tyrosine kinase, in combination with everolimus as treatment for patients with refractory metastatic colorectal cancer. *Invest New Drugs* 2015;33:187–93.
- 59 Macaulay VM, Middleton MR, Eckhardt SG, *et al.* Phase I dose-escalation study of linsitinib (OSI-906) and erlotinib in patients with advanced solid tumors. *Clin Cancer Res* 2016;22:2897–907.
- 60 Oza A, Kaye S, Van Tornout J, *et al.* Phase 2 study evaluating intermittent and continuous linsitinib and Weekly paclitaxel in patients with recurrent platinum resistant ovarian epithelial cancer. *Gynecol Oncol* 2018;149:275–82.
- 61 Davis SL, Eckhardt SG, Diamond JR, *et al.* A phase I dose-escalation study of linsitinib (OSI-906), a small-molecule dual insulin-like growth factor-1 receptor/insulin receptor kinase inhibitor, in combination with irinotecan in patients with advanced cancer. *Oncologist* 2018;23:1409–e1140.
- 62 Schirripa M, Zhang W, Heinemann V, *et al.* Single nucleotide polymorphisms in the IGF-IRS pathway are associated with outcome in mCRC patients enrolled in the FIRE-3 trial. *Int J Cancer* 2017;141:383–92.
- 63 Matsubara J, Yamada Y, Nakajima TE, *et al.* Clinical significance of insulin-like growth factor type 1 receptor and epidermal growth factor receptor in patients with advanced gastric cancer. *Oncology* 2008;74:76–83.

DISCUSSION

Fasting or calorie-restricted diets have evolved as important approaches to modulate metabolic responses as well as immune function. There is evidence that in mouse or human models of starvation, the level of protein acetylation in lymphocytes decreases, accompanied by activation of the autophagy process (Madeo et al., 2019). Likewise, a calorie-restricted diet has considerable anti-inflammatory effects and can improve immune cell function (Buck et al., 2017). Studies have found that the deacetylase SIRT3 is significantly activated in humans after 24 hours of starvation, thereby inhibiting the activation of the NLRP3 inflammasome, which ultimately leads to a decrease in the secretion of interleukin-1 β (Traba et al., 2015). Conversely, a combination of cellular metabolites and glucose significantly increased interleukin-1 β release from macrophages in lean mice after fasting, thereby promoting postprandial insulin release (Dror et al., 2017). Moreover, many studies have demonstrated that disease-associated anorexia is a highly evolutionarily conserved response that modulates immune responses by inducing systemic autophagy activation (van Niekerk et al., 2016). Next, CRMs are a class of drugs or foods that mimic the effects of calorie restriction with the potential of improved health status and a longer lifespan (Andrejeva and Rathmell, 2017). Studies have shown that starvation and various potential CRMs can increase the expression of IGFBP1 and thereby reduce the level of IGF1 in the blood, ultimately causing changes in the systemic metabolic profile (Prieto et al., 2017). Our study also confirmed that PPP can significantly induce autophagy in the brain, liver and heart. At the same time, PPP can also reduce the number of Treg cells and CD8⁺PD1⁺ effector T cells in the tumor microenvironment, and improve the immunosuppressive microenvironment. The tumor-disappeared mice possessed the immune memory function of the same type of tumor and could prevent the recurrence of the same type of tumor. Our experiment also confirmed that PPP reduced cytoplasmic protein acetylation, as determined by quantitative immunofluorescence staining. Therefore, PPP as a CRM can enhance the role of tumor immune surveillance in the body.

Furthermore, the capacity of PPP to boost ATP release from cancer cells responding to MTX-based chemotherapy is reduced in cells lacking the ER stress sensor

EIF2AK3/PERK (eukaryotic translation initiation factor 2 alpha kinase 3) or its substrate EIF2A (eukaryotic translation initiation factor 2A), as well as in cells lacking the essential autophagy protein ATG5. Of note, it appears that the autophagy-dependent increase in extracellular ATP from tumor cells (Michaud et al., 2011) plays a rate-limiting role in the therapeutic efficacy of PPP, which indeed was lost when cancer cells were genetically manipulated to express the ATP-degrading enzyme CD39 on their surface. Adenosine triphosphate (ATP) is a direct donor of intracellular energy, and ATP and its derivatives are the main signaling molecules in the tumor microenvironment and are involved in cardiac function and immune regulation (Lampropoulou et al., 2016; Littlewood-Evans et al., 2016). When cells undergo stimuli such as death or chemical stress, mechanical damage, hypoxia, or cytotoxic agents, intracellular nucleotides are released to activate immune responses (Bambouskova et al., 2018). ATP can be released in several ways, including pannexin channels (Mills et al., 2018), connexin hemichannels (Weiss et al., 2018), exocytosis (Cheng et al., 2014), and ATP transporters specific to the ATP-binding cassette family such as cystic fibrosis transmembrane conductance regulator (cystic fibrosis transmembrane conductance regulator, CFTR) mediated release across the membrane (Arts et al., 2016). ATP binds to P2R family receptors, including ionotropic P2XR and metabotropic P2YR purinergic receptors (Tomlinson et al., 2002). ATP released from dying cells can bind P2RY2 and P2RX7 purinergic receptors to promote chemotaxis and recruitment of antigen-presenting cells (APCs); in contrast, autophagy-dependent ICD also participates in ATP release, which is associated with P2RX7 interact to recruit and activate dendritic cells (Delage et al., 2010; Mirsoian et al., 2014). Activation of purinergic signaling further activates the NLR family pyran domain of the inflammasome NLRP3, resulting in the proteolytic activation of caspase-1 and promoting IL-1 β processing and release by immunostimulation, a process that further activates IL-17-mediated $\gamma\delta$ T cells (Delage et al., 2010). In the extracellular space, ATP is gradually broken down by nucleotidase CD39 and CD73 to adenosine, which is an immunosuppressive Inhibitory effect (Mirsoian et al., 2014). Adenosine activates the PKA signaling cascade by linking four G protein-coupled adenosine receptors including A1R, A2AR, A2BR and A3R, thereby enhancing adenylate cyclase-mediated generation of cAMP. Notably, the activities of A2AR and A2BR can effectively induce immunosuppression in inflammatory

diseases (Blewett et al., 2016). Activation of the adenosine-A2AR signaling axis promotes high PD-1 expression (Cancer Genome Atlas Research et al., 2015), inhibits IL-2 receptor expression and TCR stimulates the proliferation of tumor-infiltrating T cells (Ye et al., 2018), which ultimately inhibits the body's anti-tumor immune function. Meanwhile, activation of the adenosine-A2AR signaling axis promotes the recruitment of MDSCs and the expression of VEGF in mouse model tumors (Tyrakis et al., 2016), and promoted the high expression of PD-L2 and IL-10 in dendritic cells, which in turn inhibited Teff cell activity (Doedens et al., 2013). Consistently, the inhibitor of A2B receptor, PSB1115, can inhibit tumor angiogenesis and increase tumor accumulation of T cells in the microenvironment (Tyrakis et al., 2016). In many human malignancies, high levels of CD39 and CD73 are considered markers of poor prognosis (MacIver et al., 2013), and ecto-nucleoside diphosphate hydrolase inhibitors—polyoxometalate-1 have been shown to inhibit tumor growth (Xu et al., 2017). In addition to tumor cells, CD39 and CD73 are expressed in regulatory immune Treg cells and M2 macrophages (Dang et al., 2011; Xu et al., 2017). Treg cells and M2 macrophages can degrade ATP through CD39 and CD73 to produce adenosine, limiting ATP-mediated pro-inflammatory effects and further immunosuppression through the adenosine-A2AR or adenosine-A2BR signaling axis (Currie et al., 2013; Dang et al., 2011). Furthermore, there is evidence that Treg cells inhibit the antitumor activity of NK cells in a CD39-dependent pathway, thereby promoting the metastasis of melanoma (Xu et al., 2017). Therefore, targeting ATP/adenosine metabolism is an effective strategy to alleviate tumor immunosuppression. Specifically, CD39 deletion results in defects in angiogenesis and the ability of melanoma cells to migrate, thereby inhibiting tumor progression in mouse models (Al-Khami et al., 2017). Adenosine 5'-(α , β -methylene) adenosine diphosphate (APCP), a specific CD73 inhibitor, reduces the production of adenosine to attenuate breast cancer cell migration (Osinalde et al., 2016). Furthermore, evidence suggests that both CD73 inhibitors and A2AR antagonists synergize with ICIs to inhibit tumor progression in mouse models (Cancer Genome Atlas Research et al., 2015; Niu et al., 2017). At present, the combination of drugs targeting the adenosine signaling pathways with ICI has been used in clinical trials of cancer patients. The A2AR inhibitor CPI-144 has been shown to be effective in controlling refractory renal cell carcinoma (RCC; 60% disease control rate), and combined

with atezolizumab can further significantly improve control (anti-PD-L1 antibody; I/ Phase Ib trial (100% disease prevention rate) (NCT02655822) (Thommen et al., 2018).

In conclusion, we identified PPP as a non-toxic inducer of autophagic flux that acts on human and mouse cells *in vitro*, as well as mouse organs *in vivo*. Mechanistically, PPP inhibits IGF1R as well as, downstream of AKT, the mechanistic target of rapamycin complex 1 (mTORC1), coupled to the activation of the pro-autophagic transcription factors EB (TFEB) and E3 (TFE3). Cells equipped with a constitutively active AKT mutant failed to activate autophagy. PPP also stimulated the AKT-repressible activation of all three arms of the unfolded stress response (UPR), including the PERK-dependent phosphorylation of eukaryotic initiation factor 2 α (eIF2 α). Knockout of TFEB and/or TFE3 blunted the UPR while knockout of PERK or replacement of eIF2 α by a non-phosphorylatable mutant reduced TFEB/TFE3 activation and autophagy induced by PPP. This points to crosstalk between the UPR and autophagy. Of note, administration of PPP to mice improved the efficacy of immunogenic chemotherapy and immune checkpoint inhibitors relying on ATP release, HMGB1 release, and CALR exposure. This anticancer effect relied on an improved T lymphocyte-dependent anticancer immune response and was lost upon CD39 overexpression in, constitutive AKT activation in, or deletion of the essential autophagy gene Atg5 from, the malignant cells. PPP is a bioavailable, potentially useful autophagy inducer that warrants further preclinical characterization. Excessive antiautophagic signaling via IGF1R has a major negative effect on anticancer immunosurveillance, thus reducing patient prognosis. However, IGF1R and its downstream signals are amenable to pharmacological inhibition and subsequent improvement of cancer control by the immune system. These considerations should be incorporated into the future design of clinical trials in which inhibition of the IGF1R/PI3K/AKT/MTOR pathway will be combined with adequate immune stimulation with ICD inducers and/or immune checkpoint inhibitors.

ACKNOWLEDGEMENTS

I would like to give my most enormous thanks to all of you who helps me, supports me, and companies me in the past years. I cannot enjoy a so inspiring and fantastic doctoral journey without your presence.

To my supervisor Guido, thanks for your kind supervision during my Ph.D. study, your insightful perspectives and passion for science always inspire me to think about big scientific questions.

To my co-supervisor Oliver, thanks for welcoming me to the lab. You are always reliable and available whenever I need guidance or help, your support and encouragement mean a lot to me. Especially in English support, thank you very kindly and in detail to relay the important contents of the meeting to me when I had difficulty understanding. Let's continue to cross our fingers in the future.

To Dr. Didac, thanks for being my CSI member during my mid-term presentation and joining my jury as a rapporteur. Thank you very much for being able to come to France from Austria for my graduation defense.

To Dr. Nicolas, thanks for joining my jury as a rapporteur and examining my work.

To Prof. Filippo, thanks for serving as the president of my jury and examining this work.

To Prof. Véronique and Dr. Laurie, thanks for accepting my invitation to examine this work.

To Qi, thanks for being willing to give me the opportunity to work with you when I'm a new comer, and for taking me through this project and teaching me a lot.

To Jiaying, we are not only colleagues, we are neighbors, and we are good friends. Thanks for taking care of me in my life in the past. Thanks for trusting my ability enough to give me the opportunity to cooperate with you and published an SCI paper. I still remember you taught me a lot of skills and knowledge in scientific research even in my life.

To Hui Pan, thanks for the happiness you brought to me, I do enjoy the time we spent together both in and out of the lab. I also would like to thank Zhenrui for always giving me

comfort and support when I'm in trouble even if you are not in our lab. Remember, Hui, you and I are always good friends. Hui, I hope the project we are working on will be successfully completed and published in the high-impact factor SCI. Zhenrui, I hope you also could successfully complete your Ph.D. thesis and publish a good paper.

To Allan and Marion, thanks for your technical support in my projects, without you I couldn't be able to generate the massive amount and reliability of immunofluorescence data and images.

To Peng and Liwei, thanks for helping me in finalizing experiments and for your helpful advice during these three years. Your concern for me is like a brother and sister. You make me feel the warmth of home.

To Giulia, thanks for always reaching out when I need help, especially your French support has helped me with so many of my life's problems. I'm very grateful for your help during my preparation for my Ph.D. defense, and your help made everything go smoothly.

To Chiara, thanks for your tireless help in ordering mice and modifying animal projects for us, so that we can successfully complete animal experiments and obtain the unique project numbers for our published papers.

To Léa, thanks for your patience, your affability, and your help with all the doctoral school parts during these three years. You were always smiling, even when I arrived in your office without warning.

To Sabrina and Mehdi, thanks for your patience and kindness in order the experimental reagents make me complete the experiment without any doubts.

To all the members of our lab (Shuai, Hui CHEN, Sijing and so on), I do appreciate your generous help and advice in my Ph.D. projects and future careers.

To the Chinese Scholarship Council (CSC), thanks for financial support during my Ph.D. study.

To my beloved parents, I cannot appreciate more for your consistent love and support, you give me the courage to explore, to extend my limitation without worry.

REFERENCES

- Adams, T.E., Epa, V.C., Garrett, T.P., and Ward, C.W. (2000). Structure and function of the type 1 insulin-like growth factor receptor. *Cell Mol Life Sci* 57, 1050-1093.
- Adkins, I., Fucikova, J., Garg, A.D., Agostinis, P., and Spisek, R. (2014). Physical modalities inducing immunogenic tumor cell death for cancer immunotherapy. *Oncoimmunology* 3, e968434.
- Ahlmann, M., and Hempel, G. (2016). The effect of cyclophosphamide on the immune system: implications for clinical cancer therapy. *Cancer Chemother Pharmacol* 78, 661-671.
- Al-Khami, A.A., Zheng, L., Del Valle, L., Hossain, F., Wyczechowska, D., Zabaleta, J., Sanchez, M.D., Dean, M.J., Rodriguez, P.C., and Ochoa, A.C. (2017). Exogenous lipid uptake induces metabolic and functional reprogramming of tumor-associated myeloid-derived suppressor cells. *Oncoimmunology* 6, e1344804.
- Andrejeva, G., and Rathmell, J.C. (2017). Similarities and Distinctions of Cancer and Immune Metabolism in Inflammation and Tumors. *Cell Metab* 26, 49-70.
- Apetoh, L., Ghiringhelli, F., Tesniere, A., Obeid, M., Ortiz, C., Criollo, A., Mignot, G., Maiuri, M.C., Ullrich, E., Saulnier, P., *et al.* (2007). Toll-like receptor 4-dependent contribution of the immune system to anticancer chemotherapy and radiotherapy. *Nat Med* 13, 1050-1059.
- Arts, R.J., Novakovic, B., Ter Horst, R., Carvalho, A., Bekkering, S., Lachmandas, E., Rodrigues, F., Silvestre, R., Cheng, S.C., Wang, S.Y., *et al.* (2016). Glutaminolysis and Fumarate Accumulation Integrate Immunometabolic and Epigenetic Programs in Trained Immunity. *Cell Metab* 24, 807-819.
- Ashrafizadeh, M., Farhood, B., Elejo Musa, A., Taeb, S., and Najafi, M. (2020). Damage-associated molecular patterns in tumor radiotherapy. *Int Immunopharmacol* 86, 106761.
- Bambouskova, M., Gorvel, L., Lampropoulou, V., Sergushichev, A., Loginicheva, E., Johnson, K., Korenfeld, D., Mathyer, M.E., Kim, H., Huang, L.H., *et al.* (2018). Electrophilic properties of itaconate and derivatives regulate the I κ Bzeta-ATF3 inflammatory axis. *Nature* 556, 501-504.
- Bejarano, E., and Cuervo, A.M. (2010). Chaperone-mediated autophagy. *Proc Am Thorac Soc* 7, 29-39.

Bell, I.M., Stirdivant, S.M., Ahern, J., Culberson, J.C., Darke, P.L., Dinsmore, C.J., Drakas, R.A., Gallicchio, S.N., Graham, S.L., Heimbrook, D.C., *et al.* (2005). Biochemical and structural characterization of a novel class of inhibitors of the type 1 insulin-like growth factor and insulin receptor kinases. *Biochemistry* 44, 9430-9440.

Bernard, A., and Klionsky, D.J. (2013). Autophagosome formation: tracing the source. *Dev Cell* 25, 116-117.

Blewett, M.M., Xie, J., Zaro, B.W., Backus, K.M., Altman, A., Teijaro, J.R., and Cravatt, B.F. (2016). Chemical proteomic map of dimethyl fumarate-sensitive cysteines in primary human T cells. *Sci Signal* 9, rs10.

Bommareddy, P.K., Zloza, A., Rabkin, S.D., and Kaufman, H.L. (2019). Oncolytic virus immunotherapy induces immunogenic cell death and overcomes STING deficiency in melanoma. *Oncoimmunology* 8, 1591875.

Brusa, D., Migliore, E., Garetto, S., Simone, M., and Matera, L. (2009). Immunogenicity of 56 degrees C and UVC-treated prostate cancer is associated with release of HSP70 and HMGB1 from necrotic cells. *Prostate* 69, 1343-1352.

Buck, M.D., Sowell, R.T., Kaech, S.M., and Pearce, E.L. (2017). Metabolic Instruction of Immunity. *Cell* 169, 570-586.

Buytaert, E., Callewaert, G., Hendrickx, N., Scorrano, L., Hartmann, D., Missiaen, L., Vandenheede, J.R., Heirman, I., Grooten, J., and Agostinis, P. (2006). Role of endoplasmic reticulum depletion and multidomain proapoptotic BAX and BAK proteins in shaping cell death after hypericin-mediated photodynamic therapy. *FASEB J* 20, 756-758.

Cancer Genome Atlas Research, N., Brat, D.J., Verhaak, R.G., Aldape, K.D., Yung, W.K., Salama, S.R., Cooper, L.A., Rheinbay, E., Miller, C.R., Vitucci, M., *et al.* (2015). Comprehensive, Integrative Genomic Analysis of Diffuse Lower-Grade Gliomas. *N Engl J Med* 372, 2481-2498.

Cardoso, C.M., Groth-Pedersen, L., Hoyer-Hansen, M., Kirkegaard, T., Corcelle, E., Andersen, J.S., Jaattela, M., and Nylandsted, J. (2009). Depletion of kinesin 5B affects lysosomal distribution and stability and induces peri-nuclear accumulation of autophagosomes in cancer cells. *PLoS One* 4, e4424.

Casares, N., Pequignot, M.O., Tesniere, A., Ghiringhelli, F., Roux, S., Chaput, N., Schmitt, E., Hamai, A., Hervas-Stubbs, S., Obeid, M., *et al.* (2005). Caspase-dependent immunogenicity of doxorubicin-induced tumor cell death. *J Exp Med* 202, 1691-1701.

Chang, C.H., Qiu, J., O'Sullivan, D., Buck, M.D., Noguchi, T., Curtis, J.D., Chen, Q., Gindin, M., Gubin, M.M., van der Windt, G.J., *et al.* (2015). Metabolic Competition in the Tumor Microenvironment Is a Driver of Cancer Progression. *Cell* 162, 1229-1241.

Chang, C.L., Hsu, Y.T., Wu, C.C., Yang, Y.C., Wang, C., Wu, T.C., and Hung, C.F. (2012). Immune mechanism of the antitumor effects generated by bortezomib. *J Immunol* 189, 3209-3220.

Chao, M.P., Jaiswal, S., Weissman-Tsukamoto, R., Alizadeh, A.A., Gentles, A.J., Volkmer, J., Weiskopf, K., Willingham, S.B., Raveh, T., Park, C.Y., *et al.* (2010). Calreticulin is the dominant pro-phagocytic signal on multiple human cancers and is counterbalanced by CD47. *Sci Transl Med* 2, 63ra94.

Chen, H.M., Wang, P.H., Chen, S.S., Wen, C.C., Chen, Y.H., Yang, W.C., and Yang, N.S. (2012). Shikonin induces immunogenic cell death in tumor cells and enhances dendritic cell-based cancer vaccine. *Cancer Immunol Immunother* 61, 1989-2002.

Chen, J., Xie, J., Jiang, Z., Wang, B., Wang, Y., and Hu, X. (2011). Shikonin and its analogs inhibit cancer cell glycolysis by targeting tumor pyruvate kinase-M2. *Oncogene* 30, 4297-4306.

Chen, Z., Liu, L., Liang, R., Luo, Z., He, H., Wu, Z., Tian, H., Zheng, M., Ma, Y., and Cai, L. (2018). Bioinspired Hybrid Protein Oxygen Nanocarrier Amplified Photodynamic Therapy for Eliciting Anti-tumor Immunity and Abscopal Effect. *ACS Nano* 12, 8633-8645.

Cheng, L.S., Li, J., Liu, Y., Wang, F.P., Wang, S.Q., She, W.M., Wu, S.D., Qi, X.L., Zhou, Y.P., and Jiang, W. (2017). HMGB1-induced autophagy: a new pathway to maintain Treg function during chronic hepatitis B virus infection. *Clin Sci (Lond)* 131, 381-394.

Cheng, S.C., Quintin, J., Cramer, R.A., Shepardson, K.M., Saeed, S., Kumar, V., Giamarellos-Bourboulis, E.J., Martens, J.H., Rao, N.A., Aghajani-refah, A., *et al.* (2014). mTOR- and HIF-1 α -mediated aerobic glycolysis as metabolic basis for trained immunity. *Science* 345, 1250684.

Chiang, W.C., Wei, Y., Kuo, Y.C., Wei, S., Zhou, A., Zou, Z., Yehl, J., Ranaghan, M.J., Skepner, A., Bittker, J.A., *et al.* (2018). High-Throughput Screens To Identify Autophagy

Inducers That Function by Disrupting Beclin 1/Bcl-2 Binding. *ACS Chem Biol* 13, 2247-2260.

Chiu, H.W., Yeh, Y.L., Wang, Y.C., Huang, W.J., Ho, S.Y., Lin, P., and Wang, Y.J. (2016). Combination of the novel histone deacetylase inhibitor YCW1 and radiation induces autophagic cell death through the downregulation of BNIP3 in triple-negative breast cancer cells in vitro and in an orthotopic mouse model. *Mol Cancer* 15, 46.

Choi, J.H., Yoon, J.S., Won, Y.W., Park, B.B., and Lee, Y.Y. (2012). Chloroquine enhances the chemotherapeutic activity of 5-fluorouracil in a colon cancer cell line via cell cycle alteration. *APMIS* 120, 597-604.

Colangelo, T., Polcaro, G., Ziccardi, P., Muccillo, L., Galgani, M., Pucci, B., Milone, M.R., Budillon, A., Santopalo, M., Mazzoccoli, G., *et al.* (2016). The miR-27a-calreticulin axis affects drug-induced immunogenic cell death in human colorectal cancer cells. *Cell Death Dis* 7, e2108.

Cufi, S., Vazquez-Martin, A., Oliveras-Ferraros, C., Corominas-Faja, B., Cuyas, E., Lopez-Bonet, E., Martin-Castillo, B., Joven, J., and Menendez, J.A. (2013). The anti-malarial chloroquine overcomes primary resistance and restores sensitivity to trastuzumab in HER2-positive breast cancer. *Sci Rep* 3, 2469.

Currie, E., Schulze, A., Zechner, R., Walther, T.C., and Farese, R.V., Jr. (2013). Cellular fatty acid metabolism and cancer. *Cell Metab* 18, 153-161.

Dai, C., and Gu, W. (2010). p53 post-translational modification: deregulated in tumorigenesis. *Trends Mol Med* 16, 528-536.

Dang, E.V., Barbi, J., Yang, H.Y., Jinasena, D., Yu, H., Zheng, Y., Bordman, Z., Fu, J., Kim, Y., Yen, H.R., *et al.* (2011). Control of T(H)17/T(reg) balance by hypoxia-inducible factor 1. *Cell* 146, 772-784.

Davies, A.M., Lara, P.N., Jr., Mack, P.C., and Gandara, D.R. (2007). Incorporating bortezomib into the treatment of lung cancer. *Clin Cancer Res* 13, s4647-4651.

De Beck, L., Melhaoui, S., De Veirman, K., Menu, E., De Bruyne, E., Vanderkerken, K., Breckpot, K., and Maes, K. (2018). Epigenetic treatment of multiple myeloma mediates tumor intrinsic and extrinsic immunomodulatory effects. *Oncoimmunology* 7, e1484981.

Delage, B., Fennell, D.A., Nicholson, L., McNeish, I., Lemoine, N.R., Crook, T., and Szlosarek, P.W. (2010). Arginine deprivation and argininosuccinate synthetase expression in the treatment of cancer. *Int J Cancer* 126, 2762-2772.

Diederich, M., Muller, F., and Cerella, C. (2017). Cardiac glycosides: From molecular targets to immunogenic cell death. *Biochem Pharmacol* 125, 1-11.

Dikic, I., and Elazar, Z. (2018). Mechanism and medical implications of mammalian autophagy. *Nat Rev Mol Cell Biol* 19, 349-364.

Doedens, A.L., Phan, A.T., Stradner, M.H., Fujimoto, J.K., Nguyen, J.V., Yang, E., Johnson, R.S., and Goldrath, A.W. (2013). Hypoxia-inducible factors enhance the effector responses of CD8(+) T cells to persistent antigen. *Nat Immunol* 14, 1173-1182.

Dror, E., Dalmas, E., Meier, D.T., Wueest, S., Thevenet, J., Thienel, C., Timper, K., Nordmann, T.M., Traub, S., Schulze, F., *et al.* (2017). Postprandial macrophage-derived IL-1beta stimulates insulin, and both synergistically promote glucose disposal and inflammation. *Nat Immunol* 18, 283-292.

Du, H.Y., Olivo, M., Mahendran, R., Huang, Q., Shen, H.M., Ong, C.N., and Bay, B.H. (2007). Hypericin photoactivation triggers down-regulation of matrix metalloproteinase-9 expression in well-differentiated human nasopharyngeal cancer cells. *Cell Mol Life Sci* 64, 979-988.

Dudek, A.M., Garg, A.D., Krysko, D.V., De Ruyscher, D., and Agostinis, P. (2013). Inducers of immunogenic cancer cell death. *Cytokine Growth Factor Rev* 24, 319-333.

Duewell, P., Steger, A., Lohr, H., Bourhis, H., Hoelz, H., Kirchleitner, S.V., Stieg, M.R., Grassmann, S., Kobold, S., Siveke, J.T., *et al.* (2014). RIG-I-like helicases induce immunogenic cell death of pancreatic cancer cells and sensitize tumors toward killing by CD8(+) T cells. *Cell Death Differ* 21, 1825-1837.

Dunlop, E.A., and Tee, A.R. (2014). mTOR and autophagy: a dynamic relationship governed by nutrients and energy. *Semin Cell Dev Biol* 36, 121-129.

Ekman, S., Frodin, J.E., Harmenberg, J., Bergman, A., Hedlund, A., Dahg, P., Alvfors, C., Stahl, B., Bergstrom, S., and Bergqvist, M. (2011). Clinical Phase I study with an Insulin-like Growth Factor-1 receptor inhibitor: experiences in patients with squamous non-small cell lung carcinoma. *Acta Oncol* 50, 441-447.

Elliott, M.R., Chekeni, F.B., Trampont, P.C., Lazarowski, E.R., Kadl, A., Walk, S.F., Park, D., Woodson, R.I., Ostankovich, M., Sharma, P., *et al.* (2009). Nucleotides released by apoptotic cells act as a find-me signal to promote phagocytic clearance. *Nature* **461**, 282-286.

Fachri, M., Hatta, M., Massi, M.N., Santoso, A., Wikanningtyas, T.A., Dwiyantri, R., Junita, A.R., Primaguna, M.R., and Sabir, M. (2021). The strong correlation between ADAM33 expression and airway inflammation in chronic obstructive pulmonary disease and candidate for biomarker and treatment of COPD. *Sci Rep* **11**, 23162.

Feng, Y., He, D., Yao, Z., and Klionsky, D.J. (2014). The machinery of macroautophagy. *Cell Res* **24**, 24-41.

Fucikova, J., Kralikova, P., Fialova, A., Brtnicky, T., Rob, L., Bartunkova, J., and Spisek, R. (2011). Human tumor cells killed by anthracyclines induce a tumor-specific immune response. *Cancer Res* **71**, 4821-4833.

Fucikova, J., Moserova, I., Truxova, I., Hermanova, I., Vancurova, I., Partlova, S., Fialova, A., Sojka, L., Cartron, P.F., Houska, M., *et al.* (2014). High hydrostatic pressure induces immunogenic cell death in human tumor cells. *Int J Cancer* **135**, 1165-1177.

Gable, K.L., Maddux, B.A., Penaranda, C., Zavodovskaya, M., Campbell, M.J., Lobo, M., Robinson, L., Schow, S., Kerner, J.A., Goldfine, I.D., *et al.* (2006). Diarylureas are small-molecule inhibitors of insulin-like growth factor I receptor signaling and breast cancer cell growth. *Mol Cancer Ther* **5**, 1079-1086.

Galluzzi, L., Buque, A., Kepp, O., Zitvogel, L., and Kroemer, G. (2017). Immunogenic cell death in cancer and infectious disease. *Nat Rev Immunol* **17**, 97-111.

Galluzzi, L., Vitale, I., Aaronson, S.A., Abrams, J.M., Adam, D., Agostinis, P., Alnemri, E.S., Altucci, L., Amelio, I., Andrews, D.W., *et al.* (2018). Molecular mechanisms of cell death: recommendations of the Nomenclature Committee on Cell Death 2018. *Cell Death Differ* **25**, 486-541.

Gao, J., Deng, F., and Jia, W. (2019). Inhibition of Indoleamine 2,3-Dioxygenase Enhances the Therapeutic Efficacy of Immunogenic Chemotherapeutics in Breast Cancer. *J Breast Cancer* **22**, 196-209.

Garcia-Echeverria, C., Pearson, M.A., Marti, A., Meyer, T., Mestan, J., Zimmermann, J., Gao, J., Brueggen, J., Capraro, H.G., Cozens, R., *et al.* (2004). In vivo antitumor activity

of NVP-AEW541-A novel, potent, and selective inhibitor of the IGF-IR kinase. *Cancer Cell* 5, 231-239.

Garcia-Mato, A., Cervantes, B., Murillo-Cuesta, S., Rodriguez-de la Rosa, L., and Varela-Nieto, I. (2021). Insulin-like Growth Factor 1 Signaling in Mammalian Hearing. *Genes (Basel)* 12.

Garg, A.D., and Agostinis, P. (2014). ER stress, autophagy and immunogenic cell death in photodynamic therapy-induced anti-cancer immune responses. *Photochem Photobiol Sci* 13, 474-487.

Garg, A.D., Dudek-Peric, A.M., Romano, E., and Agostinis, P. (2015). Immunogenic cell death. *Int J Dev Biol* 59, 131-140.

Garg, A.D., Krysko, D.V., Vandenabeele, P., and Agostinis, P. (2012a). The emergence of phox-ER stress induced immunogenic apoptosis. *Oncoimmunology* 1, 786-788.

Garg, A.D., Krysko, D.V., Vandenabeele, P., and Agostinis, P. (2012b). Hypericin-based photodynamic therapy induces surface exposure of damage-associated molecular patterns like HSP70 and calreticulin. *Cancer Immunol Immunother* 61, 215-221.

Garg, A.D., Nowis, D., Golab, J., and Agostinis, P. (2010). Photodynamic therapy: illuminating the road from cell death towards anti-tumour immunity. *Apoptosis* 15, 1050-1071.

Garrido, G., Lorenzano, P., Sanchez, B., Beausoleil, I., Alonso, D.F., Perez, R., and Fernandez, L.E. (2007). T cells are crucial for the anti-metastatic effect of anti-epidermal growth factor receptor antibodies. *Cancer Immunol Immunother* 56, 1701-1710.

Garrido, G., Rabasa, A., Sanchez, B., Lopez, M.V., Blanco, R., Lopez, A., Hernandez, D.R., Perez, R., and Fernandez, L.E. (2011). Induction of immunogenic apoptosis by blockade of epidermal growth factor receptor activation with a specific antibody. *J Immunol* 187, 4954-4966.

Gebremeskel, S., and Johnston, B. (2015). Concepts and mechanisms underlying chemotherapy induced immunogenic cell death: impact on clinical studies and considerations for combined therapies. *Oncotarget* 6, 41600-41619.

Ghiringhelli, F., Apetoh, L., Tesniere, A., Aymeric, L., Ma, Y., Ortiz, C., Vermaelen, K., Panaretakis, T., Mignot, G., Ullrich, E., *et al.* (2009). Activation of the NLRP3

inflammasome in dendritic cells induces IL-1 β -dependent adaptive immunity against tumors. *Nat Med* 15, 1170-1178.

Girnit, L., Girnit, A., and Larsson, O. (2003). Mdm2-dependent ubiquitination and degradation of the insulin-like growth factor 1 receptor. *Proc Natl Acad Sci U S A* 100, 8247-8252.

Glick, D., Barth, S., and Macleod, K.F. (2010). Autophagy: cellular and molecular mechanisms. *J Pathol* 221, 3-12.

Golden, E.B., Frances, D., Pellicciotta, I., Demaria, S., Helen Barcellos-Hoff, M., and Formenti, S.C. (2014). Radiation fosters dose-dependent and chemotherapy-induced immunogenic cell death. *Oncoimmunology* 3, e28518.

Goncalves, R.M., Agnes, J.P., Delgobo, M., de Souza, P.O., Thome, M.P., Heimfarth, L., Lenz, G., Moreira, J.C.F., and Zanotto-Filho, A. (2019). Late autophagy inhibitor chloroquine improves efficacy of the histone deacetylase inhibitor SAHA and temozolomide in gliomas. *Biochem Pharmacol* 163, 440-450.

Guerra, F., and Bucci, C. (2016). Multiple Roles of the Small GTPase Rab7. *Cells* 5.

Gujar, S., Pol, J.G., Kim, Y., Lee, P.W., and Kroemer, G. (2018). Antitumor Benefits of Antiviral Immunity: An Underappreciated Aspect of Oncolytic Virotherapies. *Trends Immunol* 39, 209-221.

Guo, J.Y., Chen, H.Y., Mathew, R., Fan, J., Strohecker, A.M., Karsli-Uzunbas, G., Kamphorst, J.J., Chen, G., Lemons, J.M., Karantza, V., *et al.* (2011). Activated Ras requires autophagy to maintain oxidative metabolism and tumorigenesis. *Genes Dev* 25, 460-470.

Guo, J.Y., Xia, B., and White, E. (2013). Autophagy-mediated tumor promotion. *Cell* 155, 1216-1219.

Haluska, P., Carboni, J.M., Loegering, D.A., Lee, F.Y., Wittman, M., Saulnier, M.G., Frennesson, D.B., Kalli, K.R., Conover, C.A., Attar, R.M., *et al.* (2006). In vitro and in vivo antitumor effects of the dual insulin-like growth factor-I/insulin receptor inhibitor, BMS-554417. *Cancer Res* 66, 362-371.

Han, W., Pan, H., Chen, Y., Sun, J., Wang, Y., Li, J., Ge, W., Feng, L., Lin, X., Wang, X., *et al.* (2011). EGFR tyrosine kinase inhibitors activate autophagy as a cytoprotective response in human lung cancer cells. *PLoS One* 6, e18691.

Hansen, T.E., and Johansen, T. (2011). Following autophagy step by step. *BMC Biol* 9, 39.

Hartog, H., Wesseling, J., Boezen, H.M., and van der Graaf, W.T. (2007). The insulin-like growth factor 1 receptor in cancer: old focus, new future. *Eur J Cancer* 43, 1895-1904.

He, C., and Levine, B. (2010). The Beclin 1 interactome. *Curr Opin Cell Biol* 22, 140-149.

Heinrich, B., Klein, J., Delic, M., Goepfert, K., Engel, V., Geberzahn, L., Lusky, M., Erbs, P., Preville, X., and Moehler, M. (2017). Immunogenicity of oncolytic vaccinia viruses JX-GFP and TG6002 in a human melanoma in vitro model: studying immunogenic cell death, dendritic cell maturation and interaction with cytotoxic T lymphocytes. *Onco Targets Ther* 10, 2389-2401.

Hemer, S., Konrad, C., Spiliotis, M., Koziol, U., Schaack, D., Forster, S., Gelmedin, V., Stadelmann, B., Dandekar, T., Hemphill, A., *et al.* (2014). Host insulin stimulates *Echinococcus multilocularis* insulin signalling pathways and larval development. *BMC Biol* 12, 5.

Hervas-Stubbs, S., Perez-Gracia, J.L., Rouzaut, A., Sanmamed, M.F., Le Bon, A., and Melero, I. (2011). Direct effects of type I interferons on cells of the immune system. *Clin Cancer Res* 17, 2619-2627.

Hickman-Miller, H.D., and Hildebrand, W.H. (2004). The immune response under stress: the role of HSP-derived peptides. *Trends Immunol* 25, 427-433.

Huang, F.Y., Lei, J., Sun, Y., Yan, F., Chen, B., Zhang, L., Lu, Z., Cao, R., Lin, Y.Y., Wang, C.C., *et al.* (2018). Induction of enhanced immunogenic cell death through ultrasound-controlled release of doxorubicin by liposome-microbubble complexes. *Oncoimmunology* 7, e1446720.

Huang, J., Wang, Y., Guo, J., Lu, H., Lin, X., Ma, L., Teitz-Tennenbaum, S., Chang, A.E., and Li, Q. (2007). Radiation-induced apoptosis along with local and systemic cytokine elaboration is associated with DC plus radiotherapy-mediated renal cell tumor regression. *Clin Immunol* 123, 298-310.

Huang, T., Kim, C.K., Alvarez, A.A., Pangen, R.P., Wan, X., Song, X., Shi, T., Yang, Y., Sastry, N., Horbinski, C.M., *et al.* (2017). MST4 Phosphorylation of ATG4B Regulates Autophagic Activity, Tumorigenicity, and Radioresistance in Glioblastoma. *Cancer Cell* 32, 840-855 e848.

Ivashkiv, L.B., and Donlin, L.T. (2014). Regulation of type I interferon responses. *Nat Rev Immunol* 14, 36-49.

Ji, J., Fan, Z., Zhou, F., Wang, X., Shi, L., Zhang, H., Wang, P., Yang, D., Zhang, L., Chen, W.R., *et al.* (2015). Improvement of DC vaccine with ALA-PDT induced immunogenic apoptotic cells for skin squamous cell carcinoma. *Oncotarget* 6, 17135-17146.

Ji, Q.S., Mulvihill, M.J., Rosenfeld-Franklin, M., Cooke, A., Feng, L., Mak, G., O'Connor, M., Yao, Y., Pirritt, C., Buck, E., *et al.* (2007). A novel, potent, and selective insulin-like growth factor-I receptor kinase inhibitor blocks insulin-like growth factor-I receptor signaling in vitro and inhibits insulin-like growth factor-I receptor dependent tumor growth in vivo. *Mol Cancer Ther* 6, 2158-2167.

Jiang, X., Lu, W., Shen, X., Wang, Q., Lv, J., Liu, M., Cheng, F., Zhao, Z., and Pang, X. (2018). Repurposing sertraline sensitizes non-small cell lung cancer cells to erlotinib by inducing autophagy. *JCI Insight* 3.

Kawano, M., Tanaka, K., Itonaga, I., Iwasaki, T., Miyazaki, M., Ikeda, S., and Tsumura, H. (2016). Dendritic cells combined with doxorubicin induces immunogenic cell death and exhibits antitumor effects for osteosarcoma. *Oncol Lett* 11, 2169-2175.

Kenific, C.M., and Debnath, J. (2015). Cellular and metabolic functions for autophagy in cancer cells. *Trends Cell Biol* 25, 37-45.

Kepp, O., and Kroemer, G. (2020). A novel platinum-based chemotherapeutic inducing immunogenic cell death. *Oncoimmunology* 9, 1729022.

Kimmelman, A.C. (2011). The dynamic nature of autophagy in cancer. *Genes Dev* 25, 1999-2010.

Kimura, S., Noda, T., and Yoshimori, T. (2008). Dynein-dependent movement of autophagosomes mediates efficient encounters with lysosomes. *Cell Struct Funct* 33, 109-122.

Kuma, A., and Mizushima, N. (2010). Physiological role of autophagy as an intracellular recycling system: with an emphasis on nutrient metabolism. *Semin Cell Dev Biol* 21, 683-690.

Lampropoulou, V., Sergushichev, A., Bambouskova, M., Nair, S., Vincent, E.E., Loginicheva, E., Cervantes-Barragan, L., Ma, X., Huang, S.C., Griss, T., *et al.* (2016).

Itaconate Links Inhibition of Succinate Dehydrogenase with Macrophage Metabolic Remodeling and Regulation of Inflammation. *Cell Metab* 24, 158-166.

Larsson, O., Girnita, A., and Girnita, L. (2005). Role of insulin-like growth factor 1 receptor signalling in cancer. *Br J Cancer* 92, 2097-2101.

Lavandro, S., Chiong, M., Rothermel, B.A., and Hill, J.A. (2015). Autophagy in cardiovascular biology. *J Clin Invest* 125, 55-64.

Lee, P., and Gujar, S. (2018). Potentiating prostate cancer immunotherapy with oncolytic viruses. *Nat Rev Urol* 15, 235-250.

Lefranc, F., Mijatovic, T., Kondo, Y., Sauvage, S., Roland, I., Debeir, O., Krstic, D., Vasic, V., Gailly, P., Kondo, S., *et al.* (2008). Targeting the alpha 1 subunit of the sodium pump to combat glioblastoma cells. *Neurosurgery* 62, 211-221; discussion 221-212.

Li, W.W., Li, J., and Bao, J.K. (2012). Microautophagy: lesser-known self-eating. *Cell Mol Life Sci* 69, 1125-1136.

Liang, X.H., Jackson, S., Seaman, M., Brown, K., Kempkes, B., Hibshoosh, H., and Levine, B. (1999). Induction of autophagy and inhibition of tumorigenesis by beclin 1. *Nature* 402, 672-676.

Lim, V., Zhu, H., Diao, S., Hu, L., and Hu, J. (2019). PKP3 interactions with MAPK-JNK-ERK1/2-mTOR pathway regulates autophagy and invasion in ovarian cancer. *Biochem Biophys Res Commun* 508, 646-653.

Lin, A., Truong, B., Patel, S., Kaushik, N., Choi, E.H., Fridman, G., Fridman, A., and Miller, V. (2017). Nanosecond-Pulsed DBD Plasma-Generated Reactive Oxygen Species Trigger Immunogenic Cell Death in A549 Lung Carcinoma Cells through Intracellular Oxidative Stress. *Int J Mol Sci* 18.

Lin, A.G., Xiang, B., Merlino, D.J., Baybutt, T.R., Sahu, J., Fridman, A., Snook, A.E., and Miller, V. (2018). Non-thermal plasma induces immunogenic cell death in vivo in murine CT26 colorectal tumors. *Oncoimmunology* 7, e1484978.

Linder, S., Shoshan, M.C., and Gupta, R.S. (2007). Picropodophyllotoxin or podophyllotoxin does not induce cell death via insulin-like growth factor-I receptor. *Cancer Res* 67, 2899; author reply 2899-2900.

Littlewood-Evans, A., Sarret, S., Apfel, V., Loesle, P., Dawson, J., Zhang, J., Muller, A., Tigani, B., Kneuer, R., Patel, S., *et al.* (2016). GPR91 senses extracellular succinate

released from inflammatory macrophages and exacerbates rheumatoid arthritis. *J Exp Med* 213, 1655-1662.

Liu, C.C., Leclair, P., Pedari, F., Vieira, H., Monajemi, M., Sly, L.M., Reid, G.S., and Lim, C.J. (2019). Integrins and ERp57 Coordinate to Regulate Cell Surface Calreticulin in Immunogenic Cell Death. *Front Oncol* 9, 411.

Liu, J., Xia, H., Kim, M., Xu, L., Li, Y., Zhang, L., Cai, Y., Norberg, H.V., Zhang, T., Furuya, T., *et al.* (2011). Beclin1 controls the levels of p53 by regulating the deubiquitination activity of USP10 and USP13. *Cell* 147, 223-234.

Liu, M., and Li, C. (2020). Recent Advances in Activatable Organic Photosensitizers for Specific Photodynamic Therapy. *Chempluschem* 85, 948-957.

Liu, Z., Zhang, H.M., Yuan, J., Ye, X., Taylor, G.A., and Yang, D. (2012). The immunity-related GTPase Irgm3 relieves endoplasmic reticulum stress response during coxsackievirus B3 infection via a PI3K/Akt dependent pathway. *Cell Microbiol* 14, 133-146.

Long, S., GuangZhi, Y., BaoJie, G., Wei, X., YanYong, H., YingLi, W., Yang, Z., and LiHua, L. (2012). Shikonin derivatives protect immune organs from damage and promote immune responses in vivo in tumour-bearing mice. *Phytother Res* 26, 26-33.

Lu, L., Qin, A., Huang, H., Zhou, P., Zhang, C., Liu, N., Li, S., Wen, G., Zhang, C., Dong, W., *et al.* (2011). Shikonin extracted from medicinal Chinese herbs exerts anti-inflammatory effect via proteasome inhibition. *Eur J Pharmacol* 658, 242-247.

Lu, X., Fan, Q., Xu, L., Li, L., Yue, Y., Xu, Y., Su, Y., Zhang, D., and Wang, L. (2015). Ursolic acid attenuates diabetic mesangial cell injury through the up-regulation of autophagy via miRNA-21/PTEN/Akt/mTOR suppression. *PLoS One* 10, e0117400.

Lu, X., Wang, L., Mei, J., Wang, X., Zhu, X., Zhang, Q., and Lv, J. (2013). Picropodophyllin inhibits epithelial ovarian cancer cells in vitro and in vivo. *Biochem Biophys Res Commun* 435, 385-390.

Ma, Y., Aymeric, L., Locher, C., Mattarollo, S.R., Delahaye, N.F., Pereira, P., Boucontet, L., Apetoh, L., Ghiringhelli, F., Casares, N., *et al.* (2011). Contribution of IL-17-producing gamma delta T cells to the efficacy of anticancer chemotherapy. *J Exp Med* 208, 491-503.

MacIver, N.J., Michalek, R.D., and Rathmell, J.C. (2013). Metabolic regulation of T lymphocytes. *Annu Rev Immunol* 31, 259-283.

Madeo, F., Carmona-Gutierrez, D., Hofer, S.J., and Kroemer, G. (2019). Caloric Restriction Mimetics against Age-Associated Disease: Targets, Mechanisms, and Therapeutic Potential. *Cell Metab* 29, 592-610.

Martins, I., Kepp, O., Schlemmer, F., Adjemian, S., Tailler, M., Shen, S., Michaud, M., Menger, L., Gdoura, A., Tajeddine, N., *et al.* (2011). Restoration of the immunogenicity of cisplatin-induced cancer cell death by endoplasmic reticulum stress. *Oncogene* 30, 1147-1158.

Martins, I., Tesniere, A., Kepp, O., Michaud, M., Schlemmer, F., Senovilla, L., Seror, C., Metivier, D., Perfettini, J.L., Zitvogel, L., *et al.* (2009). Chemotherapy induces ATP release from tumor cells. *Cell Cycle* 8, 3723-3728.

Martins, I., Wang, Y., Michaud, M., Ma, Y., Sukkurwala, A.Q., Shen, S., Kepp, O., Metivier, D., Galluzzi, L., Perfettini, J.L., *et al.* (2014). Molecular mechanisms of ATP secretion during immunogenic cell death. *Cell Death Differ* 21, 79-91.

Menger, L., Vacchelli, E., Adjemian, S., Martins, I., Ma, Y., Shen, S., Yamazaki, T., Sukkurwala, A.Q., Michaud, M., Mignot, G., *et al.* (2012). Cardiac glycosides exert anticancer effects by inducing immunogenic cell death. *Sci Transl Med* 4, 143ra199.

Michaud, M., Martins, I., Sukkurwala, A.Q., Adjemian, S., Ma, Y., Pellegatti, P., Shen, S., Kepp, O., Scoazec, M., Mignot, G., *et al.* (2011). Autophagy-dependent anticancer immune responses induced by chemotherapeutic agents in mice. *Science* 334, 1573-1577.

Michaud, M., Xie, X., Bravo-San Pedro, J.M., Zitvogel, L., White, E., and Kroemer, G. (2014). An autophagy-dependent anticancer immune response determines the efficacy of melanoma chemotherapy. *Oncoimmunology* 3, e944047.

Mills, E.L., Ryan, D.G., Prag, H.A., Dikovskaya, D., Menon, D., Zaslona, Z., Jedrychowski, M.P., Costa, A.S.H., Higgins, M., Hams, E., *et al.* (2018). Itaconate is an anti-inflammatory metabolite that activates Nrf2 via alkylation of KEAP1. *Nature* 556, 113-117.

Minute, L., Teijeira, A., Sanchez-Paulete, A.R., Ochoa, M.C., Alvarez, M., Otano, I., Etxeberria, I., Bolanos, E., Azpilikueta, A., Garasa, S., *et al.* (2020). Cellular cytotoxicity is a form of immunogenic cell death. *J Immunother Cancer* 8.

Mirsoian, A., Bouchlaka, M.N., Sckisel, G.D., Chen, M., Pai, C.C., Maverakis, E., Spencer, R.G., Fishbein, K.W., Siddiqui, S., Monjazeb, A.M., *et al.* (2014). Adiposity induces lethal

cytokine storm after systemic administration of stimulatory immunotherapy regimens in aged mice. *J Exp Med* 211, 2373-2383.

Mitsiades, C.S., Mitsiades, N.S., McMullan, C.J., Poulaki, V., Shringarpure, R., Akiyama, M., Hideshima, T., Chauhan, D., Joseph, M., Libermann, T.A., *et al.* (2004). Inhibition of the insulin-like growth factor receptor-1 tyrosine kinase activity as a therapeutic strategy for multiple myeloma, other hematologic malignancies, and solid tumors. *Cancer Cell* 5, 221-230.

Miyamoto, S., Inoue, H., Nakamura, T., Yamada, M., Sakamoto, C., Urata, Y., Okazaki, T., Marumoto, T., Takahashi, A., Takayama, K., *et al.* (2012). Coxsackievirus B3 is an oncolytic virus with immunostimulatory properties that is active against lung adenocarcinoma. *Cancer Res* 72, 2609-2621.

Mizushima, N., Levine, B., Cuervo, A.M., and Klionsky, D.J. (2008). Autophagy fights disease through cellular self-digestion. *Nature* 451, 1069-1075.

Molino, D., Zemirli, N., Codogno, P., and Morel, E. (2017). The Journey of the Autophagosome through Mammalian Cell Organelles and Membranes. *J Mol Biol* 429, 497-514.

Montico, B., Nigro, A., Casolaro, V., and Dal Col, J. (2018). Immunogenic Apoptosis as a Novel Tool for Anticancer Vaccine Development. *Int J Mol Sci* 19.

Mulvihill, M.J., Cooke, A., Rosenfeld-Franklin, M., Buck, E., Foreman, K., Landfair, D., O'Connor, M., Pirritt, C., Sun, Y., Yao, Y., *et al.* (2009). Discovery of OSI-906: a selective and orally efficacious dual inhibitor of the IGF-1 receptor and insulin receptor. *Future Med Chem* 1, 1153-1171.

Mulvihill, M.J., Ji, Q.S., Coate, H.R., Cooke, A., Dong, H., Feng, L., Foreman, K., Rosenfeld-Franklin, M., Honda, A., Mak, G., *et al.* (2008). Novel 2-phenylquinolin-7-yl-derived imidazo[1,5-a]pyrazines as potent insulin-like growth factor-I receptor (IGF-IR) inhibitors. *Bioorg Med Chem* 16, 1359-1375.

Mulvihill, M.J., Ji, Q.S., Werner, D., Beck, P., Cesario, C., Cooke, A., Cox, M., Crew, A., Dong, H., Feng, L., *et al.* (2007). 1,3-Disubstituted-imidazo[1,5-a]pyrazines as insulin-like growth-factor-I receptor (IGF-IR) inhibitors. *Bioorg Med Chem Lett* 17, 1091-1097.

Nakamura, M., Miyamoto, S., Maeda, H., Zhang, S.C., Sangai, T., Ishii, G., Hasebe, T., Endoh, Y., Saito, N., Asaka, M., *et al.* (2004). Low levels of insulin-like growth factor type

1 receptor expression at cancer cell membrane predict liver metastasis in Dukes' C human colorectal cancers. *Clin Cancer Res* 10, 8434-8441.

Nakamura, S., and Yoshimori, T. (2017). New insights into autophagosome-lysosome fusion. *J Cell Sci* 130, 1209-1216.

Nakatogawa, H., Suzuki, K., Kamada, Y., and Ohsumi, Y. (2009). Dynamics and diversity in autophagy mechanisms: lessons from yeast. *Nat Rev Mol Cell Biol* 10, 458-467.

Nascimbeni, A.C., Codogno, P., and Morel, E. (2017). Autophagosomal membranes assemble at ER-plasma membrane contact sites. *Mol Cell Oncol* 4, e1356431.

Navarro, M., and Baserga, R. (2001). Limited redundancy of survival signals from the type 1 insulin-like growth factor receptor. *Endocrinology* 142, 1073-1081.

Nawrocki, S.T., Carew, J.S., Dunner, K., Jr., Boise, L.H., Chiao, P.J., Huang, P., Abbruzzese, J.L., and McConkey, D.J. (2005). Bortezomib inhibits PKR-like endoplasmic reticulum (ER) kinase and induces apoptosis via ER stress in human pancreatic cancer cells. *Cancer Res* 65, 11510-11519.

Ni, J., Song, J., Wang, B., Hua, H., Zhu, H., Guo, X., Xiong, S., and Zhao, Y. (2020). Dendritic cell vaccine for the effective immunotherapy of breast cancer. *Biomed Pharmacother* 126, 110046.

Niu, Z., Shi, Q., Zhang, W., Shu, Y., Yang, N., Chen, B., Wang, Q., Zhao, X., Chen, J., Cheng, N., *et al.* (2017). Caspase-1 cleaves PPARgamma for potentiating the pro-tumor action of TAMs. *Nat Commun* 8, 766.

Nuccitelli, R., McDaniel, A., Anand, S., Cha, J., Mallon, Z., Berridge, J.C., and Uecker, D. (2017). Nano-Pulse Stimulation is a physical modality that can trigger immunogenic tumor cell death. *J Immunother Cancer* 5, 32.

O'Sullivan, D., Sanin, D.E., Pearce, E.J., and Pearce, E.L. (2019). Metabolic interventions in the immune response to cancer. *Nat Rev Immunol* 19, 324-335.

Obeid, M., Tesniere, A., Ghiringhelli, F., Fimia, G.M., Apetoh, L., Perfettini, J.L., Castedo, M., Mignot, G., Panaretakis, T., Casares, N., *et al.* (2007). Calreticulin exposure dictates the immunogenicity of cancer cell death. *Nat Med* 13, 54-61.

Ogawa, M., Tomita, Y., Nakamura, Y., Lee, M.J., Lee, S., Tomita, S., Nagaya, T., Sato, K., Yamauchi, T., Iwai, H., *et al.* (2017). Immunogenic cancer cell death selectively

induced by near infrared photoimmunotherapy initiates host tumor immunity. *Oncotarget* 8, 10425-10436.

Ogier-Denis, E., Pattingre, S., El Benna, J., and Codogno, P. (2000). Erk1/2-dependent phosphorylation of Galpha-interacting protein stimulates its GTPase accelerating activity and autophagy in human colon cancer cells. *J Biol Chem* 275, 39090-39095.

Onodera, J., and Ohsumi, Y. (2005). Autophagy is required for maintenance of amino acid levels and protein synthesis under nitrogen starvation. *J Biol Chem* 280, 31582-31586.

Osinalde, N., Mitxelena, J., Sanchez-Quiles, V., Akimov, V., Aloria, K., Arizmendi, J.M., Zubiaga, A.M., Blagoev, B., and Kratchmarova, I. (2016). Nuclear Phosphoproteomic Screen Uncovers ACLY as Mediator of IL-2-induced Proliferation of CD4+ T lymphocytes. *Mol Cell Proteomics* 15, 2076-2092.

Otomo, C., Metlagel, Z., Takaesu, G., and Otomo, T. (2013). Structure of the human ATG12~ATG5 conjugate required for LC3 lipidation in autophagy. *Nat Struct Mol Biol* 20, 59-66.

Panaretakis, T., Kepp, O., Brockmeier, U., Tesniere, A., Bjorklund, A.C., Chapman, D.C., Durchschlag, M., Joza, N., Pierron, G., van Endert, P., *et al.* (2009). Mechanisms of pre-apoptotic calreticulin exposure in immunogenic cell death. *EMBO J* 28, 578-590.

Panzarini, E., Inguscio, V., Fimia, G.M., and Dini, L. (2014). Rose Bengal acetate photodynamic therapy (RBAC-PDT) induces exposure and release of Damage-Associated Molecular Patterns (DAMPs) in human HeLa cells. *PLoS One* 9, e105778.

Parodi, M., Pedrazzi, M., Cantoni, C., Aversa, M., Patrone, M., Cavaletto, M., Spertino, S., Pende, D., Balsamo, M., Pietra, G., *et al.* (2015). Natural Killer (NK)/melanoma cell interaction induces NK-mediated release of chemotactic High Mobility Group Box-1 (HMGB1) capable of amplifying NK cell recruitment. *Oncoimmunology* 4, e1052353.

Pasquereau-Kotula, E., Habault, J., Kroemer, G., and Poyet, J.L. (2018). The anticancer peptide RT53 induces immunogenic cell death. *PLoS One* 13, e0201220.

Pavlova, N.N., and Thompson, C.B. (2016). The Emerging Hallmarks of Cancer Metabolism. *Cell Metab* 23, 27-47.

Pawaria, S., and Binder, R.J. (2011). CD91-dependent programming of T-helper cell responses following heat shock protein immunization. *Nat Commun* 2, 521.

Pietrocola, F., Pol, J., Vacchelli, E., Rao, S., Enot, D.P., Baracco, E.E., Levesque, S., Castoldi, F., Jacquelot, N., Yamazaki, T., *et al.* (2016). Caloric Restriction Mimetics Enhance Anticancer Immunosurveillance. *Cancer Cell* 30, 147-160.

Pircs, K., Nagy, P., Varga, A., Venkei, Z., Erdi, B., Hegedus, K., and Juhasz, G. (2012). Advantages and limitations of different p62-based assays for estimating autophagic activity in *Drosophila*. *PLoS One* 7, e44214.

Pol, J., Vacchelli, E., Aranda, F., Castoldi, F., Eggermont, A., Cremer, I., Sautes-Fridman, C., Fucikova, J., Galon, J., Spisek, R., *et al.* (2015). Trial Watch: Immunogenic cell death inducers for anticancer chemotherapy. *Oncoimmunology* 4, e1008866.

Prassas, I., and Diamandis, E.P. (2008). Novel therapeutic applications of cardiac glycosides. *Nat Rev Drug Discov* 7, 926-935.

Prieto, I., Montemuino, S., Luna, J., de Torres, M.V., and Amaya, E. (2017). The role of immunonutritional support in cancer treatment: Current evidence. *Clin Nutr* 36, 1457-1464.

Qin, L., Xu, T., Xia, L., Wang, X., Zhang, X., Zhang, X., Zhu, Z., Zhong, S., Wang, C., and Shen, Z. (2016). Chloroquine enhances the efficacy of cisplatin by suppressing autophagy in human adrenocortical carcinoma treatment. *Drug Des Devel Ther* 10, 1035-1045.

Qu, X., Yu, J., Bhagat, G., Furuya, N., Hibshoosh, H., Troxel, A., Rosen, J., Eskelinen, E.L., Mizushima, N., Ohsumi, Y., *et al.* (2003). Promotion of tumorigenesis by heterozygous disruption of the beclin 1 autophagy gene. *J Clin Invest* 112, 1809-1820.

Radogna, F., and Diederich, M. (2018). Stress-induced cellular responses in immunogenic cell death: Implications for cancer immunotherapy. *Biochem Pharmacol* 153, 12-23.

Raymond, E., Chaney, S.G., Taamma, A., and Cvitkovic, E. (1998). Oxaliplatin: a review of preclinical and clinical studies. *Ann Oncol* 9, 1053-1071.

Rosenfeldt, M.T., O'Prey, J., Morton, J.P., Nixon, C., MacKay, G., Mrowinska, A., Au, A., Rai, T.S., Zheng, L., Ridgway, R., *et al.* (2013). p53 status determines the role of autophagy in pancreatic tumour development. *Nature* 504, 296-300.

Ruan, H., Leibowitz, B.J., Zhang, L., and Yu, J. (2020). Immunogenic cell death in colon cancer prevention and therapy. *Mol Carcinog* 59, 783-793.

Rufo, N., Garg, A.D., and Agostinis, P. (2017). The Unfolded Protein Response in Immunogenic Cell Death and Cancer Immunotherapy. *Trends Cancer* 3, 643-658.

Sato, H., Okonogi, N., and Nakano, T. (2020). Rationale of combination of anti-PD-1/PD-L1 antibody therapy and radiotherapy for cancer treatment. *Int J Clin Oncol* 25, 801-809.

Schiavoni, G., Sistigu, A., Valentini, M., Mattei, F., Sestili, P., Spadaro, F., Sanchez, M., Lorenzi, S., D'Urso, M.T., Belardelli, F., *et al.* (2011). Cyclophosphamide synergizes with type I interferons through systemic dendritic cell reactivation and induction of immunogenic tumor apoptosis. *Cancer Res* 71, 768-778.

Schirmacher, V., van Gool, S., and Stuecker, W. (2019). Breaking Therapy Resistance: An Update on Oncolytic Newcastle Disease Virus for Improvements of Cancer Therapy. *Biomedicines* 7.

Schmukler, E., Kloog, Y., and Pinkas-Kramarski, R. (2014). Ras and autophagy in cancer development and therapy. *Oncotarget* 5, 577-586.

Scotlandi, K., Manara, M.C., Nicoletti, G., Lollini, P.L., Lukas, S., Benini, S., Croci, S., Perdichizzi, S., Zambelli, D., Serra, M., *et al.* (2005). Antitumor activity of the insulin-like growth factor-I receptor kinase inhibitor NVP-AEW541 in musculoskeletal tumors. *Cancer Res* 65, 3868-3876.

Selzer, E., and Hebar, A. (2012). Basic principles of molecular effects of irradiation. *Wien Med Wochenschr* 162, 47-54.

Serrano-Del Valle, A., Naval, J., Anel, A., and Marzo, I. (2020). Novel Forms of Immunomodulation for Cancer Therapy. *Trends Cancer* 6, 518-532.

Sethuraman, S.N., Singh, M.P., Patil, G., Li, S., Fiering, S., Hoopes, P.J., Guha, C., Malayer, J., and Ranjan, A. (2020). Novel calreticulin-nanoparticle in combination with focused ultrasound induces immunogenic cell death in melanoma to enhance antitumor immunity. *Theranostics* 10, 3397-3412.

Shingu, T., Fujiwara, K., Bogler, O., Akiyama, Y., Moritake, K., Shinjima, N., Tamada, Y., Yokoyama, T., and Kondo, S. (2009). Inhibition of autophagy at a late stage enhances imatinib-induced cytotoxicity in human malignant glioma cells. *Int J Cancer* 124, 1060-1071.

Sistigu, A., Yamazaki, T., Vacchelli, E., Chaba, K., Enot, D.P., Adam, J., Vitale, I., Goubar, A., Baracco, E.E., Remedios, C., *et al.* (2014). Cancer cell-autonomous contribution of type I interferon signaling to the efficacy of chemotherapy. *Nat Med* 20, 1301-1309.

Spisek, R., Charalambous, A., Mazumder, A., Vesole, D.H., Jagannath, S., and Dhodapkar, M.V. (2007). Bortezomib enhances dendritic cell (DC)-mediated induction of immunity to human myeloma via exposure of cell surface heat shock protein 90 on dying tumor cells: therapeutic implications. *Blood* 109, 4839-4845.

Sridharan, S., Jain, K., and Basu, A. (2011). Regulation of autophagy by kinases. *Cancers (Basel)* 3, 2630-2654.

Stromberg, T., Ekman, S., Girnita, L., Dimberg, L.Y., Larsson, O., Axelson, M., Lennartsson, J., Hellman, U., Carlson, K., Osterborg, A., *et al.* (2006). IGF-1 receptor tyrosine kinase inhibition by the cyclolignan PPP induces G2/M-phase accumulation and apoptosis in multiple myeloma cells. *Blood* 107, 669-678.

Sukkurwala, A.Q., Adjemian, S., Senovilla, L., Michaud, M., Spaggiari, S., Vacchelli, E., Baracco, E.E., Galluzzi, L., Zitvogel, L., Kepp, O., *et al.* (2014). Screening of novel immunogenic cell death inducers within the NCI Mechanistic Diversity Set. *Oncoimmunology* 3, e28473.

Tai, Y.T., Podar, K., Catley, L., Tseng, Y.H., Akiyama, M., Shringarpure, R., Burger, R., Hideshima, T., Chauhan, D., Mitsiades, N., *et al.* (2003). Insulin-like growth factor-1 induces adhesion and migration in human multiple myeloma cells via activation of beta1-integrin and phosphatidylinositol 3'-kinase/AKT signaling. *Cancer Res* 63, 5850-5858.

Takamura, A., Komatsu, M., Hara, T., Sakamoto, A., Kishi, C., Waguri, S., Eishi, Y., Hino, O., Tanaka, K., and Mizushima, N. (2011). Autophagy-deficient mice develop multiple liver tumors. *Genes Dev* 25, 795-800.

Tanaka, M., Kataoka, H., Yano, S., Sawada, T., Akashi, H., Inoue, M., Suzuki, S., Inagaki, Y., Hayashi, N., Nishie, H., *et al.* (2016). Immunogenic cell death due to a new photodynamic therapy (PDT) with glycoconjugated chlorin (G-chlorin). *Oncotarget* 7, 47242-47251.

Tel, J., Hato, S.V., Torensma, R., Buschow, S.I., Figdor, C.G., Lesterhuis, W.J., and de Vries, I.J. (2012). The chemotherapeutic drug oxaliplatin differentially affects blood DC function dependent on environmental cues. *Cancer Immunol Immunother* 61, 1101-1111.

Tesniere, A., Schlemmer, F., Boige, V., Kepp, O., Martins, I., Ghiringhelli, F., Aymeric, L., Michaud, M., Apetoh, L., Barault, L., *et al.* (2010). Immunogenic death of colon cancer cells treated with oxaliplatin. *Oncogene* 29, 482-491.

Tewey, K.M., Rowe, T.C., Yang, L., Halligan, B.D., and Liu, L.F. (1984). Adriamycin-induced DNA damage mediated by mammalian DNA topoisomerase II. *Science* 226, 466-468.

Thommen, D.S., Koelzer, V.H., Herzig, P., Roller, A., Trefny, M., Dimeloe, S., Kiialainen, A., Hanhart, J., Schill, C., Hess, C., *et al.* (2018). A transcriptionally and functionally distinct PD-1(+) CD8(+) T cell pool with predictive potential in non-small-cell lung cancer treated with PD-1 blockade. *Nat Med* 24, 994-1004.

Tomlinson, I.P., Alam, N.A., Rowan, A.J., Barclay, E., Jaeger, E.E., Kelsell, D., Leigh, I., Gorman, P., Lamlum, H., Rahman, S., *et al.* (2002). Germline mutations in FH predispose to dominantly inherited uterine fibroids, skin leiomyomata and papillary renal cell cancer. *Nat Genet* 30, 406-410.

Traba, J., Kwarteng-Siaw, M., Okoli, T.C., Li, J., Huffstutler, R.D., Bray, A., Waclawiw, M.A., Han, K., Pelletier, M., Sauve, A.A., *et al.* (2015). Fasting and refeeding differentially regulate NLRP3 inflammasome activation in human subjects. *J Clin Invest* 125, 4592-4600.

Tseng, L.M., Liu, C.Y., Chang, K.C., Chu, P.Y., Shiau, C.W., and Chen, K.F. (2012). CIP2A is a target of bortezomib in human triple negative breast cancer cells. *Breast Cancer Res* 14, R68.

Tyrakis, P.A., Palazon, A., Macias, D., Lee, K.L., Phan, A.T., Velica, P., You, J., Chia, G.S., Sim, J., Doedens, A., *et al.* (2016). S-2-hydroxyglutarate regulates CD8(+) T-lymphocyte fate. *Nature* 540, 236-241.

van der Vos, K.E., Eliasson, P., Proikas-Cezanne, T., Vervoort, S.J., van Boxtel, R., Putker, M., van Zutphen, I.J., Mauthe, M., Zellmer, S., Pals, C., *et al.* (2012). Modulation of glutamine metabolism by the PI(3)K-PKB-FOXO network regulates autophagy. *Nat Cell Biol* 14, 829-837.

van Niekerk, G., Loos, B., Nell, T., and Engelbrecht, A.M. (2016). Autophagy--A free meal in sickness-associated anorexia. *Autophagy* 12, 727-734.

van Straten, D., Mashayekhi, V., de Bruijn, H.S., Oliveira, S., and Robinson, D.J. (2017). Oncologic Photodynamic Therapy: Basic Principles, Current Clinical Status and Future Directions. *Cancers (Basel)* 9.

van Vloten, J.P., Workenhe, S.T., Wootton, S.K., Mossman, K.L., and Bridle, B.W. (2018). Critical Interactions between Immunogenic Cancer Cell Death, Oncolytic Viruses, and the Immune System Define the Rational Design of Combination Immunotherapies. *J Immunol* 200, 450-458.

Vander Heiden, M.G., and DeBerardinis, R.J. (2017). Understanding the Intersections between Metabolism and Cancer Biology. *Cell* 168, 657-669.

Vera-Ramirez, L., Vodnala, S.K., Nini, R., Hunter, K.W., and Green, J.E. (2018). Autophagy promotes the survival of dormant breast cancer cells and metastatic tumour recurrence. *Nat Commun* 9, 1944.

Waksmanski, B., Dudkiewicz, J., and Dabrowski, S. (2001). Function of insulin-like growth factor (IGF-I) and its binding protein (IGFBP-1) in pathological proliferation of endometrium. *Wiad Lek* 54, 656-661.

Wang, F., Tang, J., Li, P., Si, S., Yu, H., Yang, X., Tao, J., Lv, Q., Gu, M., Yang, H., *et al.* (2018a). Chloroquine Enhances the Radiosensitivity of Bladder Cancer Cells by Inhibiting Autophagy and Activating Apoptosis. *Cell Physiol Biochem* 45, 54-66.

Wang, Q., Ju, X., Wang, J., Fan, Y., Ren, M., and Zhang, H. (2018b). Immunogenic cell death in anticancer chemotherapy and its impact on clinical studies. *Cancer Lett* 438, 17-23.

Wang, Y.J., Fletcher, R., Yu, J., and Zhang, L. (2018c). Immunogenic effects of chemotherapy-induced tumor cell death. *Genes Dis* 5, 194-203.

Warshamana-Greene, G.S., Litz, J., Buchdunger, E., Garcia-Echeverria, C., Hofmann, F., and Krystal, G.W. (2005). The insulin-like growth factor-I receptor kinase inhibitor, NVP-ADW742, sensitizes small cell lung cancer cell lines to the effects of chemotherapy. *Clin Cancer Res* 11, 1563-1571.

Webb, A.E., and Brunet, A. (2014). FOXO transcription factors: key regulators of cellular quality control. *Trends Biochem Sci* 39, 159-169.

Weiss, J.M., Davies, L.C., Karwan, M., Ileva, L., Ozaki, M.K., Cheng, R.Y., Ridnour, L.A., Annunziata, C.M., Wink, D.A., and McVicar, D.W. (2018). Itaconic acid mediates crosstalk between macrophage metabolism and peritoneal tumors. *J Clin Invest* 128, 3794-3805.

Wellenstein, M.D., and de Visser, K.E. (2018). Cancer-Cell-Intrinsic Mechanisms Shaping the Tumor Immune Landscape. *Immunity* 48, 399-416.

White, E. (2015). The role for autophagy in cancer. *J Clin Invest* 125, 42-46.

Wild, P., McEwan, D.G., and Dikic, I. (2014). The LC3 interactome at a glance. *J Cell Sci* 127, 3-9.

Wittman, M., Carboni, J., Attar, R., Balasubramanian, B., Balimane, P., Brassil, P., Beaulieu, F., Chang, C., Clarke, W., Dell, J., *et al.* (2005). Discovery of a (1H-benzimidazol-2-yl)-1H-pyridin-2-one (BMS-536924) inhibitor of insulin-like growth factor I receptor kinase with in vivo antitumor activity. *J Med Chem* 48, 5639-5643.

Wittman, M.D., Balasubramanian, B., Stoffan, K., Velaparthy, U., Liu, P., Krishnanathan, S., Carboni, J., Li, A., Greer, A., Attar, R., *et al.* (2007). Novel 1H-(benzimidazol-2-yl)-1H-pyridin-2-one inhibitors of insulin-like growth factor I (IGF-1R) kinase. *Bioorg Med Chem Lett* 17, 974-977.

Wong, D.Y., Ong, W.W., and Ang, W.H. (2015). Induction of immunogenic cell death by chemotherapeutic platinum complexes. *Angew Chem Int Ed Engl* 54, 6483-6487.

Xu, T., Stewart, K.M., Wang, X., Liu, K., Xie, M., Ryu, J.K., Li, K., Ma, T., Wang, H., Ni, L., *et al.* (2017). Metabolic control of TH17 and induced Treg cell balance by an epigenetic mechanism. *Nature* 548, 228-233.

Yamazaki, T., Hannani, D., Poirier-Colame, V., Ladoire, S., Locher, C., Sistigu, A., Prada, N., Adjemian, S., Catani, J.P., Freudenberg, M., *et al.* (2014). Defective immunogenic cell death of HMGB1-deficient tumors: compensatory therapy with TLR4 agonists. *Cell Death Differ* 21, 69-78.

Yang, J., Chen, Q., Tian, S., Song, S., Liu, F., Wang, Q., and Fu, Z. (2015a). The role of 1,25-dihydroxyvitamin D3 in mouse liver ischemia reperfusion injury: regulation of autophagy through activation of MEK/ERK signaling and PTEN/PI3K/Akt/mTORC1 signaling. *Am J Transl Res* 7, 2630-2645.

Yang, P.M., Hsieh, Y.Y., Du, J.L., Yen, S.C., and Hung, C.F. (2020). Sequential Interferon beta-Cisplatin Treatment Enhances the Surface Exposure of Calreticulin in Cancer Cells via an Interferon Regulatory Factor 1-Dependent Manner. *Biomolecules* 10.

Yang, S., Wang, X., Contino, G., Liesa, M., Sahin, E., Ying, H., Bause, A., Li, Y., Stommel, J.M., Dell'antonio, G., *et al.* (2011). Pancreatic cancers require autophagy for tumor growth. *Genes Dev* 25, 717-729.

Yang, Y., Li, X.J., Chen, Z., Zhu, X.X., Wang, J., Zhang, L.B., Qiang, L., Ma, Y.J., Li, Z.Y., Guo, Q.L., *et al.* (2012). Wogonin induced calreticulin/annexin A1 exposure dictates the immunogenicity of cancer cells in a PERK/AKT dependent manner. *PLoS One* 7, e50811.

Yang, Z., Goronzy, J.J., and Weyand, C.M. (2015b). Autophagy in autoimmune disease. *J Mol Med (Berl)* 93, 707-717.

Ye, D., Guan, K.L., and Xiong, Y. (2018). Metabolism, Activity, and Targeting of D- and L-2-Hydroxyglutarates. *Trends Cancer* 4, 151-165.

Yla-Anttila, P., Vihinen, H., Jokitalo, E., and Eskelinen, E.L. (2009). Monitoring autophagy by electron microscopy in Mammalian cells. *Methods Enzymol* 452, 143-164.

You, H., Zhang, W., Jones, M.K., Gobert, G.N., Mulvenna, J., Rees, G., Spanevello, M., Blair, D., Duke, M., Brehm, K., *et al.* (2010). Cloning and characterisation of *Schistosoma japonicum* insulin receptors. *PLoS One* 5, e9868.

Youngren, J.F., Gable, K., Penaranda, C., Maddux, B.A., Zavodovskaya, M., Lobo, M., Campbell, M., Kerner, J., and Goldfine, I.D. (2005). Nordihydroguaiaretic acid (NDGA) inhibits the IGF-1 and c-erbB2/HER2/neu receptors and suppresses growth in breast cancer cells. *Breast Cancer Res Treat* 94, 37-46.

Yu, H., and Rohan, T. (2000). Role of the insulin-like growth factor family in cancer development and progression. *J Natl Cancer Inst* 92, 1472-1489.

Zhang, H., Bosch-Marce, M., Shimoda, L.A., Tan, Y.S., Baek, J.H., Wesley, J.B., Gonzalez, F.J., and Semenza, G.L. (2008). Mitochondrial autophagy is an HIF-1-dependent adaptive metabolic response to hypoxia. *J Biol Chem* 283, 10892-10903.

Zhou, H., Forveille, S., Sauvat, A., Yamazaki, T., Senovilla, L., Ma, Y., Liu, P., Yang, H., Bezu, L., Muller, K., *et al.* (2016). The oncolytic peptide LTX-315 triggers immunogenic cell death. *Cell Death Dis* 7, e2134.

Zhou, J., Wang, G., Chen, Y., Wang, H., Hua, Y., and Cai, Z. (2019). Immunogenic cell death in cancer therapy: Present and emerging inducers. *J Cell Mol Med* 23, 4854-4865.

Zitvogel, L., Kepp, O., and Kroemer, G. (2011). Immune parameters affecting the efficacy of chemotherapeutic regimens. *Nat Rev Clin Oncol* 8, 151-160.

ANNEX 1: SCIENTIFIC PUBLICATIONS

1. **Tian AL**[#], Wu Q[#], Liu P, Zhao L, Martins I, Kepp O, Leduc M[#], Kroemer G. Lysosomotropic agents including azithromycin, chloroquine and hydroxychloroquine activate the integrated stress response. *Cell Death Dis.* 2021 Jan 6;12(1):6. doi: 10.1038/s41419-020-03324-w. PMID: 33414432; PMCID: PMC7790317.
2. Wu Q[#], **Tian AL**[#], Li B[#], Leduc M, Forveille S, Hamley P, Galloway W, Xie W, Liu P, Zhao L, Zhang S, Hui P, Madeo F, Tu Y, Kepp O, Kroemer G. IGF1 receptor inhibition amplifies the effects of cancer drugs by autophagy and immune-dependent mechanisms. *J Immunother Cancer.* 2021 Jun;9(6):e002722. doi: 10.1136/jitc-2021-002722. PMID: 34127545; PMCID: PMC8204183.
3. Wu Q[#], **Tian AL**[#], Durand S, Aprahamian F, Nirmalathasan N, Xie W, Liu P, Zhao L, Zhang S, Pan H, Carmona-Gutierrez D, Madeo F, Tu Y, Kepp O, Kroemer G. Isobacachalcone induces autophagy and improves the outcome of immunogenic chemotherapy. *Cell Death Dis.* 2020 Nov 26;11(11):1015. doi: 10.1038/s41419-020-03226-x. PMID: 33243998; PMCID: PMC7690654.
4. Deng J[#], **Tian AL**[#], Pan H, Sauvat A, Leduc M, Liu P, Zhao L, Zhang S, Chen H, Taly V, Laurent-Puig P, Senovilla L, Li Y, Kroemer G, Kepp O. Everolimus and plicamycin specifically target chemoresistant colorectal cancer cells of the CMS4 subtype. *Cell Death Dis.* 2021 Oct 21;12(11):978. doi: 10.1038/s41419-021-04270-x. PMID: 34675191; PMCID: PMC8531384.
5. Wu Q, **Tian AL**, Kroemer G, Kepp O. Autophagy induction by IGF1R inhibition with picropodophyllin and linsitinib. *Autophagy.* 2021 Aug;17(8):2046-2047. doi: 10.1080/15548627.2021.1936934. Epub 2021 Jun 10. PMID: 34110249; PMCID: PMC8386749.
6. Wu Q, **Tian AL**, Pan H, Kepp O, Kroemer G. Autophagic flux assessment by immunoblot. *Methods Cell Biol.* 2021;164:63-72. doi: 10.1016/bs.mcb.2020.10.005. Epub 2021 Mar 1. PMID: 34225919.

7. Liu P, Zhao L, Ferrere G, Alves-Costa-Silva C, Ly P, Wu Q, **Tian AL**, Derosa L, Zitvogel L, Kepp O, Kroemer G. Combination treatments with hydroxychloroquine and azithromycin are compatible with the therapeutic induction of anticancer immune responses. *Oncoimmunology*. 2020 Jul 8;9(1):1789284. doi: 10.1080/2162402X.2020.1789284. PMID: 32923151; PMCID: PMC7458592.

ANNEX 2: PAPERS NOT INCLUDED IN THIS THESIS

ARTICLE

Open Access

Lysosomotropic agents including azithromycin, chloroquine and hydroxychloroquine activate the integrated stress response

Ai-Ling Tian^{1,2}, Qi Wu^{1,2,3}, Peng Liu^{1,2}, Liwei Zhao^{1,2}, Isabelle Martins^{1,2}, Oliver Kepp^{1,2}, Marion Leduc^{1,2} and Guido Kroemer^{1,2,4,5,6}

Abstract

The integrated stress response manifests with the phosphorylation of eukaryotic initiation factor 2 α (eIF2 α) on serine residue 51 and plays a major role in the adaptation of cells to endoplasmic reticulum stress in the initiation of autophagy and in the ignition of immune responses. Here, we report that lysosomotropic agents, including azithromycin, chloroquine, and hydroxychloroquine, can trigger eIF2 α phosphorylation in vitro (in cultured human cells) and, as validated for hydroxychloroquine, in vivo (in mice). Cells bearing a non-phosphorylatable eIF2 α mutant (S51A) failed to accumulate autophagic puncta in response to azithromycin, chloroquine, and hydroxychloroquine. Conversely, two inhibitors of eIF2 α dephosphorylation, nelfinavir and salubrinal, enhanced the induction of such autophagic puncta. Altogether, these results point to the unexpected capacity of azithromycin, chloroquine, and hydroxychloroquine to elicit the integrated stress response.

Introduction

Azithromycin (AZT), chloroquine (CQ), and 3-hydroxychloroquine (HCQ) have attracted much attention over the past months as possible (and controversial) therapeutic agents for the treatment of coronavirus disease-19 (COVID-19)^{1,2}. At this point, it has not been resolved whether the frequently administered combination regimen of AZT and HCQ (often supplemented with zinc) itself reduces the morbidity and mortality of COVID-19 or whether accompanying measures (such as provision of anti-diabetic, anti-hypertensive, anti-inflammatory, and/or anti-thrombotic agents) or even placebo effects account for the clinical efficiency of AZT + HCQ,

which are more frequently observed in retrospective analyses and uncontrolled clinical studies^{3–5} than in prospective randomized studies^{6–9}.

AZT is a macrolide antibiotic, while CQ and HCQ are antimalarial drugs. HCQ is also been widely used for the treatment of rheumatoid arthritis and systemic lupus erythematosus^{10,11}. All the three agents are lysosomotropic^{12–14}, meaning that they are sufficiently lipophilic to penetrate into cells but also weak bases so that they get protonated at low pH to become trapped in lysosomes, hence gradually increasing their concentration in the lysosomal lumen until they destabilize lysosomal membranes due to detergent-like effects, causing a loss of lysosomal acidification and blockade of lysosomal functions^{15,16} that ultimately activates homeostatic circuitries including the activation of transcription factors such as TFEB and TFE3 for lysosomal biogenesis¹⁷. In addition, the loss of lysosomal acidity/function observed in cells treated with AZT, CQ, or HCQ results in the blockade of lysosomal fusion with autophagosomes, thus stalling autophagic flux and causing the accumulation of autophagosomes that cannot be eliminated^{18–20}. Moreover, CQ and

Correspondence: Oliver Kepp (captain.olsen@gmail.com) or Guido Kroemer (kroemer@orange.fr)

¹Centre de Recherche des Cordeliers, Equipe labellisée par la Ligue contre le cancer, Université de Paris, Sorbonne Université, Inserm U1138, Institut Universitaire de France, Paris, France

²Metabolomics and Cell Biology Platforms, Gustave Roussy, Villejuif, France

Full list of author information is available at the end of the article

These authors contributed equally: Ai-Ling Tian, Qi Wu, Marion Leduc

Edited by G. Melino

© The Author(s) 2021



Open Access This article is licensed under a Creative Commons Attribution 4.0 International License, which permits use, sharing, adaptation, distribution and reproduction in any medium or format, as long as you give appropriate credit to the original author(s) and the source, provide a link to the Creative Commons license, and indicate if changes were made. The images or other third party material in this article are included in the article's Creative Commons license, unless indicated otherwise in a credit line to the material. If material is not included in the article's Creative Commons license and your intended use is not permitted by statutory regulation or exceeds the permitted use, you will need to obtain permission directly from the copyright holder. To view a copy of this license, visit <http://creativecommons.org/licenses/by/4.0/>.

HCQ can stimulate lysosomal membrane permeabilization that secondarily elicits the mitochondrial pathway of apoptosis²¹, hence resulting in cell death, likely contributing to the toxicity of these agents^{22,23}.

The integrated stress response (ISR) consists in the phosphorylation of the phylogenetically conserved eukaryotic initiation factor 2 α (eIF2 α) by a series of eIF2 α kinases (EIF2K1 to 4) and plays a cardinal role in the adaptation of stress to endoplasmic reticulum (ER) stress (in particular, the accumulation of unfolded or misfolded proteins in the ER lumen)²⁴, in the innate cellular defense against viral infections (to block the translation of virus-encoded RNAs into protein)^{25–27}, as well as in the initiation of autophagy (which also can lead to the elimination of intracellular pathogens)^{28–31}. Moreover, eIF2 α phosphorylation contributes to the phenomenon of “immunogenic cell death” (ICD)^{32–34}, which likely plays a major role in connecting the virus-induced death of infected cells to immune response that ultimately lead to the active elimination of virus-infected cells by cytotoxic T lymphocytes^{35–37}. This latter effect is achieved due to the contribution of eIF2 α phosphorylation to (i) autophagy, which enables the lysosomal secretion of ATP (which is a major chemoattractant for dendritic cell precursors)^{28,29,31,38} and (ii) the exposure of the ER lumen protein calreticulin at the cell surface (where it acts as an eat-me signal to render dying/dead cells palatable to dendritic cells, allowing them to present viral antigens to T lymphocytes)^{33,39–41}.

In view of the considerable (patho)physiological relevance of ISR, we decided to investigate whether AZT, CQ, or HCQ may induce this phenomenon. Here, we show that these three agents induce signs of ISR *in vivo*, and that ISR contributes to the accumulation of stalled autophagosomes as well as to the cytotoxicity of these agents.

Results

Lysosomotropic agents induce eIF2 α phosphorylation *in vitro*

Human U2OS osteosarcoma cells stably expressing a GFP-LC3 fusion protein exhibit GFP-LC3 dots in the cytoplasm (corresponding to “autophagic puncta”)⁴² in response to the autophagy inducer torin1 (TOR, an inhibitor of mechanistic target of rapamycin, mTOR) and the lysosomal inhibitor bafilomycin A1 (BafA1, an inhibitor of the vacuolar-type H⁺-ATPase (V-ATPase) that is required for lysosomal acidification)⁴³. Similar to BafA1, the three lysosomotropic agents AZT, CQ, and HCQ did not cause any cytotoxicity in the timeframe of the experiment (Fig. 1A–D) but stimulated a dose-dependent increase in GFP-LC3 dots. The formation of GFP-LC3 puncta was observed in wild-type U2OS and human glioma H4 cells but not in cells that are deficient for the essential autophagy protein ATG5 and which

acts upstream of LC3 to facilitate lipidation and membrane association (Fig. 1E, F and Supplementary Fig. 1). Moreover, AZT, CQ, and HCQ stimulated the translocation of the transcription factors TFEB and TFE3 from the cytoplasm to the nuclei, as determined in U2OS cells expressing a GFP-TFEB fusion protein (Fig. 1G, H) or by immunofluorescence detection of TFE3 (Fig. 1I, J). AZT, CQ, and HCQ inhibited autophagic flux in U2OS RFP-GFP-LC3 tandem reporter cells, as can be expected from agents that perturb lysosomal function (Supplementary Fig. 2)^{15,16,44}. In addition, AZT, CQ, and HCQ induced the phosphorylation of eIF2 α (as measured by immunofluorescence and immunoblot using a phosphoepitope-specific antibody) (Fig. 2A, B and Supplementary Fig. 3)⁴⁵, the activation of the transcription factor CHOP (as indicated by the expression of GFP placed under the control of the CHOP promoter) (Fig. 2C, D), the upregulation of ATF6 (as indicated by the expression of an ATF6-GFP fusion protein) (Fig. 2E, F), and the activation of XBP1 (as indicated by the expression of an XBP1-GFP/Venus fusion protein in which GFP/Venus is only expressed after that IRE1 α has caused the splicing of the corresponding mRNA (Fig. 2G, H). However, in quantitative terms, the effects of AZT, CQ, and HCQ on CHOP, ATF6, and XBP1 appear relatively minor when compared to the positive controls thapsigargin and tunicamycin employed to elicit ER stress (Fig. 2C–H). Only the level of eIF2 α phosphorylation induced by AZT, CQ, and HCQ reaches that of the positive controls (Fig. 2A, B). Similarly, CQ and HCQ (but not AZT) induced a relatively low level of NF- κ B activation as compared to the positive control, tumor necrosis factor- α (Supplementary Fig. 4). We conclude that AZT, CQ, and HCQ are potent perturbators of lysosomal function as well as potent inducers of the ISR consisting in eIF2 α phosphorylation.

eIF2 α phosphorylation is required for the induction of autophagic puncta

TFEB and TFE3 are well known pro-autophagic transcription factors^{46,47}. Accordingly, their double knockout (DKO) attenuated the induction of GFP-LC3 puncta by AZT, CQ, and HCQ (Fig. 3A, B). Many autophagy inducers require eIF2 α phosphorylation as a mandatory step for the ignition of the process⁴⁸. Accordingly, we observed that a knockin mutation that renders eIF2 α non-phosphorylatable (due to the replacement of serine in position 51 by an alanine residue: genotype *eIF2 α ^{S51A/S51A}*) strongly inhibited the induction of GFP-LC3 puncta by AZT, CQ, and HCQ (Fig. 3C, D). Similarly, inhibition of ER stress with the chemical chaperone 4-phenylbutyric acid (4-PBA)⁴⁹ attenuated the induction of GFP-LC3 puncta by AZT, CQ, and HCQ (Fig. 4A, B). Conversely, treatment of the cells with two inhibitors of eIF2 α dephosphorylation, nelfinavir⁵⁰ and

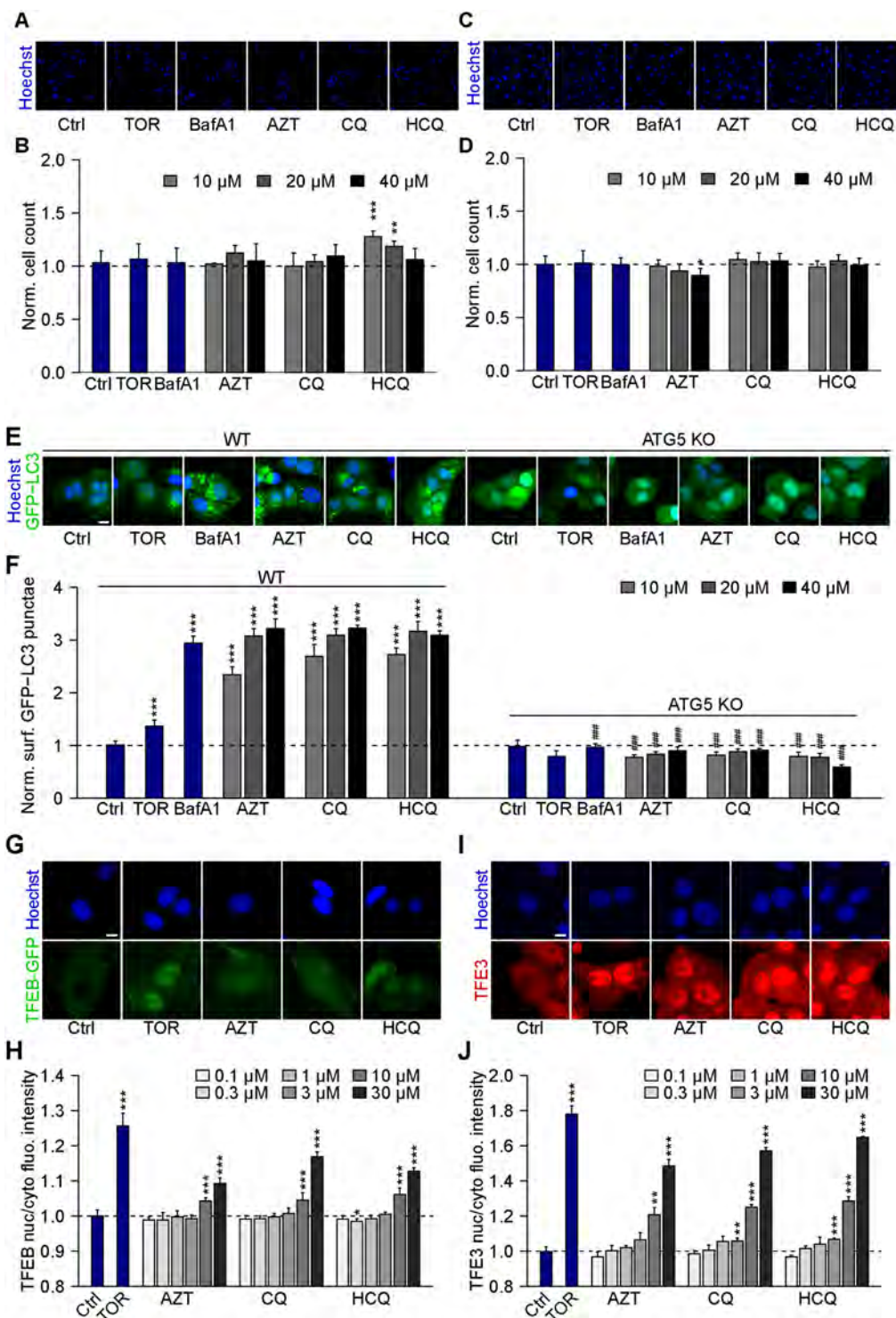


Fig. 1 (See legend on next page.)

(see figure on previous page)

Fig. 1 Chloroquine, hydroxychloroquine, and azithromycin induce the formation of LC3 puncta and trigger TFEB/TFE3 translocation. **A–D** Human osteosarcoma U2OS-GFP-LC3 (**A, B**) or human glioma H4-GFP-LC3 cells (**C, D**) were treated with chloroquine (CQ; 10, 20, 40 μ M), hydroxychloroquine (HCQ; 10, 20, 40 μ M), azithromycin (AZT; 10, 20, 40 μ M), the autophagy inducer torin 1 (TOR; 300 nM), or the inhibitor of autophagic flux bafilomycin A1 (BafA1; 100 nM) for 6 h. After fixation, healthy cells depicted by normal nuclear morphology were enumerated. Representative microscopical images are shown in **A** and **C** (AZT, CQ, and HCQ, 40 μ M) and normalized mean data are depicted as bar charts in **B** and **D**. Data are means \pm SD of four replicates ($*P < 0.05$, $**P < 0.01$, $***P < 0.001$ vs. vehicle control (Ctrl); Student's *t*-test). **E, F** U2OS-GFP-LC3 wild type or ATG5 knockout (KO) cells were treated with CQ, HCQ, or AZT (all at 10, 20, 40 μ M), TOR (300 nM), and BafA1 (100 nM) for 6 h. After fixation, GFP-LC3 dots were analyzed as a proxy for autophagy induction. Representative microscopical images are shown in **E** (AZT, CQ, and HCQ, 40 μ M) and normalized mean data are depicted as bar chart in **F**. Data are means \pm SD of four replicates ($**P < 0.01$, $***P < 0.001$ vs. vehicle control (Ctrl), and $###P < 0.001$ vs. WT; Tukey's multiple comparisons test). **G, H** U2OS cells stably expressing GFP-TFEB fusion protein were treated with CQ, HCQ, or AZT (all at 0.1, 0.3, 1, 3, 10, 30 μ M) for 6 h. TOR at 300 nM was used as a positive control for TFEB nuclear translocation. Images were analyzed and the ratio of GFP intensities in nuclei and cytoplasm was calculated to indicate TFEB translocation to nuclei (**H**). Representative images are depicted in **G** (AZT, CQ, and HCQ, 30 μ M). **I, J** U2OS cells were treated as above, and then TFE3 translocation was assessed microscopically after immunostaining (**I**). TOR at 300 nM was used as a positive control for TFE3 nuclear translocation. TFE3 intensities in the nucleus and the cytoplasm were measured, and the nucleo-to-cytoplasmic ratio of TFE3 intensities was calculated to indicate nuclear translocation of TFE3 (**J**). Data are means \pm SD of four replicates ($*P < 0.05$, $**P < 0.01$, $***P < 0.001$ vs. Ctrl, Student's *t*-test). Scale bars equal 10 μ m.

salubrial⁵¹, enhanced the formation of GFP-LC3 puncta in response to AZT, CQ, and HCQ (Fig. 4A, B and Supplementary Fig. 5).

In accord with previous work²¹, CQ and HCQ induces some degree of cellular toxicity, leading to the manifestation of apoptotic and necrotic events that can be distinguished by dual staining with annexin-V-FITC (which stains apoptotic and necrotic cells) the vital dye 4',6-diamidino-2-phenylindole (DAPI, which only stains necrotic cells)⁵². Among the genotypes evaluated in this paper (*ATG5*^{-/-}, *eIF2 α* ^{S51A/S51A}, *TFEB*^{-/-}, *TFE3*^{-/-}, *TFEB/TFE3* DKO, *PERK*^{-/-}) the *eIF2 α* ^{S51A} knockin mutation rendering *eIF2 α* non-phosphorylatable had the strongest effect on apoptosis induction by CQ and HCQ (Fig. 5A), increasing cellular killing by CQ and HCQ but not by the general tyrosine kinase inhibitor and apoptosis inducer staurosporin (STS) (Fig. 5B and Supplementary Fig. 6). These results point to the ISR as central for the effects of CQ and HCQ.

Lysosomotropic agents induce eIF2 α phosphorylation in vivo

The aforementioned results have been obtained in vitro, calling for their in vivo validation. For this, we injected mice intraperitoneally with HCQ (at a dose that inhibits autophagic flux)^{53–56} alone or in combination with AZT (supplemented in the drinking water). Of note, HCQ (but less so AZT) induced a remarkable and significant increase in *eIF2 α* phosphorylation that was detectable by immunoblot in liver extracts (Fig. 6A, B) but less so in the myocardium (Supplementary Fig 7). In addition, one single injection of HCQ was able to stimulate a significant increase in *eIF2 α* phosphorylation in several circulating leukocyte subsets (in particular neutrophil granulocytes, lymphocytes, and monocytes), as determined by immunofluorescence staining and imaging

flow cytometry (Fig. 6D, E). Thus, HCQ can induce *eIF2 α* phosphorylation in vivo, supporting the capacity of this agent to activate ISR.

Discussion

As we show in this work, lysosomotropic agents including AZR, CQ, and HCQ are capable of stimulating the ISR. The capacity of these agents to induce the cardinal hallmark of ISR, *eIF2 α* phosphorylation, is observed at similar concentrations as those required to induce the accumulation of autophagic puncta and to activate the transcription factors TFEB and TFE3 in a dose of 10–40 μ M. The accumulation of autophagic puncta induced by AZT, CQ, and HCQ requires the initial steps of autophagy, as illustrated by the fact that *ATG5*-deficient cells fail to demonstrate this phenomenon. This is in accordance with findings showing that CQ can induce non-canonical V-ATPase-dependent LC3 lipidation⁵⁷. Moreover, AZT, CQ, and HCQ were unable to elicit the accumulation of LC3-binding autophagosomes in cells expressing a non-phosphorylatable mutant of *eIF2 α* , suggesting causality between ISR and the observed phenomenon. This conjecture was further supported by the observation that two inhibitors of the dephosphorylation of *eIF2 α* enhanced autophagosome accumulation in vitro. Moreover, the apoptosis-inducing effect of CQ and HCQ was reduced in cells bearing mutant *eIF2 α* .

The ISR plays a major role in the inhibition of viral replication. Indeed, multiple viruses have developed strategies to subvert the ISR, either by directly inhibiting *eIF2 α* kinases or by deploying a decoy that resembles *eIF2 α* , hence preventing the phosphorylation of the cellular protein^{25,58,59}. In addition, a protein encoded by coronavirus counteracts the ISR at its very core by acting as a competitive inhibitor of the phospho-*eIF2 α* -*eIF2 β*

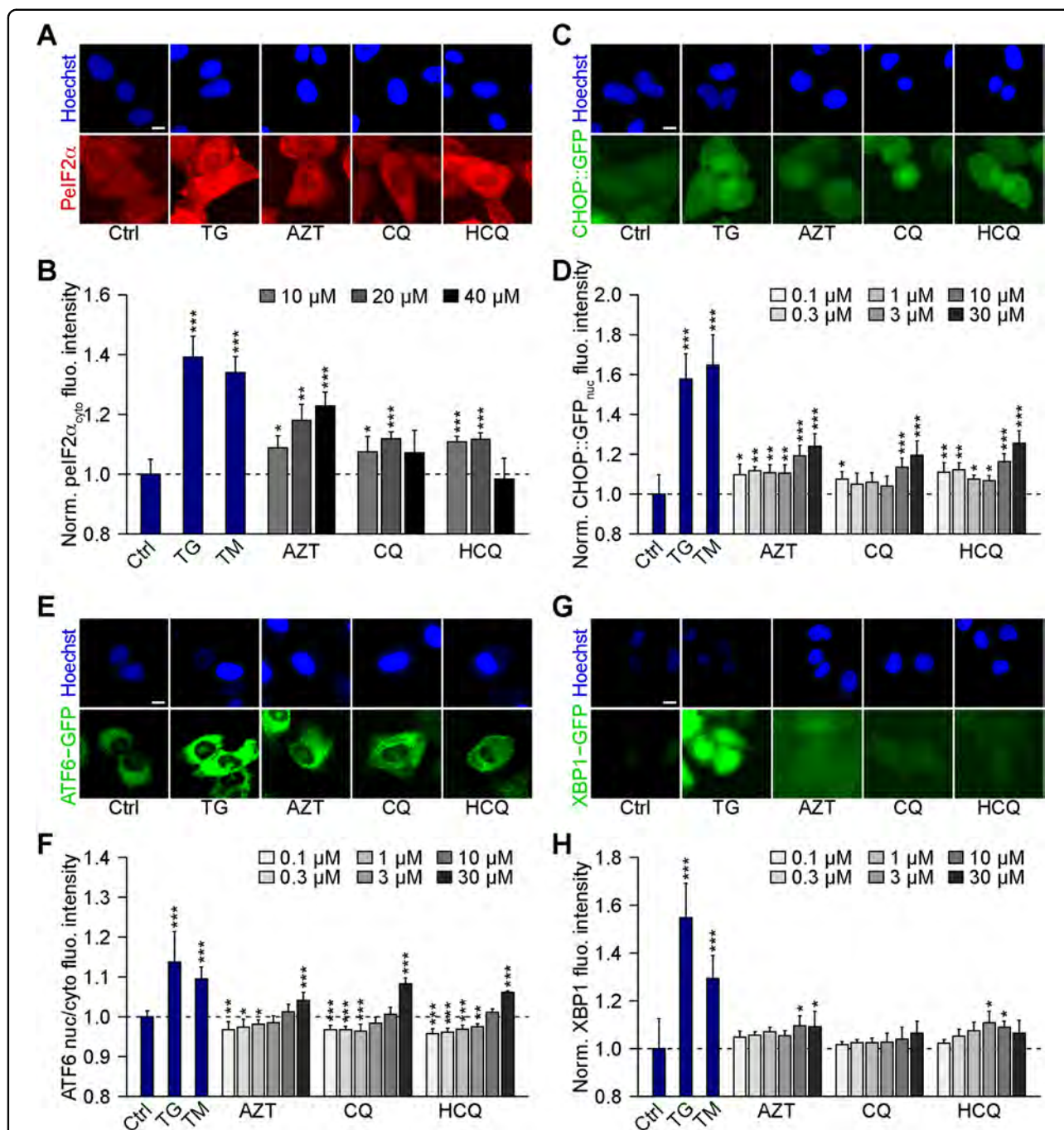


Fig. 2 Chloroquine, hydroxychloroquine, and azithromycin induce ER stress. **A, B** Human osteosarcoma U2OS cells were treated with chloroquine (CQ), hydroxychloroquine (HCQ), and azithromycin (AZT; all at 10, 20, 40 μM) for 16 h, then fixed and imaged. Tunicamycin (TM, 3 μM) and thapsigargin (TG, 3 μM) were used as positive controls for ER stress induction. PeIF2α was assessed by means of an immunofluorescence staining using a phosphoepitope-specific antibody (**A**) and the cytoplasmic intensity is depicted (**B**) (AZT, CQ, and HCQ, 40 μM). **C, D** Human osteosarcoma U2OS cells stably expressing GFP under the promoter of DDIT3 (CHOP::GFP) were treated with the indicated agents (TM (3 μM), TG (3 μM), CQ, HCQ, or AZT (all at 0.1, 0.3, 1, 3, 10, 30 μM)) for 24 h. After fixation, CHOP::GFP fluorescence was assessed microscopically as shown in **C**, and the average nuclear intensity was quantified (**D**). **E, F** U2OS cells stably expressing GFP-ATF6 were treated with the indicated agents for 24 h. After the cells were fixed, GFP-ATF6 nuclear translocation was assessed as shown in **E** (AZT, CQ, and HCQ, 30 μM), and the nuclear-to-cytoplasmic ratio of GFP-ATF6 intensity was quantified (**F**). **G, H** U2OS cells stably expressing XBP1ΔDBD-venus (for monitoring venus expression upon alternative splicing of XBP1 mRNA) were treated as above for 24 h. After fixation, XBP1s expression was assessed via fluorescent microscopy as shown (**G**) (AZT, CQ, and HCQ, 30 μM), and the average intensity was measured (**H**). Data are means ± SD of four replicates (* $P < 0.05$, ** $P < 0.01$, *** $P < 0.001$ vs. vehicle control (Ctrl), Student's *t*-test). Scale bars equal 10 μm.

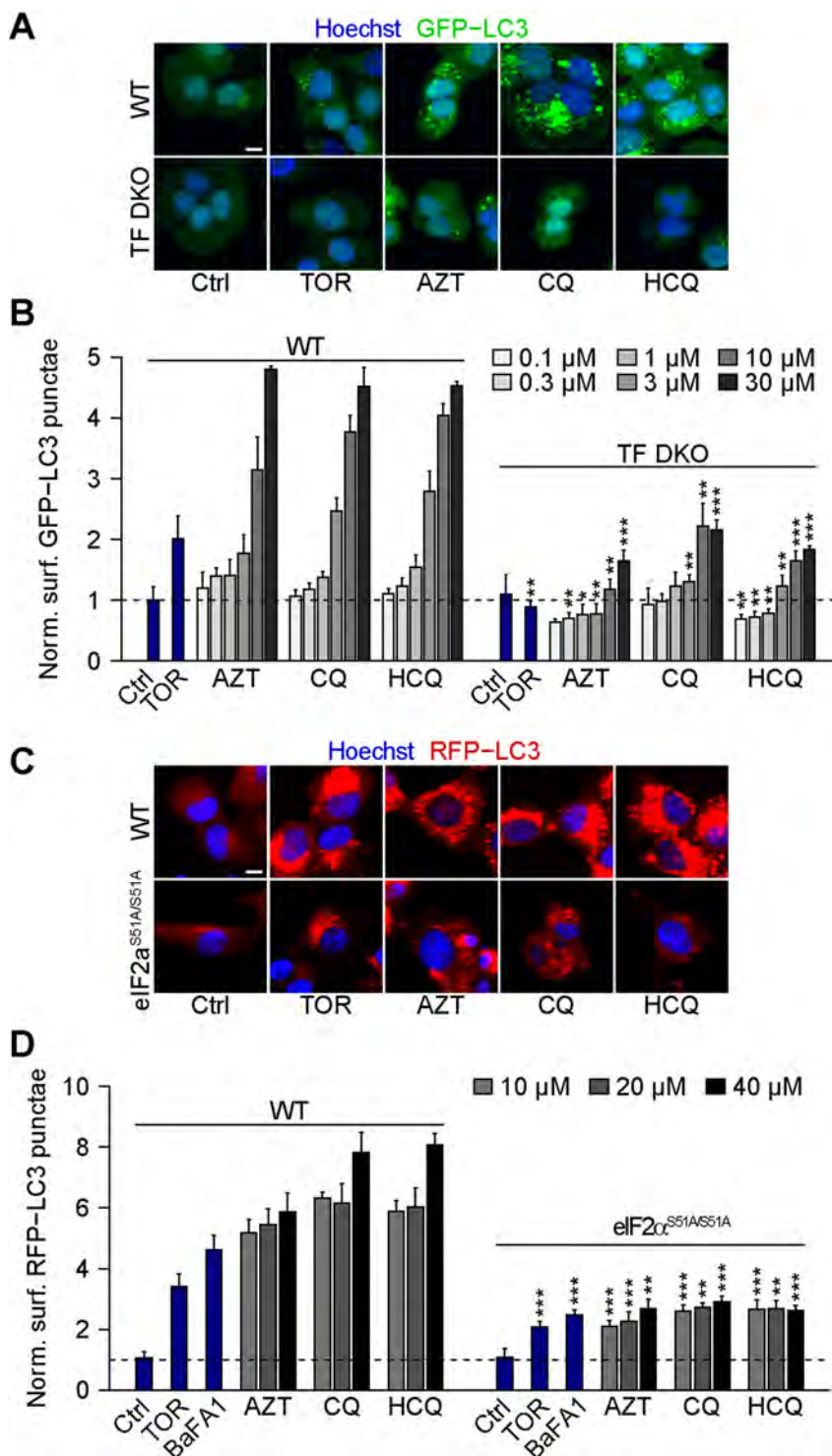


Fig. 3 Chloroquine, hydroxychloroquine, and azithromycin-induced autophagy depends on TFEB/TFE3 and eIF2α. **A, B** Human osteosarcoma U2OS wild type (WT) or TFEB/TFE3 double KO (TF DKO) cells both stably expressing GFP-LC3 were treated with the indicated compounds (torin 1 (TOR; 300 nM), chloroquine (CQ), hydroxychloroquine (HCQ), and azithromycin (AZT; all at 0.1, 0.3, 1, 3, 10, 30 μM)) for 6 h. After fixation, GFP-LC3 dots were analyzed as a proxy for autophagy. Representative images are depicted in **A** (AZT, CQ, and HCQ, 30 μM) and normalized data are shown as bar chart in **B**. Data are means ± SD of four replicates (***P* < 0.01, ****P* < 0.001 vs. WT; Student's *t*-test). **C, D** U2OS WT or Pelf2α S51A knockin cells both expressing RFP-LC3 were treated as indicated with TOR (300 nM), bafilomycin A1 (BafA1, 100 nM), CQ, HCQ, and AZT (all at 10, 20, 40 μM) for 6 h. After fixation, RFP-LC3 dots were analyzed by fluorescent microscopy. Representative images are shown in **C** (AZT, CQ, and HCQ, 40 μM) and normalized data are quantitated as a bar plot in **D**. Data are means ± SD of four replicates (***P* < 0.01, ****P* < 0.001 vs. WT; Student's *t*-test). Scale bars equal 10 μm.

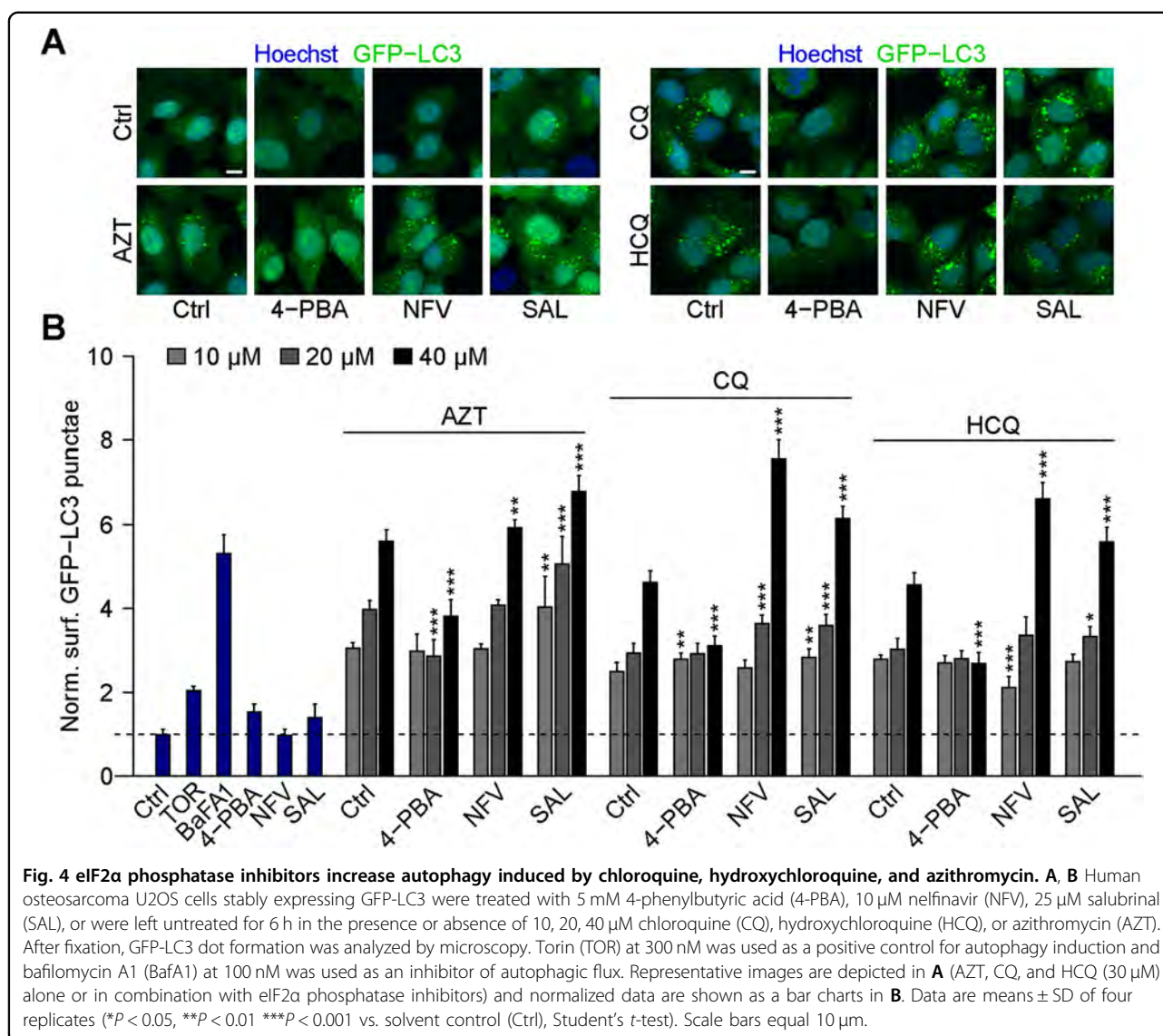


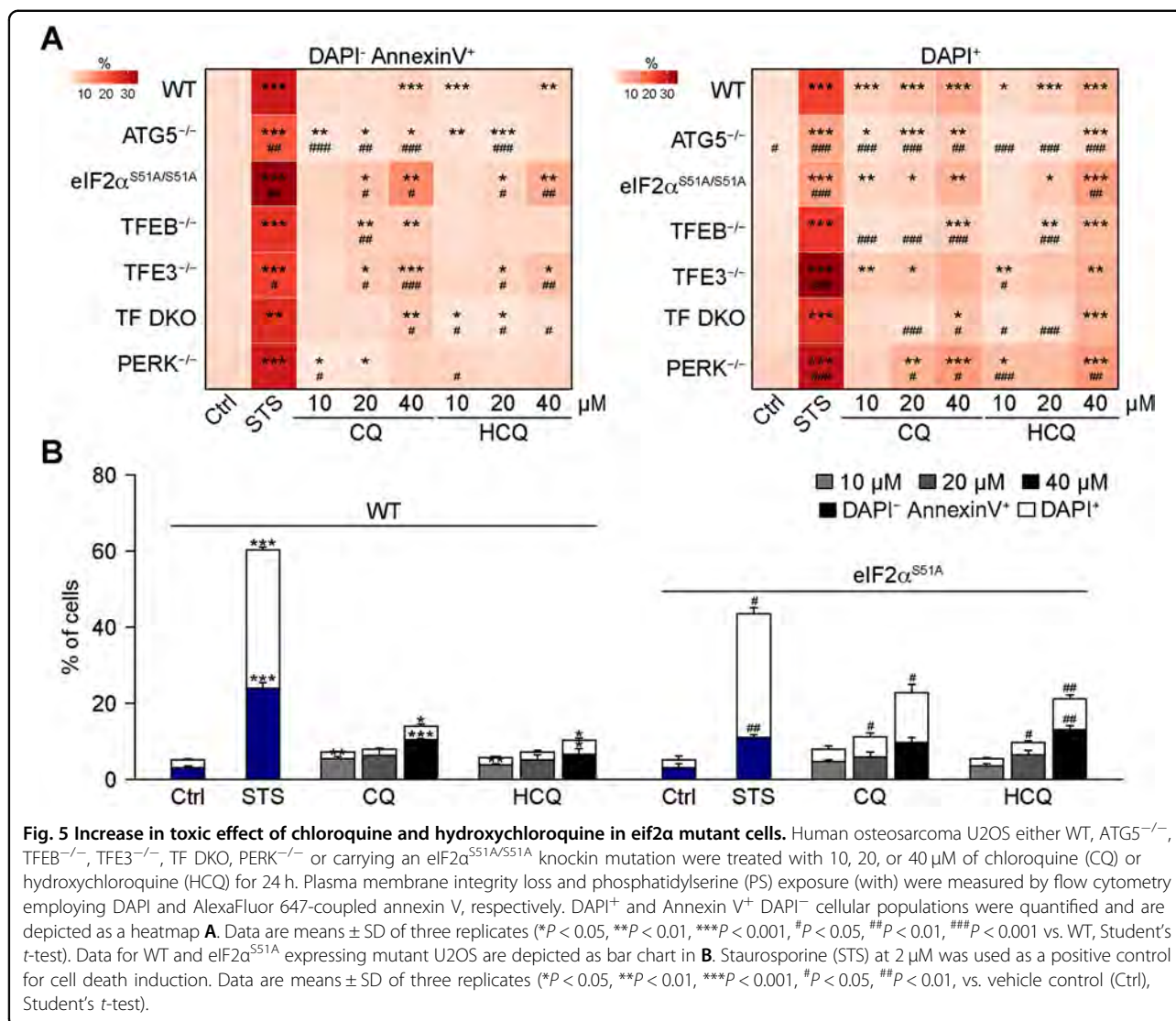
Fig. 4 eIF2 α phosphatase inhibitors increase autophagy induced by chloroquine, hydroxychloroquine, and azithromycin. **A, B** Human osteosarcoma U2OS cells stably expressing GFP-LC3 were treated with 5 mM 4-phenylbutyric acid (4-PBA), 10 μ M nelfinavir (NFV), 25 μ M salubrinal (SAL), or were left untreated for 6 h in the presence or absence of 10, 20, 40 μ M chloroquine (CQ), hydroxychloroquine (HCQ), or azithromycin (AZT). After fixation, GFP-LC3 dot formation was analyzed by microscopy. Torin (TOR) at 300 nM was used as a positive control for autophagy induction and bafilomycin A1 (BafA1) at 100 nM was used as an inhibitor of autophagic flux. Representative images are depicted in **A** (AZT, CQ, and HCQ (30 μ M) alone or in combination with eIF2 α phosphatase inhibitors) and normalized data are shown as a bar charts in **B**. Data are means \pm SD of four replicates (* P < 0.05, ** P < 0.01, *** P < 0.001 vs. solvent control (Ctrl), Student's *t*-test). Scale bars equal 10 μ m.

interaction²⁷. Hence, the question comes up whether the reported in vitro antiviral effects of CQ and HCQ^{27,60} are linked to their capacity to elicit the ISR, thus augmenting an innate immune response (such as the initiation of a type-1 interferon response^{61,62}, beyond their action on acidophilic cellular compartments^{63–65}.

The ISR also has a fundamental role in ICD. In a plausible scenario, cells infected by viruses ultimately succumb to viral infection. If the virus (or other agents) induce the ISR, cell death would be perceived as immunogenic, hence favoring the stimulation of an immune response that involves dendritic cells as antigen presenters that then “educate” cytotoxic T lymphocytes to recognize MHC class I-restricted viral peptides expressed on the surface of infected cells^{37,66}. By clearing infected cells, the immune system then can remove all virus-replicative niches from the body to subsequently establish a memory

response that protects the patient from challenges by the same or antigenically similar viruses.

We have found in the past that artificial induction of the ISR by agents that stimulate an ER stress response (such as thapsigargin injected into tumors) or inhibit the dephosphorylation of eIF2 α (such as salubrinal and a peptides inhibiting the phosphatase PP1 interacting with its cofactor GADD34) can vigorously stimulate anticancer immune responses linked to ICD^{67–70}. In this context, it is noteworthy that agents that selectively stimulate ISR but not any other manifestation of the unfolded stress response (such as the activation of ATF6 and that of IRE1/XBP1) are more efficient ICD inducers than agents with a broad effect on several arms of the unfolded stress response^{33,71,72}. In quantitative terms, when compared to appropriate positive controls (thapsigargin, tunicamycin), AZT, CQ, and HCQ induced a strong ISR but scarce ATF6 and IRE1/XBP1 activation. Hence,



these lysosomotropic agents induce a pattern of response that would be compatible with a pro-ICD action. However, further virological and immunological experimentation will be required to (in)validate this conjecture.

In essence, our results demonstrate that AZT, CQ, and HCQ stimulate the ISR. This might contribute to the potential antiviral and immunostimulatory effects of such lysosomotropic agents. However, to definitively prove the mechanistic relevance of such effects, it would be necessary to develop small animal models⁷³ in which AZT, CQ, and HCQ, alone or in combination would have significant and reproducible antiviral activity.

Materials and methods

Cell culture and chemicals

Culture media and supplements for cell culture were purchased from Gibco-Life Technologies (Carlsbad, CA, USA) and plastic ware came from Greiner Bio-One

(Kremsmünster, Austria) and Corning (Corning, NY, USA). Wild-type human osteosarcoma U2OS or human glioma H4 cells were purchased from the American Type Culture Collection (ATCC, Rockefeller, MD, USA), their derivatives stably expressing GFP-LC3, RFP-LC3, or RFP-GFP-LC3 were cultured in Dulbecco's modified Eagle's medium (DMEM) supplemented with 10% (v/v) fetal bovine serum (FBS), 10 U mL⁻¹ penicillin sodium, and 10 μg mL⁻¹ streptomycin sulfate at 37 °C in a humidified atmosphere with 5% CO₂. TFEB-deficient (TFEB^{-/-}), TFE3-deficient (TFE3^{-/-}), TFEB and TFE3-double deficient (TF DKO), ATG5-deficient (ATG5^{-/-}), and PERK-deficient (PERK^{-/-}) U2OS cells were generated by means of CRISPR/Cas9-mediated genome editing, as per the manufacturer's recommendations^{31,74}. U2OS cells stably expressing RFP-LC3 bearing a non-phosphorylatable mutant of eIF2α (eIF2α^{S51A}) were constructed by means of CRISPR/Cas9 knockin as previously detailed³¹. In

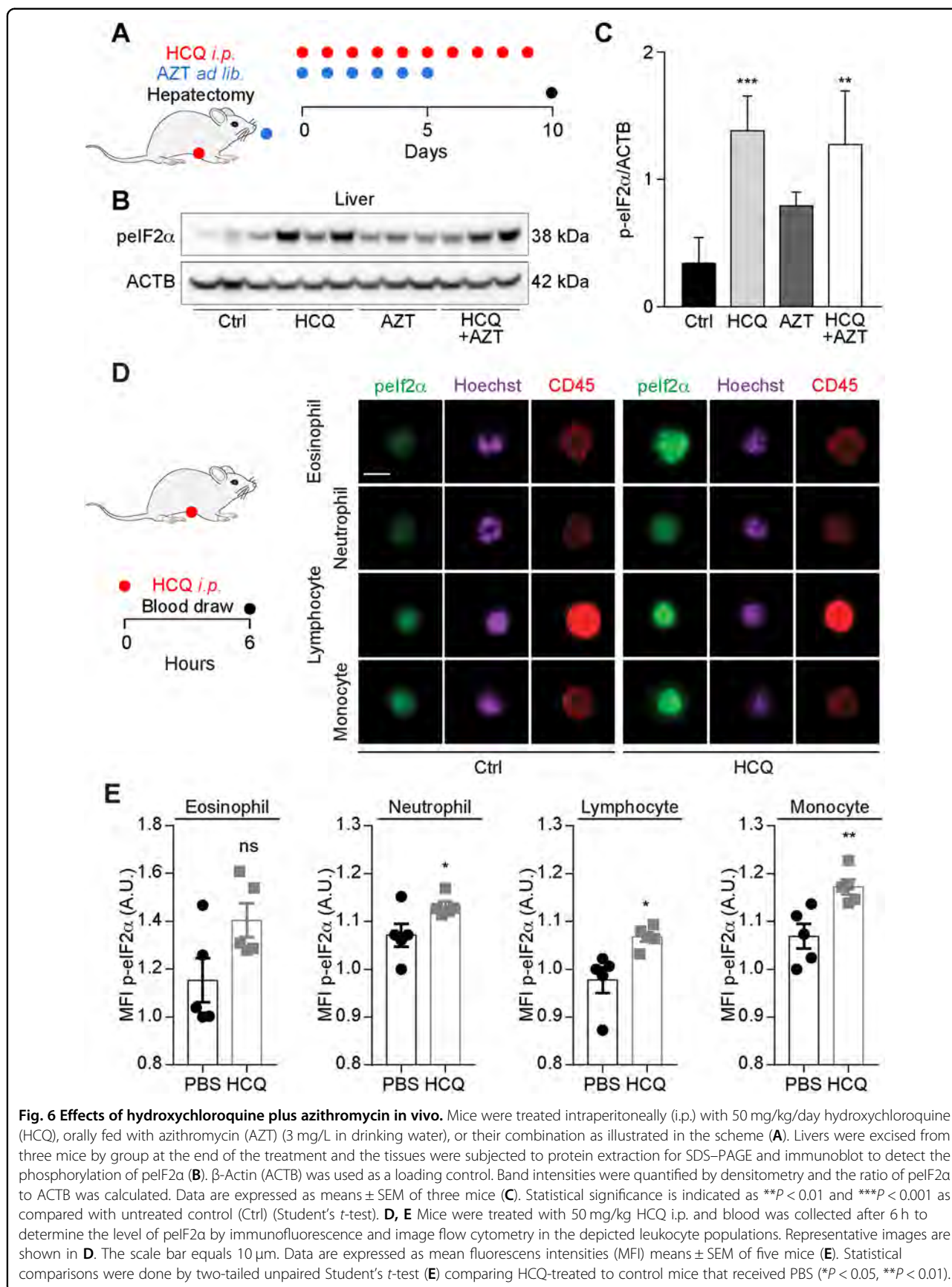


Fig. 6 Effects of hydroxychloroquine plus azithromycin *in vivo*. Mice were treated intraperitoneally (i.p.) with 50 mg/kg/day hydroxychloroquine (HCQ), orally fed with azithromycin (AZT) (3 mg/L in drinking water), or their combination as illustrated in the scheme (A). Livers were excised from three mice by group at the end of the treatment and the tissues were subjected to protein extraction for SDS-PAGE and immunoblot to detect the phosphorylation of p-eIF2α (B). β-Actin (ACTB) was used as a loading control. Band intensities were quantified by densitometry and the ratio of p-eIF2α to ACTB was calculated. Data are expressed as means ± SEM of three mice (C). Statistical significance is indicated as ****P* < 0.01 and *****P* < 0.001 as compared with untreated control (Ctrl) (Student's *t*-test). D, E Mice were treated with 50 mg/kg HCQ i.p. and blood was collected after 6 h to determine the level of p-eIF2α by immunofluorescence and image flow cytometry in the depicted leukocyte populations. Representative images are shown in D. The scale bar equals 10 μm. Data are expressed as mean fluorescens intensities (MFI) means ± SEM of five mice (E). Statistical comparisons were done by two-tailed unpaired Student's *t*-test (E) comparing HCQ-treated to control mice that received PBS (**P* < 0.05, ****P* < 0.01).

addition, U2OS cells stably expressing GFP-TFEB, a GFP under the DDIT3 promoter (CHOP::GFP), GFP-ATF6, and XBP1s- Δ DBD-venus were generated by our group in the past^{33,74}. Chloroquine diphosphate salt (CQ, #C6628), hydroxychloroquine sulfate (HCQ, #PHR1782), azithromycin (AZT, #75199), 4-phenylbutyric acid (4-PBA, #P21005), nelfinavir (NFV, #CDS021783), salubrinal (SAL, #324895), thapsigargin (TG, #T9033), tunicamycin (TM, #T7765), bafilomycin A1 (BafA1, #B1793), tumor necrosis factor- α (TNF- α , #T6674), torin1 (TOR, #475991), and staurosporine (STS, #S4400) were purchased from Sigma-Aldrich (St. Louis, MO, USA).

High-content microscopy

Human osteosarcoma U2OS-GFP-LC3 wild type or TFEB and TFE3-double deficient (TF DKO), ATG5 deficient (ATG5^{-/-}), RFP-GFP-LC3, RFP-LC3 wild type or mutant cells expressing a non-phosphorylatable knockin of eIF2 α (eIF2 α ^{S51A/S51A}) were seeded in 384-well μ clear imaging plates (Greiner Bio-One) at a density of 2×10^3 cells per well and allowed to adapt for overnight. Furthermore, ATG5^{-/-}, eIF2 α ^{S51A/S51A}, and TF DKO cells were treated for 6 h. Moreover, 2×10^3 U2OS cells either wild type or stably expressing GFP-ATF6, CHOP::GFP, GFP-TFEB, or XBP1- Δ DBD-venus were seeded in 384-well black imaging plates (Greiner Bio-One) and let adhere overnight. Cells were then treated for 6 h to assess TFEB translocation, and 24 h to monitor abundance of ATF6 and spliced XBP1 (XBP1s), or to measure CHOP expression. Next, cells were fixed with 3.7% formaldehyde (#F8775; Sigma-Aldrich) supplemented with 1 μ g/ml Hoechst 33342 (#H3570; Thermo Fisher Scientific) at 4 °C overnight. After washing the cells, the plates were sealed and analyzed by automated microscopy. Image acquisition was performed using an ImageXpress Micro XL automated microscope (Molecular Devices, Sunnyvale, CA, US) equipped with a $\times 20$ PlanApo objective (Nikon, Tokyo, Japan), followed by automated image segmentation. A minimum of four images were acquired per well, and experiments involved at least triplicate assessments.

Image segmentation and data analysis

Upon acquisition, images were segmented and analyzed using R. Briefly, cells were segmented and divided into nuclear and cytoplasmic regions based on the nuclear Hoechst staining and cytoplasmic GFP or RFP signal. After exclusion of cellular debris and dead cells, parameters of interest were normalized, statistically evaluated, and graphically depicted with R software. Using R, images were extracted and pixel intensities scaled to be visible (in the same extent for all images of a given experiment).

Immunofluorescence

Cells were treated for 16 h to detect eIF2 α phosphorylation (pEIF2 α) and TFE3 expression, or 6 h to measure p65 nuclear translocation. Then cells were fixed with 3.7% PFA at 4 °C overnight. For the immunostaining of TFE3, p65, and phospho-eIF2 α (Ser51), fixed cells were permeabilized with 0.1% Triton X-100 (#X100; Sigma-Aldrich) on ice, and unspecific antibody binding was blocked with 5% bovine serum albumin (BSA, w/v in PBS) for 1 h. Then cells were incubated with antibodies specific to TFE3 (#ab93808, 1:200; Abcam), phospho-eIF2 alpha (Ser51) (#ab32157, 1:1000; Abcam), or p65 (#4764, 1:100; Cell Signalling Technology) at 4 °C overnight. After washing with PBS twice, AlexaFluor 568-conjugated secondary antibodies (Thermo Fisher Scientific) were employed for additional 2 h at RT. Then cells were washed and imaged by automated fluorescence microscopy as described above. The nuclear-to-cytoplasm intensity ratio of TFE3 and p65 as well as the cytoplasmic intensity of phospho-eIF2 α (Ser51) were measured and normalized to controls.

Imaging cytofluorometric analysis

Six hundred microliters of total blood were diluted in 25 mL red blood cell lysis buffer (BioLegend) and incubated for 10 min at room temperature. Then the cells were washed twice in PBS, fixed with 4% PFA for 20 min at room temperature, permeabilized with 0.25% Tween-20 for 15 min at 4 °C, and blocked with 2% BSA in PBS. Cells were incubated with anti-phospho-eIF2 alpha (Ser51) and AlexaFluor 647-conjugated anti-mouse PTPRC/CD45 antibody (#clone 30-F11; BioLegend) for 1 h at room temperature. Then cells were incubated for 1 h with donkey AlexaFluor488-conjugated secondary antibody and Hoechst 33342 (0.5 μ g/ μ L). Multispectral imaging flow cytometry was performed on an AMNIS ImageStream X Mark II equipped with 375-, 488-, 561-, and 642 nm lasers using the $\times 60$ magnification lens. At least 6000 cells/sample were acquired for each sample. The analysis was performed with IDEAS software v6.2. Exclusively focused images were included in the analysis. Selection was based on the gradient RMS feature of bright field images. A compensation matrix was calculated using single color fluorescent controls. This matrix was applied to each file and singlets were then gated on aspect ratio vs. area of bright field and leukocyte subpopulations were gated on a pictogram indicating the intensity of PTPRC/CD45 staining vs. dark field. Following the intensity of pEIF2 α was quantified in each cell.

Quantification of cell death by flow cytometry

Cell death was assessed by means of the Alexa Fluor 647 Annexin V (#640943; BioLegend) and DAPI (#62248; Thermo Fisher Scientific) kit following the manufacturer's

instructions. Briefly, cells were seeded in 12-well plates (with 5×10^4 cells per well) and incubated at 37 °C in a humidified atmosphere with 5% CO₂ for 24 h, then cells were collected and washed in PBS containing 0.5% BSA before the cell pellet was resuspended in 100 µL of Annexin V Binding Buffer (#422201, BioLegend) containing Alexa Fluor 647-coupled Annexin V. Samples were then incubated at room temperature in the dark for 15 min before adding 100 µL of PBS containing 0.5% BSA and 2 µg/mL DAPI solution. Acquisitions were performed on a BD LSRFortessa™ cell analyzer (BD Biosciences, San Jose, California, USA), and data were statistically analyzed using the FlowJo 10.5.3 software (Tree Star, Ashland, Oregon, USA).

In vivo experimentation

The animal experiment was approved by the Gustave Roussy ethics committee with the project number: 24771–2020032413235413, and all procedures were performed in compliance with the governmental and institutional guidelines and regulations. Mice were kept in a temperature-controlled SPF environment (12 h light/dark cycles) with food and water ad libitum. Eight-week-old female C57Bl/6j mice were obtained from ENVIGO (France). To quantify the in vivo phosphorylation eIF2α (S51), naive mice were intraperitoneally (i.p.) treated with HCQ at a dose of 50 mg/kg/day in 200 µL PBS daily for 10 days^{75,76}; fed with AZT in autoclaved drinking water at a concentration of 3 mg/L (purchased from the local pharmacy) for 5 days, and the solution was changed daily throughout the treatment period^{77,78}. All mice were sacrificed at day 10, 4 h post-injection with HCQ, and livers and hearts were snap frozen in liquid nitrogen.

Immunoblotting

Thirty milligrams of liver tissue were dissociated in Precellys lysing tubes (#CK28; Bertin Technologies SAS, France) containing 1 mL of RIPA lysis buffer (#89901; Invitrogen) by using the Precellys 24 homogenizer (Bertin Technologies SAS) at 6500 r.p.m. for 60 s, followed by spinning at 14×10^3 g for 15 min to collect the supernatant that contains soluble proteins. Protein concentration was measured by means of by the BCA Assay (Bio-Rad, Hercules, CA, USA). The protein solution was mixed with 4× loading buffer (#NP0008; Invitrogen), and denatured at 100 °C for 10 min before subjected to western blotting. Forty micrograms of total protein were resolved on 4–12% NuPAGE Bis-Tris protein gels (#NP0336BOX; Invitrogen) and transferred to PVDF membranes (#IPFL00010; Merck Millipore). The membranes were blocked with 5% non-fat dry milk in TBST for 1 h before incubating with primary antibodies to phospho-eIF2 alpha (Ser51) (#ab32157, 1:1000; Abcam) overnight at 4 °C. Membranes were washed several times with TBST for 10 min each before incubation with HRP-conjugated secondary antibody (#4050-05;

SouthernBiotech) for 2 h at room temperature. At last, the membranes were washed again and subjected to chemiluminescence detection with the Amersham ECL Prime detection reagent kit (#RPN2236; GE Healthcare) on an ImageQuant LAS 4000 software-assisted imager. The exposed membranes were stripped and re-probed with antibodies specific to β-actin (#ab20727; Abcam) as loading control using the procedure described above. Densitometry was performed using the ImageQuant TL software (GE Healthcare, Piscataway, NJ, USA).

Image and data processing

Images were segmented using the EBIImage package (available from Bioconductor repository <https://www.bioconductor.org>) with the R software. The nuclear region was defined using a polygon mask based on the nuclear Hoechst signal, and a second polygon mask was generated using the cytoplasmic GFP or RFP signal. For the assessment of autophagic vesicles, a third mask was created on cytoplasmic regions exhibiting a high intensity signal of GFP or RFP corresponding with LC3 aggregates.

Following image segmentation, the data were extracted and reduced using the R software. After exclusion of cellular debris and dead cells, parameters of interest were normalized to controls, statistically evaluated, and graphically depicted with R software. Using R, images were extracted and pixel intensities scaled to be visible (to the same extent for all images of a given experiment).

Statistical analysis

Unless otherwise mentioned, data are reported as means ± SD of triplicate determinations and experiments were repeated at least three times yielding similar results, and statistical significance was assessed by Student's *t*-test with a *P* value adjustment based on the Benjamini–Hochberg procedure.

Acknowledgements

This study contributes to the IdEx Université de Paris ANR-18-IDEX-0001. A.-L.T. and Q.W. are supported by a CSC fellowship. G.K. is supported by the Ligue contre le Cancer (équipe labellisée); Agence National de la Recherche (ANR)—Projets blancs; ANR under the frame of E-Rare-2, the ERA-Net for Research on Rare Diseases; AMMICA US23/CNRS UMS3655; Association pour la recherche sur le cancer (ARC); Association “Ruban Rose”; Cancéropôle Ile-de-France; Chancellerie des universités de Paris (Legs Poix), Fondation pour la Recherche Médicale (FRM); a donation by Elior; European Research Area Network on Cardiovascular Diseases (ERA-CVD, MINOTAUR); Gustave Roussy Odyssey, the European Union Horizon 2020 Project Oncobiome; Fondation Carrefour; High-end Foreign Expert Program in China (GDW20171100085), Institut National du Cancer (INCa); Inserm (HTE); Institut Universitaire de France; LeDucq Foundation; the LabEx Immuno-Oncology (ANR-18-IDEX-0001); the RHU Torino Lumière; the Seerave Foundation; the SIRIC Stratified Oncology Cell DNA Repair and Tumor Immune Elimination (SOCRATE); and the SIRIC Cancer Research and Personalized Medicine (CARPEM).

Author details

¹Centre de Recherche des Cordeliers, Equipe labellisée par la Ligue contre le cancer, Université de Paris, Sorbonne Université, Inserm U1138, Institut Universitaire de France, Paris, France. ²Metabolomics and Cell Biology Platforms, Gustave Roussy, Villejuif, France. ³Department of Breast and Thyroid Surgery, Renmin Hospital of Wuhan University, Wuhan, Hubei, P. R. China.

⁴Suzhou Institute for Systems Medicine, Chinese Academy of Medical Sciences, Suzhou, China. ⁵Pôle de Biologie, Hôpital Européen Georges Pompidou, AP-HP, Paris, France. ⁶Karolinska Institutet, Department of Women's and Children's Health, Karolinska University Hospital, Stockholm, Sweden

Author contributions

Concept and design: O.K. and G.K. Writing, review, and/or revision of the manuscript: O.K., M.L., and G.K. Experimentation and analysis: A.-L.T., Q.W., P.L., L.Z., I.M., and M.L. All authors approve the final version of the article.

Conflict of interest

G.K. and O.K. are cofounders of Samsara Therapeutics, a biotech company developing autophagy inducers for the treatment of aging. The other authors have no relevant conflict of interest to declare.

Ethics approval

The animal experiment was approved by the Gustave Roussy ethics committee with the project number: 24771-2020032413235413, and all procedures were performed in compliance with the governmental and institutional guidelines and regulations.

Publisher's note

Springer Nature remains neutral with regard to jurisdictional claims in published maps and institutional affiliations.

Supplementary Information accompanies this paper at (<https://doi.org/10.1038/s41419-020-03324-w>).

Received: 4 August 2020 Revised: 1 December 2020 Accepted: 4 December 2020

Published online: 06 January 2021

References

- Gautret, P. et al. Hydroxychloroquine and azithromycin as a treatment of COVID-19: results of an open-label non-randomized clinical trial. *Int. J. Antimicrob. Agents* **56**, 105949 (2020).
- Holopigian, K., Snow, J., Seiple, W. & Siegel, I. Variability of the pattern electroretinogram. *Doc. Ophthalmol.* **70**, 103–115 (1988).
- Gautret, P. et al. Clinical and microbiological effect of a combination of hydroxychloroquine and azithromycin in 80 COVID-19 patients with at least a six-day follow up: A pilot observational study. *Travel Med. Infect. Dis.* **34**, 101663 (2020).
- Lagier, J. C. et al. Outcomes of 3,737 COVID-19 patients treated with hydroxychloroquine/azithromycin and other regimens in Marseille, France: a retrospective analysis. *Travel Med. Infect. Dis.* 101791, <https://doi.org/10.1016/j.tmaid.2020.101791> (2020).
- Mikami, T. et al. Risk factors for mortality in patients with COVID-19 in New York City. *J. Gen. Intern. Med.* <https://doi.org/10.1007/s11606-020-05983-z> (2020).
- Tang, W. et al. Hydroxychloroquine in patients with mainly mild to moderate coronavirus disease 2019: open label, randomised controlled trial. *BMJ* **369**, m1849 (2020).
- Boulware, D. R. et al. A randomized trial of hydroxychloroquine as post-exposure prophylaxis for Covid-19. *N. Engl. J. Med.* <https://doi.org/10.1056/NEJMoa2016638> (2020).
- Das, S., Bhowmick, S., Tiwari, S. & Sen, S. An updated systematic review of the therapeutic role of hydroxychloroquine in coronavirus disease-19 (COVID-19). *Clin. Drug Investig.* **40**, 591–601 (2020).
- Liu, W. et al. Efficacy and safety of antiviral treatment for COVID-19 from evidence in studies of SARS-CoV-2 and other acute viral infections: a systematic review and meta-analysis. *CMAJ* **192**, E734–E744 (2020).
- Rainsford, K. D., Parke, A. L., Clifford-Rashotte, M. & Kean, W. F. Therapy and pharmacological properties of hydroxychloroquine and chloroquine in treatment of systemic lupus erythematosus, rheumatoid arthritis and related diseases. *Inflammopharmacology* **23**, 231–269 (2015).
- Schrezenmeier, E. & Dornier, T. Mechanisms of action of hydroxychloroquine and chloroquine: implications for rheumatology. *Nat. Rev. Rheumatol.* **16**, 155–166 (2020).
- Weissmann, G. Labilization and stabilization of lysosomes. *Fed. Proc.* **23**, 1038–1044 (1964).
- Ignarro, L. J. Effects of anti-inflammatory drugs on the stability of rat liver lysosomes in vitro. *Biochem. Pharmacol.* **20**, 2847–2860 (1971).
- Carevic, O. & Djokic, S. Comparative studies on the effects of erythromycin A and azithromycin upon extracellular release of lysosomal enzymes in inflammatory processes. *Agents Actions* **25**, 124–131 (1988).
- Kuzu, O. F., Toprak, M., Noory, M. A. & Robertson, G. P. Effect of lysosomotropic molecules on cellular homeostasis. *Pharmacol. Res.* **117**, 177–184 (2017).
- Pisonero-Vaquero, S. & Medina, D. L. Lysosomotropic drugs: pharmacological tools to study lysosomal function. *Curr. Drug Metab.* **18**, 1147–1158 (2017).
- Ploper, D. & De Robertis, E. M. The MITF family of transcription factors: role in endolysosomal biogenesis, Wnt signaling, and oncogenesis. *Pharmacol. Res.* **99**, 36–43 (2015).
- Wisner-Gebhart, A. M., Brabec, R. K. & Gray, R. H. Morphometric studies of chloroquine-induced changes in hepatocytic organelles in the rat. *Exp. Mol. Pathol.* **33**, 144–152 (1980).
- Boya, P. et al. Inhibition of macroautophagy triggers apoptosis. *Mol. Cell. Biol.* **25**, 1025–1040 (2005).
- Renna, M. et al. Azithromycin blocks autophagy and may predispose cystic fibrosis patients to mycobacterial infection. *J. Clin. Investig.* **121**, 3554–3563 (2011).
- Boya, P. et al. Mitochondrial membrane permeabilization is a critical step of lysosome-initiated apoptosis induced by hydroxychloroquine. *Oncogene* **22**, 3927–3936, (2003).
- Manic, G., Obrist, F., Kroemer, G., Vitale, I. & Galluzzi, L. Chloroquine and hydroxychloroquine for cancer therapy. *Mol. Cell. Oncol.* **1**, e29911 (2014).
- Kroemer, G. & Galluzzi, L. Lysosome-targeting agents in cancer therapy. *Oncotarget* **8**, 112168–112169 (2017).
- Hetz, C., Zhang, K. & Kaufman, R. J. Mechanisms, regulation and functions of the unfolded protein response. *Nat. Rev. Mol. Cell Biol.* **21**, 421–438, (2020).
- Kepp, O. et al. Viral subversion of immunogenic cell death. *Cell Cycle* **8**, 860–869, <https://doi.org/10.4161/cc.8.6.7939> (2009).
- Johnston, B. P. & McCormick, C. Herpesviruses and the unfolded protein response. *viruses* **12**, <https://doi.org/10.3390/v12010017> (2019).
- Rabouh, H. H. et al. Inhibition of the integrated stress response by viral proteins that block p-eIF2-eIF2B association. *Nat. Microbiol.* <https://doi.org/10.1038/s41564-020-0759-0> (2020).
- Taloczy, Z. et al. Regulation of starvation- and virus-induced autophagy by the eIF2alpha kinase signaling pathway. *Proc. Natl Acad. Sci. USA* **99**, 190–195 (2002).
- Kroemer, G., Marino, G. & Levine, B. Autophagy and the integrated stress response. *Mol. Cell* **40**, 280–293 (2010).
- Costa-Mattioli, M. & Walter, P. The integrated stress response: from mechanism to disease. *Science* **368**, <https://doi.org/10.1126/science.aat5314> (2020).
- Humeau, J. et al. Phosphorylation of eukaryotic initiation factor-2alpha (eIF2alpha) in autophagy. *Cell Death Dis.* **11**, 433 (2020).
- Kepp, O. et al. eIF2alpha phosphorylation as a biomarker of immunogenic cell death. *Semin. Cancer Biol.* **33**, 86–92 (2015).
- Bezu, L. et al. eIF2alpha phosphorylation is pathognomonic for immunogenic cell death. *Cell Death Differ.* **25**, 1375–1393 (2018).
- Humeau, J. et al. Inhibition of transcription by dactinomycin reveals a new characteristic of immunogenic cell stress. *EMBO Mol. Med.* **12**, e11622 (2020).
- Uhl, M. et al. Autophagy within the antigen donor cell facilitates efficient antigen cross-priming of virus-specific CD8+ T cells. *Cell Death Differ.* **16**, 991–1005 (2009).
- Galluzzi, L., Buque, A., Kepp, O., Zitvogel, L. & Kroemer, G. Reply: the complement system is also important in immunogenic cell death. *Nat. Rev. Immunol.* **17**, 143 (2017).
- Tappe, K. A. et al. Immunogenic cell death of dendritic cells following modified vaccinia virus Ankara infection enhances CD8(+) T cell proliferation. *Eur. J. Immunol.* **48**, 2042–2054 (2018).
- Martins, I. et al. Molecular mechanisms of ATP secretion during immunogenic cell death. *Cell Death Differ.* **21**, 79–91 (2014).
- Madeo, F. et al. Phylogenetic conservation of the preapoptotic calreticulin exposure pathway from yeast to mammals. *Cell Cycle* **8**, 639–642 (2009).

40. Senovilla, L., Demont, Y., Humeau, J., Bloy, N. & Kroemer, G. Image cytometry for the quantification of ploidy and endoplasmic reticulum stress in cancer cells. *Methods Mol. Biol.* **1524**, 53–64 (2017).
41. Giglio, P. et al. PKR and GCN2 stress kinases promote an ER stress-independent eIF2alpha phosphorylation responsible for calreticulin exposure in melanoma cells. *Oncoimmunology* **7**, e1466765 (2018).
42. Bravo-San Pedro, J. M. et al. High-throughput quantification of GFP-LC3(+) dots by automated fluorescence microscopy. *Methods Enzymol.* **587**, 71–86 (2017).
43. Klionsky, D. J. et al. Guidelines for the use and interpretation of assays for monitoring autophagy (3rd edition). *Autophagy* **12**, 1–222 (2016).
44. Perera, R. M., Di Malta, C. & Ballabio, A. MiT/TFE family of transcription factors, lysosomes, and cancer. *Annu. Rev. Cancer Biol.* **3**, 203–222 (2019).
45. Bezu, L., Wu Chuang, A., Humeau, J., Kroemer, G. & Kepp, O. Quantification of eIF2alpha phosphorylation during immunogenic cell death. *Methods Enzymol.* **629**, 53–69 (2019).
46. Saftig, P. & Haas, A. Turn up the lysosome. *Nat. Cell Biol.* **18**, 1025–1027, <https://doi.org/10.1038/nbc3409> (2016).
47. Di Malta, C., Cinque, L. & Settembre, C. Transcriptional regulation of autophagy: mechanisms and diseases. *Front. Cell Dev. Biol.* **7**, 114 (2019).
48. Acevo-Rodriguez, P. S., Maldonado, G., Castro-Obregon, S. & Hernandez, G. Autophagy regulation by the translation machinery and its implications in cancer. *Front. Oncol.* **10**, 322 (2020).
49. Kolb, P. S. et al. The therapeutic effects of 4-phenylbutyric acid in maintaining proteostasis. *Int. J. Biochem. Cell Biol.* **61**, 45–52 (2015).
50. De Gassart, A. et al. An inhibitor of HIV-1 protease modulates constitutive eIF2alpha dephosphorylation to trigger a specific integrated stress response. *Proc. Natl Acad. Sci. USA* **113**, E117–E126 (2016).
51. Boyce, M. et al. A selective inhibitor of eIF2alpha dephosphorylation protects cells from ER stress. *Science* **307**, 935–939 (2005).
52. Pozarowski, P., Grabarek, J. & Darzynkiewicz, Z. *Current Protocols in Cell Biology Chapter 18*, 18.8.1–18.8.33 (John Wiley & Sons, Inc., 2004).
53. Ruiz, A. et al. Effect of hydroxychloroquine and characterization of autophagy in a mouse model of endometriosis. *Cell Death Dis.* **7**, e2059 (2016).
54. Burikhanov, R. et al. Chloroquine-inducible Par-4 secretion is essential for tumor cell apoptosis and inhibition of metastasis. *Cell Rep.* **18**, 508–519 (2017).
55. Collins, K. P., Jackson, K. M. & Gustafson, D. L. Hydroxychloroquine: a physiologically-based pharmacokinetic model in the context of cancer-related autophagy modulation. *J. Pharmacol. Exp. Therap.* **365**, 447–459 (2018).
56. Qiao, X. et al. Hydroxychloroquine Improves obesity-associated insulin resistance and hepatic steatosis by regulating lipid metabolism. *Front. Pharmacol.* **10**, 855 (2019).
57. Florey, O., Gammoh, N., Kim, S. E., Jiang, X. & Overholtzer, M. V-ATPase and osmotic imbalances activate endolysosomal LC3 lipidation. *Autophagy* **11**, 88–99 (2015).
58. Jheng, J. R., Ho, J. Y. & Horng, J. T. ER stress, autophagy, and RNA viruses. *Front. Microbiol.* **5**, 388 (2014).
59. Liu, Y. et al. The role of host eIF2alpha in viral infection. *Virology* **17**, 112 (2020).
60. Andreani, J. et al. In vitro testing of combined hydroxychloroquine and azithromycin on SARS-CoV-2 shows synergistic effect. *Microb. Pathog.* **145**, 104228 (2020).
61. Balachandran, S. et al. Essential role for the dsRNA-dependent protein kinase PKR in innate immunity to viral infection. *Immunity* **13**, 129–141 (2000).
62. Liang, Q., Deng, H., Sun, C. W., Townes, T. M. & Zhu, F. Negative regulation of IRF7 activation by activating transcription factor 4 suggests a cross-regulation between the IFN responses and the cellular integrated stress responses. *J. Immunol.* **186**, 1001–1010 (2011).
63. Carmona-Gutierrez, D. et al. Digesting the crisis: autophagy and coronaviruses. *Microb. Cell* **7**, 119–128 (2020).
64. Bonam, S. R., Muller, S., Bayry, J. & Klionsky, D. J. Autophagy as an emerging target for COVID-19: lessons from an old friend, chloroquine. *Autophagy* <https://doi.org/10.1080/15548627.2020.1779467> (2020).
65. Bello-Perez, M., Sola, I., Novoa, B., Klionsky, D. J. & Falco, A. Canonical and noncanonical autophagy as potential targets for COVID-19. *Cells* <https://doi.org/10.3390/cells9071619> (2020).
66. Galluzzi, L., Buque, A., Kepp, O., Zitvogel, L. & Kroemer, G. Immunogenic cell death in cancer and infectious disease. *Nat. Rev. Immunol.* **17**, 97–111 (2017).
67. Obeid, M. et al. Ecto-calreticulin in immunogenic chemotherapy. *Immunol. Rev.* **220**, 22–34 (2007).
68. Panaretakis, T. et al. Mechanisms of pre-apoptotic calreticulin exposure in immunogenic cell death. *EMBO J.* **28**, 578–590 (2009).
69. Kepp, O. et al. Disruption of the PP1/GADD34 complex induces calreticulin exposure. *Cell cycle* **8**, 3971–3977 (2009).
70. Martins, I. et al. Restoration of the immunogenicity of cisplatin-induced cancer cell death by endoplasmic reticulum stress. *Oncogene* **30**, 1147–1158 (2011).
71. Pozzi, C. et al. The EGFR-specific antibody cetuximab combined with chemotherapy triggers immunogenic cell death. *Nat. Med.* **22**, 624–631 (2016).
72. Liu, P. et al. Crizotinib-induced immunogenic cell death in non-small cell lung cancer. *Nat. Commun.* **10**, 1486 (2019).
73. Park, S. J. et al. Antiviral efficacies of FDA-approved drugs against SARS-CoV-2 infection in ferrets. *mBio* <https://doi.org/10.1128/mBio.01114-20> (2020).
74. Chen, G. et al. 3,4-Dimethoxychalcone induces autophagy through activation of the transcription factors TFE3 and TFEB. *EMBO Mol. Med.* <https://doi.org/10.15252/emmm.201910469> (2019).
75. Rosenfeldt, M. T. et al. p53 status determines the role of autophagy in pancreatic tumour development. *Nature* **504**, 296–300 (2013).
76. Vera-Ramirez, L., Vodnala, S. K., Nini, R., Hunter, K. W. & Green, J. E. Autophagy promotes the survival of dormant breast cancer cells and metastatic tumour recurrence. *Nat. Commun.* **9**, 1944 (2018).
77. Radhakrishnan, S. V. et al. Preventive azithromycin treatment reduces non-infectious lung injury and acute graft-versus-host disease in a murine model of allogeneic hematopoietic cell transplantation. *Biol. Blood Marrow Transpl.* **21**, 30–38 (2015).
78. Liu, P. et al. Combination treatments with hydroxychloroquine and azithromycin are compatible with the therapeutic induction of anticancer immune responses. *Oncoimmunology* **9**, 1789284 (2020).

ARTICLE

Open Access

Isobacachalcone induces autophagy and improves the outcome of immunogenic chemotherapy

Qi Wu^{1,2,3,4}, Ai-Ling Tian^{2,3,4}, Sylvère Durand^{2,3}, Fanny Aprahamian^{2,3}, Nitharsshini Nirmalathasan^{2,3}, Wei Xie^{2,3,4}, Peng Liu^{2,3,4}, Liwei Zhao^{2,3,4}, Shuai Zhang^{2,3,4}, Hui Pan^{2,3,4}, Didac Carmona-Gutierrez^{5,6,7}, Frank Madeo^{5,6,7}, Yi Tu¹, Oliver Kepp^{2,3} and Guido Kroemer^{2,3,8,9,10}

Abstract

A number of natural plant products have a long-standing history in both traditional and modern medical applications. Some secondary metabolites induce autophagy and mediate autophagy-dependent healthspan- and lifespan-extending effects in suitable mouse models. Here, we identified isobacachalcone (ISO) as a non-toxic inducer of autophagic flux that acts on human and mouse cells in vitro, as well as mouse organs in vivo. Mechanistically, ISO inhibits AKT as well as, downstream of AKT, the mechanistic target of rapamycin complex 1 (mTORC1), coupled to the activation of the pro-autophagic transcription factors EB (TFEB) and E3 (TFE3). Cells equipped with a constitutively active AKT mutant failed to activate autophagy. ISO also stimulated the AKT-repressible activation of all three arms of the unfolded stress response (UPR), including the PERK-dependent phosphorylation of eukaryotic initiation factor 2 α (eIF2 α). Knockout of TFEB and/or TFE3 blunted the UPR, while knockout of PERK or replacement of eIF2 α by a non-phosphorylatable mutant reduced TFEB/TFE3 activation and autophagy induced by ISO. This points to crosstalk between the UPR and autophagy. Of note, the administration of ISO to mice improved the efficacy of immunogenic anticancer chemotherapy. This effect relied on an improved T lymphocyte-dependent anticancer immune response and was lost upon constitutive AKT activation in, or deletion of the essential autophagy gene *Atg5* from, the malignant cells. In conclusion, ISO is a bioavailable autophagy inducer that warrants further preclinical characterization.

Introduction

Macroautophagy (to which we herein refer as “autophagy”) is a unique cell biology phenomenon that leads to cytoplasmic vacuolization in response to nutrient deprivation as well as to a myriad of other cell stress-inducing conditions¹. Portions of the cytoplasm are enveloped in two-membraned vesicles, the autophagosomes, which then fuse with lysosomes for the digestion of the autophagic

cargo by hydrolases that operate at acidic pH^{2,3}. Autophagy allows to mobilize the cell's energy reserves by digestion of cytoplasmic macromolecules and even entire organelles to recover their building blocks, including amino acids, simple sugars, and free fatty acids⁴. In addition, autophagy allows for the selective degradation of superficial, damaged, or aged cellular components, including dysfunctional organelles and potentially pathogenic protein aggregates. Genetic stimulation of autophagy has potent antiaging properties, reducing the manifestation of age-associated diseases, including arteriosclerosis, cancer, and neurodegeneration^{5–7}. Pharmacological induction of autophagy has similar broad healthspan and lifespan-extending effects, as shown in model organisms including yeast, nematodes, flies, and mice^{8–11}.

Obviously, there is much interest in identifying novel autophagy inducers that operate at low levels of toxicity

Correspondence: Yi Tu (ty701105@163.com) or Oliver Kepp (captain.olsen@gmail.com) or Guido Kroemer (kroemer@orange.fr)

¹Department of Breast and Thyroid Surgery, Renmin Hospital of Wuhan University, Wuhan, China

²Centre de Recherche des Cordeliers, Equipe labellisée par la Ligue contre le cancer, Université de Paris, Sorbonne Université, Inserm U1138, Institut Universitaire de France, Paris, France

Full list of author information is available at the end of the article

These authors contributed equally: Qi Wu, Ai-Ling Tian

Edited by G. Melino

© The Author(s) 2020



Open Access This article is licensed under a Creative Commons Attribution 4.0 International License, which permits use, sharing, adaptation, distribution and reproduction in any medium or format, as long as you give appropriate credit to the original author(s) and the source, provide a link to the Creative Commons license, and indicate if changes were made. The images or other third party material in this article are included in the article's Creative Commons license, unless indicated otherwise in a credit line to the material. If material is not included in the article's Creative Commons license and your intended use is not permitted by statutory regulation or exceeds the permitted use, you will need to obtain permission directly from the copyright holder. To view a copy of this license, visit <http://creativecommons.org/licenses/by/4.0/>.

and mediate broad antiaging and pro-health effects. Chalcones belong to the chemical class of flavonoids and are contained in multiple plants that are reputed for their dietary virtues. Based on these considerations, we have set out in the past to identify autophagy-inducing chalcones. Among a homemade library of chalcones, we identified two different agents, namely, 4,4'-dimethoxychalcone (4,4'DMC)¹² and its isomer 3,4-dimethoxychalcone (3,4-DMC)¹³ as potent autophagy inducers. Of note, both chalcones differ in their mode of action. While 4,4'DMC inhibits autophagy-suppressive GATA transcription factors^{12,14}, 3,4-DMC acts through the activation of the two related pro-autophagic transcription factors EB (TFEB) and E3 (TFE3)¹³. Irrespective of this difference, both 4,4'DMC and 3,4-DMC reduce myocardial infarction in mice. Moreover, 4,4'DMC extended the lifespan of yeast, nematodes, and flies¹², while 3,4-DMC enhanced anticancer immune responses in mice¹³. These preclinical data plead in favor of a potential medical utility for chalcones.

Driven by these considerations, we decided to identify additional pro-autophagic chalcones by screening another collection of agents. Here, we demonstrate that isobacachalcone (ISO) stimulates autophagic flux, delineate the molecular pathways involved in this effect, and suggest clinical utility for this chalcone as a stimulator of anticancer immunity in the context of immunogenic cell death (ICD)-inducing chemotherapy.

Results

Identification of ISO as an inducer of autophagic puncta

Human neuroglioma H4 cells stably transduced with a fusion protein containing green fluorescent protein (GFP) in the N- and microtubule-associated proteins 1A/1B light chain 3B (MAP1LC3B, best known as LC3) in the C-terminus (GFP-LC3) were cultured in the presence of each of the chalcones contained in the Polyphenolic Natural Compound Library from TargetMol, each used at three different concentrations (10, 25, and 50 μ M). We found that ISO, (E)-1-[2,4-dihydroxy-3-(3-methyl-2-butenyl)-phenyl]-3-(4-hydroxyphenyl)-2-propen-1-one or (E)-4,2',4'-trihydroxy-3'-prenylchalcone; 2',4,4'-trihydroxy-3'-prenyl-transchalcone consistently induced GFP-LC3 puncta at doses of 25 and 50 μ M (Fig. 1A–C). This effect was coupled to a reduction in cytoplasmic protein acetylation that could be measured by immunofluorescence assays using antibodies that recognize acetylated lysine residues (Fig. 1D, E). ISO also induced the lipidation of LC3, measurable by immunoblot analyses (in which LC3 lipidation yields a band with higher electrophoretic mobility, i.e., LC3B or LC3-II) that was even observed in the presence of bafilomycin A1, an inhibitor of autophagosome-lysosome fusion, suggesting that ISO induces autophagic flux (Fig. 1F, G). Simultaneously, ISO reduced the abundance of hemagglutinin (HA)-tagged

sequestosome 1 (SQSTM1, best known as p62) fusion protein transfected into the cells, again supporting the idea that ISO stimulates autophagic flux (Fig. 1F, H). In human osteosarcoma U2OS cells, ISO also induced GFP-LC3 puncta but failed to do so upon knockout of the essential autophagy gene *ATG5* (Fig. 1I–K), indicating that the formation of GFP-LC3 puncta is indeed coupled to autophagy. In sum, it appears that ISO is a chalcone endowed with autophagy-stimulatory properties.

ISO induces autophagic puncta through the inhibition of AKT

ISO is known to inhibit protein kinase B (PKB, best known as AKT)^{15,16}. Indeed, U2OS cells stably expressing a GFP-AKT fusion protein responded to stimulation with recombinant insulin growth factor-1 (rIGF1) by a partial translocation of the fluorescent signal to the plasma membrane, reflecting AKT activation. This effect was not detectable for a loss-of-function mutation of AKT consisting of an arginine-to-cysteine mutation in the pleckstrin homology domain of AKT (R25C) (Fig. 2A, B). In addition, ISO inhibited the activating phosphorylation of AKT (Ser473) as well as, downstream of AKT, the phosphorylation of mechanistic target of rapamycin (mTOR) (Ser448), and the mTOR complex 1 (mTORC1)-dependent phosphorylation of S6K (Thr389) (Fig. 2C). Stable transfection of U2OS cells with a constitutively active AKT mutant (T308D/S473D) inhibited the formation of ISO-induced GFP-LC3 puncta (Fig. 2D, E) as well as the lipidation of LC3 (Fig. 2F, G). In conclusion, it appears that ISO stimulates autophagy through the inhibition of AKT.

ISO induces autophagic flux in vitro and in vivo

Next, we determined whether ISO induces actual autophagic flux by means of several fluorescent reporter-based assays. First, we took advantage of a cell line stably expressing an RFP-ATG4-GFP-LC3 Δ G. When expressed in cells, the probe is cleaved into a stable/cytosolic part, RFP-LC3 Δ G (that serves as an internal control) and a degradable/quenchable part, GFP-LC3 (which is destroyed by autophagy). Hence, a diminution of the GFP-to-RFP ratio indicates the occurrence of autophagy¹⁷. ISO consistently induced a decrease in the GFP-to-RFP ratio of cells expressing RFP-ATG4-GFP-LC3 Δ G (Fig. 3A, C). We also used cells stably expressing a mCherry-GFP-p62 tandem fusion protein, in which the low pH-sensitive GFP-dependent fluorescence (but less so the pH-resistant mCherry fluorescence) was reduced upon the culture of the cells with ISO (Fig. 1B, D). Similarly, we used a rat adrenal gland (pheochromocytoma) PC12 cell line expressing a tetracycline-inducible variant of Q74-GFP, meaning that the GFP via a polyglutamine tail forms aggregates in the cytoplasm that can be degraded by macroautophagy¹⁸.

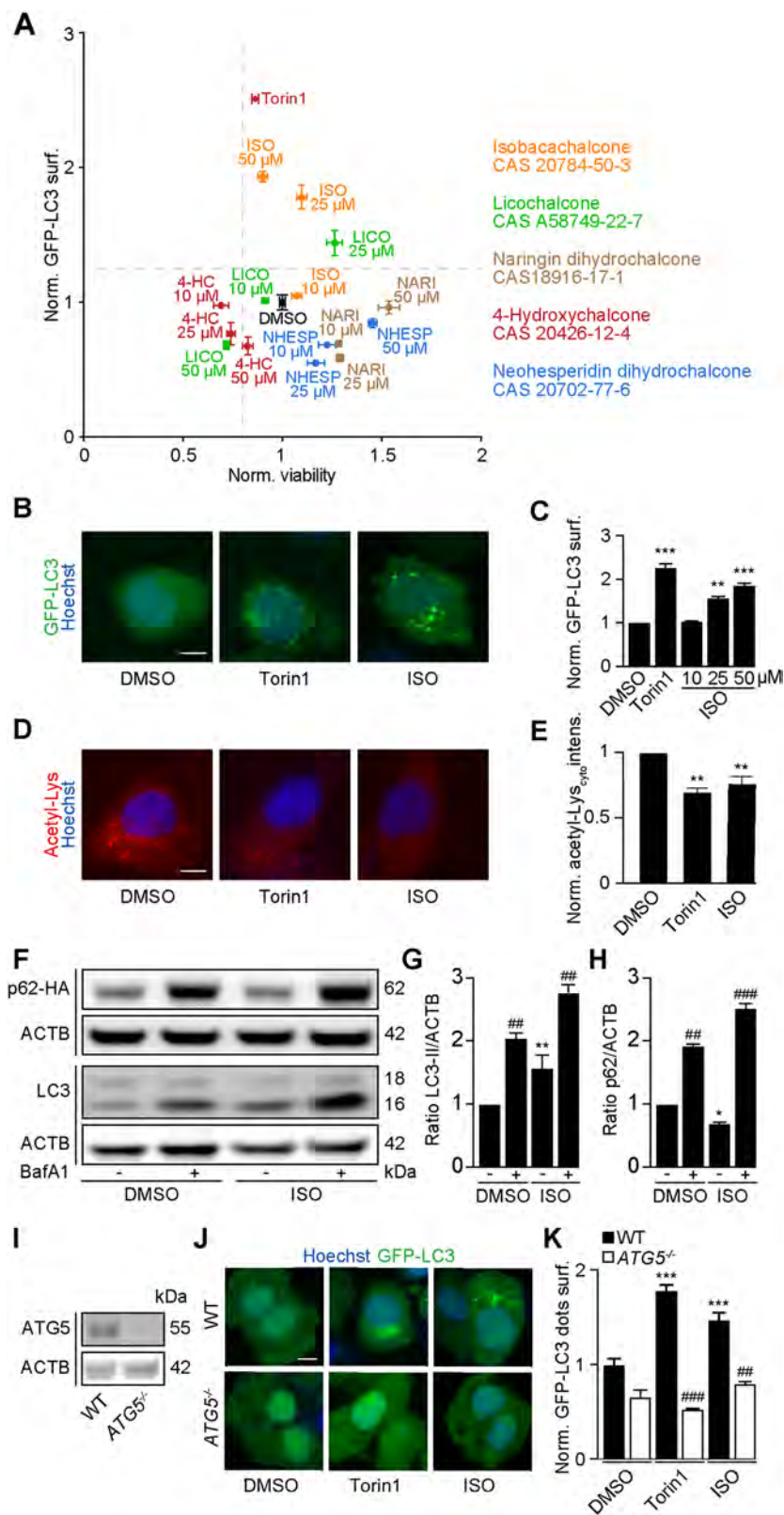


Fig. 1 (See legend on next page.)

(see figure on previous page)

Fig. 1 Isobacachalcone (ISO) is a candidate caloric restriction mimetic (CRM). **A** Human neuroglioma H4 cells stably expressing GFP-LC3 were treated with a selection of chalcones from the TargetMol library of flavonoids at the indicated concentrations. We compared the selected agents at different concentrations with the standard autophagy inducer torin 1 (300 nM), and identified conditions with significantly increased GFP-LC3 puncta formation (1.25 times of the vehicle control (DMSO)) and viability of at least 80% with respect to DMSO, as potent autophagy activation. **B, C** H4 cells stably expressing GFP-LC3 were treated with isobacachalcone (ISO) (10, 25, and 50 μ M) for 6 h. Then the cells were fixed and imaged to assess the formation of GFP-LC3 puncta (**C**). Torin 1 (300 nM) was used as a prototypical autophagy inducer. Representative images are shown in (**B**). Scale bar equals 10 μ m. Data are means \pm SD of quadruplicates (** P < 0.01; *** P < 0.001 vs. DMSO/Ctr, Student's t test). **D, E** U2OS cells were treated as described above, followed by the incubation with specific antibodies to block acetylated tubulin. Thereafter, immunofluorescence was conducted with antibodies against acetylated lysine residues and appropriate AlexaFluor-conjugated secondary antibodies. Representative images of lysine acetylation are shown in (**D**), and the decrease of acetylation in the cytoplasm was measured in (**E**). Scale bar equals 10 μ m. Data are means \pm SD of quadruplicates (** P < 0.01 vs. DMSO/Ctr, Student's t test). **F, H** U2OS cells transfected with a plasmid expressing p62 protein fused with an HA tag (HA-p62) were treated with ISO (25 μ M) in the presence or absence of bafilomycin A1 (Baf A1, 100 nM) for 6 h. SDS-PAGE and immunoblot were performed, band intensities of HA-p62 and β -actin (ATCB) were assessed, and the ratio (HA/ATCB) was calculated (**H**). In parallel samples, band intensities of LC3-II and ATCB were assessed, and their ratio (LC3-II/ATCB) was calculated (**G**). Data are means \pm SD of three independent experiments (* P < 0.05, ** P < 0.01 vs. untreated control; ## P < 0.01, ### P < 0.001 vs. without Baf A1; Tukey's multiple comparisons test). **I, K** Human osteosarcoma U2OS cell stably expressing GFP-LC3 either wild-type (WT) or ATG5 knockout (**I**) were treated with ISO (25 μ M) or torin 1 (300 nM) for 6 h. The cells were fixed, imaged, and GFP-LC3 dots were quantified (**K**). Scale bar equals 10 μ m. Data are means \pm SD of quadruplicates (** P < 0.001 vs. untreated control; ## P < 0.01, ### P < 0.001 vs. WT; Tukey's multiple comparisons test).

Again, we found that ISO reduced the number of Q74-GFP dots in this experimental system, supporting the idea that it indeed stimulates autophagic flux.

Encouraged by these findings, we determined whether ISO might inhibit the AKT pathway and induce autophagy in vivo. Multiple immunoblot experiments indicated that ISO reduces AKT, mTOR, and S6K phosphorylation while it enhances the abundance of LC3-II in the heart or liver of mice receiving intraperitoneal (i.p.) ISO injections. Thus, ISO can stimulate autophagy in vivo. Notably, the in vivo effects of ISO were not accompanied by measurable weight loss, suggesting that ISO is not toxic.

ISO induces TFEB/TFE3 activation and ER stress

U2OS cells exposed to ISO exhibited the translocation of a TFEB-GFP fusion protein from the cytoplasm to the nucleus (Fig. 4A, B). Similarly, TFE3 detectable by immunofluorescence translocated to the nucleus upon culture with ISO (Fig. 4C, D). The nuclear translocation of TFEB and TFE3 could be confirmed by cellular fractionation and immunoblot detection of the two transcription factors in the cytoplasm and nuclei (Fig. 4E–G). Accordingly, knockout of *TFEB* alone (Fig. 4H–K), *TFE3* alone (Fig. 4L–O), or their double knockout (genotype: *TFEB*^{-/-} *TFE3*^{-/-}) blunted the induction of autophagic GFP-LC3 puncta and the lipidation of LC3.

In U2OS cells equipped with biosensors of endoplasmic reticulum (ER) stress, we found that ISO induced the upregulation of CHOP (measured by using a GFP gene inserted into the genome under the control of the CHOP promoter, Fig. 5A, B) and activated the IRE1/XBP1 axis (measured by means of an XBP1 Δ DBD-venus fusion protein¹⁹ that is only in-frame for venus, a variant of GFP, when XBP1 has been spliced by IRE1, Fig. 5C, D). Similar results were obtained when signs of ER stress were

measured by immunofluorescence to detect the nuclear presence of CHOP (Fig. 5E, F) and ATF6 (Fig. 5G, H), the phosphorylation of eukaryotic initiation factor 2 α (eIF2 α) on serine 51 (Fig. 5I, J) and the expression of the spliced isoform of XBP1 (XBP1s) (Fig. 5K, L). In most of the cases, the ISO-induced signs of ER stress were comparable in magnitude to those induced by the positive controls thapsigargin (TG) and tunicamycin (TM) (Fig. 5A–L). Moreover, the expression of constitutively active AKT mutant blunted the signs of ER stress induced by ISO (Fig. 5E–L).

Interestingly, a crosstalk between the pro-autophagic and the ER stress-inducing activities of ISO was observed. Thus, *TFEB*^{-/-} *TFE3*^{-/-} cells exhibited a reduced activation of CHOP (Supplementary Fig. S1A, B) and ATF4 (Supplementary Fig. S1C, D). Such a reduced CHOP and ATF4 activation was also found for the single-gene knockout of *TFEB* or *TFE3* (Supplementary Fig. S2). Cells lacking the eIF2 α kinase 3 (EIF2AK3, best known as PERK) exhibited reduced phosphorylation of eIF2 α in response to ISO (Supplementary Fig. S1E, F), coupled to reduced formation of autophagic RFP-LC3 puncta (Supplementary Fig. S1G, H). Both the knockout of PERK and a knock-in mutation of eIF2 α rendering it non-phosphorylatable (due to the substitution of serine 51 by an alanine residue: S51A) significantly reduced the activation of TFE3 by ISO (Supplementary Fig. S1I–L). These findings suggest molecular crosstalk between the TFEB/TFE3 and the PERK/eIF2 α pathways triggered by ISO.

ISO improves the outcome of immunogenic chemotherapy

Although ISO alone had rather scarce cytotoxic activities, it was able to amplify the ATP release induced by treatment of U2OS cells with low doses of an ICD inducer (mitoxantrone, MTX), as determined by staining of cells with the ATP biosensor quinacrine (Fig. 6A, B) or by

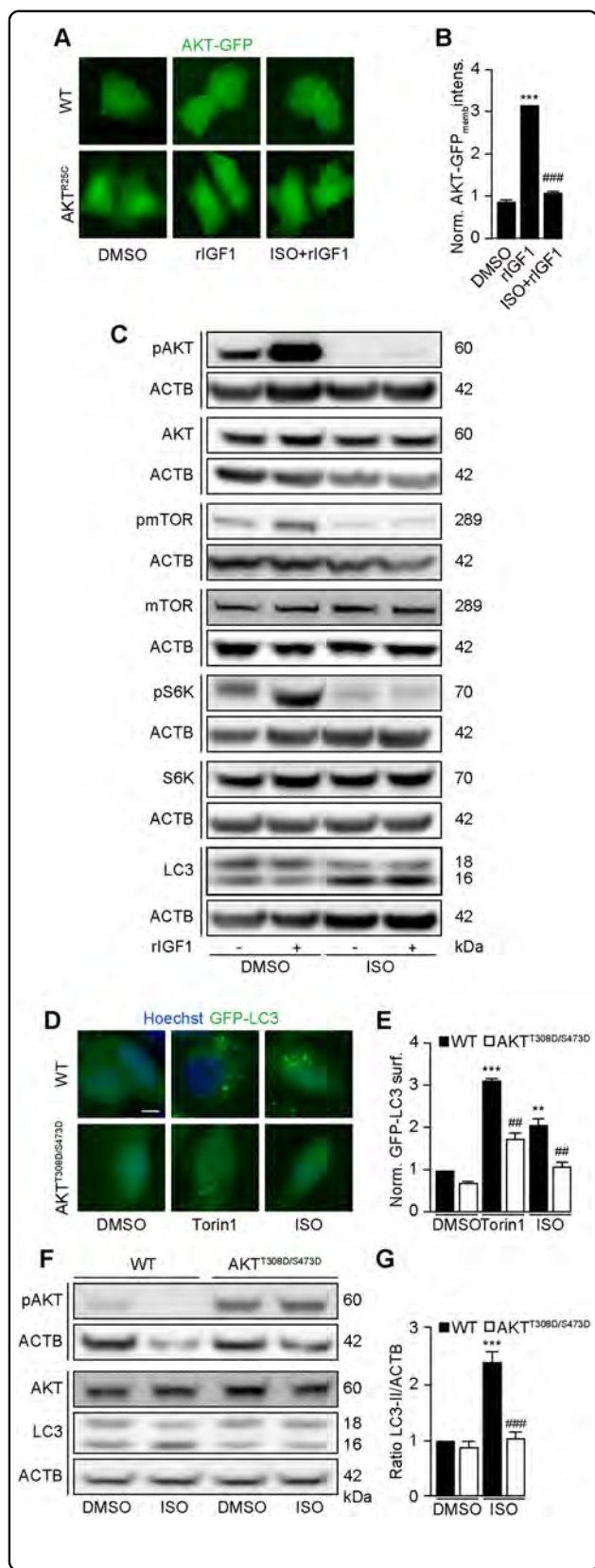


Fig. 2 Inhibition of AKT phosphorylation is pivotal to ISO-induced autophagy. **A, B** Human osteosarcoma U2OS cells stably expressing GFP-AKT or GFP-AKT^{R25C} were treated serum-deprived overnight, then the cells were treated with recombinant IGF1 (rIGF1, 10 nM) or isobacachalcone (ISO; 25 μM) combined with rIGF1. The membrane translocation of GFP-AKT was detected after 10 min (**A**), and the intensity of membranous AKT was measured (**B**). Data are means ± SD of quadruplicates (****P* < 0.001 vs. untreated control; ##*P* < 0.01, ###*P* < 0.001 vs. DMSO/Ctr; Tukey's multiple comparisons test). **C** Serum-deprived U2OS cells were treated with ISO (25 μM) with or without recombinant IGF1 (rIGF1, 10 nM) for 6 h, and parallel immunoblots were performed for detecting pAKT, AKT, pmTOR, mTOR, pS6K, S6K, and LC3-II. β-actin (ACTB) was utilized to ensure equal loading (**C**). **D, E** U2OS-GFP-LC3 cells transfected with a plasmid coding for AKT^{T308D/S473D} were treated with ISO (25 μM) or torin 1 (300 nM) for 6 h, and GFP-LC3 dots were quantified in (**E**). Scale bar equals 10 μm. Data are means ± SD of quadruplicates (***P* < 0.01, ****P* < 0.001 vs. untreated control; #*P* < 0.05, ##*P* < 0.01, ###*P* < 0.001 vs. WT; Tukey's multiple comparisons test). **F, G** U2OS cells were transfected with a plasmid expressing AKT^{T308D/S473D}. Then the cells were serum-deprived and treated with ISO (25 μM) for 6 h. Parallel immunoblot for pAKT, AKT, and LC3-II were performed, and ACTB was used to ensure equal loading. Band intensities of LC3-II and ACTB were assessed, and their ratio (LC3-II/ACTB) was calculated (**G**). Data are means ± SD of three independent experiments (***P* < 0.001 vs. untreated control; ###*P* < 0.001 vs WT; Tukey's multiple comparisons test).

measuring ATP in the supernatant of the cells using a biochemical assay (Fig. 6C–F). ATP is released from stressed cancer cells in an autophagy-dependent fashion^{20,21} and acts in the extracellular space as an important chemotactic factor that attracts myeloid immune effectors into the tumor bed, thereby setting off the molecular cascade that permits anticancer immune responses in the context of ICD^{22,23}. In contrast, ISO did not affect other autophagy-independent hallmarks of ICD²⁴, including surface exposure of calreticulin or the release of high mobility group protein B1 from low-dose MTX-treated cells (Supplementary Fig. S3). Of note, the knockouts of ATG5 (Fig. 6C) or PERK (Fig. 6D), the S51A mutation of eIF2α (Fig. 6E) or the expression of a constitutively active AKT mutant (Fig. 6F) reduced the ATP release induced by the combination of low-dose MTX and ISO, supporting the idea that the aforementioned pathways are important for this phenomenon.

Next, we determined the capacity of ISO to enhance the efficacy of ICD-inducing chemotherapy in vivo, using immunocompetent mice-bearing syngeneic cutaneous MCA205 fibrosarcomas. We chose this type of methylcholantrene-induced tumor because it is well characterized in immunosurveillance models^{25,26}, and because its growth under the skin can be considered as orthotopic. Once MCA205 tumors had been established, the mice received the ICD inducer oxaliplatin (OXA), ISO or the combination (OXA + ISO) while negative controls received vehicle alone (Fig. 6G). Of note, the combination

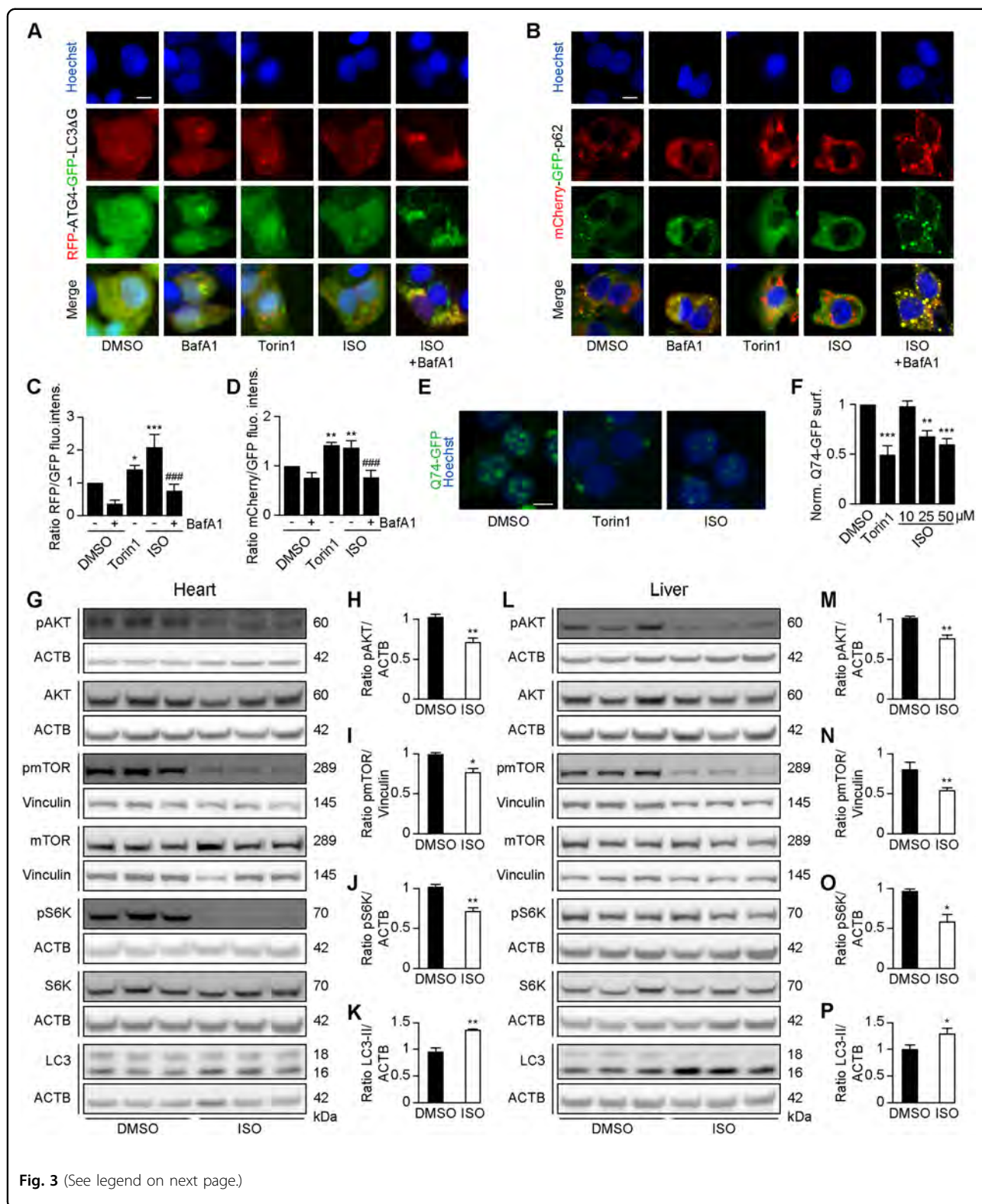


Fig. 3 (See legend on next page.)

(OXA + ISO) allowed for tumor growth control in conditions in which ISO and OXA alone had no or little effect, respectively (Fig. 6H). The anticancer activity depended on

the immune system since it was lost in mice lacking mature T cells due to the *nu/nu* mutation that causes athymia (Fig. 6I). Moreover, tumor cells engineered to lack

(see figure on previous page)

Fig. 3 ISO stimulates autophagic flux in vitro and in vivo. **A–D** Human osteosarcoma U2OS cells stably expressing the tandem reporter construct GFP-LC3-ATG4-RFP-LC3ΔG (**A**) or the tandem reporter mCherry-GFP-p62 (**B**) were treated with torin 1 (300 nM) or isobacachalcone (ISO; 25 μM) with or without bafilomycin A1 (Baf A1, 100 nM) for 6 h. After fixation, GFP and RFP fluorescence was measured by automated image analysis, and the ratio of RFP to GFP was calculated (**C, D**). Scale bar equals 10 μm. Data are means ± SD of quadruplicates (* $P < 0.05$, ** $P < 0.01$, *** $P < 0.001$ vs. untreated control, ### $P < 0.001$ vs. without Baf A1; Tukey's multiple comparisons test). **E, F** Rat adrenal gland PC12 cells stably expressing an inducible variant of Q74-GFP were treated with doxycycline (1 μg/mL) for 8 h for the induction of Q74 expression. Then the medium was changed, and ISO (10, 25, 50 μM) was added for 24 h. Torin 1 (300 nM) was used as a positive control. Representative images are shown in (**E**), and GFP-Q74 levels were quantitated in (**F**). Scale bar equals 10 μm. Data are means ± SD of quadruplicates (** $P < 0.01$, *** $P < 0.001$ vs. DMSO/Ctr, Student's *t* test). **G–M** C57BL/6 mice received two *intraperitoneal* (*i.p.*) injections of 20 mg/kg/day ISO ($n = 3$ mice per condition, $n = 2$ experiments). Organs were collected, and representative immunoblots showing regulators and LC3I-to-LC3-II conversion in the heart (**G–K**) and in the liver (**L–P**). AKT, mTOR, and p70 abundance was evaluated, and parallel samples were probed with phosphoepitope-specific antibodies. β-actin (ACTB) or vinculin levels were monitored to ensure equal protein loading (**H, J**). Band intensities of pAKT and ACTB, pmTOR and Vinculin, pS6K and ACTB, as well as LC3-II and ACTB, were assessed, and their ratios were calculated (**H–K, M–P**). Data are means ± SD ($n = 3$; * $P < 0.05$, ** $P < 0.01$ vs. DMSO/Ctr, Student's *t* test).

Atg5 or to express constitutively active AKT failed to respond to the ISO/OXA combination treatment in the immunocompetent setting (Fig. 6J, K). Analysis of the immune infiltrates of the tumors treated with ISO, OXA, or ISO + OXA (Fig. 6L) revealed that the combination treatment was particularly efficient in reducing regulatory T cells (Tregs, defined as CD3⁺CD4⁺FoxP3⁺ cells), in improving the ratio of CD8⁺ cytotoxic T lymphocytes (CTLs) over Tregs and in reducing the expression of the exhaustion marker PD-1 on CTLs (Fig. 6M–P). In conclusion, ISO stimulates anticancer immunity in the context of ICD-inducing chemotherapy.

Discussion

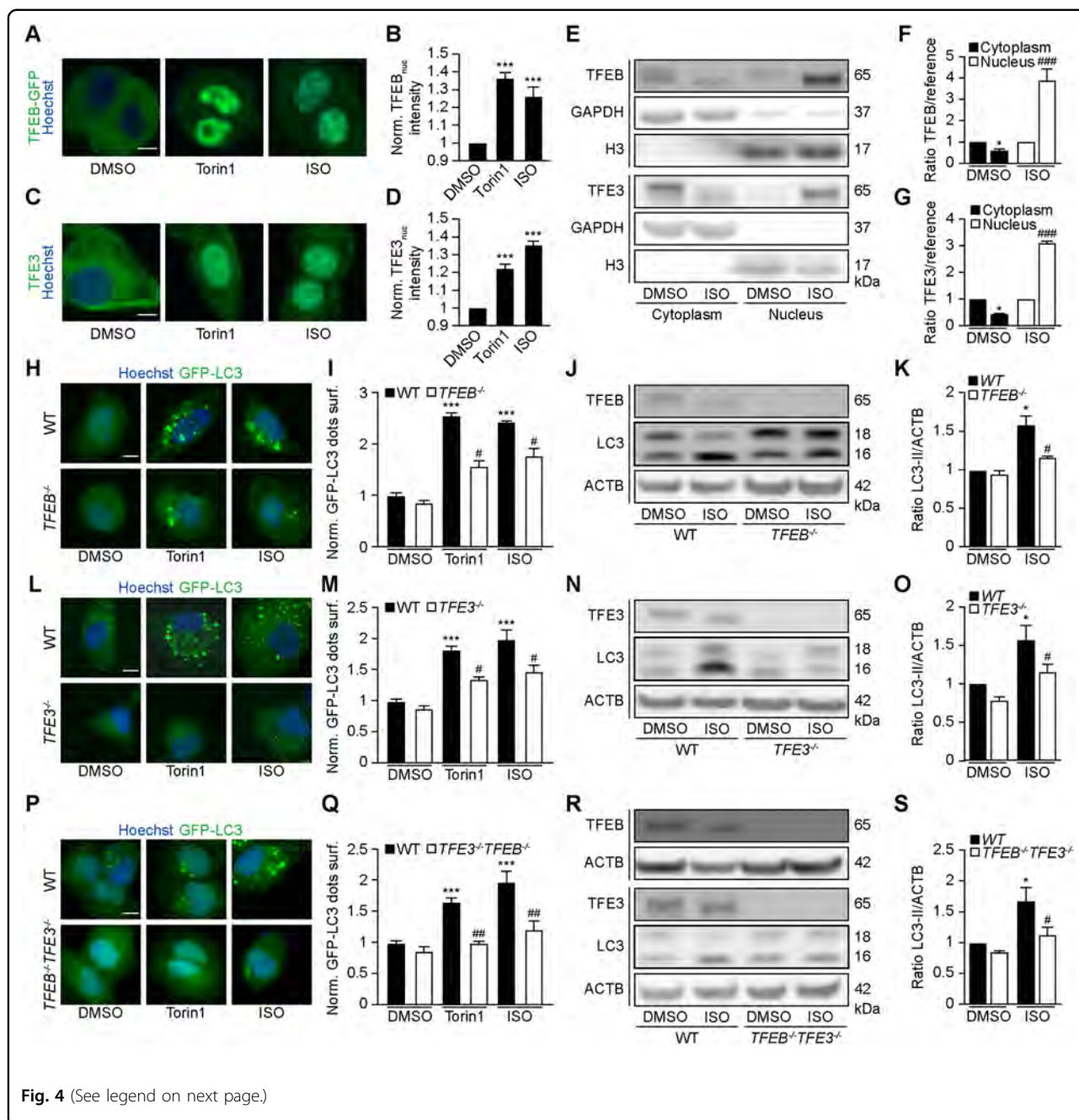
Here, we identified ISO as an autophagy inducer that inhibits AKT and mTORC1 activity and activates the pro-autophagic transcription factors TFEB and TFE3, which both are known to be activated by mTORC1 inhibition^{27,28}. We also found that ISO activates a broad ER stress response including the PERK-dependent phosphorylation of eIF2α, as a sign of the integrated stress response, which is known to be required for autophagy induction^{29–31} as well as for the induction of ICD^{32–37}. The two pathways, autophagy and ER stress induced by ISO exhibited crosstalk in thus far that (i) they both are inhibited by constitutively active AKT, (ii) TFEB/TFE3 knockout does not only reduce autophagy but also signs of ER stress, and (iii) PERK knockout or substitution of eIF2α by a non-phosphorylatable mutant reduces TFEB/TFE3 activation and autophagy. Beyond these *in vitro* phenomena, ISO induced autophagy *in vivo*, in mouse tissues, and enhanced the immune response induced by immunogenic chemotherapy against established tumors, thus improving tumor growth control through mechanisms that rely on T cells as well as AKT inhibition and autophagy induction in the cancer cells.

ISO is a chalcone that was first isolated from the multipurpose medical plant *Psoralea corylifolia*. Reportedly, ISO possesses a wide spectrum of antibacterial^{38,39} antifungal⁴⁰ antiparasitic⁴¹, antiviral^{42,43}, antitubercular⁴⁴,

antithrombotic^{45,46}, antiinflammatory^{47,48}, antioxidant⁴⁹, antiobesity⁵⁰, and phytoestrogen⁵¹ activities. Hence, ISO has a very broad range of biological activities. In cell-free enzymatic assays, ISO inhibits beta-secretase⁵², acyl-coenzyme A: cholesterol acyltransferase⁵³, severe acute respiratory syndrome coronavirus (SARS-CoV) papain-like protease⁵⁴, protein tyrosine phosphatase 1B (PTP1B)⁵⁵, carboxylesterase^{2,56}, and pancreatic lipase⁵⁷, suggesting that ISO can act on multiple pharmacological targets, shedding doubts on its specificity. Based on its broad effects, it might be suspected that ISO has direct immunostimulatory effects that help to improve immunosurveillance in the context of ICD-inducing chemotherapies. Indeed, autophagy induction may stimulate dendritic and T-cell functions^{23,58,59}.

In vitro, ISO reduces Aβ42 aggregation in SH-SY5Y cells⁶⁰ and the tumor necrosis factor-α (TNFα)-induced atrophy of C2C12 myotubes⁶¹. In rodents, ISO attenuates Parkinson's disease induced by the toxin 1-methyl-4-phenyl-1,2,3,6-tetrahydropyridine (MPTP)⁶², sephadex-induced lung injury⁶³, as well as streptozotocin-induced diabetic nephropathy⁶⁴. This suggests that ISO has a wide range of cytoprotective effects that might be explained by its autophagy-inducing activity.

With respect to its anticancer effects, ISO reportedly suppresses skin tumor promotion in an *in vivo* two-stage mouse skin carcinogenesis test using 7,12-dimethylbenz [a]anthracene (DMBA) as an initiator and 12-O-Tetradecanoylphorbol-13-acetate (TPA) as a promoter⁶⁵. ISO has cytotoxic effects on neuroblastoma⁶⁶, multiple myeloma cells^{67,68}, leukemia⁶⁹, as well as on chemoresistant carcinoma and glioblastoma cell lines⁷⁰, enhances TRAIL-induced apoptosis in prostate cancer and cervical carcinoma cells⁷¹, and reduces melanin production by B16 melanoma cells⁷². Here, we found that ISO failed to inhibit the growth of fibrosarcomas in mice when used as a standalone treatment, yet ameliorated the efficacy of ICD-inducing chemotherapy through an improved anticancer immune response. The absence of antitumor efficacy of ISO, when used as a standalone treatment, may



be linked to suboptimal dosing as well as to its pharmacokinetics, knowing that ISO has a half-life of ~6 h in rats⁷³. However, we have observed as a general pattern that autophagy induction with non-toxic agents is not sufficient to inhibit tumor growth of established tumors in mice. Thus, the biological activity of ISO is reminiscent of other autophagy inducers including 3,4-DMC¹³, hydroxycitrate, resveratrol, spermidine^{74,75}, and thiostreptone⁷⁶, all of which can ameliorate the therapeutic activity of ICD inducers in suitable mouse models but lack intrinsic anticancer properties.

Although ISO has multiple pharmacological effects and targets, several of the *in vitro* effects of ISO correlated with the inhibition of the AKT/mTORC1 pathway, and expression of a constitutively active AKT mutant largely reversed the ISO-induced signs of cellular stress including autophagy (with its upstream events, mTORC1 inhibition and TFEB/TFE3 activation) and ER stress (at all levels of the unfolded stress response, including its PERK/eIF2 α /ATG4/CHOP, ATG6, and IRE1 α /XBP1 arms), as shown in human U2OS cells. Moreover, mouse cancer cells stably expressing a constitutively active AKT enzyme

(see figure on previous page)

Fig. 4 ISO induces TFEB- and TFE3-dependent autophagy. **A, B** Human osteosarcoma U2OS cells stably expressing GFP-TFEB fusion protein were treated with torin 1 (300 nM) and isobacachalcone (ISO, 25 μ M) for 6 h. Representative images are shown in **(A)** and TFEB translocation was assessed by measuring GFP intensities in the nuclei **(B)**. Scale bar equals 10 μ m. Data are means \pm SD of quadruplicates ($^{***}P < 0.001$ vs. DMSO/Ctr, Student's *t* test). **C, D** U2OS cells were treated with torin 1 (300 nM) and ISO (25 μ M) for 6 h, and then, endogenous TFE3 translocation was assessed by immunostaining **(C)**. Nuclear TFE3 intensities are depicted in **(D)**. Scale bar equals 10 μ m. Data are means \pm SD of quadruplicates ($^{***}P < 0.001$ vs. DMSO/Ctr, Student's *t* test). **E–G** U2OS cells were treated with ISO (25 μ M) for 6 h or were left untreated. Cytoplasmic and nuclear fractions were assessed for nuclear translocation of the transcription factors TFEB and TFE3 in parallel samples by SDS–PAGE. GAPDH and H3 were used to ensure equal loading in the cytoplasmic and nuclear fractions, respectively. Band intensities of TFEB, TFE3, GAPDH, and H3 were assessed and their ratios (TFEB or TFE3/GAPDH, and TFEB or TFE3/H3) were calculated in **(F, G)**. ($^{\dagger}P < 0.05$, $^{**}P < 0.01$, $^{***}P < 0.001$ vs. cytoplasmic DMSO; $^{\#}P < 0.05$, $^{\#\#}P < 0.01$, $^{\#\#\#}P < 0.001$ vs. nuclear DMSO; Tukey's multiple comparisons test). **H–K** U2OS cells stably expressing GFP-LC3 either wild-type (WT) or knockout for TFEB were treated with torin 1 (300 nM) or ISO (25 μ M) for 16 h. LC3-II expression and TFEB deficiency were visualized by SDS–PAGE and immunoblot **(J)**. Band intensities of LC3-II and β -actin (ACTB) were assessed, and their ratio (LC3-II/ACTB) was calculated in **(K)**. Representative images are shown in **(H)**, and GFP-LC3 dots were quantified as indicators of autophagy **(I)**. Scale bar equals 10 μ m. Data are means \pm SD of quadruplicates ($^{***}P < 0.001$ vs. untreated control; $^{\#}P < 0.05$ vs. WT; Tukey's multiple comparisons test). **L–O** U2OS cells stably expressing GFP-LC3 either WT or knockout for TFE3 were treated with torin 1 (300 nM) and ISO (25 μ M) for 16 h. LC3-II expression and TFE3 deficiency were monitored by SDS–PAGE and immunoblot **(N)**. Band intensities of LC3-II and ACTB were assessed, and their ratio (LC3-II/ACTB) was calculated in **(O)**. Representative images are shown in **(L)**, and GFP-LC3 dots were quantified **(M)**. Scale bar equals 10 μ m. Data are means \pm SD of quadruplicates ($^{\dagger}P < 0.05$, $P < 0.001$ vs. untreated control; $^{\#}P < 0.05$ vs. WT; Tukey's multiple comparisons test). **P–S** U2OS cell stably expressing GFP-LC3 either wild-type or double knockout for TFEB and TFE3 cells were treated with torin 1 (300 nM) and ISO (25 μ M) for 16 h. LC3-II expression and TFEB/TFE3 deficiency were checked in parallel samples by SDS–PAGE and immunoblot **(R)**. Band intensities of LC3-II and ACTB were assessed, and the ratio (LC3-II/ACTB) was calculated **(S)**. Representative images are shown in **(P)**, and GFP-LC3 dots were quantified as indicators of autophagy **(Q)**. Scale bar equals 10 μ m. Data are means \pm SD of quadruplicates ($^{\dagger}P < 0.05$, $^{***}P < 0.001$ vs. untreated control; $^{\#}P < 0.05$, $^{\#\#}P < 0.01$ vs. WT; Tukey's multiple comparisons test).

(or lacking the essential autophagy gene *Atg5*) became resistant against the anticancer activity of ISO combined with ICD induction, suggesting some sort of 'specificity' for the ISO effect. However, at this point, it is not clear whether ISO may directly inhibit AKT or an enzyme upstream of AKT (such as phosphatidylinositol 3-kinases). Reportedly, ISO inhibits PTP1B⁵⁵, which would result in the activation, not the inhibition of the AKT pathway. Hence, the precise molecular target of ISO remains elusive.

ISO was initially isolated from *Psoralea corylifolia*, but has also been identified in other plants, including in *Angelica keiskei*⁵⁰, *Artocarpus species*⁴⁶, *Cullen corylifolium*⁷⁷, *Dorstenia barteri*³⁸, *Erythrina fusca*⁷⁸, *Fatoua pilosa*⁴⁴, *Morus alba*⁷⁹, and *Piper longum*⁷². This suggests that ISO is rather prevalent in plants, perhaps contributing to the broad pro-health effects of plant-enriched diets^{80,81}. However, additional studies are required to confirm this conjecture.

In summary, here we identified a particular chalcone, ISO, as a potent autophagy inducer that acts *in vitro* and *in vivo*, on human cell lines and mouse organs, respectively. Through the induction of autophagy, ISO is able to stimulate anticancer immune responses in the context of immunogenic chemotherapy.

Materials and methods

Cell culture and chemicals

Culture media and supplements for cell culture were obtained from Life Technologies (Carlsbad, California, USA) and plastic materials came from Greiner Bio-One (Kremsmünster, Austria) and Corning (Corning, NY, USA).

Rat adrenal gland PC12 cells stably expressing doxycycline-inducible Q74-GFP were cultured in Roswell Park Memorial Institute (RPMI)-1640 containing 5% fetal bovine serum and 10% horse serum⁸². Human neuroglioma H4 cells, human osteosarcoma U2OS cells, MCA205 murine fibrosarcoma, and all the other cells were maintained in Dulbecco's modified Eagle's medium (DMEM), supplemented with 10% (v/v) fetal bovine serum (FBS), 10 U mL⁻¹ penicillin sodium and 10 μ g mL⁻¹ streptomycin sulfate at 37 °C in a humidified atmosphere with 5% CO₂. TFEB-deficient (*TFEB*^{-/-}), TFE3-deficient (*TFE3*^{-/-}), TFEB and TFE3-double deficient (*TFEB*^{-/-}*TFE3*^{-/-}), ATG5-deficient (*ATG5*^{-/-}), and PERK-deficient (*PERK*^{-/-}) U2OS-GFP-LC3 cell lines and TFEB and TFE3-double deficient (*TFEB*^{-/-}*TFE3*^{-/-}) in H4-GFP-LC3 cells were generated by means of the CRISPR/Cas-mediated genome editing, as per the manufacturer's recommendations¹³. U2OS cells stably expressing RFP-LC3 bearing a mutant non-phosphorylation of eIF2 α (eIF2 α ^{S51A}) were constructed using the CRISPR-Cas9 technology as previously detailed³¹. In addition, U2OS cells stably expressing GFP-TFEB, CHOP::GFP, and XBP1s-DDBD-venus were generated by our group in the past^{13,36}. MCA205 cells stably expressing shRNAs interfering with the expression of TFE3/TFEB or ATG5, and a mutant phosphorylation AKT T308D/S473D were also constructed as recommended by the manufacturer^{13,74,83}. The Polyphenolic Natural Compound Library library and ISO were purchased from TargetMol (Boston, Massachusetts, USA); torin 1 (TOR), thapsigargin (TG), tunicamycin (TM), bafilomycin A1 (Baf A1), mitoxantrone (MTX), and oxaliplatin (OXA) were obtained from Sigma-Aldrich (St. Louis, Missouri, USA).

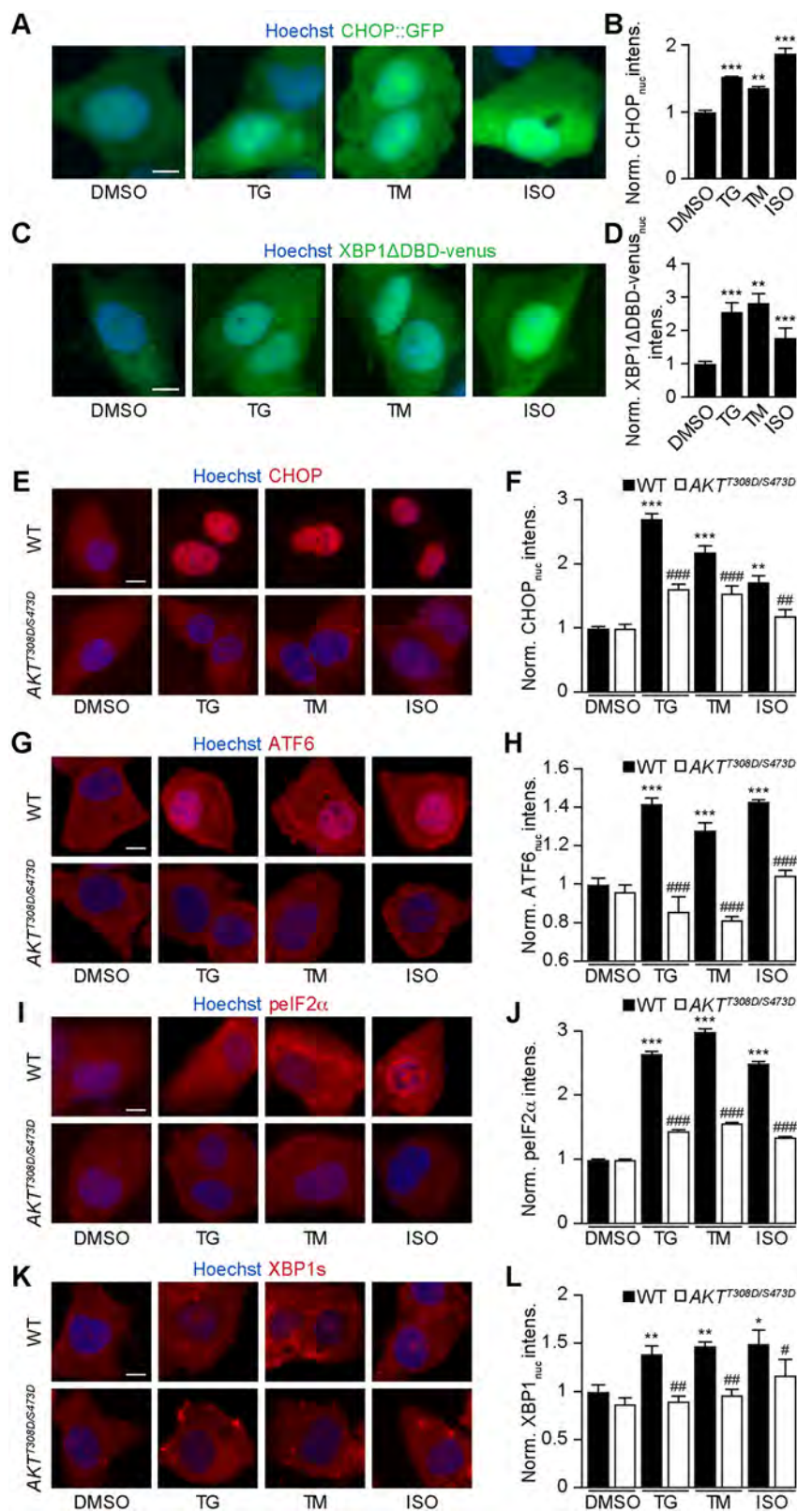


Fig. 5 (See legend on next page.)

(see figure on previous page)

Fig. 5 ISO stimulates ER stress via the inhibition of AKT phosphorylation. **A, B** Human osteosarcoma U2OS cells stably expressing GFP under the CHOP promoter (CHOP::GFP) were treated with the indicated agents (tunicamycin, TM (3 μ M), TG thapsigargin (3 μ M), isobacachalcone ISO (25 μ M)) for 24 h. GFP nuclear translocation is shown in **(A)**, and the average nuclear intensity of GFP was quantified in **(B)**. Scale bar equals 10 μ m. Data are means \pm SD of quadruplicates (** P < 0.01, **** P < 0.001 vs. untreated control; Student's t test). **C, D** U2OS cells stably expressing XBP1 Δ DBD-venus (for monitoring venus expression upon alternative splicing of XBP1 mRNA) were treated as indicated for 16 h. XBP1s expression is shown in **(C)**, and the average nuclear intensity was measured in **(D)**. Scale bar equals 10 μ m. Data are means \pm SD of quadruplicates (** P < 0.01, **** P < 0.001 vs. untreated control; Student's t test). **E–L** U2OS wild-type (WT) or knock-in for AKT^{T308D/S473D} cells were treated with TM (3 μ M), TG (3 μ M), ISO (25 μ M) 24 h for assessing CHOP, 6 h for measuring pEIF2 α , and 16 h for monitoring ATF6 and XBP1s. After fixation, the cells were stained with corresponding primary antibodies followed by an AlexaFluor-568 secondary antibody. Nuclei were counterstained with Hoechst 33342. CHOP nuclear expression is shown in **(E)**, and the average nuclear intensity of CHOP was quantified in **(F)**. ATF6 nuclear translocation is shown in **(G)**, and the average nuclear intensity of ATF6 was quantified in **(H)**. pEIF2 α was assessed by means of immunofluorescence staining **(I)**, and the average cytoplasmic intensity of cells was depicted in **(J)**. XBP1s activation is shown in **(K)**, and the average nuclear intensity was measured in **(L)**. Scale bar equals 10 μ m. Data are means \pm SD of quadruplicates (* P < 0.05, ** P < 0.01, **** P < 0.001 vs. untreated control; # P < 0.05, ## P < 0.01, ### P < 0.001 vs. WT; Tukey's multiple comparisons test).

High-content microscopy

Human osteosarcoma U2OS and neuroglioma H4 cells stably expressing GFP-LC3 or RFP-LC3 and rat adrenal gland PC12 cells stably expressing doxycycline-inducible Q74-GFP were seeded in 384-well black imaging plates at a density of 2000 cells per well and allowed to adapt for overnight. Cells were treated with the indicated agents for 6 h, subsequently, cells were fixed with 3.7% paraformaldehyde (PFA, w/v in PBS) (F8775, Sigma-Aldrich) at 4 °C overnight and stained with 1 μ g/ml Hoechst 33342 in PBS. Moreover, 2000 U2OS cells either wild-type or stably expressing HMGB1-GFP/CALR-RFP, GFP-ATF6, CHOP::GFP, GFP-TFEB, or XBP1-DBD-venus were seeded in 384-well black imaging plates (Greiner Bio-One) and let adhere overnight. Cells were then treated for 6 h to detect TFEB translocation, 16 h to assess ATF6 translocation and spliced XBP1 (XBP1s) levels, or 24 h to measure CHOP promoter activity. For CALR redistribution and HMGB1 release, cells were incubated for 8 h or 24 h respectively. Next, cells were fixed with 3.7% formaldehyde supplemented with 1 μ g/ml Hoechst 33342 (H3570, Thermo Fisher Scientific) at 4 °C overnight. Subsequently, the fixative was exchanged to PBS, and the plates were analyzed by automated microscopy. Image acquisition was performed using an ImageXpress Micro XL automated microscope (Molecular Devices, Sunnyvale, CA, USA) equipped with a \times 20 PlanApo objective (Nikon, Tokyo, Japan), followed by automated image processing with the custom module editor within the MetaXpress software (Molecular Devices). At least four view fields were acquired per well, and experiments involved at least triplicate assessment. Cellular regions of interest, cytoplasm and nucleus, were defined and segmented by using the MetaXpress software (Molecular Devices). After exclusion of cellular debris and dead cells from the dataset, parameters of interest were normalized, statistically evaluated, and graphically depicted with R software. Using R, images were extracted and pixel intensities scaled to be visible (in the same extent for all images of a given experiment).

Immunofluorescence

Human osteosarcoma U2OS cells were treated for 6 h to detect eIF2 α phosphorylation (pEIF2 α) and TFE3, 16 h to assess ATF6 and spliced XBP1 (XBP1s) levels, or 24 h to measure CHOP expression. Then cells were fixed by 3.7% PFA at 4 °C overnight. For staining, fixed cells were then permeabilized with 0.1% Triton X100 on ice, and blocked with 5% bovine serum albumin (BSA, w/v in PBS) for 1 h. Next, cells were incubated with antibodies specific to TFE3 (#ab93808, 1:400, Abcam), phospho-eIF2 alpha (Ser51) (#ab32157, 1:1000, Abcam), ATF6 (#ab37149, 1:200, Abcam), XBP1 (#ab37152, 1:250, Abcam) or CHOP (#2895, 1:500, Cell Signaling Technology) at 4 °C overnight. After washed by PBS twice, AlexaFluor conjugates (Thermo Fisher Scientific) against the primary antibody were applied for 2 h at RT. Finally, cells were washed and imaged by automated fluorescence microscopy as described above. The nuclear intensity of TFE3, ATF6, XBP1s or CHOP and cytoplasmic intensity of phospho-eIF2 α (Ser51) were measured and normalized on Ctrl.

Immunoblotting

The tissues (~30 mg) were dissociated in Precellys lysing tubes (#CK28_2 mL, Bertin Technologies SAS, Montigny-le-Bretonneux, France) containing 1 mL of radioimmunoprecipitation assay buffer (RIPA) lysis buffer (#89901, Invitrogen, Carlsbad, CA, USA) by using the Precellys 24 homogenizer (Bertin Technologies SAS) at 6500 rpm for 5 min, followed by spinning at 14,000 \times g for 15 min to collect the supernatant that contains soluble proteins. For cells, the protein extracts were dissolved in RIPA buffer and obtained by ultrasonication for 3 \times 10 s and centrifuging at 12,000 \times g for 15 min to collect the supernatant that contains soluble proteins. Protein concentration was measured by means of the BCA Assay (Bio-Rad, Hercules, CA, USA). The protein solution was mixed with 4 \times loading buffer (# NP0008, Invitrogen), and denatured at 100 °C for 15 min before subjected to western blotting. The total protein (~30 μ g) were resolved on

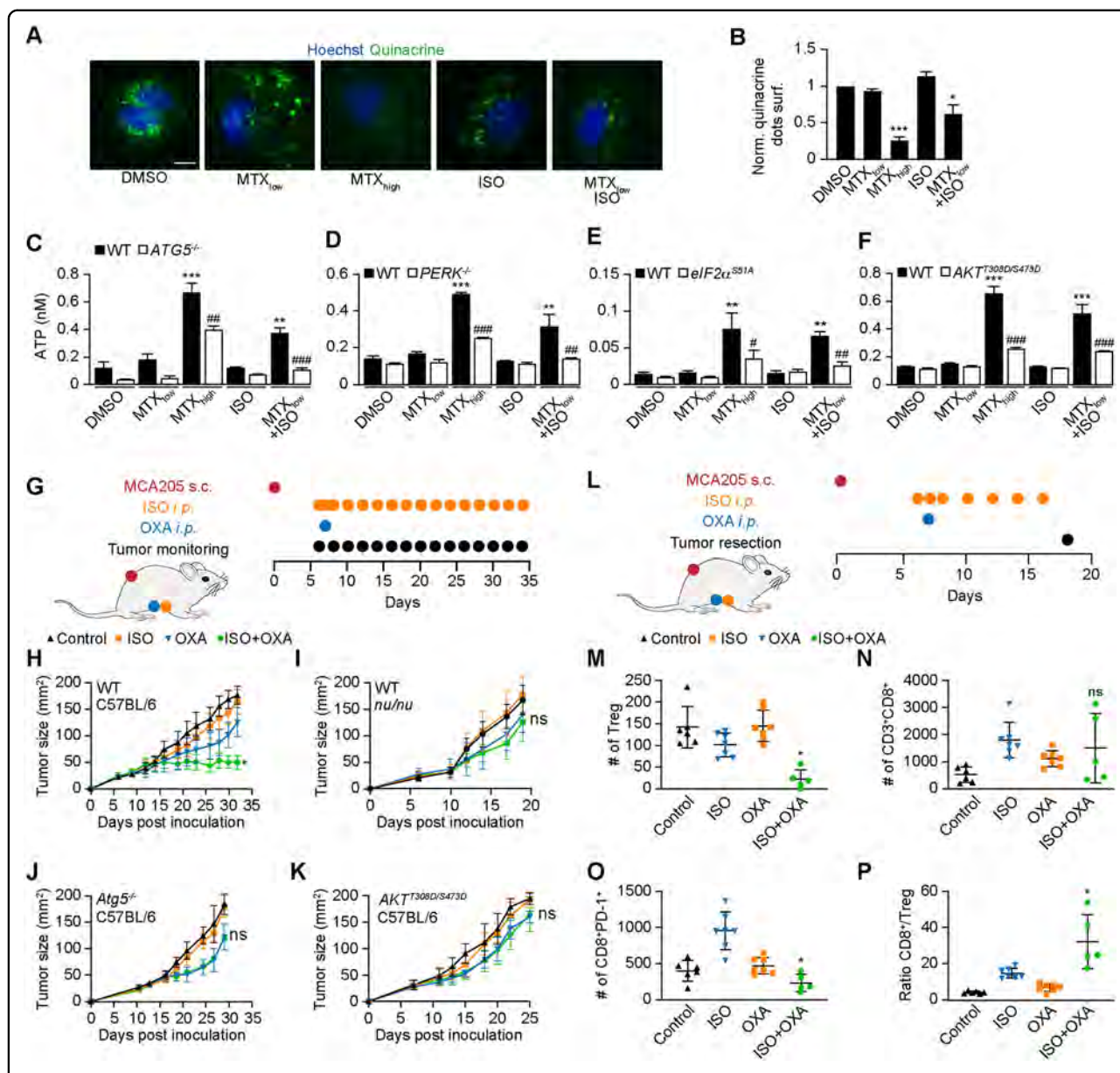


Fig. 6 ISO mediates improvement of anticancer chemotherapy. **A, B** Human osteosarcoma U2OS cells were treated with isobacachalcone (ISO, 25 μM) in the presence of low doses of the immunogenic cell death (ICD) inducer mitoxantrone (MTX, 1 μM) for 6 h. High-dose MTX (5 μM) was used as a positive control. The ATP-sensitive agent quinacrine was used to monitor intracellular ATP content. Representative images are shown in **(A)**, and the abundance of quinacrine was quantified in **(B)**. Scale bar equals 10 μm. Data are means ± SD of quadruplicates ($P < 0.05$, $***P < 0.001$ vs. untreated control Tukey's multiple comparisons test). **C–F** Human neuroglioma H4 cell stably expressing GFP-LC3 either wild-type (WT) or ATG5 knockout, human osteosarcoma U2OS wild-type, PERK knockout or eIF2α^{S51A} knock-in cells, murine fibrosarcoma MCA205 WT or AKT^{T308D/S473D} knock-in cells were treated with ISO (25 μM) alone or in combination with low doses of MTX (1 μM) for 6 h, as described above. High-dose MTX (5 μM) was used as a positive control. Extracellular ATP levels were measured by luciferase conversion ($*P < 0.01$, $***P < 0.001$ vs. untreated control; $^{\#}P < 0.05$, $^{\#\#}P < 0.01$, $^{\#\#\#}P < 0.001$ vs. WT; Tukey's multiple comparisons test). **G, L** Schematic overview of the in vivo treatment of murine fibrosarcoma MCA205-bearing mice with oxaliplatin (OXA) and ISO, alone or in combination. **H–K** Growth kinetic of murine fibrosarcoma MCA205 cells WT **(H)**, Atg5KD **(J)**, or AKT^{T308D/S473D} knock-in **(K)** growing in immunocompetent C57BL/6 mice, treated as indicated in **(G)**. Athymic mice (nu/nu) mice **(I)** were inoculated subcutaneously with murine fibrosarcoma MCA205 cells. When tumors became palpable, mice received a systemic intraperitoneal injection of ISO alone or together with OXA. $n \geq 6$ mice per group. Results (means ± SD tumor growth curves) are plotted ($P < 0.05$ or ns, not statistically significant vs. OXA). **M–P** Murine fibrosarcoma MCA205 cells were evolving in immunocompetent C57BL/6 mice, treated as indicated in **(L)**. Cytofluorometric characterization of tumor-infiltrating lymphocytes, in particular CD4⁺FOXP3⁺CD25⁺ regulatory T cells (Treg) **(M)**, CD3⁺CD8⁺ cytotoxic T lymphocytes **(N)**, CD8⁺PD1⁺ T lymphocytes **(O)**, and the ratio of CD3⁺CD8⁺ T cells over Treg **(P)** are depicted. Data are means ± SD ($n \geq 5$) ($P < 0.05$ or ns, not statistically significant vs. OXA; Student's *t* test).

4–12% NuPAGE Bis-Tris protein gels (#NP0322, Thermo Fisher Scientific) and electrotransferred to 0.2 μ M polyvinylidene fluoride (PVDF) membranes (#1620177, Bio-Rad). The membranes were blocked with 0.05% Tween 20 (#P9416, Sigma-Aldrich) v-v in Tris-buffered saline (TBS) (TBST) (#ET220, Euromedex) supplemented with 5% nonfat powdered milk (w:v in TBS), followed by an overnight incubation at 4 °C with primary antibodies specific for LC3B (#2775, 1:1000, Cell Signaling Technology), HA (#ROAHAHA, 1:1000, Sigma-Aldrich), phospho-P70 (Thr389) (#9234, 1:1000, Cell Signaling Technology), P70 (#9202, 1:1000, Cell Signaling Technology), TFE3 (#4240, 1:1000, Cell Signaling Technology), TFE3 (#ab93808, 1:1000, Abcam), phospho-AKT (Ser473) (#4060, Cell Signaling Technology), AKT (#4691, Cell Signaling Technology), phospho-mTOR (Ser2448) (#2971, Cell Signaling Technology), mTOR (#2983, Cell Signaling Technology), H3 (#9715, 1:1000, Cell Signaling Technology). Membranes were washed three times with TBST for 10 min each before incubated with HRP-conjugated goat-anti-rabbit secondary antibody (CliniScience) for 2 h at room temperature. At last, the membranes were washed again and subjected to chemiluminescence detection with the Amersham ECL Prime detection reagent kit (GE Healthcare, Piscataway, NJ, USA) on an ImageQuant LAS 4000 software-assisted imager. Samples from cells or organs were aliquoted and run on separate gels. Equal loading was controlled by Coomassie staining. The abundance of control proteins (such as β -actin (ACTB, #ab 20727, 1:10000, Abcam), glyceraldehyde-3-phosphate dehydrogenase (GAPDH) (#2118, 1:5000, Cell Signaling Technology), vinculin (#13901, 1:1000, Cell Signaling Technology) vinculin, or non-phosphorylated proteins such as AKT, S6K, mTOR) in each sample was determined in parallel samples. Quantification was performed by densitometry using the Image J software.

Nuclear extraction experiment

U2OS-GFP-LC3 cells were collected and processed with the Nuclear Extraction Kit (#ab113474, Abcam) following the manufacturer's methods. The GAPDH antibody (#2118, 1:1000, Cell Signaling Technology) was used as the cytoplasmic control, and H3 (#9715, 1:1000, Cell Signaling Technology) was selected as the nuclear control.

Detection of protein deacetylation

U2OS cells stably expressing GFP-LC3 (~2000 cells/well) were seeded in 384-well microplates overnight. After experimental treatments, cells were fixed with 3.7% PFA containing 10 μ g/ml Hoechst 33342 overnight at 4 °C. Thereafter, cells were incubated with an antibody specific for acetyl-alpha-tubulin (#5335, 1:500, Cell Signaling Technology) in 5% BSA (w/v in PBS) for 1 h to block non-specific binding sites and acetylated tubulins, followed by

overnight incubation at 4 °C with an antibody specific to acetylated lysine residues (#623402, 1:400, BioLegend, San Diego, California, USA). After washing three times with PBS, cells were incubated in AlexaFluor-568-conjugated secondary antibodies (Life Technologies) for 2 h at room temperature. Fluorescent images were acquired and analyzed as described before.

ATP release assays

Intracellular ATP levels were detected by quinacrine stain assay (Calbiochem) kits, subsequently, the images of quinacrine were obtained by high-content microscopy and the cytoplasmic intensity of quinacrine was quantitated described above. Extracellular ATP levels were measured by the ENLITEN ATP Assay System Bioluminescence Detection Kit (Promega, Madison, Michigan, USA; #FF2000) following the manufacturer's methods. Luminescence was detected by means of a Paradigm I3 multimode plate reader (Molecular Devices).

Animal experimentation

The animal experiments were approved by the Gustave Roussy ethical committee with project number 24771–2020032413235413, and all procedures were performed under the governmental and institutional guidelines and regulations. All mice were maintained in a temperature-controlled and pathogen-free environment with 12-h light/dark cycles, with food and water ad libitum. Animal experiments were conducted in compliance with the EU Directive 63/2010 and protocols 2019_030_20590 and were approved by the Ethical Committee of the Gustave Roussy Campus Cancer (CEEA IRCIV/IGR no. 26, registered at the French Ministry of Research).

For tumor growth experiments, 7-week-old female wild-type C57BL/6 mice or athymic female nude mice (*nu/nu*) were obtained from Envigo, France (Envigo, Huntingdon, UK). MCA205 wild-type (WT), or continuous activation of AKT T308D/S473D cells (4×10^5), MCA205 cells carrying an ATG5 knockdown (WT, 6×10^5) were subcutaneously injected into C57BL/6 hosts. When tumors became palpable, mice were treated with 20 mg/kg ISO dissolved in corn oil (Sigma-Aldrich) or an equivalent volume of vehicle alone or in combination with 10 mg/kg oxaliplatin (OXA, Sigma-Aldrich) by intraperitoneal injection. On the following days, mice well-being and tumor growth were monitored and documented. Animals were sacrificed when tumor size reached the ethical endpoint or signs of obvious discomfort were observed following the EU Directive 63/2010 and our Ethical Committee advice.

Ex vivo phenotyping of the tumor immune infiltrate

Tumors were harvested, weighed, and transferred on ice into gentleMACS C tubes (Miltenyi Biotec, Bergisch Gladbach, Germany) containing 1 mL of RPMI medium.

Tumors were dissociated first mechanically with scissors, then enzymatically using Miltenyi Biotec mouse tumor dissociation kit (Miltenyi Biotec) and a GentleMACS Octo Dissociator according to the manufacturer's instructions. The dissociated bulk tumor cell suspension was resuspended in RPMI-1640, sequentially passed through 70- μ m MACS Smart-Strainer (Miltenyi Biotec), and washed twice with PBS. Finally, bulk tumor cells were homogenized in PBS at a concentration corresponding to 250 mg of the initial tumor weight per milliliter. Prior to staining of tumor-infiltrating lymphocytes (TILs) for flow cytometry analysis, samples (~50 mg) were incubated with LIVE/DEAD[®] Fixable Yellow Dead Cell dye (Thermo Fisher Scientific) to discriminate viable cells from damaged cells. Fc receptors were blocked with anti-mouse CD16/CD32 (clone 2.4G2, Mouse BD Fc Block, BD Pharmingen) before staining with fluorescent-labeled antibodies targeting T-cell surface markers. Surface staining of murine immune cell populations infiltrating the tumor was performed with the following fluorochrome-conjugated antibodies: anti-CD45-AF700, anti-CD3-BV421, anti-CD8-PE, anti-CD4-Percp.Cy5.5, anti-CD25-PE/Cy7, and anti-PD-1-APC/Cy7 (BioLegend). Then, cells were fixed and permeabilized in eBioscience Foxp3/Transcription Factor Staining Buffer (Thermo Fisher Scientific) and stained for intracellular Foxp3. Finally, stained samples were run through a BD LSR II flow cytometer. Data were acquired using BD FACSDiva software (BD Biosciences) and analyzed using FlowJo software (TreeStar). Absolute counts of leukocytes and tumor cells were normalized considering the following parameters: the weight of the harvested tumor and total volume of the dissociated tumor cell suspension (cell concentration typically set to 250 mg/mL in PBS), the proportion of the whole-cell suspension, and proportion of the cell suspension used for cytometry.

Statistical analysis

Unless otherwise mentioned, data are reported as means \pm SD of triplicate determinations, and experiments were repeated at least three times yielding similar results. Statistical significance was assessed by Student's *t* test. TumGrowth and GraphPad were used to analyze in vivo data arising from murine models⁸⁴. TumGrowth is available at Github/Kroemerlab. *P* values of 0.05 or less were considered to denote significance (**P* < 0.05; ***P* < 0.01; ****P* < 0.001; ns, not significant).

Acknowledgements

Q.W., A.T., H.P., and W.X. are supported by the Chinese scholarship council. S.Z. receives funding from the Scientific Research Training Program for Young Talents, Union Hospital, Tongji Medical College, Huazhong University of Science and Technology. O.K. receives funding by the Île de France DIM ELICIT initiative. G.K. is supported by the Ligue contre le Cancer (équipe labellisée); Agence National de la Recherche (ANR)—Projets blancs; A.N.R. under the frame of E-Rare-2, the ERA-Net for Research on Rare Diseases; AMMICA US23/CNRS UMS3655; Association pour la recherche sur le cancer (ARC); Association

"Le Cancer du Sein, Parlons-en!"; Cancéropôle Ile-de-France; Chancellerie des universités de Paris (Legs Poix), Fondation pour la Recherche Médicale (FRM); a donation by Elior; European Research Area Network on Cardiovascular Diseases (ERA-CVD, MINOTAUR); Gustave Roussy Odyssey, the European Union Horizon 2020 Project Oncobiome; Fondation Carrefour; High-end Foreign Expert Program in China (GDW20171100085), Institut National du Cancer (INCa); Inserm (HTE); Institut Universitaire de France; LeDucq Foundation; the LabEx Immuno-Oncology (ANR-18-IDEX-0001); the RHU Torino Lumière; the Seerave Foundation; the SIRIC Stratified Oncology Cell DNA Repair and Tumor Immune Elimination (SOCRATE); and the SIRIC Cancer Research and Personalized Medicine (CARPEM). We are grateful to the support of the Gustave Roussy, Université Paris-Saclay, Plate-forme Imagerie et Cytométrie (PFIC). UMS AMMICA INSERM US23-CNRS 3655. Villejuif, F-94805, France; F.M. is grateful to the Austrian Science Fund FWF (SFB-LIPOX F3007 & F3012, W1226, P29203, P29262, P27893, and P31727); the Austrian Federal Ministry of Education, Science and Research and the University of Graz for grants Unkonventionelle Forschung-InterFast and flysleep (BMWFW-80.109/0001-WF/V/3b/2015) and the field of excellence program BioHealth. We acknowledge support from NAWI Graz, the BioTechMed-Graz flagship project EPIAge.

Author details

¹Department of Breast and Thyroid Surgery, Renmin Hospital of Wuhan University, Wuhan, China. ²Centre de Recherche des Cordeliers, Equipe labellisée par la Ligue contre le cancer, Université de Paris, Sorbonne Université, Inserm U1138, Institut Universitaire de France, Paris, France. ³Metabolomics and Cell Biology Platforms, Gustave Roussy Cancer Center, Université Paris Saclay, Villejuif, France. ⁴Faculty of Medicine, Université Paris Saclay, Kremlin-Bicêtre, France. ⁵Institute of Molecular Biosciences, NAWI Graz, University of Graz, Graz, Austria. ⁶BioTechMed-Graz, Graz, Austria. ⁷Field of Excellence BioHealth, University of Graz, Graz, Austria. ⁸Suzhou Institute for Systems Medicine, Chinese Academy of Medical Sciences, Suzhou, China. ⁹Pôle de Biologie, Hôpital Européen Georges Pompidou, AP-HP, Paris, France. ¹⁰Karolinska Institutet, Department of Women's and Children's Health, Karolinska University Hospital, Stockholm, Sweden

Conflict of interest

F.M. is cofounder of The Longevity Labs. D.C.-G., F.M., O.K., and G.K. are cofounders of Samsara Therapeutics. G.K. is cofounder everImmune and Therafast Bio. The remaining authors declare no conflict of interest.

Publisher's note

Springer Nature remains neutral with regard to jurisdictional claims in published maps and institutional affiliations.

Supplementary Information accompanies this paper at (<https://doi.org/10.1038/s41419-020-03226-x>).

Received: 1 October 2020 Revised: 5 November 2020 Accepted: 6 November 2020

Published online: 26 November 2020

References

- Levine, B. & Kroemer, G. Biological functions of autophagy genes: a disease perspective. *Cell* **176**, 11–42 (2019).
- Nakamura, S. & Yoshimori, T. New insights into autophagosome-lysosome fusion. *J. Cell Sci.* **130**, 1209–1216 (2017).
- Kawabata, T. & Yoshimori, T. Autophagosome biogenesis and human health. *Cell Discov.* **6**, 33 (2020).
- Lopez-Otin, C., Galluzzi, L., Freije, J. M. P., Madeo, F. & Kroemer, G. Metabolic control of longevity. *Cell* **166**, 802–821 (2016).
- Rubinsztein, D. C., Marino, G. & Kroemer, G. Autophagy and aging. *Cell* **146**, 682–695 (2011).
- Hansen, M., Rubinsztein, D. C. & Walker, D. W. Autophagy as a promoter of longevity: insights from model organisms. *Nat. Rev. Mol. Cell Biol.* **19**, 579–593 (2018).
- Leidal, A. M., Levine, B. & Debnath, J. Autophagy and the cell biology of age-related disease. *Nat. Cell Biol.* **20**, 1338–1348 (2018).

8. Madeo, F., Eisenberg, T., Pietrocola, F. & Kroemer, G. Spermidine in health and disease. *Science* **359**, <https://doi.org/10.1126/science.aan2788> (2018).
9. Nakamura, S. & Yoshimori, T. Autophagy and longevity. *Mol. Cells* **41**, 65–72 (2018).
10. Madeo, F., Carmona-Gutierrez, D., Hofer, S. J. & Kroemer, G. Caloric restriction mimetics against age-associated disease: targets, mechanisms, and therapeutic potential. *Cell Metab.* **29**, 592–610 (2019).
11. Lopez-Otin, C. & Kroemer, G. Decelerating ageing and biological clocks by autophagy. *Nat. Rev. Mol. Cell Biol.* **20**, 385–386 (2019).
12. Carmona-Gutierrez, D. et al. The flavonoid 4,4'-dimethoxychalcone promotes autophagy-dependent longevity across species. *Nat. Commun.* **10**, 651 (2019).
13. Chen, G. et al. 3,4-Dimethoxychalcone induces autophagy through activation of the transcription factors TFE3 and TFEB. *EMBO Mol. Med.* **11**, e10469 (2019).
14. Zimmermann, A. et al. Targeting GATA transcription factors—a novel strategy for anti-ageing interventions? *Micro. Cell* **6**, 212–216 (2019).
15. Jing, H. et al. Abrogation of Akt signaling by Isobavachalcone contributes to its anti-proliferative effects towards human cancer cells. *Cancer Lett.* **294**, 167–177 (2010).
16. Li, Y. et al. Isobavachalcone isolated from *Psoralea corylifolia* inhibits cell proliferation and induces apoptosis via inhibiting the AKT/GSK-3beta/beta-catenin pathway in colorectal cancer cells. *Drug Des. Devel Ther.* **13**, 1449–1460 (2019).
17. Kaizuka, T. et al. An autophagic flux probe that releases an internal control. *Mol. Cell* **64**, 835–849 (2016).
18. Narain, Y., Wyttenbach, A., Rankin, J., Furlong, R. A. & Rubinsztein, D. C. A molecular investigation of true dominance in Huntington's disease. *J. Med. Genet.* **36**, 739–746 (1999).
19. Senovilla, L. et al. An immunosurveillance mechanism controls cancer cell ploidy. *Science* **337**, 1678–1684 (2012).
20. Michaud, M. et al. Autophagy-dependent anticancer immune responses induced by chemotherapeutic agents in mice. *Science* **334**, 1573–1577 (2011).
21. Martins, I. et al. Molecular mechanisms of ATP secretion during immunogenic cell death. *Cell Death Differ.* **21**, 79–91 (2014).
22. Ma, Y. et al. Anticancer chemotherapy-induced intratumoral recruitment and differentiation of antigen-presenting cells. *Immunity* **38**, 729–741 (2013).
23. Ma, Y., Galluzzi, L., Zitvogel, L. & Kroemer, G. Autophagy and cellular immune responses. *Immunity* **39**, 211–227 (2013).
24. Kroemer, G., Galluzzi, L., Kepp, O. & Zitvogel, L. Immunogenic cell death in cancer therapy. *Annu. Rev. Immunol.* **31**, 51–72 (2013).
25. Shankaran, V. et al. IFN γ and lymphocytes prevent primary tumour development and shape tumour immunogenicity. *Nature* **410**, 1107–1111 (2001).
26. Vacchelli, E. et al. Chemotherapy-induced antitumor immunity requires formyl peptide receptor 1. *Science* **350**, 972–978 (2015).
27. Settembre, C. et al. A lysosome-to-nucleus signalling mechanism senses and regulates the lysosome via mTOR and TFEB. *EMBO J.* **31**, 1095–1108 (2012).
28. Di Malta, C. & Ballabio, A. TFEB-mTORC1 feedback loop in metabolism and cancer. *Cell Stress* **1**, 7–10 (2017).
29. Kroemer, G., Marino, G. & Levine, B. Autophagy and the integrated stress response. *Mol. Cell* **40**, 280–293 (2010).
30. Shen, S. et al. Cytoplasmic STAT3 represses autophagy by inhibiting PKR activity. *Mol. Cell* **48**, 667–680 (2012).
31. Humeau, J. et al. Phosphorylation of eukaryotic initiation factor-2alpha (eIF2alpha) in autophagy. *Cell Death Dis.* **11**, 433 (2020).
32. Zitvogel, L. et al. Immunogenic tumor cell death for optimal anticancer therapy: the calreticulin exposure pathway. *Clin. Cancer Res.* **16**, 3100–3104 (2010).
33. Martins, I. et al. Restoration of the immunogenicity of cisplatin-induced cancer cell death by endoplasmic reticulum stress. *Oncogene* **30**, 1147–1158 (2011).
34. Kepp, O. et al. eIF2alpha phosphorylation as a biomarker of immunogenic cell death. *Semin Cancer Biol.* **33**, 86–92 (2015).
35. Semeraro, M. et al. The ratio of CD8(+)/FOXP3 T lymphocytes infiltrating breast tissues predicts the relapse of ductal carcinoma in situ. *Oncimmunology* **5**, e1218106 (2016).
36. Bezu, L. et al. eIF2alpha phosphorylation is pathognomonic for immunogenic cell death. *Cell Death Differ.* <https://doi.org/10.1038/s41418-017-0044-9> (2018).
37. Humeau, J. et al. Inhibition of transcription by dactinomycin reveals a new characteristic of immunogenic cell stress. *EMBO Mol. Med.* **12**, e11622 (2020).
38. Mbaveng, A. T. et al. Antimicrobial activity of the crude extracts and five flavonoids from the twigs of *Dorstenia barteri* (Moraceae). *J. Ethnopharmacol.* **116**, 483–489 (2008).
39. Dzoyem, J. P., Hamamoto, H., Ngameni, B., Ngadjui, B. T. & Sekimizu, K. Anti-microbial action mechanism of flavonoids from *Dorstenia* species. *Drug Disco. Ther.* **7**, 66–72 (2013).
40. ElSohly, H. N., Joshi, A. S., Nimrod, A. C., Walker, L. A. & Clark, A. M. Antifungal chalcones from *Maclura tinctoria*. *Planta Med.* **67**, 87–89 (2001).
41. Sandjo, L. P. et al. Individual and combined antiparasitic effect of six plant metabolites against *Leishmania amazonensis* and *Trypanosoma cruzi*. *Bioorg. Med. Chem. Lett.* **26**, 1772–1775 (2016).
42. Wang, H. M. et al. Isobavachalcone inhibits post-entry stages of the porcine reproductive and respiratory syndrome virus life cycle. *Arch. Virol.* **163**, 1263–1270 (2018).
43. Wang, Y., Liu, T. X., Wang, T. Y., Tang, Y. D. & Wei, P. Isobavachalcone inhibits Pseudorabies virus by impairing virus-induced cell-to-cell fusion. *Virology* **17**, 39 (2020).
44. Chiang, C. C., Cheng, M. J., Peng, C. F., Huang, H. Y. & Chen, I. S. A novel dimeric coumarin analog and antimycobacterial constituents from *Fatoua pilosa*. *Chem. Biodivers.* **7**, 1728–1736 (2010).
45. Tsai, W. J., Hsin, W. C. & Chen, C. C. Antiplatelet flavonoids from seeds of *Psoralea corylifolia*. *J. Nat. Prod.* **59**, 671–672 (1996).
46. Jantan, I., Mohd Yasin, Y. H., Jamil, S., Sirat, H. & Basar, N. Effect of prenylated flavonoids and chalcones isolated from *Artocarpus* species on platelet aggregation in human whole blood. *J. Nat. Med.* **64**, 365–369 (2010).
47. Shin, H. J., Shon, D. H. & Youn, H. S. Isobavachalcone suppresses expression of inducible nitric oxide synthase induced by Toll-like receptor agonists. *Int. Immunopharmacol.* **15**, 38–41 (2013).
48. Lee, K. M., Kim, J. M., Baik, E. J., Ryu, J. H. & Lee, S. H. Isobavachalcone attenuates lipopolysaccharide-induced ICAM-1 expression in brain endothelial cells through blockade of toll-like receptor 4 signaling pathways. *Eur. J. Pharm.* **754**, 11–18 (2015).
49. Haraguchi, H., Inoue, J., Tamura, Y. & Mizutani, K. Antioxidative components of *Psoralea corylifolia* (Leguminosae). *Phytother. Res.* **16**, 539–544 (2002).
50. Lee, H. et al. Isobavachalcone from *Angelica keiskei* inhibits adipogenesis and prevents lipid accumulation. *Int. J. Mol. Sci.* **19**, <https://doi.org/10.3390/ijms19061693> (2018).
51. Xin, D. et al. Phytoestrogens from *Psoralea corylifolia* reveal estrogen receptor-subtype selectivity. *Phytotherapy* **17**, 126–131 (2010).
52. Choi, Y. H. et al. In vitro BACE-1 inhibitory phenolic components from the seeds of *Psoralea corylifolia*. *Planta Med.* **74**, 1405–1408 (2008).
53. Choi, J. H. et al. Bavachin and isobavachalcone, acyl-coenzyme A: cholesterol acyltransferase inhibitors from *Psoralea corylifolia*. *Arch. Pharm. Res.* **31**, 1419–1423 (2008).
54. Kim, D. W. et al. Phenolic phytochemical displaying SARS-CoV papain-like protease inhibition from the seeds of *Psoralea corylifolia*. *J. Enzym. Inhib. Med. Chem.* **29**, 59–63 (2014).
55. Li, W. et al. Evaluation of licorice flavonoids as protein tyrosine phosphatase 1B inhibitors. *Bioorg. Med. Chem. Lett.* **23**, 5836–5839 (2013).
56. Li, Y. G. et al. Fructus *Psoraleae* contains natural compounds with potent inhibitory effects towards human carboxylesterase 2. *Fitoterapia* **101**, 99–106 (2015).
57. Hou, X. D. et al. Pancreatic lipase inhibitory constituents from *Fructus psoraleae*. *Chin. J. Nat. Med.* **18**, 369–378 (2020).
58. Bantug, G. R., Galluzzi, L., Kroemer, G. & Hess, C. The spectrum of T cell metabolism in health and disease. *Nat. Rev. Immunol.* **18**, 19–34 (2018).
59. Vodnala, S. K. et al. T cell stemness and dysfunction in tumors are triggered by a common mechanism. *Science* **363**, <https://doi.org/10.1126/science.aau0135> (2019).
60. Chen, X., Yang, Y. & Zhang, Y. Isobavachalcone and bavachinin from *Psoraleae fructus* modulate Abeta42 aggregation process through different mechanisms in vitro. *FEBS Lett.* **587**, 2930–2935 (2013).
61. Hur, J., Kim, M., Choi, S. Y., Jang, Y. & Ha, T. Y. Isobavachalcone attenuates myotube atrophy induced by TNF- α through muscle atrophy F-box signaling and the nuclear factor erythroid 2-related factor 2 cascade. *Phytother. Res.* **33**, 403–411 (2019).
62. Jing, H. et al. Isobavachalcone attenuates MPTP-induced Parkinson's disease in mice by inhibition of microglial activation through NF- κ B pathway. *PLoS ONE* **12**, e0169560 (2017).
63. Gao, D., Liu, F., Li, Z. & Guan, Y. Isobavachalcone attenuates Sepsis-induced lung injury via activation of A20 and NRF2/HO-1 in rats. *Eur. J. Pharm.* **848**, 49–54 (2019).

64. Dong, W. H., Chu, Q. Q., Liu, S. Q., Deng, D. T. & Xu, Q. Isobavachalcone ameliorates diabetic nephropathy in rats by inhibiting the NF-kappaB pathway. *J. Food Biochem.* e13405, <https://doi.org/10.1111/jfbc.13405> (2020).
65. Akihisa, T. et al. Chalcones and other compounds from the exudates of *Angelica keiskei* and their cancer chemopreventive effects. *J. Nat. Prod.* **69**, 38–42 (2006).
66. Nishimura, R. et al. Isobavachalcone, a chalcone constituent of *Angelica keiskei*, induces apoptosis in neuroblastoma. *Biol. Pharm. Bull.* **30**, 1878–1883 (2007).
67. Zhao, S. et al. Autophagy inhibition enhances isobavachalcone-induced cell death in multiple myeloma cells. *Int. J. Mol. Med.* **30**, 939–944 (2012).
68. Szliszka, E., Jaworska, D., Ksek, M., Czuba, Z. P. & Krol, W. Targeting death receptor TRAIL-R2 by chalcones for TRAIL-induced apoptosis in cancer cells. *Int. J. Mol. Sci.* **13**, 15343–15359 (2012).
69. Yang, L. et al. Isobavachalcone reveals novel characteristics of methuosis-like cell death in leukemia cells. *Chem. Biol. Interact.* **304**, 131–138 (2019).
70. Kuete, V. et al. Cytotoxicity of three naturally occurring flavonoid derived compounds (artocarpesin, cycloartocarpesin and isobavachalcone) towards multi-factorial drug-resistant cancer cells. *Phytomedicine* **22**, 1096–1102 (2015).
71. Szliszka, E. et al. Chalcones enhance TRAIL-induced apoptosis in prostate cancer cells. *Int. J. Mol. Sci.* **11**, 1–13 (2009).
72. Ohno, O. et al. Inhibitory effects of bakuchiol, bavachin, and isobavachalcone isolated from *Piper longum* on melanin production in B16 mouse melanoma cells. *Biosci. Biotechnol. Biochem.* **74**, 1504–1506 (2010).
73. Ma, T. et al. Determination of isobavachalcone in rat plasma by LC-MS/MS and its application to a pharmacokinetic study. *J. Pharm. Biomed. Anal.* **107**, 50–55 (2015).
74. Pietrocola, F. et al. Caloric restriction mimetics enhance anticancer immunosurveillance. *Cancer Cell* **30**, 147–160 (2016).
75. Ando, S. et al. DNA-binding characteristics of aclarubicin as compared with daunorubicin and doxorubicin. *Anticancer Res.* **8**, 409–415 (1988).
76. Kepp, O. & Kroemer, G. Autophagy induction by thiostrepton for the improvement of anticancer therapy. *Autophagy* **16**, 1166–1167 (2020).
77. Kim, D. H. et al. Modulation of inducible nitric oxide synthase expression in LPS-stimulated BV-2 microglia by prenylated chalcones from *Cullen corvifolium* (L.) Medik. through inhibition of I-kappaBalpha degradation. *Molecules* **23**, <https://doi.org/10.3390/molecules23010109> (2018).
78. Innok, P., Rukachaisirikul, T. & Suksamrarn, A. Flavanoids and pterocarpanes from the bark of *Erythrina fusca*. *Chem. Pharm. Bull. (Tokyo)* **57**, 993–996 (2009).
79. Yang, Y., Wang, H. Q. & Chen, R. Y. Flavonoids from the leaves of *Morus alba* L. *Yao Xue Xue Bao* **45**, 77–81 (2010).
80. Miller, V. et al. Fruit, vegetable, and legume intake, and cardiovascular disease and deaths in 18 countries (PURE): a prospective cohort study. *Lancet* **390**, 2037–2049 (2017).
81. Dalgaard, F. et al. Associations between habitual flavonoid intake and hospital admissions for atherosclerotic cardiovascular disease: a prospective cohort study. *Lancet Planet Health* **3**, e450–e459 (2019).
82. Wang, Y. et al. Autophagy induction by thiostrepton improves the efficacy of immunogenic chemotherapy. *J. Immunother. Cancer* **8**, <https://doi.org/10.1136/jitc-2019-000462> (2020).
83. Pietrocola, F. et al. Aspirin recapitulates features of caloric restriction. *Cell Rep.* **22**, 2395–2407 (2018).
84. Enot, D. P., Vacchelli, E., Jacquilot, N., Zitvogel, L. & Kroemer, G. TumGrowth: an open-access web tool for the statistical analysis of tumor growth curves. *Oncotarget* **7**, e1462431 (2018).

ARTICLE OPEN



Everolimus and plicamycin specifically target chemoresistant colorectal cancer cells of the CMS4 subtype

Jiayin Deng^{1,2,3,4,9} , Ai-Ling Tian^{2,3,4,9}, Hui Pan^{2,3,4}, Allan Sauvat^{3,4}, Marion Leduc^{3,4}, Peng Liu^{3,4} , Liwei Zhao^{3,4}, Shuai Zhang^{3,4}, Hui Chen^{2,3,4}, Valérie Taly⁴, Pierre Laurent-Puig^{4,5} , Laura Senovilla^{3,4,5} , Yingqiu Li¹  , Guido Kroemer^{3,4,6,7,8}   and Oliver Kepp^{3,4}  

© The Author(s) 2021

Colorectal cancers (CRC) can be classified into four consensus molecular subtypes (CMS), among which CMS1 has the best prognosis, contrasting with CMS4 that has the worst outcome. CMS4 CRC is notoriously resistant against therapeutic interventions, as demonstrated by preclinical studies and retrospective clinical observations. Here, we report the finding that two clinically employed agents, everolimus (EVE) and plicamycin (PLI), efficiently target the prototypic CMS4 cell line MDST8. As compared to the prototypic CMS1 cell line LoVo, MDST8 cells treated with EVE or PLI demonstrated stronger cytostatic and cytotoxic effects, increased signs of apoptosis and autophagy, as well as a more pronounced inhibition of DNA-to-RNA transcription and RNA-to-protein translation. Moreover, nontoxic doses of EVE and PLI induced the shrinkage of MDST8 tumors in mice, yet had only minor tumor growth-reducing effects on LoVo tumors. Altogether, these results suggest that EVE and PLI should be evaluated for their clinical activity against CMS4 CRC.

Cell Death and Disease (2021)12:978; <https://doi.org/10.1038/s41419-021-04270-x>

INTRODUCTION

Colorectal cancer (CRC) represents a continuous therapeutic challenge calling for personalized approaches that are based on molecular stratification systems. Thus, beyond the tumor-node metastasis (TNM) classification of CRC stages, anatomical criteria (right versus left, colonic versus rectal cancer), and histological evaluation (low-grade versus high-grade), additional variables have been used to distinguish different categories of CRC [1, 2]. For instance, CRC has been classified as a function of the activated oncogenes (e.g., KRAS-positive versus KRAS-negative CRC) [3], as a function of the immune infiltrates (the immunoscore reflecting the density of CD3⁺ and CD8⁺ T cells) [4, 5] or as a function of microsatellite instability (MSI) resulting from DNA mismatch repair (MMR) defects [6]. All these classifications have clinical utility as exemplified by the fact that KRAS-positive CRC are resistant against the anti-epidermal growth factor receptor (anti-EGFR) antibody cetuximab [7, 8], immunoscore-positive resectable CRC have an intrinsically good prognosis and can be spared adjuvant chemotherapy [9, 10], and MMR-deficient, MSI-high cancers are particularly susceptible to immunotherapy with the PD-1-blocking antibody nivolumab [11–13].

In a collective attempt to unify distinct classification systems, the CRC subtyping consortium identified four consensus molecular subtypes (CMS): CMS1 (microsatellite instability immune), CMS2 (canonical), CMS3 (metabolic), and CMS4 (mesenchymal) [14]. Among the subtypes, CMS1, which is characterized by genomic and chromosomal instability and strong immune infiltration, has a particularly good prognosis [15], while the CMS4 subtype has a particularly poor prognosis, which may be explained by cancer cell-intrinsic features reflecting epithelial–mesenchymal transition and dedifferentiation [16, 17].

Of note, the susceptibility of distinct CRCs to anticancer drugs correlates with the CMS classification, as determined in primary colorectal cancers, cell lines, and patient-derived xenografts [18, 19], as well as retrospective clinical studies [20, 21]. Based on the observation that CMS4 cells are particularly resistant against chemotherapeutic interventions, we employed high-throughput screening to identify drugs that selectively act on such cells. Here, we report that everolimus (EVE) and plicamycin (PLI) are particularly efficient against a CMS4 cell line in preclinical experiments.

¹MOE Key Laboratory of Gene Function and Regulation, State Key Laboratory of Biocontrol, School of Life Sciences, Sun Yat-sen University, Guangzhou, China. ²Université Paris Sud, Paris Saclay, Faculty of Medicine, Kremlin Bicêtre, France. ³Metabolomics and Cell Biology Platforms, Gustave Roussy Cancer Center, Université Paris Saclay, Villejuif, France. ⁴Centre de Recherche des Cordeliers, Equipe labellisée par la Ligue contre le cancer, Université de Paris, Sorbonne Université, Inserm U1138 and CNRS SNC 5096, Institut Universitaire de France, Paris, France. ⁵Unidad de Excelencia Instituto de Biología y Genética Molecular (IBGM), Universidad de Valladolid – CSIC, Valladolid, Spain. ⁶Pôle de Biologie, Institut du Cancer Paris Carpem, APHP, Hôpital Européen Georges Pompidou, Paris, France. ⁷Suzhou Institute for Systems Medicine, Chinese Academy of Medical Sciences, Suzhou, Jiangsu, China. ⁸Karolinska Institutet, Department of Women's and Children's Health, Karolinska University Hospital, Stockholm, Sweden. ⁹These authors contributed equally: Jiayin Deng, Ai-Ling Tian. email: lsslyq@mail.sysu.edu.cn; kroemer@orange.fr; captain.olsen@gmail.com
Edited by Professor Gerry Melino

Received: 11 June 2021 Revised: 19 September 2021 Accepted: 5 October 2021

Published online: 21 October 2021

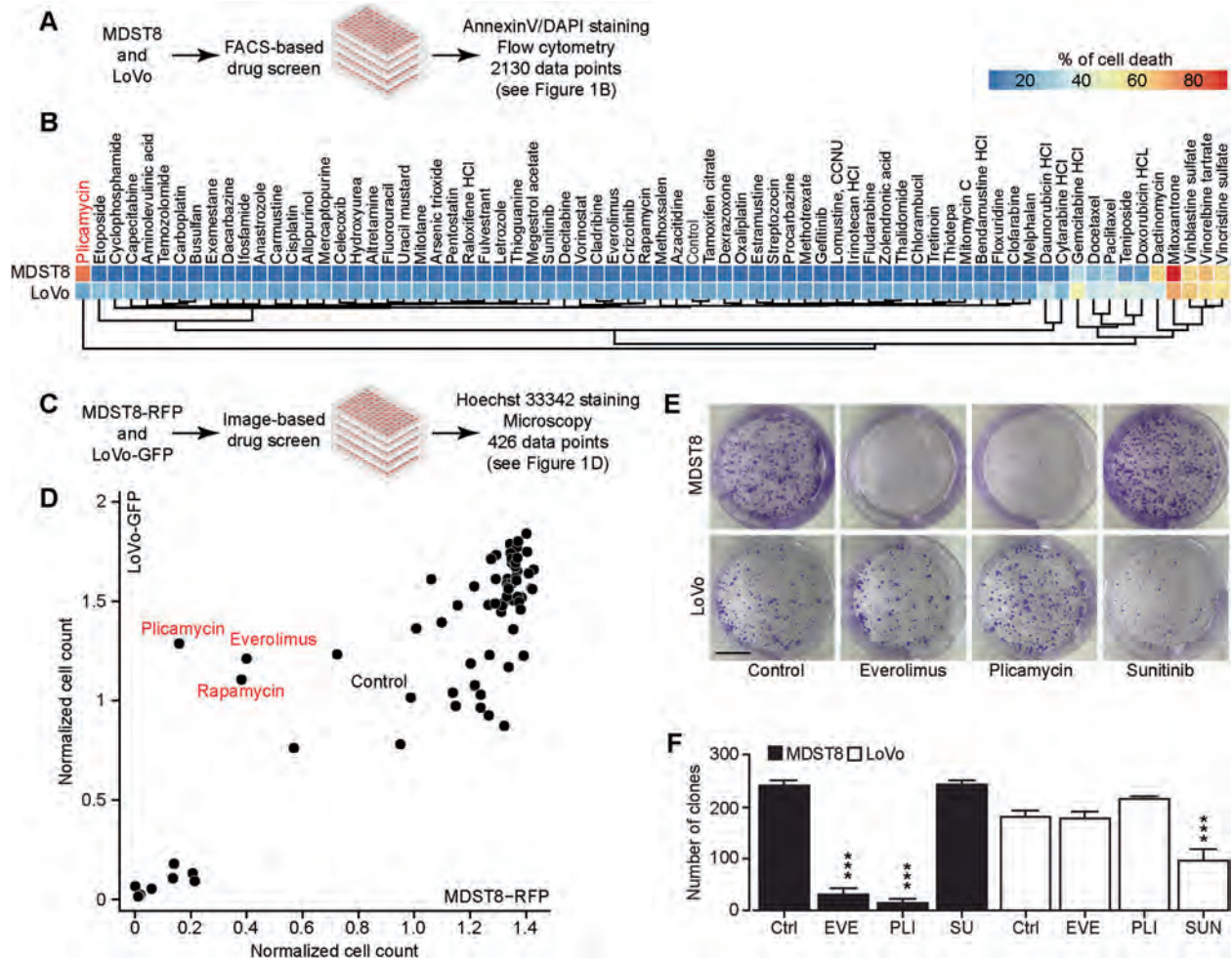


Fig. 1 Chemical compound screen discovers that plicamycin and everolimus specifically target MDST8. **A** Scheme of the screening campaigns. **B** MDST8 or LoVo cells were treated with 71 drugs in the anticancer library at a concentration of 0.1 μM for 72 h. The percentage of AnnexinV^{high}DAPI^{high} cells was measured by flow cytometry as an indicator for cell death. Each parameter depicts the mean value of three times repeated experiments and is depicted in a hierarchically clustered heatmap. The blue and red tiles in the heatmap represent the percentage of AnnexinV^{high}DAPI^{high} death cells range from 0 to 100%. **C** Identification of plicamycin, everolimus, and rapamycin as chemicals that specifically kill MDST8 but not LoVo cells. MDST8-RFP or LoVo-GFP cells were treated with 71 drugs in the anticancer library at the concentration of 0.1 μM for 72 h. Debris and cells depicting nuclear pyknosis were excluded, and healthy cells were enumerated. The untreated control was normalized to 1. **D** Results reported in a bi-parametric plot, showing the normalized healthy cell counts after treatment comparing between MDST8-RFP and LoVo-GFP. **E** Images show representative pictures of colonies formed as observed upon crystal violet staining after treatment of MDST8 and LoVo cells with 10 nM everolimus (EVE), 10 nM plicamycin (PLI), or 2 μM sunitinib (SUN) for 3 to 4 weeks. **F** The bar chart represents the number of clones with a size greater than or equal to 50 μm^2 . Error bars indicate SEM. Asterisks refer to significant effects for treatments versus control (Ctrl) (paired Student's *t* test, ****p* < 0.001).

RESULTS

Identification of everolimus and plicamycin as CMS4-targeting agents

LoVo cells represent the good-prognosis microsatellite instable-enriched CMS1 CRC subtype, while MDST8 cells represent the poor-prognosis mesenchymal CMS4 CRC subtype, as determined by transcriptomic analyses [19] and validated by quantitative reverse transcriptase-polymerase chain reactions (qRT-PCR) for a selected panel of mRNAs (Supplementary Fig. S1). Since CMS4 tumors have a poor prognosis [14, 22] and CMS4 cells are notoriously resistant to chemotherapeutic drugs [19], we designed a dual-screening campaign for identifying drugs that would kill MDST8 cells more efficiently than LoVo cells. In the first approach, both cell lines were cultured in the presence of a collection of ~70 distinct small-molecule anticancer drugs, and the frequency of apoptotic or necrotic cells was determined by Annexin V-AF647/DAPI staining, considering both Annexin V-AF647⁺DAPI⁻ and

Annexin V-AF647⁺DAPI⁺ cells as a desirable outcome (Fig. 1A, B and Supplementary Fig. S2A, B). In the second approach, LoVo cells were stably transduced with green fluorescent protein (GFP) and MDST8 cells with red-fluorescent protein (RFP), cultured in the presence of the drugs, and then subjected to automated quantification of the proportion of green and red cells in each culture (Fig. 1C, D and Supplementary Fig. S2C). Both approaches revealed that MDST8 cells were generally more resistant against anticancer drugs, in accord with the published literature [19], with the notable exception of plicamycin (PLI), which was identified in both screens as an MDST8-specific drug, and two inhibitors of the mechanistic target of rapamycin complex 1 (mTORC1), rapamycin and everolimus (EVE), which were identified in the second screen. As a note, the tyrosine kinase inhibitors sunitinib (SUN) and crizotinib (CRIZ) preferentially killed LoVo cells but not MDST8 cells (Fig. 1E, F and Supplementary Fig. S2A, B). Clonogenic assays (Fig. 1E, F) confirmed that both PLI and EVE reduced the number of

viable colonies of MDST8 but not of LoVo cells. Hence, we decided to continue the characterization of these two agents, EVE and PLI, as potential CMS4-targeting agents.

Selective induction of MDST8 cell stress and death by everolimus and plicamycin

We continued the comparative analysis of clinically approved EVE and PLI on LoVo and MDST8 cells to characterize specific vulnerabilities of the latter cell line. Annexin V-AF647/DAPI staining revealed that MDST8 cells were selectively killed by plicamycin while presenting both early apoptotic (Annexin V-AF647⁺DAPI⁻) and necrotic (Annexin V-AF647⁺DAPI⁺) events. In contrast, MDST8 cells were resistant against the anticancer agents oxaliplatin (OXA) and sunitinib (SUN) in conditions in which a sizeable fraction of LoVo cells died (Fig. 2A–C). The differential PLI sensitivity (and SUN resistance) of CMS4 cells over CMS1 cells was confirmed for another pair of human colorectal cancer cell lines, namely, Colo320HSR and HCT116, which represent the CMS4 and CMS1 subtypes, respectively (Supplementary Fig. S3). Moreover, PLI (and to less degree EVE) induced a higher level of caspase-3 activation (measured with a fluorogenic substrate) in MDST8 than in LoVo cells (Fig. 2D, E), and PLI (and to less degree EVE) caused the release of cytochrome C from mitochondria (measured by an immunofluorescence assay that assesses the reduction of the staining intensity) more efficiently in MDST8 than in LoVo cells (Fig. 3). Moreover, MDST8 but not LoVo cells manifested an elongation of mitochondria stained with MitoTracker, as well as a reduction of MitoTracker staining (Supplementary Fig. S4). Other cellular assays confirmed the selective susceptibility of MDST8 cells to EVE and PLI as compared to LoVo cells. Thus, both EVE and PLI caused an accumulation of cells in the G0/G1 phase of the cell cycle (measured by propidium iodide staining of ethanol-permeabilized, RNase-treated cells, and cytofluorometry) with a concomitant reduction of cells in the S and G2/M phase in MDST8 but not in LoVo cells (Fig. 4A, B). Although neither EVE nor PLI induced DNA damage assessed by immunofluorescence detection of nuclear γ -histone 2 A.X foci (Fig. 4C, D), both agents caused a reduction in DNA-to-RNA transcription and RNA-to-protein translation in MDST8 but not in LoVo cells, as measured by quantifying the cellular incorporation of the RNA precursor ethacrynic uridine (EU) and the protein precursor L-azidohomoalanine (AHA), respectively (Fig. 4E–H). Finally, the autophagy-association redistribution of microtubule-associated proteins 1A/1B light chain 3B (hereafter referred to as LC3) fused to GFP (GFP-LC3), the lipidation of LC3 causing an increase in its electrophoretic mobility (annotated as LC3-II), and the decrease in the autophagic substrate sequestosome-1 (SQSTM1, best known as p62) were observed in MDST8 but not in LoVo cells cultured with EVE or PLI (Fig. 5). Altogether, these results demonstrate that MDST8 cells are sensitive to the induction of cytostatic cell stress and cell death by EVE and PLI, respectively.

In vivo treatment of MDST8 tumors with everolimus and plicamycin

As a final proof that MDST8 tumors can be treated with the drugs identified in this study, we inoculated mice with MDST8 or, as a control, LoVo cells. Once palpable tumors had been established, the mice received systemic injections of either EVE or PLI on a biweekly basis (Fig. 6A, B). While MDST8 tumors reduced their volume in response to EVE and PLI, LoVo tumors continued their progression (Fig. 6C, D and Supplementary Fig. S5A, B). This drug effect was not accompanied by any manifest signs of toxicity (and in particular weight loss, Supplementary Fig. S5C, D) and caused a significant extension of lifespan in mice carrying MDST8 but not LoVo tumors (Fig. 6E, F). In a limited number of cases, we stopped the treatment of MDST8-bearing mice at day 65 post-inoculation. For those mice that lacked palpable tumor masses after EVE or PLI treatment, discontinuation of the drugs did not result in recurrence of the

tumors, suggesting that these animals had been definitively cured from their cancers. In contrast, when macroscopic tumors had not been fully eliminated, discontinuation of EVE or PLI resulted in regrowth of most cancers, contrasting with the continuous shrinkage of the majority of tumors that underwent further therapy (Fig. 6G, H). These results suggest that tumors usually remained sensitive to EVE and PLI throughout the treatment phase, for up to 3 months (from day 37 to day 117). Altogether, these results demonstrate that MDST8 tumors can be held in check by continuous, nontoxic administration of EVE and PLI.

DISCUSSION

This work demonstrates that two mechanistically unrelated drugs, everolimus (EVE, an inhibitor of mTORC1) and plicamycin (PLI, a DNA-binding agent that inhibits RNA synthesis) efficiently target the CMS4 cell line MDST8, both in vitro and in vivo. It will be interesting to determine the molecular mechanisms explaining why MDST8 cells are selectively susceptible to these agents. Moreover, it will be important to evaluate the potential clinical utility of these agents for the treatment of CMS4 colorectal cancers.

Everolimus is FDA approved for a series of indications including hormone receptor-positive, HER2-negative advanced breast cancer (in combination with aromatase inhibitors), neuroendocrine tumors (NET) of gastrointestinal (GI) or lung origin, advanced renal carcinoma, renal angiomyolipoma associated with tuberous sclerosis complex (TSC), subependymal giant cell astrocytoma (SEGA) associated with TSC [23]. Clinical trials on colorectal cancer patients largely failed when EVE was used as a single agent [24, 25] or combined with the anti-VEGF-A antibody bevacizumab [26] or the insulin receptor/insulin-like growth factor R receptor inhibitor linsitinib [27] for the treatment of refractory metastatic colorectal cancer. However, stable disease was induced in 50% of patients with refractory metastatic colorectal cancer when EVE was combined with tivozanib (an oral VEGF receptor-1, -2, -3 inhibitor) [28], and a 60% response rate was reported when EVE was combined with the chemotherapeutic agent irinotecan and the anti-EGFR antibody panitumumab [29]. Currently, there is one clinical trial (NCT02890069) that recruits colorectal cancer patients to combine EVE with the PD-1-blocking antibody PDR001. It may be interesting to apply the CMS classification to these trials and to re-evaluate the possibility that patients bearing cancers falling into the CMS4 category obtain clinical benefit from treatment with EVE alone or in combination with other agents.

Plicamycin (which is often referred to as "mithramycin A") has been clinically evaluated for the treatment of Ewing sarcoma (NCT01610570), as well as for the treatment of lung, esophagus, and other thoracic cancers (NCT01624090). A Phase I/II that is currently recruiting patients with primary thoracic malignancies or extrathoracic neoplasias with pleuropulmonary metastases evaluates the effects of continuous intravenous infusion of mithramycin (NCT02859415). However, PLI has not been evaluated in the context of colorectal cancer, apart from one phase II study reporting a major regression of one rectal adenocarcinoma in response to this agent [30]. Of note, this inhibitor of DNA-to-RNA transcription has been reported to target colorectal cancer stem cells [31], perhaps due to the inhibition of the transcription factor Sp1 [32]. Interestingly, it appears that inhibition of transcription by plicamycin is well detectable in the susceptible CMS4 cell line MDST8 but not in the resistant CMS1 cell line LoVo.

It will be important to evaluate whether the mechanism that we explored here comes into action in vivo and whether patients with CMS4 colorectal cancer might benefit from PLI, alone or in combination with EVE. Indeed, in the xenograft models, both PLI and EVE exhibit satisfactory preclinical activity against CMS4 cancers. Future clinical trials might establish whether these two drugs can be advantageously combined to achieve efficient tumor shrinkage without major side effects.

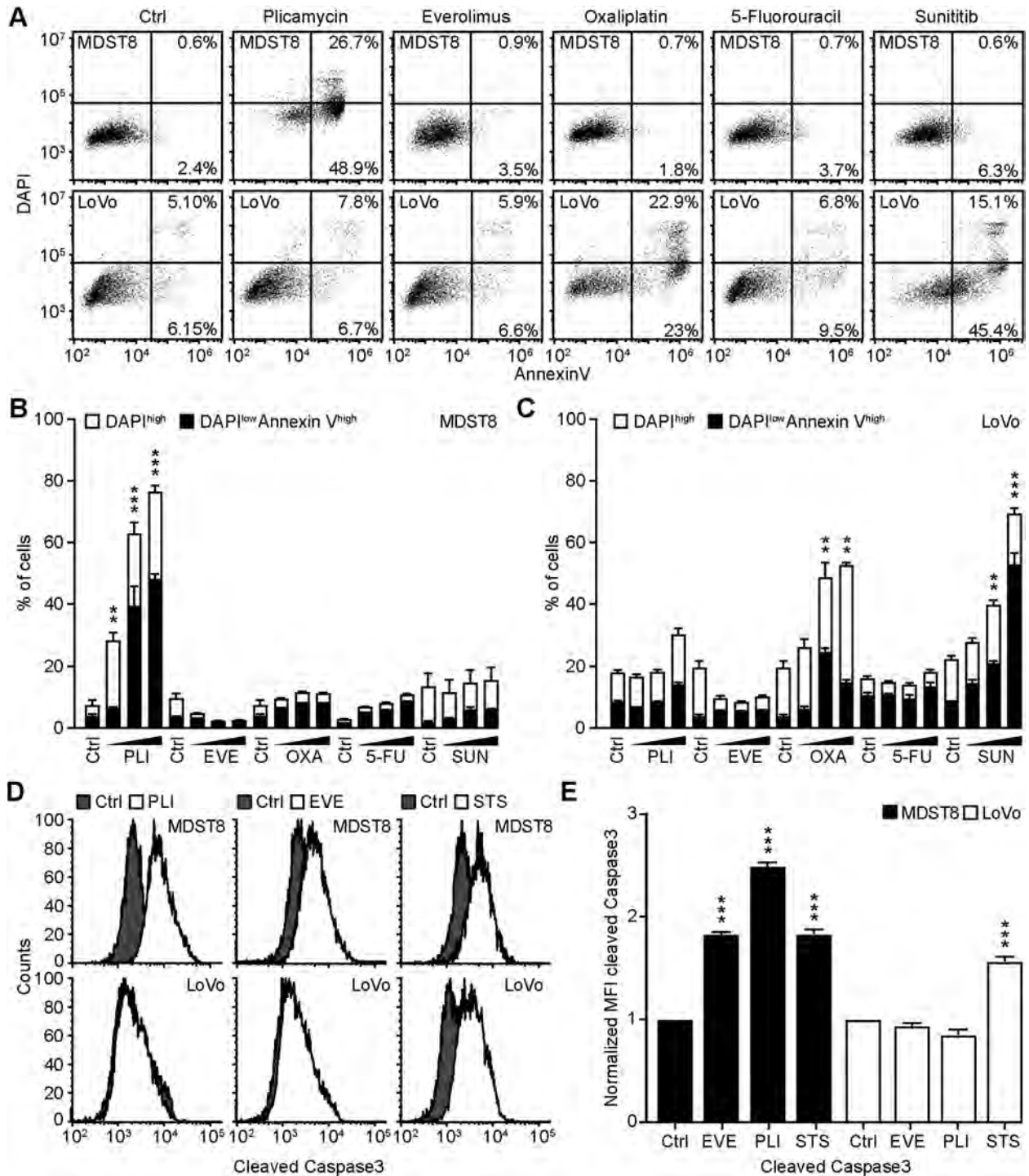


Fig. 2 Plicamycin induces cell death in MDST8. Wild-type (WT) MDST8 and LoVo cells were treated with plicamycin (PLI at 25, 50, and 100 nM for 72 h), everolimus (EVE at 10, 100 nM and 1 μ M for 72 h), oxaliplatin (OXA; 2.5, 5 and 10 μ M for 48 h), 5-fluorouracil (5-FU; 2.5, 5 and 10 μ M for 48 h), sunitinib (SUN; 2.5, 5 and 10 μ M for 48 h). Then, cells were stained with the DAPI and Annexin V to measure apoptotic cell death (A–C). **A** Representative dot plots of untreated MDST8 and LoVo controls (Ctrl) or treated with plicamycin 100 nM, EVE 1 μ M, OXA 10 μ M, 5-FU 10 μ M, and SUN 10 μ M. Numbers indicate the percentage of cells in each quadrant. **B, C** The frequency of dying (DAPI^{low}AnnexinV^{high}) and dead (DAPI^{high}) cells among the MDST8 (**B**) and LoVo (**C**) cells elicited by the corresponding drugs, as determined by analysis with the FlowJo software. Data are depicted as mean values of three independent experiments. **D, E** MDST8 cells were treated with 50 nM PLI, 0.1 μ M EVE or the positive control staurosporine (STS) 0.1 μ M for 48 h. Caspase-3 activation was measured by flow cytometric analysis upon staining with specific antibodies. Representative histograms are shown in (**D**). Normalized mean fluorescent intensity (MFI) of cleaved caspase-3 for each condition is depicted as bar chart (**E**). Error bars indicate SEM. Asterisks refer to significant effects for treatments versus control (paired Student's *t* test; ***P* < 0.01, ****P* < 0.001).

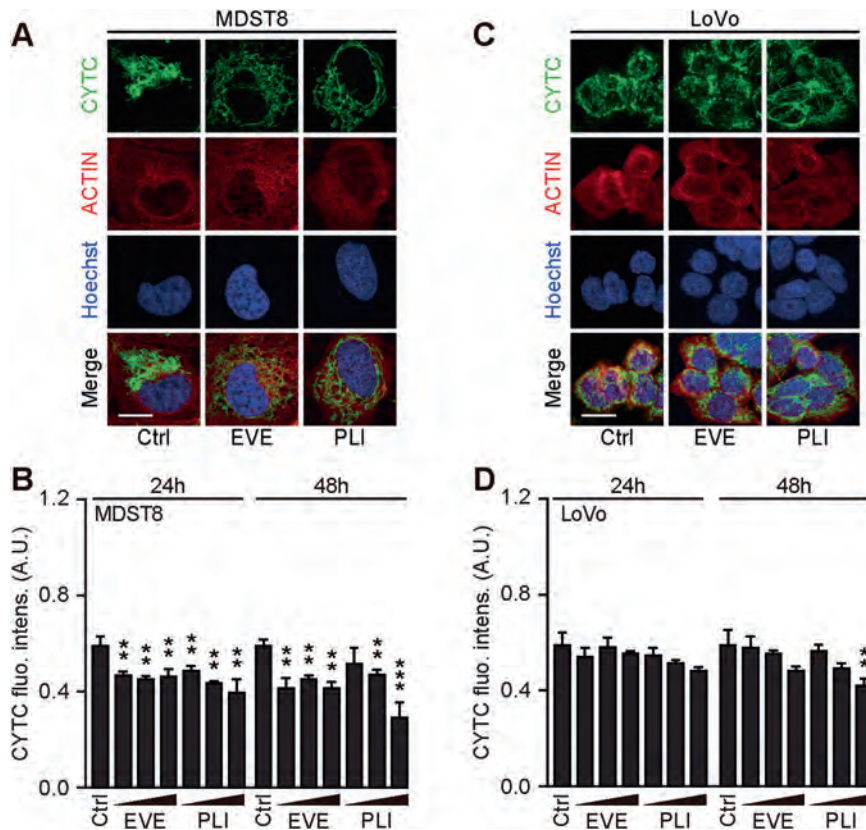


Fig. 3 Mitochondrial cytochrome c release in response to plicamycin treatment. Wild-type (WT) MDST8 and LoVo cells were treated 25, 50, or 100 nM plicamycin (PLI) or 10 nM, 100 nM, 1 μ M everolimus (EVE) for 24 h or 48 h followed by immunofluorescence staining with antibodies specific for cytochrome c and subsequent assessment by confocal microscopy. Representative images of cells in each condition are shown. Scale bars represent 10 μ m. **A, C** Images were quantified of cytoplasmic cytochrome c intensity and are reported as a bar chart (**B, D**). Error bars indicate SEM. Asterisks refer to significant effects for treatments versus control (paired Student's t test; Error bars indicate SEM. Asterisks refer to significant effects for treatments versus control (paired Student's t test; ** $P < 0.01$, *** $P < 0.001$).

MATERIALS AND METHODS

Cell lines

Human colon Colo320HSR, HCT116, LoVo, and MDST8 cells were purchased from the American Type Cancer Collection (ATCC). MDST8 and LoVo wild-type cells were transduced with LentiBrite™ H2B-RFP and H2B-GFP lentiviral particles (Merck Millipore, Burlington, MA, USA), respectively, following the manufacturer's instructions, to obtain MDST8 H2B-RFP and LoVo H2B-GFP. In addition, both MDST8 and LoVo wild-type cells were transduced with LentiBrite™ GFP-LC3 lentiviral particles (Merck Millipore, Burlington, MA, USA), to obtain MDST8 GFP-LC3 and LoVo GFP-LC3 cells, as described [33–35].

Cell culture

MDST8 and MDST8 GFP-LC3 cells were cultured in Dulbecco's Modified Eagle medium with high glucose (Thermo Fisher Scientific, Carlsbad, CA, USA) while the medium of LoVo and LoVo GFP-LC3 was Ham's F-12K (Kaighn's) (Thermo Fisher Scientific). Both media were supplemented with 10% fetal bovine serum (Gibco™ Thermo Fisher Scientific), 10 U/mL penicillin sodium, and 10 U/mL streptomycin sulfate (Thermo Fisher Scientific), and cells were kept in a humidified incubator with 5% CO₂ at 37 °C. Cell culture plastic was purchased from Corning (Corning, NY, USA) and Greiner Bio-One (Kremsmünster, Austria).

Compounds and reagents

A custom-arrayed anticancer library was used [36]. Oxaliplatin came from Accord Healthcare (Ahmedabad, India). Sunitinib (PZ0012), crizotinib (PZ0191), 5-fluorouracil (F6627), everolimus (SML2282), rapamycin (R8781), plicamycin (M6891), staurosporine (S5921), thapsigargin (T9033) methotrexate (M7824), and DMSO were purchased from Sigma-Aldrich. The MAD2 inhibitor M21-1 (312271-03-7) was from Cayman. Everolimus

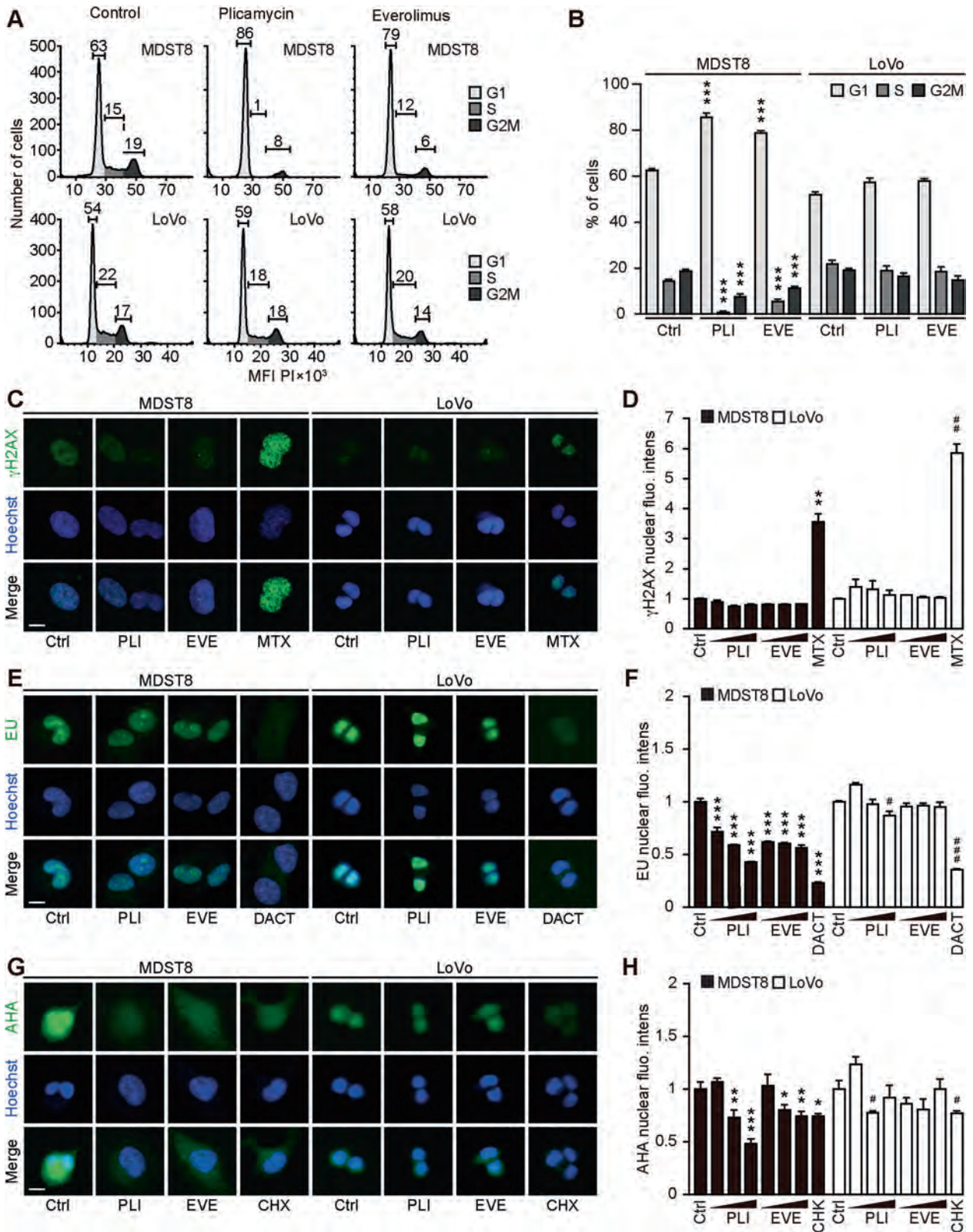
(HY-10218) and plicamycin (HY-A0122) for in vivo experimentation were purchased from MedChemExpress. Hoechst 33342 (H3570) and Lipofectamine® 2000 were purchased from Thermo Fisher Scientific. Propidium iodide (P4864), formaldehyde (F8775), and Triton X-100 (T8787) were purchased from Sigma-Aldrich (St. Louis, MO, USA).

Flow cytometric analysis

For high-throughput screening, cancer cells were seeded in 96-well plates (1×10^4 cells/well) in 100 μ L cell culture medium and let adapt for 24 h before treatment. Then cells were treated with the 71 chemicals of the anticancer library at 0.1 μ M, 1 μ M, or 10 μ M final concentration for 48 h or 72 h. Then cells were collected in 96-well V-shape plates (Greiner Bio-One, Frickenhausen, Germany), washed with PBS, and then the cell pellets were resuspended in 100 μ L Annexin V Binding Buffer (422201, Biolegend) containing 0.2 μ L Annexin V (640919, Biolegend) and 0.1 μ L DAPI. Samples were then incubated in the dark for 15 min. After that, the plates were immediately subjected to flow cytometry acquisition using a high-throughput sampler mounted on a BD LSRFortessa flow cytometer (Beckton Dickinson, Franklin Lakes, NY, USA). Data were further processed with the FlowJo software (LLC, Ashland, OR, USA) to assess the percentage of Annexin V⁺ and DAPI⁺ dying and dead cells, respectively [37]. Then the data were imported into the free available software R (<https://www.r-project.org>) and integrated with the heatmap packages from the Bioconductor repository (<https://bioconductor.org/>) to graphically depict data as a heatmap.

Assessment of caspase activity

Cells were seeded in 12-wells plates (5×10^4 cells/well). The next day, cells were treated with 0.1 μ M everolimus, 100 nM plicamycin, or 0.1 μ M staurosporine for 48 h. After that, cells were collected and fixed with



intracellular (IC) Fixation Buffer (00-8222-49, Invitrogen) and permeabilized with Permeabilization Buffer (00-8333-56, Invitrogen) and finally stained with a rabbit anti-human/mouse caspase-3 Alexa Fluor® 488-conjugated monoclonal antibody (IC835G, Invitrogen) for flow cytometric analysis. The mean fluorescence intensity was analyzed with the FlowJo software.

Cell cycle analysis

Cells were seeded in 12-wells plates (5×10^4 cells/well) and let adapt overnight. The next day, cells were treated with 0.1 μM everolimus, 50 nM plicamycin, or 5 μM sunitinib for 48 h. After the treatment, the supernatant was discarded and the cells were collected and transferred into flow cytometry tubes. Cells were agitated and fixed in cold 70% ethanol for

Fig. 4 Cellular stress response to everolimus and plicamycin. **A, B** Alterations in the cell cycle progression in response to plicamycin (PLI) or everolimus (EVE) were studied by flow cytometry. Human colon cancer MDST8 and LoVo cells were treated with 50 nM PLI or 100 nM EVE for 48 h, then fixed and stained with FxCycle™ PI/RNase, followed by flow cytometric assessment. Representative cell cycle histograms of MDST8 and LoVo cells are shown in **(A)** and the percentage of cells in each cell cycle phase are depicted as a bar chart in **(B)**. Error bars indicate SEM. Asterisks refer to significant effects for treatments versus control (paired Student's *t* test, **P* < 0.05, ***P* < 0.01, ****P* < 0.001). **C–H** MDST8 and LoVo cells were pre-treated with EVE at 0.01, 0.1, and 1 μM, or with PLI at 12.5, 25, and 50 nM for 24 h; with mitoxantrone (MTX) at 1 μM for 16 h; with dactinomycin (DACT) at 2 μM, or cycloheximide (CHX) at 50 μM for 6 h followed by fixation and permeabilization. Then, cells were incubated with a rabbit anti-phospho-histone H2A.X (γH2A.X) antibody and stained with an anti-rabbit Alexa Fluor-488-coupled secondary antibody. The formation of nuclear γH2A.X⁺ foci is shown in **(C)** and the average nuclear intensity of the γH2A.X signal was quantified **(D)**. Cells were pre-treated with the aforementioned compounds in a complete medium and followed by an additional hour of treatment in the presence of 100 mM 5-ethynyl uridine (EU). After fixation, cells were permeabilized, and EU was stained with an Alexa Fluor-488-coupled azide. Representative images are shown for each treatment **(E)**. The EU intensity in the nucleus of each condition was ranked between the untreated control (control, Ctrl, 0% transcription inhibition) and the control that was not incubated with EU (corresponding to 100% transcription inhibition) **(F)**. Cells were pre-treated with the aforementioned compounds in complete medium followed by washout and treatment pursued in the methionine-free medium for 30 min. Afterward, the treatments were continued in methionine-free medium supplemented with 50 μM L-azidohomoalanine (AHA) for 1 h and AHA incorporation was detected after fixation, permeabilization, and blocking by the addition of an Alexa Fluor-488-coupled azide. Then, images were acquired **(G)**, and AHA intensity in the cells was ranked between the untreated control (Ctrl, 0% translation inhibition) and control without AHA (corresponding to 100% translation inhibition) **(H)**. Data information: representative images of EVE 1 μM, PLI 50 nM and MTX 1 μM are shown **(C)**; EVE 0.1 μM, PLI 25 nM, and DACT 2 μM are shown **(E)**; EVE 1 μM, PLI 50 nM, and CHX 50 μM are shown **(G)**. Scale bars represent 20 μm. One representative experiment among three is shown as mean ± SD, and *P*-values indicating differences to controls were calculated with Student's *t* test: **P* < 0.05, ***P* < 0.01, ****P* < 0.001 versus untreated MDST8 control; #*P* < 0.05, ##*P* < 0.01, ###*P* < 0.001 versus untreated LoVo control **(D, F, H)**.

2 min and kept in the dark at 4 °C overnight. Then the cells were washed three times with PBS and resuspended in 500 μL FxCycle™ PI/RNase staining solution (F10797, Thermo Fisher). The samples were incubated for 15–30 min at room temperature, protected from light, and finally analyzed on a Cytoflex (Beckman Coulter) flow cytometer. Data analysis was performed with the FlowJo software.

High-throughput screening

Wild-type cells were seeded in 384-well black imaging plates (Greiner Bio-One) at a density of 1.5×10^3 cells/well and let adhere for 24 h. The next day, cells were treated with drugs of an anticancer compound library in 0.1 μM concentration for 72 h. For viability assessment, cells were fixed with 3.7% formaldehyde containing 1 μg/mL Hoechst 33342 for 1 h at room temperature. The fixative was exchanged to PBS and viability was assessed by automated microscopy.

Automated fluorescence microscopy

MDST8 GFP-LC3 or LoVo GFP-LC3 cells were seeded in 96-well black imaging plates at a density of 1.5×10^3 cells/well. The next day, cells were treated with everolimus (10, 100 nM, and 1 μM), plicamycin (25, 50, and 100 nM), or torin (0.3 μM), and incubated for 6, 24 or 48 h. After that, cells were stained with MitoTracker™ Orange (M7510, Thermo Fisher) [38] and then fixed with 3.7% formaldehyde containing Hoechst 33342. Automated fluorescence microscopy was conducted by means of a robot-assisted Molecular Devices IXM XL Biolumager and a Molecular Devices IXM-C (Molecular Devices, Sunnyvale, CA, USA) equipped with either a SpectraX or an Aura II light source (Lumencor, Beaverton, OR, USA), adequate excitation and emission filters (Semrock, Rochester, NY, USA) and a 16-bit monochromes sCMOS PCO.edge 5.5 camera (PCO Kelheim, Germany) or an Andor Zyla camera (Belfast, Northern Ireland) and a ×20 PlanAPO objective (Nikon, Tokyo, Japan) were used to acquire a minimum of four view fields per well, followed by automated image processing with the custom module editor within the MetaXpress software (Molecular Devices) and/or R employing the EBIImage and RBioFormats packages. Image segmentation was performed using the MetaXpress software (Molecular Devices). Following the exclusion of cellular debris and dead cells from the dataset, parameters of interest were normalized, statistically evaluated, and graphically depicted with R software [39]. Cytoplasmic ROIs were used for the quantification of cytochrome *c* intensity. To quantify GFP-LC3 aggregation, a segmentation mask of high-intensity dots was generated in the cytoplasm of cells.

Monitoring mitochondrial cytochrome *c* release

Wild-type cells were plated onto coverslips previously coated with 10 μg/mL poly-L-lysine in a 12-well plate. The next day, cells were treated with 0.1 μM everolimus, 50 nM plicamycin, or 0.1 μM staurosporine for 24 h or 48 h. After the treatment, cells were stained with MitoTracker, fixed with 3.7% formaldehyde, as described previously, and permeabilized with 0.2% Triton X-100 for 10 min. Then the cells were incubated with Alexa Fluor® 647

coupled anti-cytochrome *c* antibody (612310, Biolegend) overnight at 4 °C in the dark. Finally, cells were washed with PBS and mounted with Fluoromount-G™ mounting medium (00-4958-02, Thermo Fisher). Fluorescence confocal microscopy was carried out using a Leica TCS SP8 Confocal Microscope with a ×63 oil immersion objective (Leica Microsystems, Wetzlar, Germany). Images were acquired from randomly selected fields of cells. Subsequently, the percentage of each subtype was evaluated for each treatment and a minimum of 30 cells were considered for the analysis. Image analysis was performed with the LAS X software (Leica) and R.

Clonogenic assay

MDST8 and LoVo cells were seeded in six-well plates at 1×10^3 cells per well. After 24 h, cells were treated with 10 nM everolimus, 10 nM plicamycin, or 2 μM sunitinib for 3 weeks (MDST8) or 4 weeks (LoVo). After that, the supernatant was discarded and the cells were incubated with 500 μL of crystal violet (Sigma) for 10 min. Then, cells were washed with deionized water, images were acquired and the area of each colony was quantified through Fiji's ColonyArea plugin, as described [40].

Quantitative RT-PCR

Total RNA extraction of cultured cells was performed with the GeneJET RNA Purification Kit (Life Technologies). In total, 2.5 μg RNA was then reverse transcribed into cDNA with the Maxima First Strand cDNA Synthesis Kit (Life Technologies). The expression of the genes of interest (Table 1) was analyzed by means of SYBR® green-based quantitative PCR using the Power SYBR™ Green PCR Master Mix in a StepOnePlus Real-Time PCR System (Applied Biosystems, Foster City, CA, USA). qRT-PCR data were normalized to the expression levels of the housekeeping gene hypoxanthine phosphoribosyltransferase 1 (HPRT1) and data were depicted as a Volcano plot employing R.

Protein immunoblots

Protein was extracted with RIPA lysis and extraction Buffer (89900; Thermo Scientific) in the presence of phosphatase and protease inhibitors (A32961; Thermo Scientific) followed by sonication. Then, protein content was measured by a DC™ Protein Assay Kit II (5000112; Bio-Rad) following the manufacturer's protocol. Protein was denatured at 100 °C, and 30 μg of proteins and 10 μL PAGE Ruler prestained protein ladder (26616; Thermo Scientific) were separated by polyacrylamide gel electrophoresis (PAGE) using 4–12% Bis-Tris Novex™ NuPAGE™ protein gels (NP0336PK2; Invitrogen) in Novex™ NuPAGE™ MES SDS migration buffer (1x) (NP000202; Invitrogen). Afterward, proteins were transferred to EtOH-activated PVDF membranes (88518; Thermo Scientific) in transfer buffer (25 mM Tris; 190 mM glycine; 10% ethanol in H₂O) at 200 mA and 120 V for 1.5 h. Membranes were washed in Tris-buffered saline with Tween-20 buffer (TBST; 20 mM Tris, pH 7.5; 150 mM NaCl; 0.1% Tween-20 in H₂O) and then blocked with 5% skim milk in TBST for 1 h. Membranes were exposed to primary antibody (anti-LC3B antibody; ab192890; Abcam) at 1:2000;

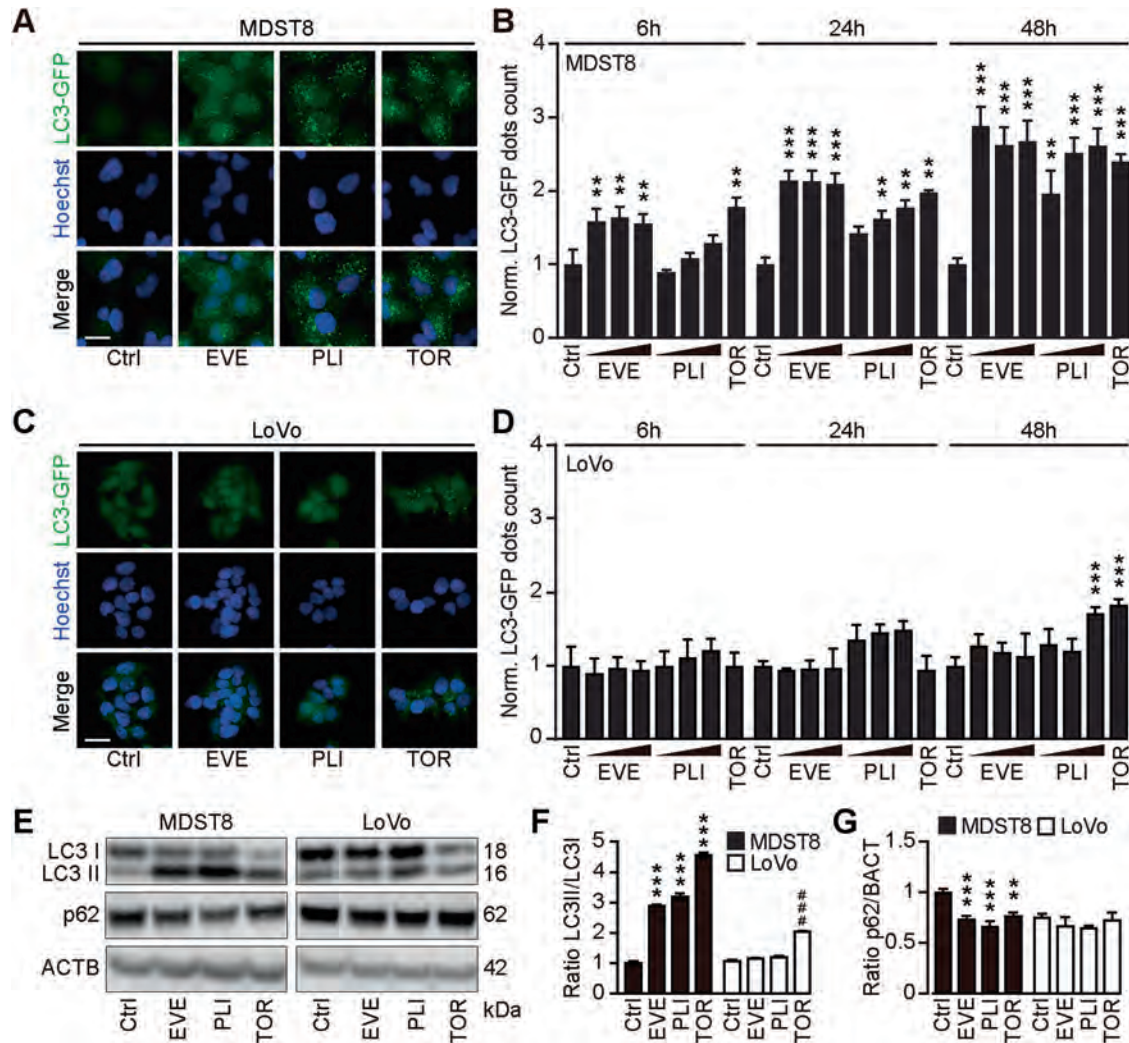


Fig. 5 Everolimus induces autophagy in MDST8. **A** MDST8 and **C** LoVo cells stably expressing GFP-LC3 were treated with plicamycin (PLI; 25, 50, and 100 nM), everolimus (EVE; 10, 100 nM and 1 μ M) or torin1 (TOR; 0.1 μ M) for 6 h 24 h and 48 h. After fixation and nuclear staining with Hoechst 33342, the images were acquired by confocal microscopy. Representative images are depicted for each cell line. The scale bar equals 20 μ m. **B**, **D** GFP-LC3 dots area were quantified. For each assessed parameter and cell line, data were normalized to the untreated control. Data represent means \pm SD. Each condition was compared to the untreated control by means of a paired Student's *t* test (***P* < 0.01, ****P* < 0.001). **E–G** Human colon cancer MDST8 or LoVo cells were treated with EVE (0.1 μ M) or PLI (50 nM) for 72 h. TOR (300 nM) was used for 6 h as a prototypical autophagy inducer. SDS-PAGE and immunoblot were performed, band intensities of LC3-I, LC3-II, p62, and β -actin (ACTB) were assessed, and the ratio LC3-II/LC3-I (**F**) and p62/ACTB (**G**) were calculated. Data are means \pm SD of three independent experiments (***P* < 0.01, ****P* < 0.001 versus untreated MDST8 control; ##*P* < 0.001 versus untreated LoVo control; Tukey's multiple comparisons test).

p62/SQSTM1 monoclonal antibody (H00008878-M01, Abnova) at 1:1000 diluted in 5% BSA in TBST overnight at 4 $^{\circ}$ C. Next, membranes were washed three times with TBST and then were incubated with 1:25000 appropriate horseradish peroxidase (HRP)-coupled secondary antibody (goat anti-rabbit IgG (H + L) (4050-05, SouthernBiotech); goat anti-mouse IgG (H + L) (1031-05, SouthernBiotech)) for 1 h at room temperature. Proteins were revealed with Amersham ECL Prime Western Blotting Detection Reagent (RPN2232; GE Healthcare Life Sciences). Anti-beta actin antibody (ab49900; Abcam) at 1:50,000 was used to verify equal loading.

Evaluation of DNA damage by quantification of phospho-histone H2A.X

Two thousand cells per well were cultured in 384-well μ Clear imaging plates. The next day, cells were treated for 24 h. Following, cells were fixed with 3.7% formaldehyde supplemented with 1 μ g/mL Hoechst 33342 for 1 h, permeabilized with 0.5% Triton X-100 for 15 min and blocked with 3% BSA for 1 h. Cells were further incubated with 1:1000 rabbit antibody specific for phospho-histone H2A.X (γ H2A.X) overnight at 4 $^{\circ}$ C. After several PBS washing steps, 1:2000 anti-rabbit Alexa Fluor-488-coupled antibodies were added. Following several PBS washing steps, the DAPI and GFP

signals were acquired with a confocal microscope IXM-C (Molecular Devices) and quantified as described before [41, 42].

Evaluation of RNA transcription by EU incorporation

Transcription was analyzed by measuring the incorporation of Click-iT chemistry-detectable 5-ethynyl uridine (EU) (C10327; Invitrogen) as described before [43]. In short, 2×10^3 cells per well were seeded in 384-well μ Clear imaging plates. The next day, cells were pre-treated for 24 h and washed and treatment was pursued in the presence of 1 mM 5-ethynyl uridine (EU) for 1 h. Following, the cells were fixed with 3.7% formaldehyde supplemented with 1 μ g/mL Hoechst 33342 for 1 h and permeabilized with 0.5% Triton X-100 for 15 min. Alexa Fluor-488-coupled azide was then added for 1 h. The intensity of the GFP signal (EU) in the nucleus was measured by microscopy, and the inhibition of transcription was calculated as a fold change in fluorescence intensity as compared to controls.

Protein translation study by AHA incorporation

Translation was measured by assessing the incorporation of L-azido-homoalanine (AHA) (C10289; Invitrogen), a labeled form of methionine by

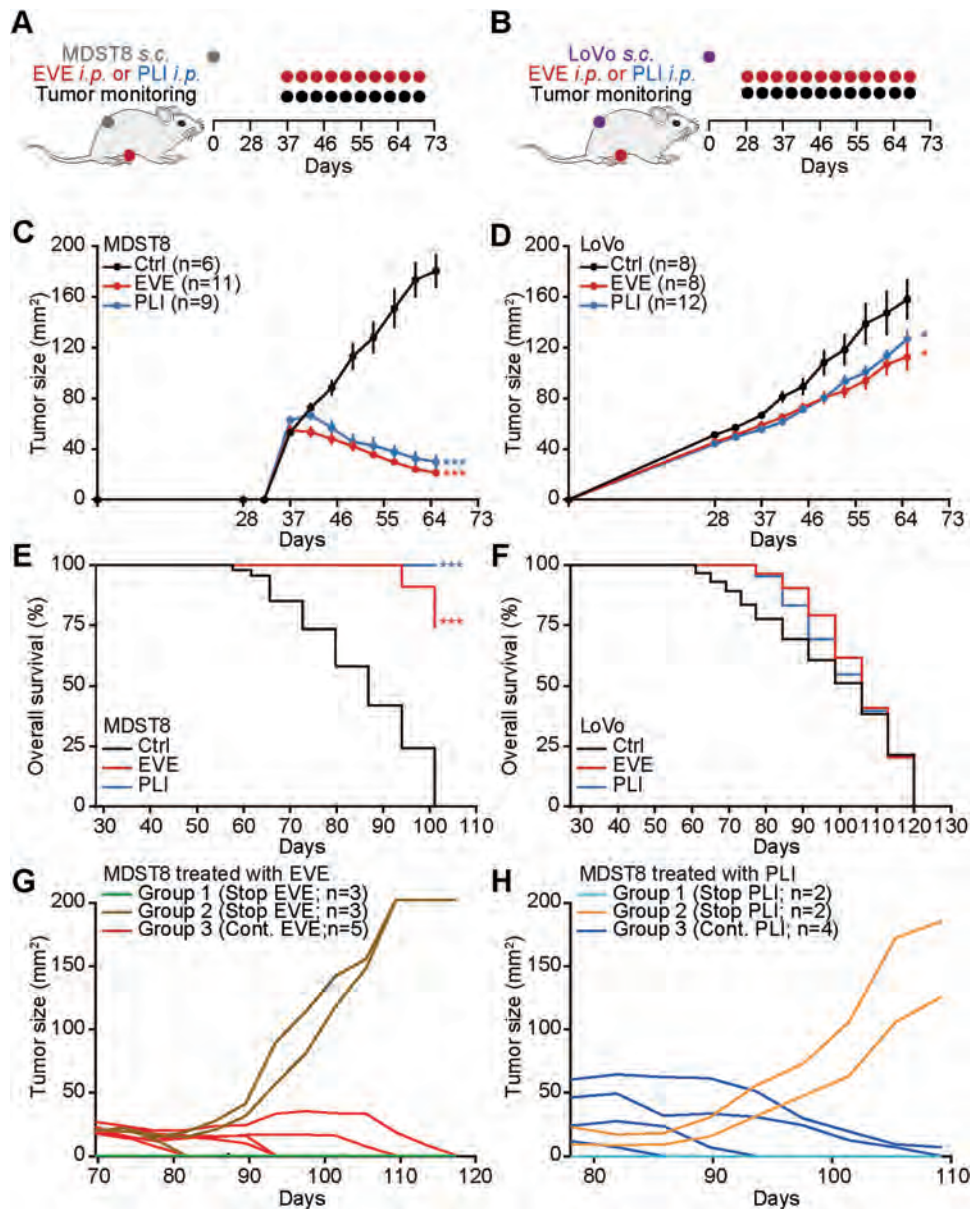


Fig. 6 Everolimus and plicamycin exhibit anticancer effects against CMS4 tumors. **A, B** Schematic overview of the treatment schedule of LoVo or MDST8 tumors with everolimus (EVE) and plicamycin (PLI) in vivo. **C–H** Five million human colon cancer MDST8 or LoVo cells were injected subcutaneously (s.c.) into the flank of athymic immunodeficient *nu/nu* mice. When tumors became palpable, mice received a systemic intraperitoneal injection of EVE or PLI. $n \geq 6$ mice per group. Results (means \pm SD tumor growth curves) are plotted ($*P < 0.05$, $***P < 0.001$). Overall survival is depicted, and P values ($***P < 0.001$) were calculated with a Log-rank test (**E, F**). After EVE/PLI treatment, mice bearing MDST8 tumors were divided into three different groups, and tumor growth was monitored upon continuation or discontinuation of the treatment as indicated (**G, H**).

Click-iT chemistry as described [44]. In short, 2×10^3 cells per well were seeded in 384-well μ Clear imaging plates. The next day, cells were treated for 24 h. After several PBS washing steps, the cells were incubated 30 min in the presence of methionine-free medium. They were further treated for 1 h in methionine-free medium in the presence of 50 μ M AHA. Afterward, the cells were fixed with 3.7% formaldehyde supplemented with 1 μ g/mL Hoechst 33342 for 1 h, permeabilized with 0.5% Triton X-100 for 15 min, and blocked with 3% BSA for 1 h. Then, Alexa Fluor-488-coupled azide was added for 1 h and AHA incorporation was measured by microscopy as a fold change in GFP fluorescence intensity.

In vivo tumor treatment

Established tumors were assessed for their response to everolimus- and plicamycin-based chemotherapy. To this aim, colon cancers were established subcutaneously (s.c.) in athymic *nu/nu* mice by injection of

5×10^6 MDST8 or LoVo cells. When tumors became palpable, 200 μ L of the chemotherapeutics (everolimus diluted in 90% corn oil, 4 mg/kg; plicamycin diluted in 40% PEG300, 5% Tween-80 and 45% saline, 1.5 mg/kg) or the diluent alone were injected intraperitoneally (i.p.) and tumor growth was monitored for the following weeks [5].

Experimental animals

In vivo experimentation. Seven- to eight-week-old female wild-type *nu/nu* mice were purchased from Envigo France (Gannat, France) and were kept at the Gustave Roussy Campus Cancer in a specific pathogen-free and environmental temperature-controlled animal facility with 12 h day, 12 h night cycles, and received food and water ad libitum. Animal experiments were conducted in compliance with the EU Directive 63/2010 and were approved by the Ethical Committee of the Gustave Roussy Campus Cancer (CEEA IRCIV/IGR no. 26, registered at the French Ministry of Research).

Table 1. RT-qPCR primers [45].

Human gene	Forward sequence	Reverse sequence
HPRT1	CCTGGCGTCGTGATTAGTGA	CGAGCAAGACGTTTCAGTCCT
CDH2	ACAGTGGCCACCTACAAAGG	CCGAGATGGGGTTGATAATG
SLUG	GGTCAAGAAGCATTTCACCG	CACAGTGTATGGGGCTGTATG
VIM	CCCTCACCTGTGAAGTGGAT	TCCAGCAGCTTCTGTAGGT
MMP2	TCTCCTGACATTGACCTTGGC	CAAGGTGCTGGCTGAGTAGATC
MMP9	TTGACAGCGGACAAGAAGTGG	GCCATTCACGTCGTCTTAT
MMP13	TCCCAGGAATTGGTGATAAAGTAGA	CTGGCATGACGCGAACAATA
CYP1B1	CACTGCCAACACCTCTGTCTT	CAAGGAGCTCCATGGACTCT
GAS1	AAAGTCTTCAACGGGCTGCGCT	TCCTTGACCGACTCGCAGATGG
HTR2B	TGTCCTTGGCGTGGCTGAT	TGGCACAGAGATGCATGATGGA
RGS4	AACACAATTCTCCACAACAA	CTGCCAGCCACATCA
FRMD6	AAGGACTGCCACCTCTTGG	AGTTCCCAAGATCAGCCTGC
INHBA	GCAGTCTGAAGACCACCTC	ATGATCCAGTCATTCCAGCC
CDX2	TTCACTACAGTCGCTACATCACC	TTGTTGATTTCTCTCTCTTGC
ZEB1	GCACAAGAAGAGCCACAAGTA	GCAAGACAAGTTCAGGGTTC
SP1	TGGCAGCAGTACCAATGGC	CCAGGTAGTCTGTGAGAAGTTC
HSP70	AGCTGGAGCAGGTGTGTAAC	CAGCAATCTTGGAAAGGCC
MAD2L1	TTCTCATTGCGCATCAAC	TCCAGGACCTCACCCTT
AIF1	GTTCCAGCGATGGCATGTTC	ACGCGGCCTTTTCTGTTC
HOPX	GCTCATTTCTGGGCTGTTA	GGATTTCCACCTGTCCTCTG

Primers utilized for the detection of CMS-related mRNA expression profiles.

Statistical analysis

Unless otherwise mentioned, data are reported as means \pm SD of triplicate determinations, and experiments were repeated at least three times yielding similar results. Statistical significance was assessed by Welch's and Student's *t* test. TumGrowth and GraphPad were used to analyze *in vivo* data raised in murine models [5]. TumGrowth is available at <https://github.com/kroemerlab>. *P* values of 0.05 or less were considered to denote significance (**P* < 0.05; ***P* < 0.01; ****P* < 0.001; ns, not significant).

DATA AVAILABILITY

Data are available from the corresponding authors upon reasonable request.

REFERENCES

- Markowitz SD, Bertagnolli MM. Molecular origins of cancer: molecular basis of colorectal cancer. *N. Engl J Med.* 2009;361:2449–60.
- Dekker E, Tanis PJ, Vleugels JLA, Kasi PM, Wallace MB. Colorectal cancer. *Lancet.* 2019;394:1467–80.
- Bos JL. *ras* oncogenes in human cancer: a review. *Cancer Res.* 1989;49:4682–9.
- Galon J, Costes A, Sanchez-Cabo F, Kirilovsky A, Mlecnik B, Lagorce-Page C, et al. Type, density, and location of immune cells within human colorectal tumors predict clinical outcome. *Science.* 2006;313:1960–4.
- Enot DP, Vacchelli E, Jacquilot N, Zitvogel L, Kroemer G. TumGrowth: an open-access web tool for the statistical analysis of tumor growth curves. *Oncoimmunology.* 2018;7:e1462431.
- Loeb LA. Microsatellite instability: marker of a mutator phenotype in cancer. *Cancer Res.* 1994;54:5059–63.
- Lievre A, Bachet JB, Le Corre D, Boige V, Landi B, Emile JF, et al. KRAS mutation status is predictive of response to cetuximab therapy in colorectal cancer. *Cancer Res.* 2006;66:3992–5.
- Lievre A, Bachet JB, Boige V, Cayre A, Le Corre D, Buc E, et al. KRAS mutations as an independent prognostic factor in patients with advanced colorectal cancer treated with cetuximab. *J Clin Oncol.* 2008;26:374–9.
- Anitei MG, Zeitoun G, Mlecnik B, Marliot F, Haicheur N, Todosi AM, et al. Prognostic and predictive values of the immunoscore in patients with rectal cancer. *Clin Cancer Res.* 2014;20:1891–9.
- El Sissy C, Kirilovsky A, Zeitoun G, Marliot F, Haicheur N, Lagorce-Page C, et al. Therapeutic implications of the immunoscore in patients with colorectal cancer. *Cancers.* 2021;13:1281.
- Kroemer G, Galluzzi L, Zitvogel L, Fridman WH. Colorectal cancer: the first neoplasia found to be under immunosurveillance and the last one to respond to immunotherapy? *Oncoimmunology.* 2015;4:e1058597.
- Bilgin B, Sendur MA, Bulent Akinci M, Sener Dede D, Yalcin B. Targeting the PD-1 pathway: a new hope for gastrointestinal cancers. *Curr Med Res Opin.* 2017;33:749–59.
- Thomas J, Leal A, Overman MJ. Clinical development of immunotherapy for deficient mismatch repair colorectal cancer. *Clin Colorectal Cancer.* 2020;19:73–81.
- Guinney J, Dienstmann R, Wang X, de Reynies A, Schlicker A, Soneson C, et al. The consensus molecular subtypes of colorectal cancer. *Nat Med.* 2015;21:1350–6.
- Becht E, de Reynies A, Giraldo NA, Pilati C, Buttard B, Lacroix L, et al. Immune and stromal classification of colorectal cancer is associated with molecular subtypes and relevant for precision immunotherapy. *Clin Cancer Res.* 2016;22:4057–66.
- Thanki K, Nicholls ME, Gajjar A, Senagore AJ, Qiu S, Szabo C, et al. Consensus molecular subtypes of colorectal cancer and their clinical implications. *Int Biol Biomed J.* 2017;3:105–11.
- Marisa L, Svrcek M, Collura A, Becht E, Cervera P, Wanherdrick K, et al. The balance between cytotoxic T-cell lymphocytes and immune checkpoint expression in the prognosis of colon tumors. *J Natl Cancer Inst.* 2018;110:68–77.
- Sveen A, Bruun J, Eide PW, Eilertsen IA, Ramirez L, Murumagi A, et al. Colorectal cancer consensus molecular subtypes translated to preclinical models uncover potentially targetable cancer cell dependencies. *Clin Cancer Res.* 2018;24:794–806.
- Linnekamp JF, Hooff SRV, Prasetyanti PR, Kandimalla R, Buikhuizen JY, Fessler E, et al. Consensus molecular subtypes of colorectal cancer are recapitulated in *in vitro* and *in vivo* models. *Cell Death Differ.* 2018;25:616–33.
- Okita A, Takahashi S, Ouchi K, Inoue M, Watanabe M, Endo M, et al. Consensus molecular subtypes classification of colorectal cancer as a predictive factor for chemotherapeutic efficacy against metastatic colorectal cancer. *Oncotarget.* 2018;9:18698–711.
- Mooi JK, Wirapati P, Asher R, Lee CK, Savas P, Price TJ, et al. The prognostic impact of consensus molecular subtypes (CMS) and its predictive effects for bevacizumab benefit in metastatic colorectal cancer: molecular analysis of the AGITG MAX clinical trial. *Ann Oncol.* 2018;29:2240–6.
- Bramsen JB, Rasmussen MH, Ongen H, Mattesen TB, Orntoft MW, Arnadottir SS, et al. Molecular-subtype-specific biomarkers improve prediction of prognosis in colorectal cancer. *Cell Rep.* 2017;19:1268–80.

23. Hasskarl J. Everolimus. *Recent Results Cancer Res.* 2018;211:101–23.
24. Altomare I, Hurwitz H. Everolimus in colorectal cancer. *Expert Opin Pharmacother.* 2013;14:505–13.
25. Ng K, Taberero J, Hwang J, Bajetta E, Sharma S, Del Prete SA, et al. Phase II study of everolimus in patients with metastatic colorectal adenocarcinoma previously treated with bevacizumab-, fluoropyrimidine-, oxaliplatin-, and irinotecan-based regimens. *Clin Cancer Res.* 2013;19:3987–95.
26. Altomare I, Bendell JC, Bullock KE, Uronis HE, Morse MA, Hsu SD, et al. A phase II trial of bevacizumab plus everolimus for patients with refractory metastatic colorectal cancer. *Oncologist.* 2011;16:1131–7.
27. Bendell JC, Jones SF, Hart L, Spigel DR, Lane CM, Earwood C, et al. A phase Ib study of linsitinib (OSI-906), a dual inhibitor of IGF-1R and IR tyrosine kinase, in combination with everolimus as treatment for patients with refractory metastatic colorectal cancer. *Invest N. Drugs.* 2015;33:187–93.
28. Wolpin BM, Ng K, Zhu AX, Abrams T, Enzinger PC, McCleary NJ, et al. Multicenter phase II study of tivozanib (AV-951) and everolimus (RAD001) for patients with refractory, metastatic colorectal cancer. *Oncologist.* 2013;18:377–8.
29. Schwark WS, Haluska M. Prophylaxis of amygdala kindling-induced epileptogenesis: comparison of a GABA uptake inhibitor and diazepam. *Epilepsy Res.* 1987;1:63–9.
30. Baum M. A clinical trial of mithramycin in the treatment of advanced malignant disease. *Br J Cancer.* 1968;22:176–83.
31. Quami W, Dutta R, Green R, Katiri S, Patel B, Mohapatra SS, et al. Mithramycin A inhibits colorectal cancer growth by targeting cancer stem cells. *Sci Rep.* 2019;9:15202.
32. Zhao Y, Zhang W, Guo Z, Ma F, Wu Y, Bai Y, et al. Inhibition of the transcription factor Sp1 suppresses colon cancer stem cell growth and induces apoptosis in vitro and in nude mouse xenografts. *Oncol Rep.* 2013;30:1782–92.
33. Bravo-San Pedro JM, Pietrocola F, Sica V, Izzo V, Sauvat A, Kepp O, et al. High-throughput quantification of GFP-LC3(+) dots by automated fluorescence microscopy. *Methods Enzymol.* 2017;587:71–86.
34. Kepp O, Chen G, Carmona-Gutierrez D, Madoe F, Kroemer G. A discovery platform for the identification of caloric restriction mimetics with broad health-improving effects. *Autophagy.* 2020;16:188–9.
35. Wang Y, Xie W, Humeau J, Chen G, Liu P, Pol J, et al. Autophagy induction by thiostrepton improves the efficacy of immunogenic chemotherapy. *J Immunother Cancer.* 2020;8.
36. Bezu L, Sauvat A, Humeau J, Gomes-da-Silva LC, Iribarren K, Forveille S, et al. eIF2alpha phosphorylation is pathognomonic for immunogenic cell death. *Cell Death Differ.* 2018;25:1375–93.
37. Sica V, Maiuri MC, Kroemer G, Galluzzi L. Detection of apoptotic versus autophagic cell death by flow cytometry. *Methods Mol Biol.* 2016;1419:1–16.
38. Mettievier D, Dallaporta B, Zamzami N, Larochette N, Susin SA, Marzo I, et al. Cytofluorometric detection of mitochondrial alterations in early CD95/Fas/APO-1-triggered apoptosis of Jurkat T lymphoma cells. Comparison of seven mitochondrion-specific fluorochromes. *Immunol Lett.* 1998;61:157–63.
39. Cerrato G, Leduc M, Muller K, Liu P, Zhao L, Humeau J, et al. Oleate-induced aggregation of LC3 at the trans-Golgi network is linked to a protein trafficking blockade. *Cell Death Differ.* 2020;28:1733–52.
40. Bravo-San Pedro JM, Kepp O, Sauvat A, Rello-Varona S, Kroemer G, Senovilla L. Clonogenic assays to detect cell fate in mitotic catastrophe. *Methods Mol Biol.* 2021;2267:227–39.
41. Rello-Varona S, Lissa D, Shen S, Niso-Santano M, Senovilla L, Marino G, et al. Autophagic removal of micronuclei. *Cell Cycle.* 2012;11:170–6.
42. Michels J, Vitale I, Senovilla L, Enot DP, Garcia P, Lissa D, et al. Synergistic interaction between cisplatin and PARP inhibitors in non-small cell lung cancer. *Cell Cycle.* 2013;12:877–83.
43. Humeau J, Sauvat A, Cerrato G, Xie W, Loos F, Iannantuoni F, et al. Inhibition of transcription by dactinomycin reveals a new characteristic of immunogenic cell stress. *EMBO Mol Med.* 2020;12:e11622.
44. Loos F, Xie W, Sica V, Bravo-San Pedro JM, Souquere S, Pierron G, et al. Artificial tethering of LC3 or p62 to organelles is not sufficient to trigger autophagy. *Cell Death Dis.* 2019;10:771.
45. De Sousa EMF, Wang X, Jansen M, Fessler E, Trinh A, de Rooij LP, et al. Poor-prognosis colon cancer is defined by a molecularly distinct subtype and develops from serrated precursor lesions. *Nat Med.* 2013;19:614–8.

ACKNOWLEDGEMENTS

JD, A-LT, HP, SZ, and HC are supported by the China Scholarship Council. OK receives funding by the DIM ELICIT initiative of the Ile de France and Institut National du Cancer (INCa); GK, VT, and PLP are supported by the Ligue contre le Cancer (équipes labellisées, Program “Equipe labellisée LIGUE”; no. EL2016.LNCC (VT/PLP)); Agence National de la Recherche (ANR)—Projets blancs; ANR under the frame of E-Rare-2, the ERA-Net for Research on Rare Diseases; AMMICA US23/CNRS UMS3655; Association pour la recherche sur le cancer (ARC); Association “Le Cancer du Sein, Parlons-en!”; Cancéropôle Ile-de-France; Chancellerie des universités de Paris (Legs Poix), Fondation pour la Recherche Médicale (FRM); a donation by Elior; European Research Area Network on Cardiovascular Diseases (ERA-CVD, MINOTAUR); Gustave Roussy Odyssea, the European Union Horizon 2020 Project Oncobiome; Fondation Carrefour; INCa; Inserm (HTE); Institut Universitaire de France; LeDucq Foundation; the LabEx Immuno-Oncology (ANR-18-IDEX-0001); the RHU Torino Lumière; the Seerave Foundation; the SIRIC Stratified Oncology Cell DNA Repair and Tumor Immune Elimination (SOCRATE); and the SIRIC Cancer Research and Personalized Medicine (CARPEM). We are grateful to the support of the Gustave Roussy, Université Paris-Saclay, Plateforme Imagerie et Cytométrie (PFIC), UMS AMMICA INSERM US23-CNRS 3655.

AUTHOR CONTRIBUTIONS

JD, AT, and HP conducted experiments, AS and ML analyzed the data. PL, LZ, SZ, and HC advised assisted sample preparation. VT, PL, LS, and YL supervised the project. GK and OK led the project and prepared the publication.

COMPETING INTERESTS

GK and OK are cofounders of Samsara Therapeutics. GK is a cofounder of Therfast Bio. The remaining authors declare no competing interests.

ADDITIONAL INFORMATION

Supplementary information The online version contains supplementary material available at <https://doi.org/10.1038/s41419-021-04270-x>.

Correspondence and requests for materials should be addressed to Yingqiu Li, Guido Kroemer or Oliver Kepp.

Reprints and permission information is available at <http://www.nature.com/reprints>

Publisher's note Springer Nature remains neutral with regard to jurisdictional claims in published maps and institutional affiliations.



Open Access This article is licensed under a Creative Commons Attribution 4.0 International License, which permits use, sharing, adaptation, distribution and reproduction in any medium or format, as long as you give appropriate credit to the original author(s) and the source, provide a link to the Creative Commons license, and indicate if changes were made. The images or other third party material in this article are included in the article's Creative Commons license, unless indicated otherwise in a credit line to the material. If material is not included in the article's Creative Commons license and your intended use is not permitted by statutory regulation or exceeds the permitted use, you will need to obtain permission directly from the copyright holder. To view a copy of this license, visit <http://creativecommons.org/licenses/by/4.0/>.

© The Author(s) 2021

Titre : L'inhibition du récepteur IGF1 amplifie les effets des médicaments anticancéreux par l'autophagie et les mécanismes immuno-dépendants

Mots clés : Autophagie, picropodophylline, récepteur du facteur de croissance analogue à l'insuline 1, cancer

Résumé :

Un certain nombre de produits végétaux naturels induisent l'autophagie et médient la durée de vie dépendante de l'autophagie et les effets de prolongation de la durée de vie dans des modèles de souris appropriés. Ici, nous avons identifié la picropodophylline (PPP) comme un inducteur non toxique du flux autophagique qui agit sur les cellules humaines et de souris *in vitro*, ainsi que sur les organes de souris *in vivo*. Mécaniquement, PPP inhibe IGF1R ainsi qu'en aval d'AKT, la cible mécaniste du complexe de rapamycine 1 (mTORC1), couplé à l'activation des facteurs de transcription pro-autophagiques EB (TFEB) et E3 (TFE3). Les cellules équipées d'un mutant AKT constitutivement actif n'ont pas réussi à activer l'autophagie. Le PPP a également stimulé l'activation répressible par AKT des trois bras de la réponse au stress déplié (UPR), y compris la phosphorylation dépendante de PERK du facteur d'initiation eucaryote 2 α (eIF2 α). L'inactivation de TFEB et / ou TFE3 a émoussé l'UPR tandis que l'inactivation de PERK ou le remplacement de eIF2 α par un mutant non phosphorylable a réduit l'activation de TFEB / TFE3 et l'autophagie induite par PPP. Cela indique une diaphonie entre l'UPR et l'autophagie. Il convient de noter que l'administration de PPP à des souris a amélioré l'efficacité de la chimiothérapie immunogène et des inhibiteurs de point de contrôle immunitaire en s'appuyant sur la libération d'ATP, la libération de HMGB1 et l'exposition au CALR. Cet effet anticancéreux reposait sur une amélioration de la réponse immunitaire anticancéreuse dépendante des lymphocytes T et était perdu lors de la surexpression de CD39, de l'activation constitutive de l'AKT ou de la suppression du gène essentiel de l'autophagie Atg5 des cellules malignes. En conclusion, le PPP est un inducteur d'autophagie biodisponible et potentiellement utile qui justifie une caractérisation préclinique plus poussée.

Title : IGF1 receptor inhibition amplifies the effects of cancer drugs by autophagy and immune-dependent mechanisms

Keywords : Autophagy, picropodophyllin, insulin-like growth factor 1 receptor, cancer

Abstract :

A number of natural plant products induce autophagy and mediate autophagy-dependent healthspan and lifespan-extending effects in suitable mouse models. Here, we identified picropodophyllin (PPP) as a non-toxic inducer of autophagic flux that acts on human and mouse cells *in vitro*, as well as mouse organs *in vivo*. Mechanistically, PPP inhibits IGF1R as well as, downstream of AKT, the mechanistic target of rapamycin complex 1 (mTORC1), coupled to the activation of the pro-autophagic transcription factors EB (TFEB) and E3 (TFE3). Cells equipped with a constitutively active AKT mutant failed to activate autophagy. PPP also stimulated the AKT-repressible activation of all three arms of the unfolded stress response (UPR), including the PERK-dependent phosphorylation of eukaryotic initiation factor 2 α (eIF2 α). Knockout of TFEB and/or TFE3 blunted the UPR while knockout of PERK or replacement of eIF2 α by a non-phosphorylatable mutant reduced TFEB/TFE3 activation and autophagy induced by PPP. This points to crosstalk between the UPR and autophagy. Of note, administration of PPP to mice improved the efficacy of immunogenic chemotherapy and immune checkpoint inhibitors relying on ATP release, HMGB1 release, and CALR exposure. This anticancer effect relied on an improved T lymphocyte-dependent anticancer immune response and was lost upon CD39 overexpression in, constitutive AKT activation in, or deletion of the essential autophagy gene Atg5 from, the malignant cells. In conclusion, PPP is a bioavailable, potentially useful autophagy inducer that warrants further preclinical characterization.